The Role of Silica in Mineralising Tissues

A thesis submitted in partial fulfilment of the
requirements of the Nottingham Trent University
for the degree of Doctor of Philosophy

by

Ana Maria Caballero-Alías

November 1999

Department of Chemistry & Physics
The Nottingham Trent University

To my parents,

Francisco and Antonia.

ACKNOWLEDGEMENTS

I would like to thank my supervisor Dr. C.C. Perry for the opportunity to carry out this research and for her guidance, advice and support throughout. I would like to thank to Dr. S. Aubonnet, Dr. S. Din, Dr. T. Keeling-Tucker, Ms L. Heath, Mr. M. Gardener, Mr. C. McLean, Dr. M. Webb, members of the Inorganic research group of the Nottingham Trent University (past and present) for bearing with me during the last three years. I would like to thank to Dr. J. Hargreaves for assistance with the XRD and with the X-ray line broadening analysis. I would also like to thank him for his advice and support during the project. I thank Ms. P. Fleming, Mr. M. Sladen, Mr. R. Bentham and Mr. D. Chambers-Asman for technical assistance. I thank Mr. D. Lacy for assistance with the TEM. I thank Ms. D. Whitmore for photographic reproduction. I thank the undergraduate students Mr. G. Copper, Ms N. Tzioumaki and Mr. C. Simpson for their contribution to this research.
I would like to thank Prof. S. Downes of Smith&Nephew (second supervisor). I thank Ms. S. Anderson of the Nottingham University for performing the biological studies of the silica-coatings and writing the paper. I thank Dr. C Scotchford of the Nottingham University and Dr. S. Kirk of the Nottingham Trent University for their help in the isolation of the bone mineral. I thank Mr. B. Shaw of the Nottingham University for assistance with the TEM sample processing. I thank Dr. A. Slawin of the Loughborough University for allowing me to use the XRD spectrophotometer at Loughborough University when the XRD at the NTU was down. I thank Dr. P. Day of Manchester University for performing the AA aluminium analyses and AES silicon analysis reported in this study.
I thank the BFWG Charitable Foundation for financial support. I would like to thank my friends Adrian and Jo.
Finally I would like to thank my parents, Francisco and Antonia, and sisters, Antonia and Pilar, for being so caring and supportive during the entire time of this research.

"El Universo vegetal susurra apenas hasta que la tempestad pone en accion toda la música terrestre. De aquellas tierras, de aquel barro, de aquel silencio, he salido yo a andar, a cantar por el mundo".

Pablo Neruda
Memorias

ABSTRACT

Hydroxyapatite is the principal inorganic constituent of human bone and teeth and its formation has widely been investigated. The formation of crystalline hydroxyapatite is preceded by an amorphous calcium phosphate precipitate, the composition of which depends on the reaction solution. The effect of pH, T, precursors and ionic medium on the precipitation of calcium phosphate have been investigated. At both 23 °C and 37 °C , with the pH neutral to alkaline and at moderate supersaturation conditions, apatite is the main phase precipitated. The material is non-stochiometric (Ca/P=1.3 to 1.8) and poorly crystalline. At high supersaturation calcium phosphate dibasic and apatite form.
In higher animals silicon has been shown to be an essential trace element and its involvement in bone mineralisation is well established. Since silica seems to have an important role to play in mineralisation processes, studies of the precipitation of calcium phosphate have been carried out in the presence of silica. Calcium phosphate crystals were precipitated from a solution containing 10 mM $Ca(NO_3)_2$ and 6 mM $(NH_4)_2HPO_4$ in the presence of soluble silicon species (0-0.409 mM) at both 23°C and 37°C from solutions at an initial pH of 7.4. Results showed that silica promotes calcium phosphate precipitation and crystallisation. Electron microscopy analysis showed that soluble silicon species act as nucleation sites for apatite crystals. By contrast, it is believed that aluminium might play a role in the development of bone fragility and inhibit bone mineralisation. The effect of aluminium on calcium phosphate precipitation has also been investigated. Calcium phosphate was precipitated from a solution containing 10 mM $Ca(NO_3)_2$ and 6 mM $(NH_4)_2HPO_4$ in the presence of freshly prepared aluminium chloride (7.5 and 75 μM) at both 23°C and 37°C from solutions at an initial pH of 7.4. The presence of aluminium decreased the crystallinity of the principal phases. Electron microscopy analysis showed that aluminium species were incorporated into apatitic material and into complex amorphous aggregates. The presence of aluminium chloride in the reaction medium appeared to inhibit the transformation of amorphous calcium phosphate and/or octacalcium phosphate to stoichiometric hydroxyapatite.
In the early 90's, Birchall hypothesised that silicon species could be involved in a mechanism to protect against aluminium poisoning. Birchall and co. workers showed that Si could lessen the toxic effect of Al in a variety of organisms. Some studies have shown that silicic acid could release and excrete aluminium from the body stores including bone. Based on these studies, the ability of silicic acid to ameliorate the effect of aluminium on crystal composition, crystallinity and morphology have been investigated. The presence of silicon in the aluminium-containing reaction medium (up to 0.082mM) appeared to enhance the formation of hydroxyapatite at room temperature. The presence of silicon did not improve the crystallinity of dicalcium phosphate dihydrated but it seemed to improve the transformation of amorphous phosphate and/or octacalcium phosphate into hydroxyapatite. Although the hydroxyapatite crystals were not as crystalline as the control they were more perfect than the crystals formed in the presence of aluminium in the reaction media.
The bioactivity of a silica-coating was assessed using the simulated body fluid method. The osteoblast response to a silica-coating was also assessed. Primary human osteoblast cells were seeded on the surface of upright silica-coated discs. Results showed that silica-coated surfaces stimulate apatite precipitation and may promote mineralisation of osteoblast cells *in vitro*.

CONTENTS

LIST OF ABBREVIATIONS

ACP, amorphous calcium phosphate, $Ca_3(PO_4)_2$ 3-4.5H_2O

CP calcium phosphate

DCP, dicalcium phosphate, monetite $CaHPO_4$

MCP, monocalcium phosphate, $Ca(H_2PO_4)_2$

MCPH, monocalcium phosphate hydrated, $Ca(H_2PO_4)_2.H_2O$

DCPD, dicalcium phosphate dihydrated, brushite $CaHPO_4.2H_2O$

EtOH, ethanol

HAP, hydroxyapatite $Ca_{10}(PO_4)_6(OH)_2$

OCP, octacalcium phosphate, $Ca_8H_2(PO_4)_6.5H_2O$

QMC, Queen's Medical Center

RT room temperature

SBF, simulated body fluid

SRM, standard reference material

TCP, tricalcium phosphate, $Ca_3(PO_4)_2$

TEOS, tetraethylorthosilicate.

TTCP, tetracalcium phosphate, $Ca_4(PO_4)_2O$

CHAPTER 1: INTRODUCTION

1.1 THE FORMATION OF PRECIPITATES

1.1.1 Nucleation

The generation of crystals from solution is of particular significance not only in analytical chemistry but also in physiology and in the geochemical sciences. In the field of physiology, nucleation occurs under normal conditions (e.g. bone growth) and under abnormal conditions (bladder, kidney, gout, etc.).

Nucleation or the birth of crystals from solution is a process which controls the number, size, structure, and morphology of precipitated crystals[1].

The interaction between ions and between molecules which leads to cluster formation and to the evolution of crystals has been likened to a chemical reaction. Similarly to a chemical reaction, before crystallisation can occur the energy barrier to nucleation must be overcome. There must be a degree of supersaturation before spontaneous crystallisation will occur.

The largest cluster which may exist before spontaneous crystallisation occurs is usually referred to as the critical cluster or nucleus. The process for the crystallisation of a molecular species can be represented as follows:

$A + A \leftrightarrow A_2$

$A_2 + A \leftrightarrow A_3$

$A_{x-1} + A \leftrightarrow A_x$

$A_x + A \xrightarrow{\text{nucleation}} A_{x+1}$

$A_{x+1} + A \longrightarrow$ crystal growth where A = molecule.

There are two different forms of precipitate nucleation: heterogeneous nucleation and homogeneous nucleation[1]. Heterogeneous nucleation occurs at a supersaturation level lower than that required for homogeneous nucleation (fig. 1.1).

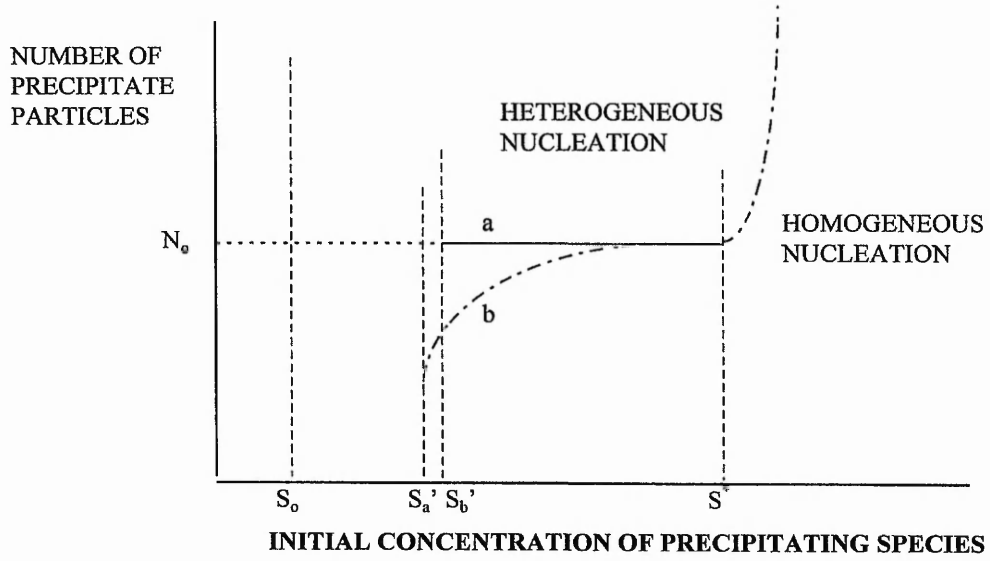

Figure 1.1 Typical curves for the number of precipitate particles produced as a function of the initial concentration. Curve *a* is for a system of N_o impurity particles, each equally efficient in catalysing heterogeneous nucleation. Curve *b* corresponds to the precipitation onto N_o impurities of varying nucleation efficiency. Heterogeneous nucleation occurs at a supersaturation s' and homogeneous nucleation occurs at a much higher (critical) supersaturation s^*; s_o is the solubility of the precipitant.

In heterogeneous nucleation, the influence of solids other than the precipitating phase and impurities is strong. The influence of the substrate can affect the energy barrier to nucleation and the formation of precipitates can be catalysed by impurities, (e.g. lattice match between precipitate crystal and impurity substrate)[1]. Homogeneous nucleation occurs only at high supersaturation values.

The nature of the initiating nucleus will affect the structural morphology of the product. If the critical nucleus size is less than one unit cell, amorphous or partially crystalline material is produced. Agglomeration of small crystallites into larger aggregates also favours an amorphous precipitate[1].

1.1.2 Crystal growth

The way in which a crystal grows depends upon the structure of its surface in contact with the solution[1]. Some molecules will move out from the crystal surface and will be replaced by solvent molecules; some molecules from the solution will adsorb onto the crystal surface. The surface is in dynamic equilibrium with the solution and when the solution is supersaturated the equilibrium will be disturbed[2].

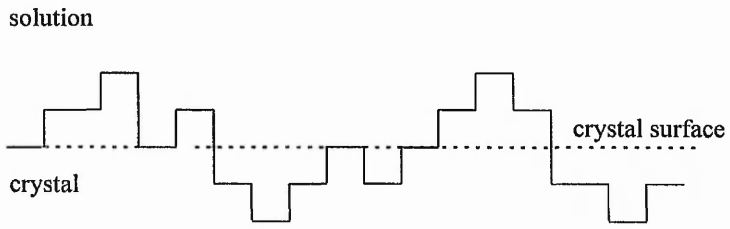

Figure 1.2 Schematic representation of the development of a surface.

Molecules from solution will absorb at the top of the layer and at the bottom molecules of solvent will diffuse out of the lattice layer to be replaced by solute molecules; thus the disordered layers move upwards leaving behind an ordered crystal (fig. 1.2). Each molecule is incorporated into the crystal without any discontinuous change in the essential structure of the interface. Macroscopic crystals are unlikely to be perfect; they will normally contain lattice dislocations and other imperfections[1,2].

1.1.3 Impurities and additives

When a crystal grows from an impure solution or from one containing an additive, it will reject the impurity if the impurity is less soluble in the crystal than in the solution. As the interface moves, impurities may be rejected into the solution more rapidly than they can be carried away by diffusion. In consequence the impurity concentration in the solid will be

determined by the impurity concentration in the enriched diffusion layer and not by the mean concentration in the solution[2].

The impurities may adsorb onto the crystal from the neighbouring enriched solution and the molecules after certain time may desorb back into the solution. An advancing growth layer on meeting an adsorbed molecule may brush it ahead until it desorbs, or, if the impurity is more strongly adsorbed and less mobile on the surface, surround and partially embed it. Succeeding growth layers will repeat the process and the chances of the impurity desorbing decrease the more deeply it is embedded[3].

During crystallisation, the largest crystals are those which would have nucleated first at the highest solute concentrations and are subjected to rates of growth varying from the highest to the lowest rate. They will be the most impure crystals and unless there is diffusion within the crystal, they will be most impure near their centres. Smaller crystals born later and grown more slowly will be more pure. When Ostwald ripening occurs, these smaller crystals will dissolve and the larger crystals will grow. The new growth on the latter will be purer than the dissolved crystals[2].

The distribution of impurity molecules will not only be radial but may be anisotropic since the growth and adsorption are likely to be different for different faces[4]. For example, the presence of lead ions cause potassium chloride crystals to grow in an octahedral habit[1] (fig. 1.3). Low concentrations (<1%) cause the disappearance of the (1 0 0) faces and the appearance of the octahedral (1 1 1) planes. Higher concentrations (>1%) cause higher-index planes to appear, giving a faceted sphere[1].

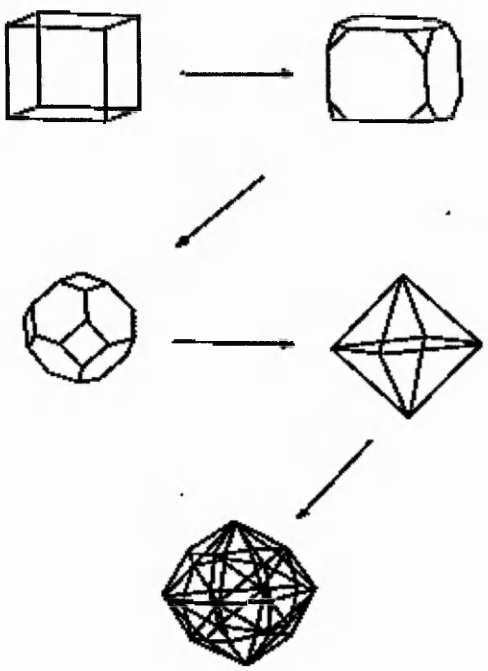

Figure 1.3 Some possible modifications of a cubic system showing first the formation of the octahedral faces, then higher-index faces[1].

1.1.4 Ostwald ripening

A supersaturated state does not spontaneously transform directly into the phase which is the most stable of the possible states but into the phase which is less stable than itself[5]. If the immediate product of a crystallisation or other phase change is the unstable form, then , during ageing, this may transform into the stable or a more stable form. The mechanism of the transformation will vary with the conditions[2].

Nucleation of the stable form may have occurred to a small extent alongside the nucleation and growth of the major product, the unstable form. The stable form has the lowest solubility but as it is likely to be present as smaller crystals with enhanced solubility these may either dissolve back into solution or grow at the expense of the unstable form. On the other hand no stable nuclei may have been formed, and if the unstable product is to

transform, nuclei of the stable form must be created. It seems likely that these nuclei will not be formed within the solution but will be generated from the unstable crystals[2]. The new phase may be of a different lattice structure to the parent crystal, or with different orientation or conformation of molecules on lattices sites, or be different in composition[6,7,8,9].

1.1.5 Morphology

The morphology or physical appearance of precipitates is determined by nucleation and growth rates, colloidal stability, recrystallisation and ageing processes, and various habit modifications brought about either by ions or molecules present in solution or by the solvent itself[1,2]. The first feature affecting the grain size of precipitates is its solubility[10,11]. The final particle size will depend upon the number of nucleation sites and the amount of material precipitated. With little material in solution the growth rate will be slow at controllable levels of supersaturation. The degree of supersaturation also strongly affects the degree of crystal perfection[12]. At concentrations close to those of homogeneous crystal nucleation, the critical nucleus is typically the size of a few unit cells; however, at higher concentrations the critical nucleus is much smaller and looses its identity with the new phase[13]. For simple compounds the ions or molecules will rapidly reorganise to satisfy the minimum energy requirement of the regular lattice; however, there are many complicated structures known where it is not easy for the ions or molecules to rearrange in the appropriate configuration (e.g. apatites, silicates, cholesterol, and most polymers and enzymes). There is often an intermediate amorphous gel structure from which the molecules undergo a transition state before attaining its normal structure[1].

The rate of growth also influences the morphology. For slow growth rates, precipitate particles often take on a compact, well-defined shape which is related to the crystal structure. At faster rates of growth, changes in crystal habit are observed and at higher supersaturations dendritic growth usually occurs[14,15]. Crystals produced at low supersaturation are compact and small, at higher concentrations are large and dendritic, and at still higher concentration are much smaller, but compact, and agglomerated[16,17,18].

The addition of foreign ions to a crystallising solution causes changes in the crystallisation process which are partially described by the changes in growth rate and coprecipitation involving the foreign ion[19]. The added ions may have a cation, anion, or neither in common with the crystallising phase, and the effect of habit modification may be brought about as a result of changes in a lattice dimension by incorporated ions or surface blocking[20]. Habit modifications may then be observed[21-23].

1.2 BIOMINERALISATION

Mineralisation in living organisms is defined as the deposition of inorganic chemical compounds under normal or pathologic conditions. In mammals, mineralisation is synonymous with calcification because the major inorganic minerals deposited are calcium containing compounds. The most familiar calcified structure is bone. Bone refers to a family of materials each with a different structural motif (eg. dentin, mineralised tendons), but all having in common the basic building block, the mineralised collagen fibril[24].

Bone not only has a mechanical function providing the architecture of the human body, but is also the major reservoir of calcium and phosphate necessary for a wide variety of metabolic functions[25].

The components of bone are classified as organic and inorganic. The organic constituents are made up of acidic glycoproteins, proteoglycans, a host of serum proteins and type I collagen, a fibrous protein that constitutes the extracellular matrix of bone, and water[26]. The collagen fibrils constitute a three dimensional framework on which crystals form[24,26]. The range of mineral contents of bone is between about 45 and 85 % by mass and approximately half of that by volume[24]. The mineral can exist in three different possible compartments in relation to the collagen fibrils: 1) within the fibrils, 2) on the surface of the fibrils and 3) between the fibrils, but not in direct contact with them[26].

1.2.1 The processes of calcification

Bone mineralisation occurs in the extracellular space. The process in which the mineral is deposited within an organic matrix has been extensively reviewed[24,26-38]. Calcification depends on the interaction of cells, extracellular macromolecules and other matrix components. The extracellular macromolecules, particularly collagen, non-collagenous proteins, proteoglycans, proteolipids, and glycoproteins regulate the manner in which the mineral is deposited. Smaller molecules and ions, such as pyrophosphate[28,32], carbonate[39,40], magnesium[41-43], and nucleoside triphosphates[41,44] as well as certain hormones[44,45] and non-matrix proteins[46-49] are involved in the regulation of *in vivo* calcification and the production of the calcifiable matrix.

Although physiological solutions such as plasma or lymph, are supersaturated with respect to hydroxyapatite[50], apatite precipitation does not occur spontaneously within them. Physiological solutions can maintain their metastability with higher free calcium and phosphate concentrations because of the chelation of these ions by macromolecules and because of the presence of calcification inhibitors[28,38]. Extracellular macromolecules and

certain cells (osteoblasts, odontoblasts, chondroblasts, etc.) are believed to control calcification by increasing local calcium and phosphate concentrations, providing sites for crystal growth and deposition, and controlling mineralisation in areas where mineral formation is not desired.

Three different mechanisms have been proposed to explain the calcification process:

a) *Physiochemical mechanisms*. It was first suggested that collagen could provide a suitable template for the formation of the apatite which would grow from collagen by epitaxy[51]. However electron microscopic studies failed to confirm an association between the first detectable mineral crystals and collagen fibrils[52].

A second theory was the "amorphous calcium phosphate" hypothesis[37]. Non-crystalline compounds called amorphous calcium phosphate (ACP) are formed from calcium and phosphate prior to the appearance of crystalline apatite. ACP was thought to compose mostly of tricalcium phosphate. Once formed, ACP converted to crystalline mineral.

A third physicochemical theory was that apatite mineral was formed through a simpler, but crystalline, intermediate, namely octacalcium phosphate[53].

b) *Local ion-concentrating mechanisms*. One of the most important theories has been the phosphatase theory, introduced by Robinson[54] in the 1920s. He and his co-workers showed that phosphatases were highly concentrated within bone and cartilage during the process of initial mineralisation[55]. Robinson proposed that phosphatase functions at the calcification front were to hydrolyse a naturally occurring phosphate ester substrate, producing a localised high concentration of phosphate ions and a supersaturated condition for calcium and phosphate ions. This would cause spontaneous nucleation of a calcium phosphate mineral phase. However, the theory was challenged on several points. First, no natural substrate was identified for bone alkaline phosphatase to act upon. Iodoacetate and

fluoride, which could inhibit mineralisation in rachitic rat, did not inhibit alkaline phosphatase under the experimental conditions used by Robinson. Finally, in biological fluids, in which it was shown that calcium and phosphate concentrations were metastable with regard to apatite, apatite never spontaneously precipitated.

A second theory relied on the attraction of calcium ions to certain acidic phospholipids, (e.g. phosphatidyl serine) which had been identified in calcifying regions of cartilage[56]. Phosphatidyl serine and other phospholipids could act as a non-energy-requiring calcium trap localised at the site of mineralisation.

Phosphoproteins have also been shown to be present in higher concentration at the mineralisation front, suggesting a possible role in mineralisation[57].

c) *Removal of calcification inhibitors*. In the calcification sites, inhibitors are present and can prevent the formation of mineral. Thus mineralisation could only occur at sites where local enzymatic and other anti-inhibitory activity could remove inhibitors (such as pyrophosphate). The proposal that pyrophosphate could serve as a mineral inhibitor was first suggested by Fleisch and Neuman[32], who showed that pyrophosphate had two effects on apatite: 1) preventing its formation from metastable calcium phosphate solutions and 2) preventing its dissolution once formed. Thus the phosphatase hypothesis was revitalised by showing that this enzyme could promote mineralisation not only providing orthophosphate, but locally destroying pyrophosphate at the precise site of mineralisation.

Proteoglycans had also been implicated as calcification inhibitors because of their ability to chelate Ca^{2+}. Acidic proteoglycans which are abundant in cartilage matrix[58] are present in lower concentrations in bone and dentin[28]. Anionic proteoglycans would have to be degraded in order to allow progressive mineralisation. There is biochemical, histochemical

and electron microscopic evidence of proteoglycan removal at sites of incipient calcification[59-61].

A second mode of calcification, not always present, involves the release of so-called matrix vesicles into the extracellular space, which also induces crystals to form. The matrix vesicles contribute to the mineralisation of the intercollagen fibril compartment[28].

1.2.2 The nature of the initial mineral

The nature of the initial mineral deposited in calcified tissues is uncertain. Literature reports the presence of a variety of calcium phosphate phases such as amorphous calcium phosphate[62,63], brushite[64,65] and octacalcium phosphate[66] in addition to hydroxyapatite itself. It has been suggested that brushite is the first mineral to form in the process of calcification[65].

The presence of brushite has been confirmed in newly mineralised tissue from the bony part of the tibias of 17-day-old chick embryos[65]. However brushite, which accounts for approximately 1% of the total mineralised tissue, is not found in mature bone[67]. *In vitro* studies suggested that brushite might act as a precursor to hydroxyapatite deposition, and that hydroxyapatite growth could occur on the brushite crystals[64,68]. However, brushite forms *in vitro* at a lower pH than that which is believed to exit in the extracellular matrix[69]. It is most likely that the earliest mineral deposited in bone osteoid is a less perfect hydroxyapatite than that of mature bone. The identification of all the mineral phases that exist within the living organism is extremely difficult and the determination of the precise nature of the first mineral formed is one of the major unsolved problems in the field of calcification.

1.2.3 The nature of the mature bone mineral

It was once believed that mature bone was a mixture of an X-ray amorphous tricalcium phosphate (ACP) and hydroxyapatite (HAP), but nowadays it is known that the mature bone is formed from poorly crystalline carbonated apatite crystals named Dahllite[26]. They crystals are plate-shaped, with average lengths and widths of 50 x 25 nm[26]. The crystals are very thin, with thickness appearing to be remarkably uniform 2-6 nm (fig. 1.4). These crystals are extremely small and they may be the smallest biologically formed crystals known. Although the crystals are plate-shaped, they have hexagonal symmetry[70]. It has been proposed that this is because they grow via an octacalcium phosphate transition phase[66]. Octacalcium phosphate crystals are plate-shaped and have a structure very similar to apatite except for the presence of an hydrated layer[70].

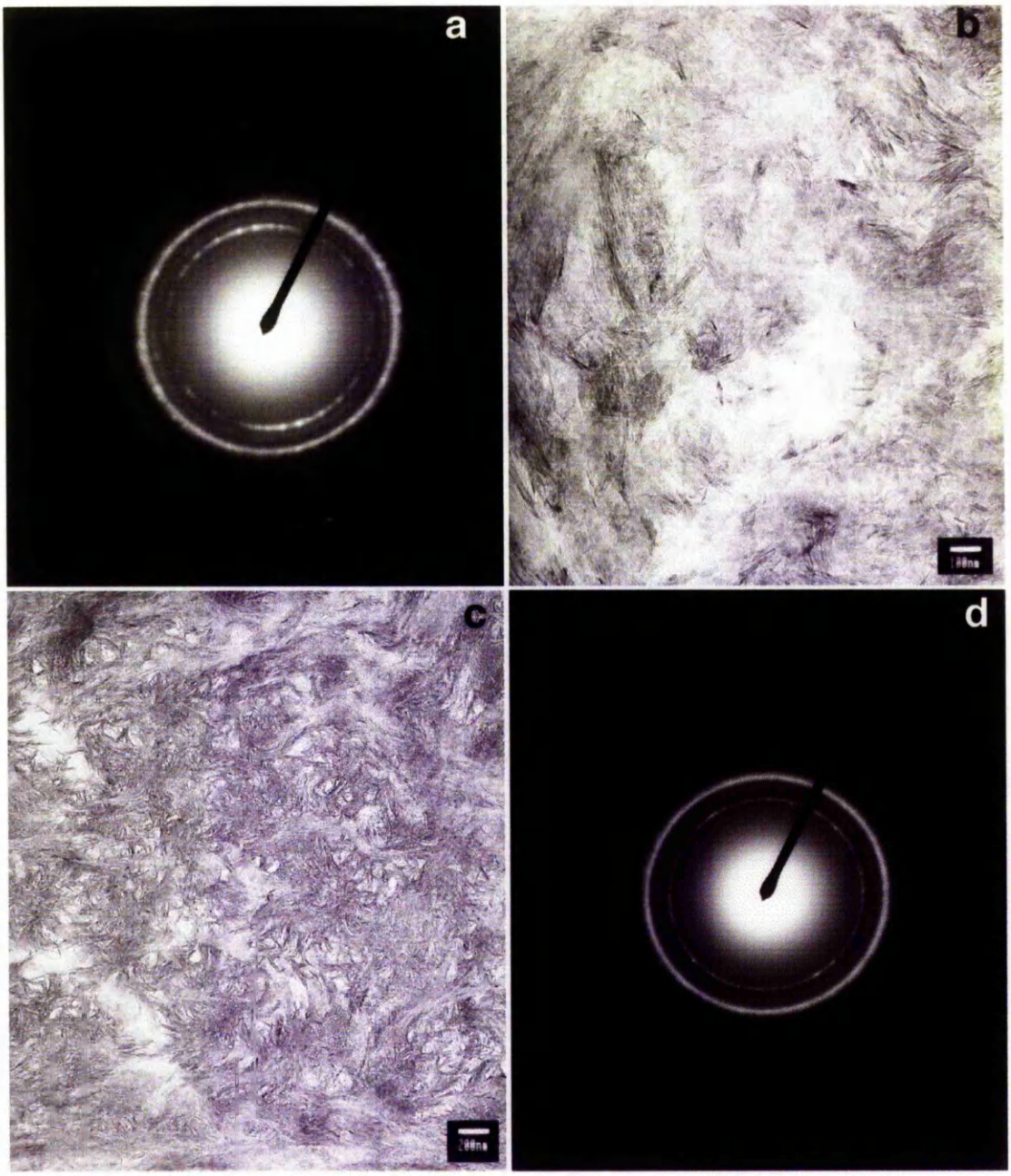

Figure 1.4 a) Electron diffraction of b) femoral head cortical bone, c) femoral head cancellous bone and d) electron diffraction of c) (see appendix IV for protocol for the preparation of bone samples for TEM analysis).

1.3 CALCIUM PHOSPHATES

Calcium Phosphates form a large family of isomorphous materials. Each one has different properties depending on its crystallographic characteristics. Table 1.1 summarises the crystallographic characteristics of some of the crystalline calcium phosphate phases.

NAME	MOLECULAR FORMULA	SYMMETRY GROUP	SYSTEM	Ca/P
Hydroxyapatite (HAP)	$Ca_{10}(PO_4)_6(OH)_2$	$P2_1/b$	Monoclinic	1.67
Non-stoichiometric hydroxyapatite (AP)	$Ca_{10-x}(HPO_4)_x(PO_4)_{6-x}(OH)_{2-x} \cdot nH_2O$ $0<x<1$, n=0-2.5	$P6_3/m$	Hexagonal	1.4-2
Hydroxycarbonateapatite (HCA)	$Ca_{10}(PO_4)_6(CO_3)_3(OH)$	$P2_1/b$	Monoclinic	1.67
Monocalcium Phosphate (MCP)	$Ca(H_2PO_4)_2$	-	Triclinic	0.50
Monocalcium Phosphate hydrated (CPMH)	$Ca(H_2PO_4)_2. H_2O$	-	Triclinic	0.50
Dicalcium Phosphate (DCP)	$CaHPO_4$	P-1 (2)	Triclinic	1.00
Dicalcium Phosphate dihydrated (DCPD)	$CaHPO_4.2H_2O$	Ia	Monoclinic	1.00
Amorphous Calcium Phosphate (ACP)	$Ca_3(PO_4)_2 \cdot nH_2O$	-	-	1.50
Tricalcium Phosphate (TCP)	$Ca_3(PO_4)_2$	R3m	Rhombohedral	1.50
Tetracalcium Phosphate (TTCP)	$Ca_3(PO_4)_2CaO$	$P2_1$ (4)	Monoclinic	2.00
Octacalcium Phosphate (OCP)	$Ca_3(PO_4)_2.CaHPO_4$	P-1	Triclinic	1.33

Table 1.1 Name, molecular formulae, symmetry group, system and Ca/P ratio of calcium phosphates.

The structure of the relevant calcium phosphate phases found in this work are described below.

1.3.1 Hydroxyapatite structure (HAP)

Because of its crystallographical similarity to various calcified tissue of vertebrates, hydroxyapatite, $Ca_{10}(PO_4)_6(OH)_2$ (HAP), has been well studied for biological applications as a substituted material for damaged teeth or bone.

DeJong[71] was the first to observe the similarity between the X-ray diffraction pattern of bone powder and the pattern obtained from the basic calcium phosphate mineral, hydroxyapatite. In fact the X-ray diffraction and electron diffraction patterns (Fig.1.4) of bone powder are identical to the pattern obtained from non-stoichiometric synthetic HAP. The crystal structure of non-stoichiometric HAP belongs to the space group $P6_3/m$ in the hexagonal system with the lattice parameters, $a(b=)9.432$ Å and $c=6.881$ Å (ref.)[70]. A simplified unit cell of HAP is shown in Fig. 1.5.

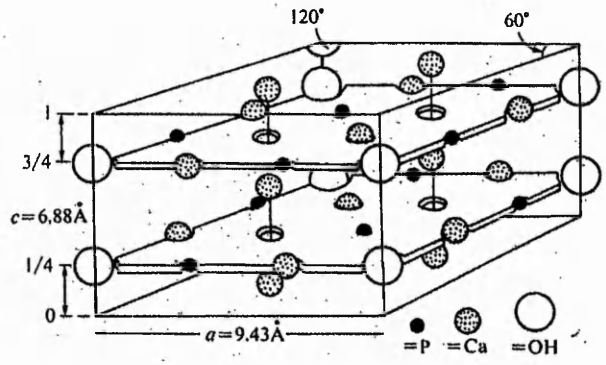

Figure 1.5 Simplied view of the unit cell of hydroxyapatite[70].

The two oxygen atoms of the PO_4-tetrahedron locate on the mirror planes at z=1/4 and 3/4, and the other two symmetrically occupy the sites above and below the planes. Calcium ions occupy two different sites; the column Ca at z=0,1/2 and the screw axis Ca at z=1/4, 3/4. Three of the screw axis Ca^{2+} form a triangle on a mirror plane (Fig. 1.6)[70].

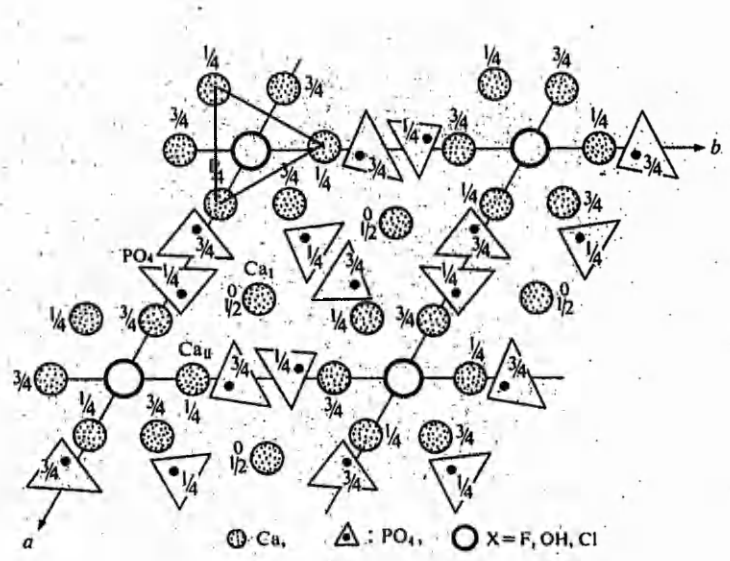

Figure 1.6 Crystal structure of apatite[70].

The arrangement of OH^- ions surrounded by a Ca^{2+}-triangle along the *c* axis is also characteristic of the HAP structure. Most wet-chemically synthesised HAP powders are non-stoichiometric. The following formula is mainly used for the explanation of the non-stoichiometry.

$$Ca_{10-x}(HPO_4)_x(PO_4)_{6-x}(OH)_{2-x} \cdot nH_2O \quad 0<x<1, n=0\text{-}2.5$$

The crystal structure of stoichiometric HAP belongs to the space group $P2_1/b$[71,72]. It is monoclinic pseudohexagonal. It has been postulated that the monoclinic phase results from a statistical disorder of the OH^- ion around the mirror plane (Fig.1.7).

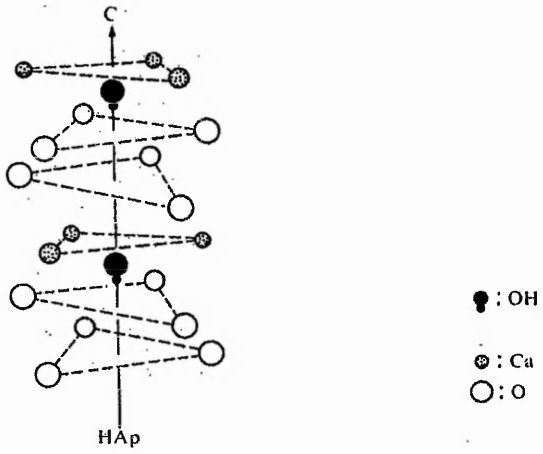

Figure 1.7 A cross-section of the apatite lattice parallel to the *c*-axis[70].

Such displacements of OH^- ions from the mirror plane changes the 6_3 axes into the 2_1 axes and the mirror plane into a b axial glide plane. There are two non-equivalent crystallographic sites for Ca^{2+}. Each Ca_I ion is surrounded by 9 oxygens from 6 PO_4^{3-} groups and Ca_{II} by 7 oxygens from PO_4^{3-} and 1 OH^- group.

1.3.2 Octacalcium phosphate structure (OCP)

Octacalcium phosphate belongs to the space group *P*-1 in the triclinic system[70,73]. OCP consists of alternative stackings of an "apatitic layer" with $4[Ca_3(PO_4)_2 \cdot 0.5H_2O]$ at z = -1/4, 1/4 and a "hydrated layer" with $4[CaHPO_4 \cdot 2H_2O]$ at z=1/4, 3/4 (fig.1.8).

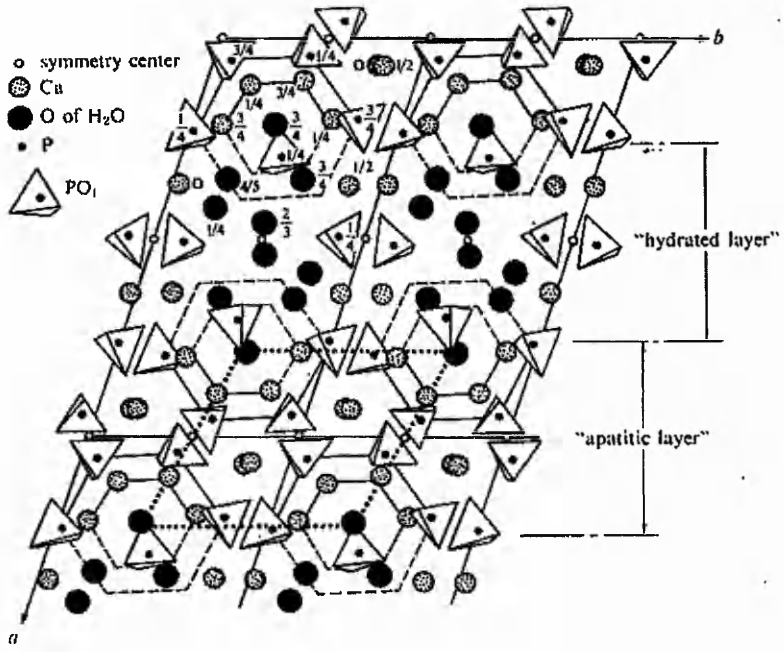

Figure 1.8 Structure of OCP projected down the *c*-axis. Heights are slightly idealised[70].

The x-ray diffraction pattern resembles that of HAP. A characteristic x-ray diffraction peak of OCP is from the (100) plane. The composition of the hydrated layer corresponds to that of brushite $CaHPO_4 \cdot 2H_2O$. It contains four HPO_4^{2-} groups which two of them form pillars as [Ca-HPO_4-Ca], and the other two are linked tightly to the apatitic layer through oxygen. The chemical formula of OCP is written by:

$$Ca_8(HPO_4)_2(PO_4)_4 \cdot 5H_2O$$

1.3.3 Brushite (DCPD)

The original studies by Beevers[74] suggested that brushite ($CaHPO_4 \cdot 2H_2O$) has a monoclinic cell of space group *I2/a* or *Ia*. Further studies by Jones[75] and Berry[76] concluded that the space group for brushite was *Ia*. Brushite converts to monetite ($CaHPO_4$, DCP) at 37°C and above. Monetite has a triclinic cell of space group *P-1(2)*.

1.3.4 Amorphous Calcium Phosphate (ACP)

ACP is amorphous with the composition of $Ca_3(PO_4)_2 \cdot nH_2O$ (n=3-4.5; 15-20% H_2O), which corresponds to a calcium-deficient HAP with the composition $Ca_9H_2(PO_4)_6(OH_2) \cdot nH_2O$. ACP forms mostly as spherical particles of ca. 300-1000 Å in diameter. X-ray diffraction of ACP gives an amorphous pattern. ACP is not a simple accumulation of HAP unit lattices[70]. It has been proposed that ACP is composed of clusters. Each cluster has a unit having the composition of $Ca_9(PO_4)_6$ with ca. 9.5 Å in diameter centring on the Ca_I site of the HAP structure. ACP has been found to contain no HPO_4^{2-} groups. ACP seems to be glass-like amorphous phase without HPO_4^{2-} groups.

1.4 SILICON AND BONE MINERAL

Silicon is the second most abundant element in the earth's crust after oxygen and it is an element required in trace amounts for life. It can be found combined with aluminium to form the aluminosilicates of rocks, clays, and soil minerals, and dissolved as soluble silica-silicic acid, $Si(OH)_4$. At approximately neutral pH silicic acid is uncharged and has a solubility of 2mM, above which polycondensation produces oligomeric silicic acids and colloidal particles of hydrated silica, $SiO_2 \cdot xH_2O$[77]. Silicic acid is found in the interstitial water of soils, lakes, rivers and oceans. Marine organisms such as diatoms, radiolaria, *etc.* use silica to construct their exoskeletons[78]. Some plants such as the primitive plant *Equisetum* have silica deposits that exhibit a wide range of structural motifs at the microscopic level[79-81].

The human ingestion of silicon in its most bioavailable form, silicic acid, has been estimated to be 30 mg Si per day with 60% of this from cereals and 20% from water and drinks[77].

The involvement of silica in osteogenesis and connective tissue metabolism is well-established. In the early 1970s, almost simultaneously, Carlisle[82] and Schwarz[83] published similar results demonstrating the essentiality of silicon in chicks and rats respectively. In both studies, silicon deficiency produced defective collagenous connective tissue formation and defects in the growth of bone. Experiments with chicks showed that birds on a silicon-deficient diet presented small and flexible bone structures[82]. Their femora and tibiae fractured more easily under pressure than those birds on a silicon-supplemented diet (fig 1.9).

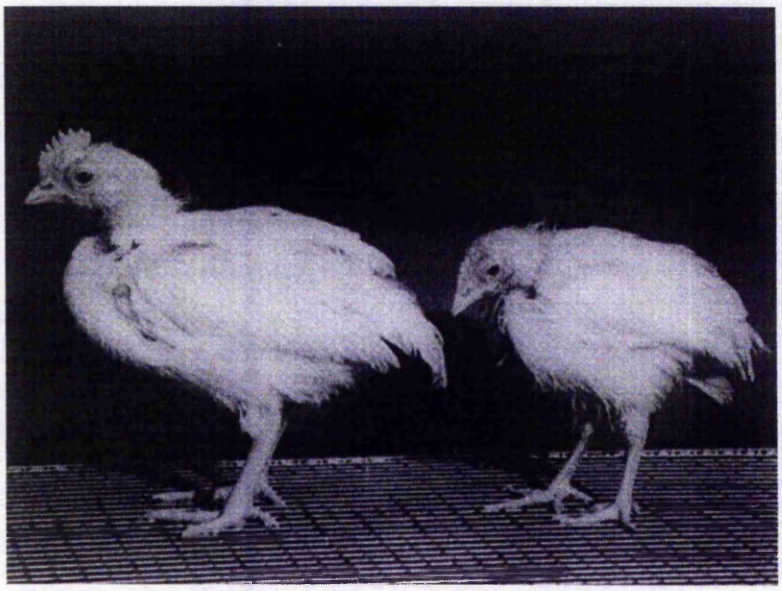

Figure 1.9 Four-week old chicks on silicon supplemented diet (left) and low-silicon basal diet (right)[82].

Rats maintained on low silicon diets showed skull and pigmentation abnormalities[83]. Later on, Carlisle showed that silicon was present in osteoblast cells and it was concentrated at the mineralisation front in growing bone[84]. The analysis of bone from animals maintained on a silicon-deficient diet presented a reduction in the proportion of collageneous organic matrix.

The effect of silicon not only appears to be on the synthesis of collagen but also on the formation of the bone mineral itself[85].

The level of silica in connective tissues (100 ppm) and in regions of active calcification is approximately 100 times higher than most other tissues (1-2 ppm)[86]. As a minor constituent of saliva[87], it has been suggested to influence the mineralisation of dental plaque and promote the formation of calculus[88]. Silicon concentration in dental plaque is enhanced in areas with hard drinking water, where silicon is present in higher concentrations than normal , or as a result of the consumption of foods with a high silicon content, such as certain cereals[89].

Studies of the effect of different silicon species on the formation of calcium phosphate have shown that silica can act as an heterogeneous nucleation substrate and that the formation of HAP nuclei is favoured over other calcium phosphate (CP) nuclei.[90]. Recent studies have shown that silica and silicate ions promote calcification[91,92]. Tanizawa *et al.*, (1995)[92], proposed that ACP is formed in an early stage followed by formation of DCPD and HAP. They reported that the transformation was enhanced by the presence of silica. The effects observed were attributed to polymeric silicon species rather than monomeric silicon species.

1.5 ALUMINIUM AND BONE MINERAL

Aluminium is the most abundant metallic element in the Earth's crust, the third most abundant element overall. It can be found in measurable quantities in food, soil, water and air[93]. Aluminium can be found as insoluble sulphates, phosphates, silicates and hydroxides as well as in solution in the bedrock and soils[94]. Until recently, the majority of aluminium was locked in the soils and minerals in these insoluble forms and significant amounts were

found in only few natural waters. However, with the advent of acid deposition, the buffering capacity of soils and natural waters is slowly decreasing and as a consequence of this, their pH falls to levels which allow for the mobilisation of aluminium from its mineral stores[95].

Despite being present at trace levels in almost all vegetation and animals, even a small increase in the concentration of aluminium can have deleterious effects. In animals, aluminium can cause growth disorders and disturbed neurological functions. It is believed that aluminium is involved in Alzheimer disease[96] and amyotrophic lateral sclerosis, a type of Parkinson's disease[97]. Aluminium is also associated with skeletal toxicities such as low bone remodelling and defective mineralisation[98] but the exact mechanism of aluminium toxic actions on bone is still under debate. It is not clear whether the aluminium-associated defect in mineralisation is due to a physicochemical impairment of hydroxyapatite formation by deposition of aluminium at the bone-osteoid interface or to an effect of aluminium on osteoblast function essential for normal mineralisation. Osteomalacia in patients on long-term hemodialysis has also been associated with aluminium accumulation in bone[99,100]. Several studies have been carried out to clarify the physicochemical effect of aluminium on the *in vitro* formation and growth of HAP[101]. Aluminium chloride has been shown to delay the formation of calcium phosphate mineral from supersaturated solution and the transformation of ACP to HAP, and to inhibit growth of poorly crystalline HAP[101]. It has also been reported that the adsorption of aluminium to HAP crystals inhibits their dissolution rate[102].

1.6 BIOMATERIALS

A large number of materials are available for osseous repair and reconstruction. However, bone-bonding is restricted to a limited number of "surface-reactive materials". These materials, named bioactive implants, create an environment compatible with bone growth and develop a layer of biologically active hydroxycarbonateapatite (HCA) on their surfaces during implantation. The HCA crystals bind to collagen fibrils and form a strong interface between the organic matrix and inorganic material. Hydroxyapatite ceramic is a material chemically similar to bone mineral and consequently is one of the few materials characterised as bioactive capable of undergoing bonding osteogenesis '*in vivo*'[103]. Hydroxyapatite coating of a metal substrate is an alternative to obtain an implant that can be used in tensile load-bearing applications[103-105]. Tricalcium phosphate, $Ca_3(PO_4)_2$, together with hydroxyapatite, is one of the most widely investigated calcium phosphate ceramics. It has been reported to possess good biocompatible properties[103].

In the last 25 years, silicate glass-ceramics containing calcium phosphate have been developed for application in prosthetic or bone implant materials. In the early 1970s, Hench and co-workers discovered and developed bioactive glasses. These glasses are registered as Bioglass® and their constituents are Na_2O-CaO-P_2O_5-SiO_2. Other researchers such as Kokubo, (1992)[107], and Li, (1994)[108] have developed glass-ceramics by modifying Bioglass®, decreasing or substituting Na_2O and adding MgO. Some bioactive glasses are osteoproductive, what means that they can bind with both bone and soft tissues due to an intracellular and an extracellular response at their interface. Bone cells (osteoblasts) in contact with the bioactive surface undergo rapid proliferation and quickly form new bone[109]. It has been proposed that the rapid bone formation is a result of soluble silica

being released from the glass which activates genes in the cell to produce growth factors[110,111].

1.7 AIMS

1. To develop methods to identify and characterise calcium phosphate materials by FT-IR, XRD, TEM and EDX analysis,

2. To study the effects of pH, T , concentration and initial precursors on the formation of calcium phosphate and establish a model system to produce these materials,

3. To study the effects of soluble silica species and aluminium (III) species on calcium phosphate nucleation and transformation,

4. To study the possible ameliorating effects of soluble silica species on the toxic effect of aluminium (III) species on calcium phosphate formation, and

5. To assess the bioactivity of a silica gel based surface.

1.8 REFERENCES

1. Walton, A.G. (1967). The Formation and Properties of Precipitates. Ed. by Interscience Publishers. New York.
2. Dunning, W.J. (1971). Ripening and Ageing Processes in Precipitates in Tooth Enamel, vol. 2. Ed. by Fearnhead & Stack. John Wright & Sons.
3. Chernov, A.A. and Khadzhi, C.E. (1968). Trapping of Colloidal Inclusions in the Growth of Quartz Crystals. *J. Cryst. Growth* **3**(4):641.
4. Buckley, H.E. (1949). Habit Modifications in Crystals as a Result of the Introduction of Impurities During Growth. *Discuss. Faraday Soc.* **5**:243.
5. Ostwald, W. (1986-1902). Lehrbuch Allgemeine Chemie, Vol. II ii, pp 444. Englemann, W. Leipzig.
6. Mehl, R.F. (1943). Decomposition of Austenite by Nucleation and Growth Processes. *J. Iron Steel Inst.* **159**:113.

7. Hedges, J.M. and Mitchell, J.W. (1953). Polyhedral Substructures in Crystals of AgBr. *Phil. Mag.* **44**(223):357.
8. Garner, W.E. (1955). In Chemistry of the Solid State. Ed. Garner, W.E. Chapter 8. Butterworths, London.
9. Dunning, W.J. (1969). Materials Science Research, Vol IV. Eds. Gray, T.J. and Frechette, V., pp. 112. Plenum Press, New York.
10. Hofer, E. (1939). Relation Between the Solubility of Crystals and their Size in Precipitation from a Solution. *Z. Physik. Chem.* **183A**:455.
11. Egli, P.H. and Zerfoss S. (1949). General Principles of Crystal Growth. *Discuss. Faraday Soc.* **5**:64.
12. Gordon, L., Salutsky, J.L. and Willard, H.H. (1959). Precipitation from Homogeneous Solutions. Wiley, New York.
13. von Weimarn, P.P., (1925). The Precipitation Laws. *Chem. Rev.* **2**:217.
14. Suito, E. and Takiyama, K. (1954). Formation and Aging of Precipitates. I Electron Microscopic Investigations of the Formation of Barium Sulfate Precipitates. *Bull. Chem. Soc. Japan* **27**:121.
15. Black, J.J., Insley, M.J. and Parfitt, G.D. (1964). Precipitation of AgCl from Homogeneous Solution. *J. Phot. Sci.* **12**:86.
16. Kern, R. (1953). Effect of Supersaturation of the Mother Liquor on Crystal Habit. *Compt. Rend.* **236**:830.
17. Kern, R. and Tillman, M. (1953). Influence of Degree of Supersaturation and of Impurities on Crystal Habit. *Compt. Rend.* **236**:942.
18. Kolthoff, I.M. and van't Riet, B. (1959). Formation and Aging of Precipitates. Precipitation of $PbSO_4$. *J. Phys. Chem.* **63**:817.
19. Lewin, S.Z. (1955). The Crystal Growth of Lead Chloride from Aqueous Solution. *J. Phys. Chem.* **59**:1030.
20. Raynaud, J.H. and Pouradier, J. (1955). Precipitation of mixtures of AgI and AgBr. *J. Chim. Phys.* **52**:133.
21. Kuznetsov, V.D. (1953). Crystals and Crystallisation. Gostekhizdat, Moscow.
22. Eckert, T.S. and France, W.G. (1927). Adsorption at Crystal Faces I. The Growth and Solution of Single Cooper Sulfate Crystals in the Presence of Gelatin and Dyes. *J. Am. Ceram. Soc.* **10**:579.

23. Keenan, F.G. and France, W.G. (1927). Adsorption at Crystal Solutions Interfaces (II). Individual Macroscopic K Alum Crystals Grown in the Presence of Gelatin and Dyes. *J. Am. Ceram. Soc.* **10**:821.

24. Weiner, S. (1985). Organization of Extracellularly Mineralised Tissues: A Comparative Study of Biological Crystal Growth. *CRC Critical Rev. Biochem.* **20**(4):365.

25. Simkiss, K. (1975). Bone and Biomineralisation. Studies in Biology, 53. Edited by Arnorld, E. London.

26. Weiner, S. and Wagner, H.D. (1998). The Material Bone: Structure-Mechanical Function Relations. *Annu. Rev. Mater. Sci.* **28**:271.

27. Alcok, N.W. (1972). Calcification of Cartilage. *Clin. Orthop.* **86**:287.

28. Anderson, H.C. (1980). Calcification Processes. *Path. Ann.* **15**:45.

29. Bachra, B.N. (1970). Calcification of Connective Tissue. *Int. Rev. Conn. Tiss. Res.* **5**:165.

30. Becker, G.L. (1977). Calcification Mechanisms: Roles for Cells and Mineral. *J. Oral Pathol.* **6**:307.

31. Bernard, G.W. (1972). Ultrastructural Observations of Initial Calcification in Dentine and Enamel. *J. Ultrastruct. Res.* **41**:1.

32. Fleisch, H. and Neuman, W.F. (1961). Mechanism of Calcification: Role of Collagen, Polyphosphate, and Phosphatase. *Am. J. Physiol.* **200**:1296.

33. Glimcher, M.J. (1976). Composition, Structure and Organisation of Bone and other Mineralised Tissues and the Mechanism of Calcification. In Handbook of Physiology-Endocrinology VII, pp. 25. Williams and Wilkins, Co., Baltimore.

34. Irving, J.T. (1973). Theories of Mineralisation of Bone. *Clin. Orthop.* **97**:225.

35. Krampitz, G., and Witt, W. (1979). Biochemical Aspects of Biomineralisation. *Topics Curr. Chem.* **78**:57.

36. Nancollas, G.H. (1977). The Mechanism of Biological Mineralization. *J. Crystal Growth* **42**:185.

37. Posner, A.S. (1969). Crystal Chemistry of Bone. *Physiol. Rev.* **40**:760.

38. Boskey, A.L. (1981). Current Concepts of Physiology and Biochemistry of Calcification. *Clin. Res. and Rel. Res.* **157**:225.

39. LeGeros, R.Z. (1977). Apatites from Aqueous and Non-aqueous Systems: Relation to Biological Apatites. First Int'l. Congress on Phosphorous Compounds, Rabat, IMPHOS, **199**:347.

40. LeGeros, R.Z., LeGeros, J.P., and Sherra, W.P. (1971). Conversion of Monetite, $CaHPO_4$ to Apatites: Effect of Carbonate on the Crystallinity and the Morphology of the Apatite Crystallites. *Adv. X-Ray Anal.* **14**:57.

41. Blumenthal, N.C., Betts, F., and Posner, A.S. (1977). Stabilisation of Amorphous Calcium Phosphate by Mg and ATP. *Calcif. Tiss. Res.* **23**:245.

42. Boskey, A.L. and Posner, A.S. (1974). Magnesium Stabilisation of Amorphous Calcium Phosphate: A Kinetic Study. *Mat. Res. Bull.* **9**:907.

43. Nancollas, G.H., Amjad, Z. and Koutsoukos, P. (1979). Calcium Phosphates-Speciation, Solubility and Kinetic Considerations. ACS Symp. 93, Chemical Modeling in Aqueous Systems pp. 475.

44. Peck, W.A. and Klahr, S. (1979). Cyclic Nucleotides in Bone and Mineral Metabolism. *Adv. Cyclic Nucleotide Res.* **11**:90.

45. Raisz, L.G., Maina, D.M., Gworek, S.C., Dietrich, J.W. and Canalis, E.M. (1978). Hormonal Control of Bone Collagen Synthesis *in vitro*: Inhibitory Effect of 1-hydroxylated Vitamin D Metabolites. *Endocrinology* **102**:731.

46. Hay, D.J. and Moreno, E.C. (1979). Differential Adsorption and Chemical Affinities of Proteins for Apatitic Surfaces. *J. Dent. Res.* **58B**:930.

47. Rath, N.C. and Reddi, A.H. (1979). Collagenous Bone Matrix is a Local Mitogen. *Nature* **278**:855.

48. Reddi, A.H., and Anderson, W.A. (1976). Collagenous Bone Matrix-Induced Endochondral Ossification and Hemopoiesis. *J. Cell Biol.* **69**:557.

49. Urist, M.R. and Mikulski, A.J. (1979). A Soluble Bone Morphogenetic Protein Extracted from Bone Matrix with a Mixed Aqueous and Non-aqueous Solvent. *Proc. Soc. Exp. Biol. Med.* **162**:48.

50. Neuman, W.F. and Neuman, M. (1953). The Nature of the Mineral Phase of Bone. *Chem. Rev.* **53**:1.

51. Glimcher, M., Hodge, A.J., Schimtt, F.O. (1957). Macromolecular Aggregation States in Relation to Mineralisation: The Collagen Hydroxyapatite System as Studied *in vitro*. *Proc. Natl. Acad. Sci. USA* **43**:860.

52. Dudley, H.R., and Spiro, D. (1961). The Fine Structure of Bone Cells. *J. Biophys. Biochem. Cytol.* **11**:627.

53. Brown, W.E. (1966). Crystal Growth of Bone Mineral. *Clin. Orthop. Rel. Res.* **44**:205.

54. Robinson, R. (1923). The Possible Significance of Hexose Phosphoric Esters in Ossification. *Biochem. J.* **17**:286.

55. Fell, H.B. and Robinson, R. (1929). The Growth, Development and Phosphatase Activity of Embryonic Avian Femora and Limb-buds Cultivated *in vitro*. *Biochem. J.* **23**:767.

56. Irving, J.T. and Wutier, R.E. (1968). Histochemistry and Biochemistry of Calcification with Special Reference to the Role of Lipids. *Clin. Orthop. Rel. Res.* **56**:237.

57. Weinstock, M. and Leblond, G.P. (1973). Radioautographic Visualisation of the Deposition of a Phosphoprotein at the Mineralisation Front in Dentin of the Rat Incisor. *J. Cell Biol.* **56**:838.

58. Matukas, V.J., Panner, B.J., and Orbinson, J.L. (1967). Studies on Ultrastructural Identification and Distribution of Protein-Polysaccharide in Cartilage Matrix. *J. Cell Biol.* **32**:365.

59. Jibril, A.O. (1967). Proteolytic Degradation of Ossifying Cartilage Matrix and the Removal of Acid Mucopolysaccharide prior to Bone Formation. *Biochim. Biophys. Acta* **136**:162.

60. Hirschmann, A, and Dziewaitkowski, D.D. (1966). Protein-polysaccharide loss during Endochondral Ossification. Immunochemical Evidence. *Science* **154**:393.

61. Matukas, V.J., and Krikos, G.A. (1968). Evidence for Changes in Proteinpolysaccharides Associated with the Onset of Calcification in Cartilage. *J. Cell Biol.* **39**:43.

62. Termine, J.D. (1972). Mineral Chemistry and Skeletal Biology. *Clin. Orthop.* **85**:207.

63. Termine, J.D. and Posner, A.S. (1966). Infrared Analysis of Rat Bone; Age Dependency of Amorphous and Crystalline Fractions. *Science* **153**:1523.

64. Neuman, W.F. and Bareham, B.J. (1975). Evidence for the presence of Secondary Calcium Phosphate in Bone and its Stabilisation by Acid Production. *Calcif. Tiss. Res.* **18**:161.

65. Roufosse, A.H., Landis, W.J., Sabine, W.K. and Glimcher, M.J. (1979). Identification of Brushite in Newly Deposited Bone Mineral from Embryonic Chicks. *J. Ultrastr. Res.* **68**:235.

66. Brown, W.E., and Chow, L.C. (1976). Chemical Properties of Bone Mineral. *Ann. Rev. Mater. Sci.* **6**:213.

67. Glick, P.L. (1980). Ultrastructural Aspects of Dentin Mineralisation. *Trans. 26. Orthop. Res. Soc.* **5**:26.

68. Francis, M.D. and Webb, N.C. (1971). Hydroxyapatite Formation from a Hydrated Calcium Monohydrated Phosphate Precursor. *Calcif. Tiss. Res.* **6**:335.

69. Pita, J.C. and Howell, D.S. (1978). Microbiochemical Studies of Cartilage. In The Joints and Synovial Fluid, Vol 10, pp274, Academic Press, New York.

70. Kanazawa, T. (1989). 'Materials Science Monographs, 52: Inorganic Phosphate Materials'. Elsevier.

71. DeJong, W.F. (1926). La Substance minerale dans les os. *Rec. Trav. Chim.* **45**:445.

72. Van Rees, H.B., Mengeot, M. and Kostiner, E. (1973). Monoclinic-Hexagonal Transition in Hydroxyapatite and DeuteroHydroxyapatite Single Crystals. *Mat. Res. Bull.* **8**:1307.

73. Hitmi, N., LaCabanne, C. and Young, R.A. (1986).)H-Dipole Reorientability in Hydroxyapatites. Effect of Tunnel Size. *J. Phys. Chem. Solids* **47**:533.

74. Beevers, C.V. and Raistrick, B. (1954). Properties of the Ca Phosphates. *Nature* **173**:542.

75. Jones, D.W. and Smith, J.A.S. (1962). Structure of Brushite, $CaHPO_4 \cdot H_2O$. *J. Chem. Soc.* 1414.

76. Berry, E.E. and Baddiel, C.B. (1967). The Infra-red Spectrum of Dicalcium Phosphate Dihydrated (brushite). *Spectrochim. Acta.* **23A**:2089.

77. Birchall, J.D. (1995). The Essentiality of Silicon in Biology. *Chem. Soc. Rev.*, **24**(5):351.

78. Harrison, C.C. (1996). Silified Diatoms, Sponges and Plants; Experts in Amorphous Structure Regulation. *Abs. Papers Am. Chem. Soc.*, **212**(1):155.

79. Harrison, C.C. (1996). Evidence for Intramineral Macromolecules Containing Protein from Plant Silicas. *Phytochem.*, **41**(1):37.

80. Perry, C.C. (1989). 'Chemical Studies of Biogenic Silica'. In Biomineralisation. Chemical and Biochemical Perspectives, Chapter 8, pp223-256. Edited by Mann, S., Webb, J. and Williams, R.J.P.VCH Publishers. Germany.

81. Perry, C.C., Fraser, M.A. and Hughes, N.P. (1991). Macromolecular Assemblages in Controlled Biomineralisation. *ACS Symposium Series*, **444**:316.

82. Carlisle, E.M. (1972). Silicon: An essential Element for the Chick. *Science*, **178**:619.

83. Schwarz, K. (1972).Growth-promoting Effects of Silicon in Rats. *Nature*, **239**:333.

84. Carlisle, E.M. (1986). Silicon as an Essential Trace Element in Animal Nutrition. In Silicon Biochemistry. Ciba Foundation Symposium 121, pp.123. Wiley, Chichester.

85. Damen, J.J.M. and ten Cate, J.M. (1989). Calcium Phosphate Precipitation is Promoted by Silicon. In Recent Advances in the Study of Dental Calculus. Edited by Ten Cate and Damen. OUP, Oxford.

86. Iler, R.K. (1970). The Chemistry of Silica. John Wiley&Sons. Wiley-Intersicence. New York.

87. Swift, P (1967). A Method for the Trace Elemental Analysis of Dental Tissues. *Br. Dent. J.* **123**:326.

88. Rølla, G. Gaare, D., Langmyhr, F.J. and Helgeland, K. (1989). Silicon in Calculus and its Potential Role in Calculus Formation. In Recent Advances in the Study of Dental Calculus, pp97. Edited by Ten Cate and Damen. OUP, Oxford.

89. Sangster, A.G. and Hodson, M.J. (1986). Silica in Higher Plants: In Silicon Biochemistry, Ciba Foundation Symposium 121, pp.90. Wiley, Chichester.

90. Hidaka S., Okamoto, Y. and Abe, K. (1993). Possible Regulatory Roles of Silicic Acid, Silica, and Clay Minerals in the Formation of Calcium Phosphate Precipitates. *Archs. Oral. Biol.* **38**:405.

91. Damen, J.J.M. and Ten Cate, J.M. (1989). The Effect of Silicic Acid on Calcium Phosphate Precipitation. *J. Dent. Res.*, **68**(9):1355.

92. Tanizawa, Y. and Suzuki, T. (1995). Effects of Silicate Ions on the Formation and Transformation of Calcium Phosphates in Neutral Aqueous-Solutions. *J. Chem. Soc.:Faraday Trans.*, **94**(19):3499.

93. Epstein, S.G. (1988). In Geochemistry and Health, pp. 189. Edited by Thornton, I., Science Reviews Ltd., Northwood.

94. Kennedy, I.R. (1992). Acid Soil and Acid Rain. Wiley, New York.

95. Boyle, R.H. and Boyle, R.A. (1983). Acid Rain. Schocken Books, New York.

96. Perl, D.P. and Brody, A.R. (1980). Alzheimer's Disease: X-Ray Spectrometric Evidence of Aluminium Accumulation in Neurofibrillary Tangle-Bearing Neurons. *Science* **208**:297.

97. Martin, R.B. (1988). Aluminium and its Role in Biology. In Metals Ions in Biological Systems, pp. 1. Edited by Sigel, H. and Sigel, A., Marcel Decker, New York.

98. Quarles, L.D. (1991). Paradoxical Toxic and Trophic Osseous Actions of Aluminium: Potential Explanations. *Miner. Electrolyte Metab.* **17**:233.

99. Perides, A.M., Edwards, W.G., Jr., Cullu, U.S., Jr., McCall, J.T., Ellis, H.A. (1980). Hemodialysis Encephalopathy with Osteomalacic Fractures and Muscles Weakness. *Kidney Int.* **18**:115.

100. Walker, G.S., Aaron, J.E., Peacock, M., Robinson, P.J.A., Davison, A.M. (1982). Dialysate Aluminum Concentration and Renal Bone Disease. *Kidney Int.* **21**:411.

101. Posner, A.S., Blumenthal, N.C., Boskey, A.L. (1986). Model of Aluminum-induced Osteomalacia: Inhibition of Apatite Formation and Growth. *Kidney Int.* **18**:S17.

102. Christoffersen, M.R. and Christoffersen, J. (1985). The Effect of Aluminium on the Rate of Dissolution of Calcium Hydroxyapatite —A Contribution to the Understanding of Aluminium-Induced Bone Diseases. *Calcif. Tiss. Int.* **37**:673.

103. De Bruijn-JD (1993). 'Calcium Phosphate Biomaterials: Bone-bonding and Biodegradation Properties'. Edited by Offsetdrukkerij Haveka B.V., Alblasserdam.

104. Chen-J, Wolke-JGC, and de Groot-K (1994). Microstructure and Crystallinity in Hydroxyapatite Coatings. *Biomaterials,* **15**(5):396.

105. Thomas, I.M. (1994). *Sol-Gel Optics: Processing and Applications*, pp. 141. Edited by Klein, L.C.

106. Hench, L.L., Splinter, R.J.M., Allen, W.C., Greenlee, T.K. (1971). Bonding Mechanisms at the Interface of Ceramic Prosthetic Materials. *J. Biomed. Mater. Res. Biomed. Mater. Symp.* **2**:117.

107. Kokubo, T. (1992). 'Bioactivity of Glasses and Glass-Ceramics'. Bone-Bonding. Reed Healthcare Communications, pp 31-46. Ducheyne, Kokubo & Van Blitterswijk eds.

108. Li, P., and De-Groot, K. (1994). Better Bioactive Ceramics Through Sol-Gel Process. *J. Sol-Gel Sci. Technol.*, **2**:797.

109. Hench, L.L. (1995). Bioactive Implants. *Chemistry & Industry,* **14**:547.

110. Vrouwenvelder, W.C.A., Groot, C.G., & de Groot, K. (1993). Histological and Biochemical Evaluation of Osteoblast Cultures on Bioactive Glass, Hydroxyapatite, Titanium-Alloy, and Stainless-Steel. *J. Biomed. Mater. Res.*, **27**:465.

111. Keeting, P.E., Oursler, M.J, Wiegand, K.E., Bonde, S.K., (1992). Zeolite-A Increases Proliferation, Differentiation, and Transforming Growth-Factor-Beta Production in Normal Adult Human Osteoblast-like Cells *in* vitro. J. *Bone Miner. Res.*, **7**(11):1281.

CHAPTER 2: EXPERIMENTAL METHODS

2.1 Transmission Electron Microscopy (TEM)[1-5]

The TEM probes the internal structure of solids and allows access to microstructural or ultrastructural detail that may not be visible by the human eye.

The principles of light microscopy also follow for electron microscopy. Three important attributes of microscopes should be considered: resolution, contrast and magnification. Features in a magnified image subtend an enlarged viewing angle at the eye, and are thus more easily detected than in the object itself. The magnifying system must be capable of: 1) carrying sufficiently fine detail (the system's resolving power), and 2) providing adequate contrast between features in the image.

Optics can be approached from two viewpoints. In geometrical optics, we assume that the imaging radiation travels in straight lines except when it is refracted by the lenses; this enables us to explain magnification and some aspects of contrast, but gives no information on why resolution might be limited. Wave optics, on the other hand, involves consideration of the wave nature of the radiation, of diffraction and interference, and clearly demonstrates the limits to resolution and explains some other mechanisms of contrast enhancement.

In terms of geometrical optics, the lenses of microscopes can be compared to three familiar instruments: a camera, a projector and a magnifying glass (which is itself a simple microscope).

The condenser acting like a camera lens throws an image of a light-source on to the specimen. The objective, like lens of a projector, forms a magnified image (the primary image) of an object placed just in front of its first focal plane. In a light microscope, the

eyepiece acts as a magnifying glass providing further magnification of the central portion of the primary image. In a transmission electron microscope subsequent 'projector-type' lenses form further images, the final one of these on the screen or film.

Magnification is arguably the least important of the three attributes of the microscope, and certainly the easiest to achieve; any microscope can be arranged to produce images of any magnification by simple manipulation of lenses and distances. Magnification is useful up to the point where it is just sufficient to enable the eye to resolve the finest detail of interest; any more is empty magnification.

The resolving power of the light microscope has been close to its theoretical limit for the past 100 years, and the optical systems of light microscopes are technologically almost perfect. As an example, an electron microscope image of a specimen may contain useful information down to about 3nm. A total magnification of 100,000 will enlarge 3nm detail up to 300 μm and make it comfortably visible. However, since photographic film can be enlarged at least fivefold without significant loss of quality, this magnification of 100,000 might be made up from a magnification of 20,000 in the microscope and 5 in the enlarger. Increasing magnification reduces the area of the specimen observed. Doubling the magnification reduces the area observed by a factor of 4. A tenfold increase in magnification reduces the area of view to one-hundredth. The electrons which illuminate the viewing screen or film to an appropriate brightness all must pass through the tiny area of specimen being observed; hence, other things being equal, for constant screen brightness we must subject the specimen to irradiation by electrons increasing with the square of the magnification. Furthermore, an area of $1mm^2$, at a magnification of 10,000, will require about 10,000 micrographs for complete coverage. Using the lowest adequate magnification

will thus provide maximum information about the specimen, minimum specimen damage by irradiation, and lowest costs for photography.

The contrast of the image is produced by the absorption of the incident electron beam by the specimen. The amount of contrast is dependent on the atomic number of the material. In order to create contrast in the image, the scattered electrons must be separated from the unscattered electrons using the objective lens aperture. If there were no objective aperture most of the electrons would recombine with the unscatterred electrons and form a featureless image. When the objective aperture is introduced parts of the image with high mass and/or density will appear darker.

Fine detail can be enhanced by phase contrast on each side of focus. The objective aperture must be sufficiently large to allow the diffracted beam and the undeviated beam to interfere. At high magnifications it can be an advantage to enhance certain regular spacings (e.g. lattice fringes) defocusing the image. Defocusing will enhances certain spacings but it will also reduce the visibility of others for the same defocus. Although it is possible to calculate the amount of defocus required, in practice it is easier to take a through-focal series of micrographs and select the underfocused image which improves the fine level of detail of the desired feature.

2.1.1 Electron diffraction[6,7]

Diffraction describes the interaction of waves with an object, and the relative sizes of wave and object determine the importance of the effect. Diffraction in effect 'encodes' information about the object in the radiation.

Electron diffraction patterns produced in the electron microscope can be of three different types:

a) Ring pattern (polycrystalline specimen).

b) Spot pattern (single crystal region of the specimen).

c) Kikuchi line pattern (single crystal region of the specimen).

Ring and spot patterns were the common patterns obtained in the characterisation of the materials presented in this thesis.

The major use of ring patterns is in the identification of phases using extraction replicas. These diffraction patterns also arise from very fine grain size polycrystalline material. For a given beam direction a number of precipitate particles within the area illuminated by the beam will be oriented to satisfy the Bragg law for all allowed reflecting planes. However, one individual precipitate will produce a specific beam reflected from a particular (hkl) plane, such that the angle between it and the incident beam is 2θ, satisfying the Bragg law. For randomly oriented particles and a specific reflecting plane (hkl) these beams will lie in a cone with apex angle $4\theta_{(hkl)}$ centered on the incident beam direction to produce a ring in the diffraction pattern. Since a number of {hkl} planes will reflect depending on the structure factor a series of concentric rings will be produced to a particular set of (hkl) reflections, as indexed.

Using a spot pattern it is possible to determine the sample orientation in the microscope; the crystal can be quickly surveyed and the accessibility of certain orientations and hence diffracting vectors determined. Details of the fine structure of the pattern can be used to obtain information on the defect structure of the specimen.

2.1.2 Energy Dispersive X-ray Analysis (EDAX)[8,9]

When a high speed incident electron strikes a specimen it may generate an X-ray, the energy or wavelength of which is detected and counted by a suitable detector. A

bombarding electron with sufficient energy may completely displace an inner shell electron from a specimen atom. An unstable ion is produced and an outer electron drops into the inner shell vacancy. This transition results in the emission of a characteristic X-ray. Hence chemical information concerning the specimen is obtained. X-rays are detected by a lithium drifted silicon detector attached to the microscope column. The X-rays pass through the window of the detector and create electron hole pairs in the lithium drifted silicon crystal. A charge pulse is created, which is proportional to the energy of the X-ray. This is then amplified and passes to a multichannel analyser where the signals are sorted according to their energy. This energy is characteristic for each element. By measuring the different energies, the elements present in the specimen are determined.

The detection and counting of X-rays may be performed using an energy dispersive spectrometer (EDS) detection system. The production of an X-ray spectrum in this way is often referred to as the energy dispersive analysis of X-rays (EDAX).

TEM analyses were performed using a JEOL 2010 TEM with a LaB_6 electron gun filament operating at 200 KeV. Energy Dispersive X-ray Analysis was performed using the attached PentafetST X-ray detector and TEMQUANT function within the Link-Isis software from Oxford Instruments.

The TEM was calibrated to check the camera length using an aluminium standard. As the d-spacings are already known, diffraction patterns are obtained at the camera length to be used with the samples and a back calculation performed to obtain the exact length.

2.1.3 Specimen Preparation

Specimens for transmission electron microscopy study were prepared by placing drops of the suspension directly on holey-carbon formvar-coated copper grids at specific time points in the reaction, e.g. 1, 5, 15, and 30 min of reaction. Excess water was removed by blotting with filter paper. For analysis of the dried final precipitate, powder samples were suspended in acetone and then dropped onto holey carbon coated copper grids which were allowed to dry in air.

2.2 Scanning Electron Microscope (SEM)[10,11]

The scanning electron microscope is used to study the surface or near surface structure of specimens. The SEM has a similar setup to that of the TEM as it requires the use of an electron gun, electromagnetic lenses and apertures to image the specimen. However the placement of the beam deflector or scanning coils, below the objective lens is where the two instruments differ.

SEM analysis were performed using a Cambridge Stereoscan 600 SEM operating at 25KV.

2.2.1 Specimen Preparation

The powdered sample was dispersed on double-sided sticky tape that had been mounted on aluminium SEM stubs. In order to obtain a sharp image the samples were rendered electrically conducting by coating with a thin layer of gold.

2.3 Fourier Transform-InfraRed Spectroscopy (FT-IR)[12-18.]

From the infrared spectrum it also is possible to obtain structural information. Molecules are excited to a higher energy when they absorb infrared radiation. A molecule

absorbs the frequencies of infrared radiation which match the natural vibration frequencies of the molecule. They correspond to the range encompassing the stretching and bending vibrational frequencies of the bonds in a covalent molecule. The energy absorbed serves to increase the amplitude of the vibrational motions of the bonds in the molecule. Only those bonds with a dipole moment can absorb infrared radiation. They must have an electrical dipole which changes at the same frequency as the incoming radiation in order for the energy to be transferred. The absorptions of each type of bond are found in specific parts of the infrared region.

The infrared spectrum can also be used as a fingerprint. Since every type of bond has a different natural frequency of vibration, and since bonds of the same type of different compounds are in slightly different environments, molecules with different structures would not have the same infrared spectrum. By comparing the infrared spectra of substances thought to be identical you can establish whether they are identical or not.

The FT-IR spectrometer operates on a different principle from the dispersive spectrometer. The design of the optical pathway produces a pattern called an interferogram which contains all the frequencies which make up the infrared spectrum (a plot of intensity versus time). By the mathematical operation (Fourier-transform) the individual absorption frequencies are separated from the interferogram and a spectrum identical to that obtained with a dispersive spectrometer is produced. The FT-IR spectrometer can acquire the interferogram of a sample in less than a second. It is possible to collect dozens of interferograms of the same sample and accumulate them. The spectrum obtained from the sum of the accumulated interferograms has a better signal-to-noise ratio. The FT-IR spectrometer is faster and more sensitive than the dispersive spectrometer.

A computer-interfaced FT-IR operates in a single-beam mode. The computer software automatically substracts the spectrum of the background, which is previously collected, from the sample spectrum. The spectrum obtained is identical to that obtained from a traditional double-beam dispersive spectrometer.

To determine the infrared spectrum of a compound, it must be place in a sample holder which must be constructed of ionic substances, typically NaCl or KBr.
The main disadvantage of KBr is that it absorbs water which may interfere with the spectrum that is obtained. If a good disk is prepared, the spectrum will not have interfering bands since KBr is transparent down to 400 cm^{-1}.

FT-IR was performed using a Nicolet Magna-IR^{TM} Spectrometer 750 with a DTGS (KBr) detector and a KBr beam splitter. Resolution was set at 4 cm^{-1} and 64 scans collected.

2.3.1 Specimen preparation

For FT-IR Spectroscopy analysis, the powder samples were analysed as potassium bromide (KBr) discs. Approximately 0.5 mg of sample was ground with 100 mg of KBr in an agate mortar and compressed into a thin, homogeneous disc using an hydraulic press at 10K tons.

2.4 X-Ray Diffraction (XRD)[19-24]

X-ray diffraction analysis is a non-destructive technique and requires only a small amount of sample. The method determines the actual compound or compounds present in the sample, and is able to distinguish different crystalline forms of the same compound. As with other types of electromagnetic radiation, interaction between the electric vector of X-ray radiation and the electrons of the matter through which it passes results in scattering.

When X-rays are scattered by the ordered environment in a crystal, both constructive and destructive interference occurs among the scattered rays because the distance between the scattering centers is of the same order of magnitude as the wavelength of the radiation, and this results in diffraction.

The powder X-ray diffraction method is useful in qualitative phase analysis because every crystalline material has its own characteristic powder pattern. The powder patterns have two characteristic features:

a) the *d*-spacings of the lines

b) the intensities of the lines (I/I_1)

Materials are identified from these values in conjunction with the JCPDS (Joint Committee on Powder Diffraction Standards) Powder Diffraction File. This contains sets of cards containing X-ray data for known crystalline phases.

X-ray diffraction was performed on samples using a Hiltonbrooks modified Philips PW1050 Powder Diffractometer with CuKα radiation at Kα=1.540562Å. The samples were scanned over the range 10-40° of 2θ, at 0.02° of 2θ step size.

2.4.1 Specimen preparation

For x-ray diffraction analysis, powdered samples were packed into the hollow of a cavity in a glass sample holder and smoothed off by sliding a flat glass slide over the surface.

2.5 Preparation of calcium phosphate materials[25, 26]

Synthesis of apatites can be brought about by wet, dry and hydrothermal methods.

1. Dry chemical methods by solid-state reactions. An heterogeneous mixture of appropriate solid ingredients when heated to an optimum temperature can lead to the formation of a desired lattice through solid state diffusion of the constituent ions. They have the advantage of providing stoichoimetric HAP powders. The synthesis is usually carried out at high temperatures (1200-1400 °C).

2. Wet chemical methods use either precipitation from mixed aqueous solutions or the hydrolysis of calcium phosphates. They are the most suited for preparation of appreciable quantities of apatites. HAP powders produced by wet chemical methods generally possess high surface areas and fine particle size. Non-stoichiometry (Ca-deficiency; Ca/P < 1.67) and low crystallinity are also characteristics of HAP obtained by precipitation synthesis. These are mainly due to the fact that a gel of amorphous calcium phosphate (ACP) with low Ca/P ratio (~ 1.5) precipitates initially and much water is incorporated in ACP. Crystallinity and Ca/P ratio depend on various factors such as pH, aging time and temperature and the type and concentration of starting materials.

3. Hydrothermal methods as the name implies, deal with the application of high temperatures to aqueous solutions to facilitate the precipitation of crystals of dimensions larger than those attainable using ordinary wet methods. Because the aqueous precipitating medium at atmospheric pressure has its boiling point as the upper limiting temperature, heating under high pressure enables this limit to be exceeded. The principal advantage of such methods has been to enhance considerably the crystallinity and purity of the product.

The method used in this study was a wet method. It was based on precipitation from aqueous solutions. It was a modification of the method suggested by Hayek and Stadlman, (1955)[27]. Figure 2.1 shows a schematic representation of the method.

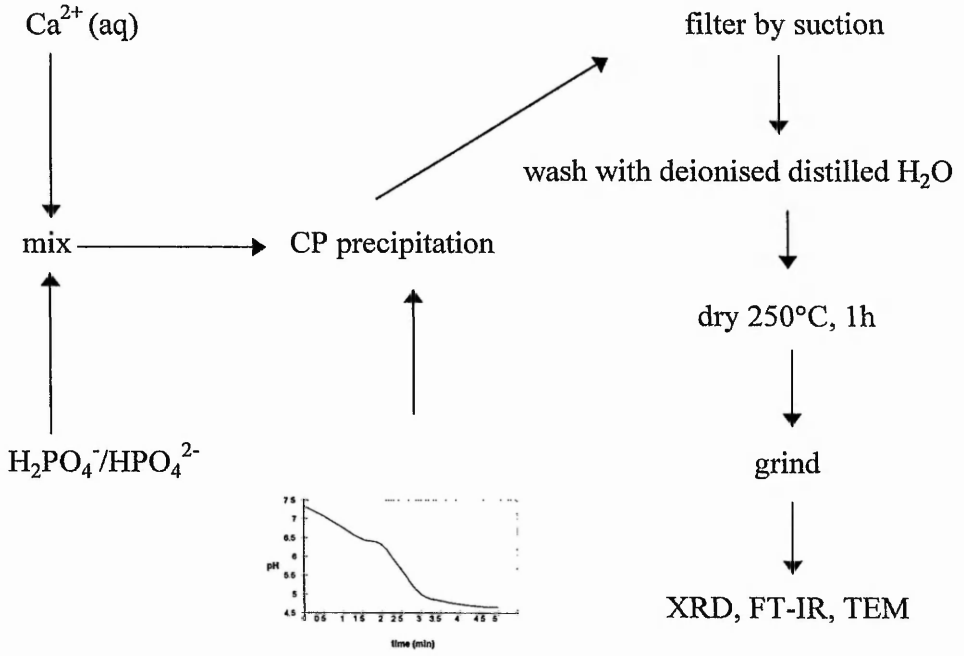

Figure 2.1 Schematic representation of the method used to precipitate calcium phosphates

The calcium solution (pH 5.1) was added to the phosphate solution, the pH of which had previously been adjusted to 7.4 by the addition of an acid or base. The precipitation reaction was carried out at 23°C (RT) and 37°C (in a thermostatically controlled water bath). The reaction was constantly stirred using a magnetic stirrer. The effect of different parameters such as T, pH, precursors, initial precursor concentrations, and the presence of other ions in the reactive solutions were assessed.

The precipitate was dried at different temperatures to assess changes in crystal phases and crystalline sizes. Table 2.1 shows the crystallites sizes for the reflections corresponding to the Miller Indexes (0 0 2) and (2 1 2) for the precipitate formed at 37°C (see chapter 3).

T (°C)	(0 0 2)	(2 1 1)
40	171	43
110	156	45
250	166	44

Table 2.1 Crystallites sizes (Å) for the precipitate formed at 37°C. The Miller Indexes correspond to HAP (JCPDS 9-432), ($p<0.05$ compared to control).

No changes were observed up to a temperature of 250°C which was the temperature chosen to dry the precipitate to eliminate any volatile nitrate salts formed during the precipitation[26].

2.6 Preparation of silica thin films[28]

13 mm round Thermanox® Coverslips were coated with silica sol-gel by the spin coating method which is a fast and convenient method for preparing sol-gel coatings.

Figure 2.2 illustrates a Basic Spin Coating system. The coverslip to be coated was attached to a motor-driven turntable and the coating solution is applied from the top to the center of the coverslip.

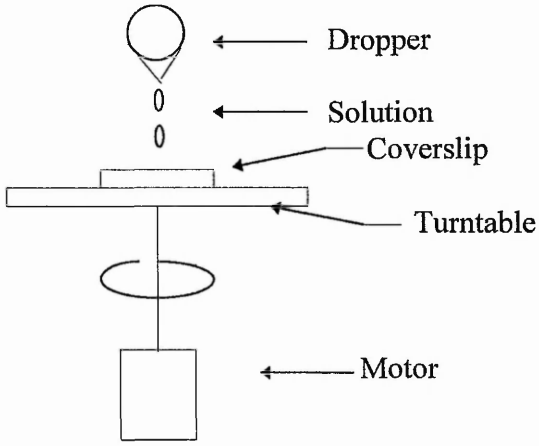

Fig 2.2 Schematic Diagram of a Basic Spin Coater (Thomas, 1994)[28].

An excess of sol-gel solution was applied from the dropper to the coverslip while the latter is rotating. The solution deposited on the center of the coverslip moves radially outwards driven by centrifugal force. On reaching the edge of the coverslip excess solution is thrown off in droplets. The solution film solidifies by solvent evaporation or by gelation and a thin coating was obtained which covers the surface of the substrate.

2.6.1 Preparation of silica sol-gel[29]

10 ml of TEOS was mixed with 10.23 ml of dry ethanol in a beaker. After stirring for 10-15 seconds, 3.165 ml of 0.2 M HCl was added (1TEOS:4EtOH:4H_2O:0.045HCl). The beaker was covered and the solution was stirred for 1h. The sol-gel solution was used to prepare the silica thin films onto the coverslips. The thin films were assessed for bioactivity.

The coverslips were also sent to Queen Medical Center at the University of Nottingham for biological studies.

2.7 Identification of Calcium Phosphate Phases

Different phases of calcium phosphate form during precipitation depending on the experimental conditions. To identify the phases present by FT-IR analysis, combinations of commercial dicalcium phosphate (DCP) and hydroxpapatite (HAP) were used at ratios of 100%, 75/25%, 50/50%, 25/75% and 0% (w/w) of DCP/HAP. To identify the phases formed by XRD analysis, combinations of commercial dicalcium phosphate (DCP) and hydroxyapatite (HAP) in the ratio DCP:HAP; 100%, 80/20%, 60/40%, 40%60, 20/80% and 0% in weight were used with corundum as an internal standard reference material. Figure 2.3e shows the spectrum obtained from commercial HAP with significant bands at 1094 cm^{-1}, 1035 cm^{-1}, 961 cm^{-1}, 634 cm^{-1} , 601 cm^{-1} and 564 cm^{-1}. When HAP is diluted with DCP there is no major change in the spectrum until 75% DCP by weight is present in the sample, Figure 2.3b, where there is a broadening of the top of the band at 1035 cm^{-1}, a loss of a recognisable band at 601 cm^{-1} and an increase in intensity of the band at ca. 905 cm^{-1}.

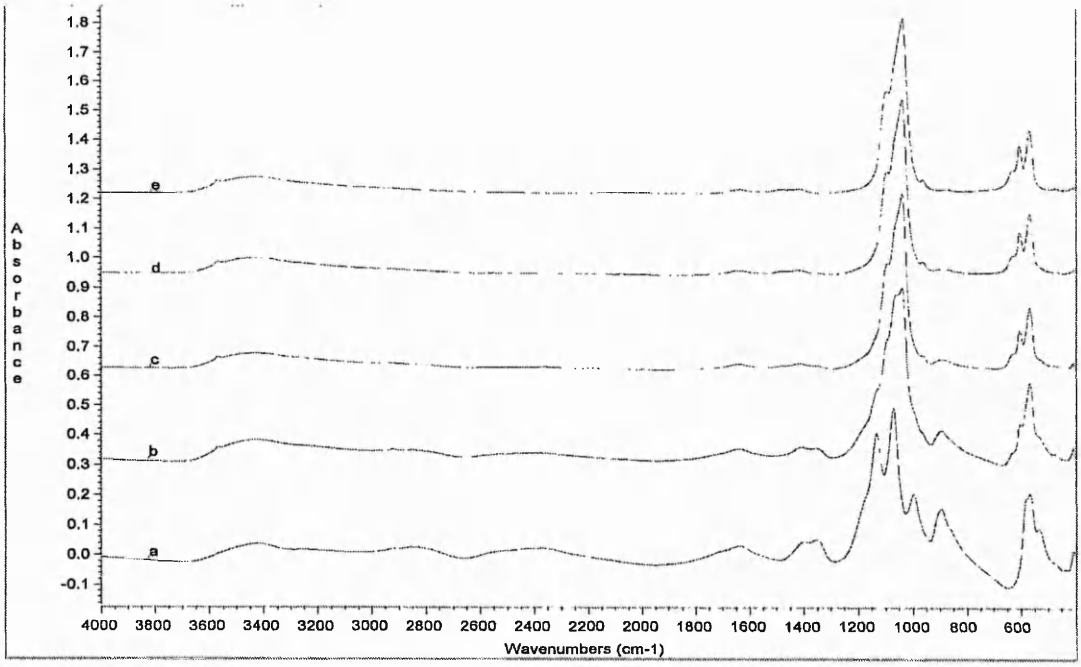

Figure 2.3 FT-IR spectra of mixtures of commercial DCP and HAP a) 100 % DCP, b) 75/25 % DCP/HAP, c) 50/50 % DCP/HAP, d) 25/75 % DCP/HAP and e) 100 % HAP.

These changes are due to the superposition of the infrared spectrum of DCP on that of HAP. Even when there is an excess of DCP in a given sample it is very difficult to confirm its presence using infrared spectroscopy and other techniques must be employed.

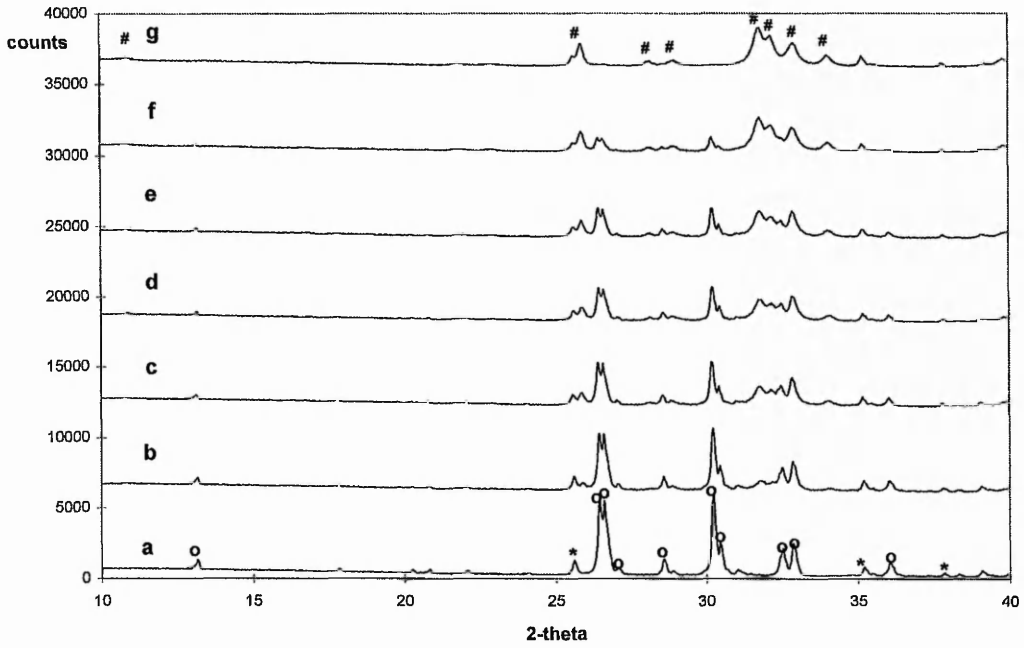

Figure 2.4 XRD spectra of mixtures of commercial DCP and HAP a) 100 % DCP, b) 80/20 % DCP/HAP, c) 60/40 % DCP/HAP, d) 50/50 % DCP/HAP, e) 40/60 % DCP/HAP, f) 20/80 % DCP/HAP and g) 100% HAP. *SRM, #HAP, ° DCP.

X-ray diffraction data obtained from mixtures of commercial HAP and DCP, figure 2.4a-g, show that it is possible to identify 20% DCP in the presence of well crystalline HAP (fig 2.4f). It is also possible to identify up to 20% of crystalline HAP in the presence of DCP. With increasing concentration of HAP, the reflections at ca. 2θ=10°, 26° and 32° corresponding to HAP become more prominent while the main reflections for DCP at ca. 2θ=13°, 26.6° and 30° decrease.

2.8 References

1. Beeston, B.E.P, Horne, R.W. and Markham, R. (1987). Practical Methods in Electron Microscopy,Vol.1, Glauert, A.M., North-Holland.
2. Chescoe, D. and Goodhew, P.J. (1990). The Operation of Transmission and Scanning Electron Microscopes. Microscopy Handbooks 20. Oxford Science Publications. Royal Microscopical Society. Oxford University Press, New York.
3. Fryer, J.R. (1979). The Chemical Applications of Transmission Electron Microscope, Academic Press, London.
4. Joy, D.C., Roming Jr., A.D. and Goldstein, J.I. (1986). Principles of Analytical Electron Microscopy, Plenum Press, New York.
5. Watt, I.M. (1985). The Principles and Practice of Electron Microscope. Cambridge.
6. Edington, J.W. Electron Diffraction in the Electron Microscope. In Practical Electron Microscopy in Materials Science, Philips Technical Library.
7. Goodhew, P.J. and Humphreys, F.J. (1988). Electron Microscopy and Analysis, 2nd Edition, Edited by Taylor and Francis.
8. Chandler, J.A. (1987). X-ray Microanalysis in the electron Microscope in Practical Methods in Electron Microscopy, Glauert, A.M., North-Holland.
9. Williams, D.B. (1984). Practical Analytical Electron Microscopy in Materials Science, Verlag Chemie International.
10. Lawes, G. (1987). Scanning Electron Microscopy and X-Ray Microanalysis, Analytical Chemistry, by Open Learning, Wiley. New York.
11. Newbury, D.E., Joy, D.C., Echlin, P., Fiori, C.E. and Goldstein, J.I. (1986). Advanced Scanning Electron Microscope and X-Ray Microanalysis, Plenum Press, New York.
12. Glasser, L. (1987). Fourier Transform for Chemist: Part I. Introduction to the Fourier Transform. *J. Chem. Ed.*, **64**(10)A228.
13. Griffiths, P.R. and De Haseth, J.A. (1986). Fourier Transform Infrared Spectroscopy, Wiley. New York.
14. Nakamishi, K. and Solomon, P.H. (1977). Infrared Spectroscopy, 2nd Edition, Holden-Day, San Francisco.
15. Perkins, W.D. (1986). Fourier Transform-Infrared Spectroscopy. Part I Instrumentation. *J. Chem. Ed.*, **63**(1):A5.

16.Perkins, W.D. (1986). Fourier Transform-Infrared Spectroscopy. Part II Applications. *J. Chem. Ed.*, **64**(12):A296.

17.Perkins, W.D. (1986). Fourier Transform-Infrared Spectroscopy. Part III Advantages of FT-IR. *J. Chem. Ed.*, **64**(11):A269.

18.Smith, A.L. (1979). Applied Infrared Spectroscopy, Wiley, New York.

19.Chesick, J.P (1989). Fourier Analysis and Structure Determination. Part III: X-Ray Crystal Structure Analysis. *J. Chem. Ed.*, **66**(5):413.

20.Cullity, B.D. (1978). Elements of X-Ray Diffraction, 2nd ed., Addison-Wesley. Massachusetts.

21.Enemark, J.H. (1988). Introducing Chemists to X-Ray Structure Determination. *J. Chem. Ed.* **65**(6):491.

22.Jenkins, R., Anderson, R., and McCarthy, G.J. Use of the Power Diffraction File. An Education Resource Package. JCPDS International Centre for Diffraction Data, Pennsylvania, U.S.A.

23.Klug, H.P., Alexander, L.E. (1974). X-Ray Diffraction Procedures for Polycrystalline and Amorphous Materials, 2nd Edition, John Wiley, New York.

24.Pope, C.G. (1997). X-Ray Diffraction and the Bragg Equation. *J. Chem. Ed.*, **74**(1):129.

25.Kanazawa, T. (1989). Materials Science Monographs, 52: Inorganic Phosphate Materials, Elsevier.

26.Narasaraju, T.S.B. and Phebe, D.E. (1996). 'Some Chemical Aspects of Hydroxyapatite'. *J. Mater. Science*, **31**:1.

27.Hayek, E and W. Stadlmann, W. (1955).Preparation of Pure Hydroxyapatite for Adsorption Uses. *Angew. Chem.* 67.

28.Thomas, I.M. (1994). Optical Coating Fabrication, in Sol-Gel Optics: Processing and Applications, Klein.

29.Brinker, C.J. and Scherer, G.W. (1990). Sol-Gel Science. The Physics and Chemistry of Sol-Gel Processing. Academic Press.

CHAPTER 3: CHARACTERISATION OF CALCIUM PHOSPHATE CRYSTALS

3.1 Introduction

Over the last 50 years much has been written about the formation of "calcium phosphates" from aqueous solutions. The main reason for all these studies is that calcium phosphate, in particular hydroxyapatite is chemically and structurally very similar to the main inorganic component of bone[1].

Hydroxyapatite does not normally precipitate directly from solution although it has been shown to grow from seeded solutions[2-10].

It was found that at higher supersaturations apatite did not precipitate directly from solution but a precursor phase was formed which was amorphous to electron diffraction, named amorphous calcium phosphate, thereafter ACP[11]. However, evidence suggesting that at the lowest supersaturations, without seeding, apatite could nucleate directly from solution without the formation of precursor phases has been presented by Boskey *et al.* (1976)[12].

The transformation of ACP to HAP has been described as an autocatalytic conversion process[13, 14] with the first crystals appearing on the surface of the amorphous phase[15]. The composition of ACP depends on the reaction solution[16, 17] and it has been reported to have an effect on the final HAP precipitated[18]. Numerous studies have also been carried out to investigate the formation of the intermediate crystal phases formed from the conversion of ACP[19-25]. Crystal phases which have been proposed as precursors to HAP formation are DCPD[26], OCP[27] and TCP[28].

As the final apatite precipitate is not a stoichiometric hydroxyapatite, some investigations of the structure of non-stoichiometric or Ca-deficient apatites have been made[29]. It is also important to note that the solution parameters of pH, temperature and ionic concentration have a large effect on the type of calcium phosphate precipitated from solutions containing Ca^{2+} and

HPO_4^{2-} ions[27, 30,-32]. Table 3.1 summarises the experimental conditions which have been used in the preparation of apatite crystals and the main conclusions obtained from those studies.

Starting materials	Conditions	Temp (°C)	Ca/P molar ratio	Results	Ref.
$Ca(NO_3)_2/CaCl_2$ 0.75 M $(NH_4)_2HPO_4$ 0.25 M	pH=10.5	25	1.71	autocatalytic conversion of ACP to HAP	Eanes *et al.* (1965)
$CaCl_2$ 1.3x10^{-2} M Na_2HPO_4	pH=7.4 seeded	25	1.2-1.6	crystal growth occurs in two stage process with a precursor Ca/P close to 1.5	Nancollas *et al.* (1970)
$CaCl_2$ 4x10^{-3} M NaH_2PO_4 4x10^{-3} M	pH=7.4 non-stirred additives: NaCl citrate EDTA gelatin	25 37	1	less precipitate formed with increasing [NaCl] gelatin enhanced secondary precipitation citrate decreased the rate of recrystallisation no evidence of specific interaction of EDTA with calcium phosphate crystals	Füredi-Milhofer *et al.* (1971)
$CaCl_2$ 3 mM Na_2HPO_4 3 mM	pH=7.4	25	1	ACP appeared as a template to OCP nucleation	Brecevic *et al.* (1972)
$Ca(OH)_2$ 0.9-1.3 mM H_3PO_4 0.8-1.1 mM	pH=7.4	25	1	SEM studies of the growth of hydroxyapatite	Meyer *et al.*(1972)
$CaCl_2$ 10.4 mM Na_2HPO_4 10.4 mM	pH=7.4 buffered TRIS	25	1-2.3	amorphous calcium phosphate has two morphologically distinct form: spheroidal and discoidal	Eanes *et al.* (1973)
$CaCl_2$ 8.0 mM Na_2HPO_4 3.4 mM	pH=7.6-8.0 NaCl 0.16M	35	1-2.3		
$CaCl_2$ H_3PO_4 high and low supersaturating solutions	pH=7.4 seeded	25	1.67	OCP&HAP at high supersaturation HAP at low supersaturation	Nancollas *et al.* (1974)
$Ca(NO_3)_2$ 1.33-3.9 mM Na_2HPO_4 1.0-2.4 mM	pH=7.5 buffered 25 mM HEPES seeded	20	1-2	seeding did not affect the formation of apatite crystals but reduced the amount of free ACP formed	Eanes (1976)
$CaCl_2xNa_2HPO_4$ 0.25-1.7 mM^2	pH=7.4 NaCl 0.15 M	26.5	1.0-1.7	growth of HAP occurred by ripening process	Boskey *et al.* (1976)
$Ca(NO_3)_2$ 0.2-1.15M K_2HPO_4+ KH_2PO_4 0.12- 0.74 M	pH=6.70-8.50	26	1.55-1.70	OCP intermediate in the conversion of ACP to HAP	Feenstra *et al.* (1979)
$CaCl_2$ 0.15-3.00 mM KH_2PO_4 0.075-1.8mM	pH=6-8.5 seeded	37	1-1.66	solubility decreased in DCPD>TCP>OCP>HAP	Koutsoukos *et al.* (1980)
$CaCl_2$ 1-7 mM NaH_2PO_4 1 mM	pH=6.3-9.1	37	0.4-2	ACP had Ca/P < 1.5	Walton *et al.* (1981)
$CaCl_2$ 0.1-10mM Na_2HPO_4 0.1-100mM	pH=7.0	23		DCPD stabilisation	Cheng *et al.* (1983)

Table 3.1 Summary of studies on calcium phosphate formation over the last 30 years.

Starting materials	Conditions	Temp (°C)	Ca/P molar ratio	Results	Ref.
$CaCl_2$ 10 mM K_2HPO_4 6-7.5 mM	7.40	15 30 42	1.67 1.33	DCPD formed independently of ACP Formation of OCP or d-HAP through ACP2	Christoffersen *et al.* (1989)
$Ca(NO_3)_2$ $5.71x10^{-4}$-$5.71x10^{-2}$ M KH_2PO_4 $3.43x10^{-4}$-$3.43x10^{-2}$M	various pH	RT	1.67	HPO_4^{2-} retarding parameter of crystallisation	Lazic *et al.* (1995)
$Ca(NO_3)_2$ 4-16 mM K_2HPO_4+ KH_2PO_4 various	pH controlled by changing K_2HPO_4+ KH_2PO_4	25 50	1	ACP transformed into DCPD at 25°C and into OCP at 50°C	Tsuge *et al.* (1996)

Table 3.1 continued Summary of studies on calcium phosphate formation over the last 30 years.

Despite all the previous studies on calcium phosphate precipitation, there are still some contradictory questions such as: does DCPD hydrolyse to HAP?, does ACP really transform into DCPD or does DCPD forms independently?, is OCP an intermediate phase in the conversion of ACP to HAP?. The aim of the current study presented below was to determine which calcium phosphates formed under various conditions of pH, T and concentrations of calcium and phosphate and to answer some of the above questions using specific conditions for the precipitation of calcium phosphate before going on to study of the effect of certain ions on the formation of calcium phosphate. The nucleation and crystal growth of calcium phosphate crystals was also studied.

3.2 Experimental

3.2.1 Materials

Sodium dihydrogen orthophosphate dihydrate 98% ($NaH_2PO_4.2H_2O$) from East Anglia Chemicals, diammonium phosphate dibasic 99% ($(NH_4)_2HPO_4$) from Sigma Chemical Co,

calcium nitrate anhydrous 98+% ($Ca(NO_3)_2$ from Avocado Research Chemicals Ltd., calcium chloride dihydrate 98% ($CaCl_2 \cdot 2H_2O$) from Aldrich, sodium chloride 99% (NaCl) from BDH were used.

Standards: Calcium phosphate monobasic (CaH_2PO_4) from Sigma Chemical Co, calcium phosphate dibasic ($CaHPO_4$) from Sigma Chemical Co, calcium phosphate tribasic (Hydroxyapatite, $Ca_5(PO_4)_3(OH)$ from Sigma Chemical Co, and β-Tricalcium phosphate ($Ca_3(PO_4)_2$) from Fluka Chemika (see Appendix I for XRD and FT-IR spectra).

3.2.2. Method

Experiments were carried out by following the method described in Chapter 2. The effect of T, pH, precursors and the concentration of calcium and phosphate solutions was studied. The precipitations were carried out at 23°C (room temperature) and 37°C (thermostatically controlled water bath). $CaCl_2/NaH_2PO_4$ and $Ca(NO_3)_2/(NH_4)_2HPO_4$ solutions were used to study the effect of the precursors on the nature of the final precipitate. At 23°C the precipitations were carried out by first keeping the pH constant with the addition of 1M $(NH_4)OH$ during the precipitation reaction and second, prior to adjusting the phosphate solution to pH 7.4 with 1M HNO_3 before the addition of the calcium solution, without further pH control. Three different concentrations of calcium and phosphate solutions were used to study the effect of concentration on the final precipitate: 3.2 mM and 6 mM, 6 mM and 10 mM, and 0.145 M and 0.242 mM for $Ca(NO_3)_2$ and $(NH_4)_2HPO_4$ respectively. The precipitates were calcined at 600°C and 1000°C for 10 h to study phase changes of the final precipitate on heating. For experiments at the 6 mM (Ca^{2+}) and 10 mM (HPO_4^{2-}) concentrations, the solutions were prepared in 0.15M NaCl and during the precipitation reaction , the reaction mixture was continuously

stirred and the pH monitored using a pH93 reference pH meter (Radiometer Copenhagen). After 30 min, the reaction mixture was filtered, rinsed with distilled deionised H_2O and dried at 250°C for 1h to eliminate any volatile ammonium salts produce during the precipitation process. The method of Hidaka *et al.* (1991)[33] was used to follow the formation and transformation of calcium phosphate phases by monitoring the rate of change of pH with time. Samples were analysed by TEM, EDX, FT-IR and XRD (see chapter 2).

Statistics

The mean ± standard deviation was calculated using the t-test Student. Statistical comparisons were made by the F-distribution test. The difference was considered significant at $p < 0.05$.

3.3 Results

3.3.1 Effect of temperature

The precipitate formed at 23 °C depended upon the initial solution concentrations used for the precipitation reaction (see section 3.3.3) . The precipitate formed at 23 °C using 0.242 M Ca^{2+} and 0.145 M $HPO_4^{2-}/H_2PO_4^-$ (Ca/P 1.67) was dicalcium phosphate (for 10 mM Ca^{2+} and 6 mM HPO_4^{2-} see section 3.3.3). This was confirmed by FT-IR analysis (Fig 3.1). The FT-IR spectrum showed bands at 998, 1070 and 1128 cm^{-1} corresponding to HPO_4^{2-} stretching modes and at the range 600-500 cm^{-1} corresponding to the OPO bending modes[34].

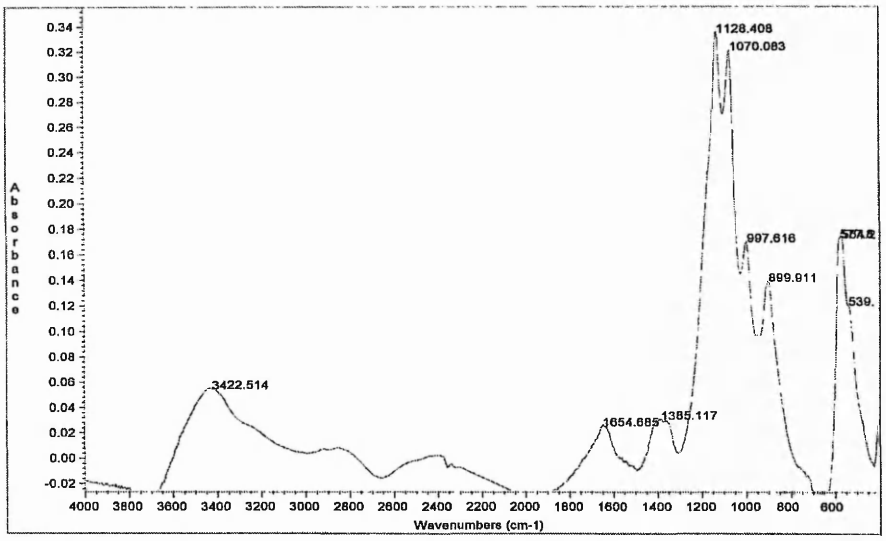

Fig 3.1. FT-IR spectra of precipitate formed by mixing 0.242 M and 0.145 M solutions of calcium nitrate and diammonium hydrogen phosphate at 23 °C after drying at 250°C for 1h.

X-ray diffraction analysis also confirmed that the calcium phosphate formed was DCP (N.B. after heating at 250°C for 1h), JCPDS 9-80. Figure 3.2 shows the XRD pattern of the dried precipitate with the main reflections and their corresponding Miller Indices.

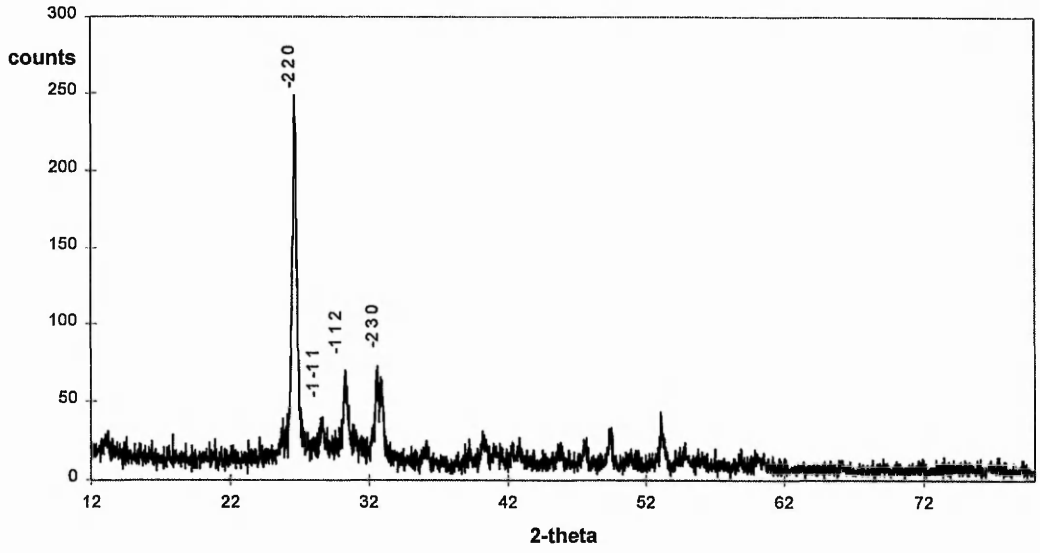

Fig 3.2. XRD pattern of precipitate formed by mixing 0.242 M and 0.145 M solutions of calcium nitrate and diammonium hydrogen phosphate at 23 °C after drying at 250°C for 1h.

EDX analysis in the transmission mode by TEM showed a Ca/P molar ratio 0.93 ± 0.05, indicating a lack of stoichiometry (Ca/P molar ratio for stoichiometric DCP is 1). The product was unstable under the electron beam indicating that it was highly hydrated. This agreed with the XRD data which showed a poorly crystalline material (fig. 3.2).

SEM analysis of the precipitate showed that the crystals had a plate-like morphology (Fig 3.3). A higher magnification view in the TEM mode showed that these plates were formed from lath-like subunits aligned parallel to one another (Fig 3.6b). Table 3.2 lists the d-spacings and Miller indices obtained by electron diffraction (appendix II) and correspond to calcium phosphate dibasic (JCPDS 9-80).

d-spacings (Å)	**Miller indices (DCP JCPDS 9-80)**
2.953	(-1 1 2)
2.910	(2 -1 1)

Table 3.2 d-spaces (Å) obtained from ED analysis and Miller indices for the material precipitated at 23°C after drying at 250°C for 1h.

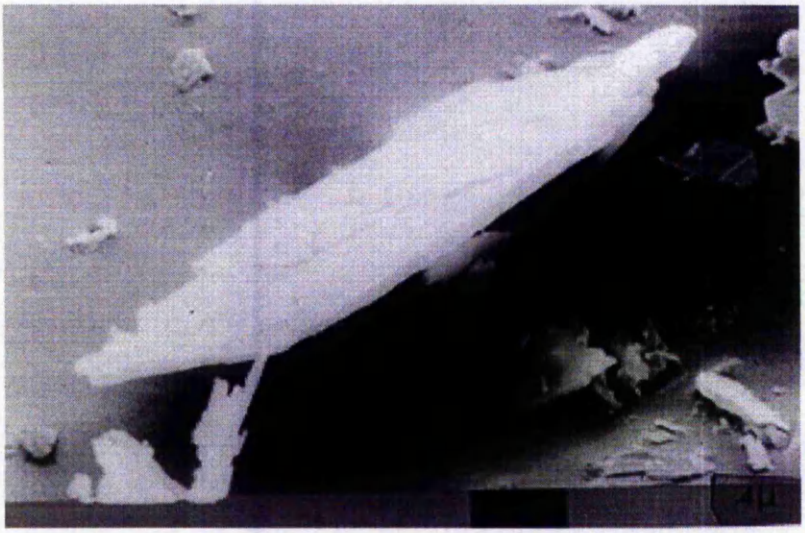

Fig. 3.3 SEM micrograph of precipitate formed by mixing 0.242 M and 0.145 M solutions of calcium nitrate and diammonium hydrogen phosphate at 23 °C after drying at 250°C for 1h.

The precipitate formed at 37 °C depended upon the concentration and precursors used for precipitation (see section 3.3.3 and 3.3.4) . When concentrations of 10 mM Ca^{2+} and 6 mM HPO_4^{2-} (Ca/P 1.67) were used to precipitate calcium phosphate crystals, the main calcium phosphate phase formed was apatite (fig 3.4). The FT-IR spectrum showed bands at 1098, 1035 cm^{-1} assigned to the antisymmetric PO stretching mode, at 961 cm^{-1} assigned to the symmetric P-O stretching mode. The band at 3567 cm^{-1} is attributed to the OH stretching mode and at 633 cm^{-1} to the OH vibrational mode. The bands at 603 and 566 cm^{-1} are assigned to the O-P-O bending modes[35,36].

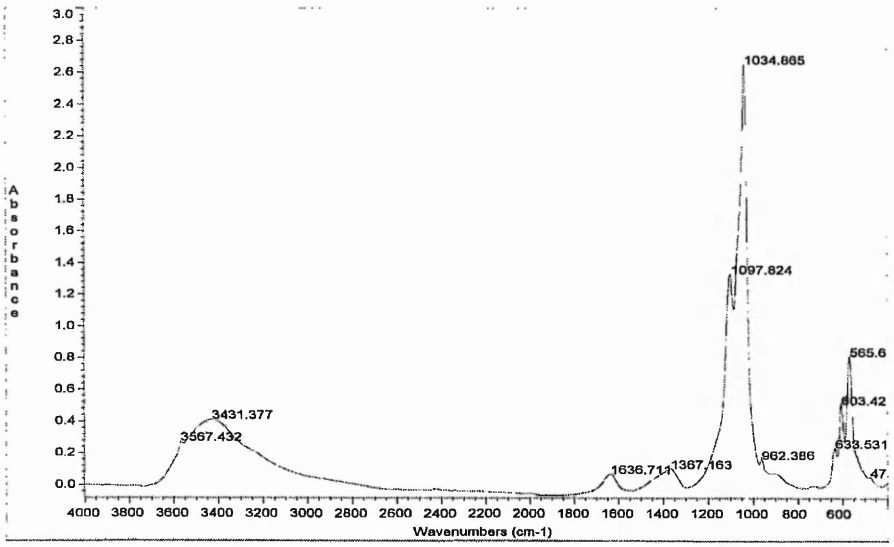

Fig 3.4 FT-IR spectrum of precipitate formed at 37 °C by the mixing 10 mM calcium nitrate and 6 mM diammonium hydrogen phosphate after drying at 250°C for 1h..

XRD analysis showed the main reflections corresponding to hydroxyapatite at ca. 25.5 2-theta degrees and ca. 32 2-theta degrees. The broad reflections observed in the XRD spectra indicate that the crystals are very small and poorly crystalline, JCPDS 9-432, (Fig 3.5).

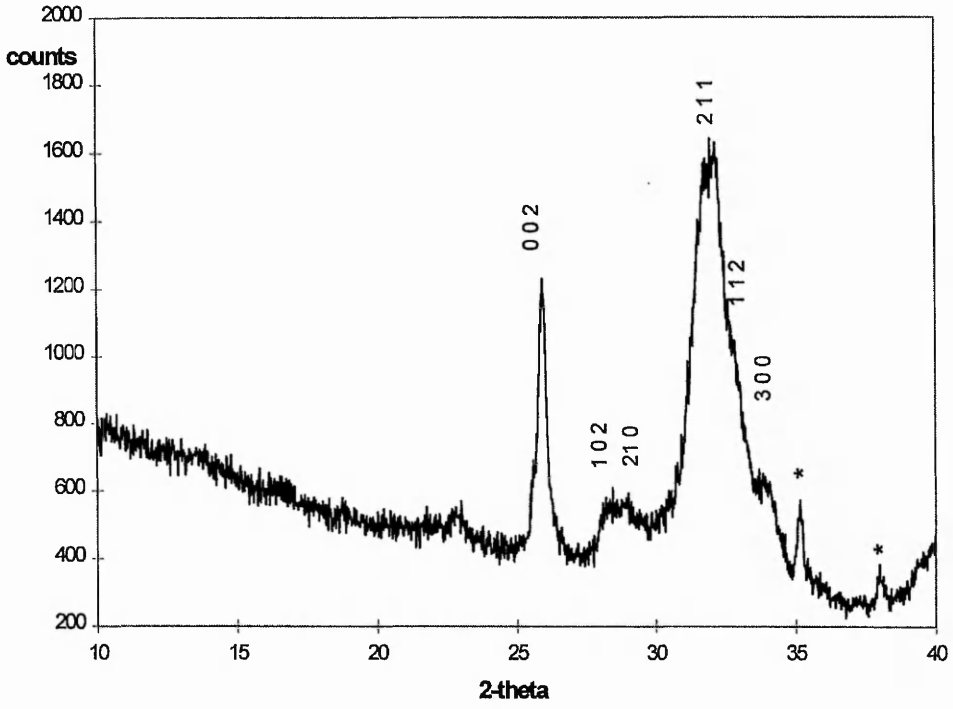

Fig 3.5 XRD pattern of precipitate formed at 37 °C by the mixing 0.242 M calcium nitrate and 0.145 M diammonium hydrogen phosphate after drying at 250°C for 1h.. *SRM

TEM analyses showed that the crystals were agglomerated and had a needle-like morphology typical of non-stoichiometric hydroxyapatite crystals (Fig.3.6a)[18]. The electron diffraction patterns obtained corresponded to polycrystalline materials. The precipitate was also highly hydrated and it decomposed under the electron beam. It had a Ca/P molar ratio of 1.56 ± 0.22. The Ca/P ratio was not the stoichiometric value expected for hydroxyapatite (Ca/P=1.67).

Table 3.3 lists the d-spacings and Miller indexes obtained by electron diffraction (appendix II) for the precipitate formed at 37°C then dried at 250°C for 1h.

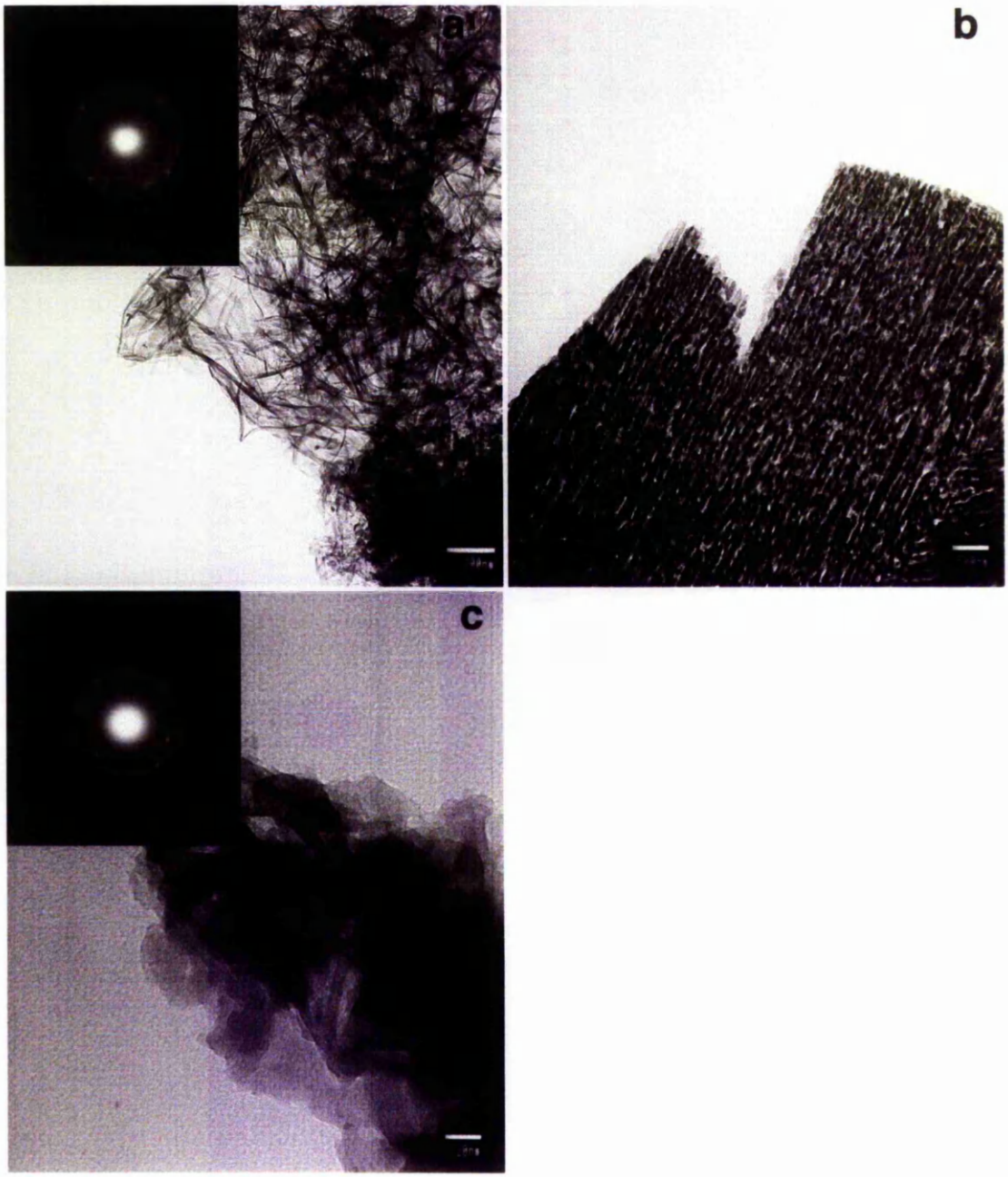

Continuation Figure 3.6 Calcium phosphate was precipitated from a solution containing 0.242 M $Ca(NO_3)_2$ and 0.145 M $(NH_4)_2HPO_4$ at a) 37°C, b) 23°C and c)23°C and pH=7.4, and then dried at 250°C for 1h. The d-spacings obtained from the electron diffraction pattern for the material formed at 37°C were ca. 3.46 Å attributed to the HAP Miller Index (0 0 2) (JCPDS 9-432). The d-spacings obtained from the electron diffraction pattern for the material formed at 23°C and pH=7.4 were ca. 3.44 Å and 2.80 Å attributed to the HAP Miller Indices (0 0 2) and (2 1 1) (JCPDS 9-432).

d-spacings (Å) from electron diffraction analysis	d-spacings (Å) from HAP (JCPDS 9-432)	Miller Indices HAP (JCPDS 9-432)
3.522	3.51	2 0 1(w)
3.462	3.44	0 0 2(s)
2.822	2.814	2 1 1 (s)
2.788	2.778	1 1 2(s)
1.753	1.754	4 0 2(m)
1.746	1.722	0 0 4(m)

Table 3.3 lists the d-spacings obtained for the precipitate formed at 37°C by the mixing 10 mM calcium nitrate and 6 mM diammonium hydrogen phosphate after drying at 250°C for 1h..

3.3.2 Effect of pH

The effect of pH was studied using 0.242M $Ca(NO_3)_2$ and 0.145M $(NH_4)_2HPO_4$ as precursors at a temperature of 23°C. During precipitation the pH was kept constant ca. 7.4 ± 0.1 by the addition of 1M $(NH_4)OH$. The precipitate formed under these conditions was apatite confirmed by FT-IR and XRD analysis (fig 3.7, and fig 3.8). The precipitate showed the same structural and chemical characteristics as the precipitate formed at 37°C with 10 mM Ca^{2+} and 6 mM HPO_4^{2-} (fig. 3.6c). The FT-IR spectra showed bands at 1034 cm^{-1} and 962 cm^{-1} corresponding to the P-O stretching mode and at 603 cm^{-1} and 565 cm^{-1} corresponding to O-P-O bending mode. It also showed the HAP characteristic band at 3568 cm^{-1} corresponding to an OH^- stretching mode although the band expected at 630 cm^{-1} was a shoulder. The shift to higher wavenumber observed for the band at 1097 cm^{-1} and the appearance of the band at 906 cm^{-1} showed the presence of HPO_4^{2-} in the material[37].

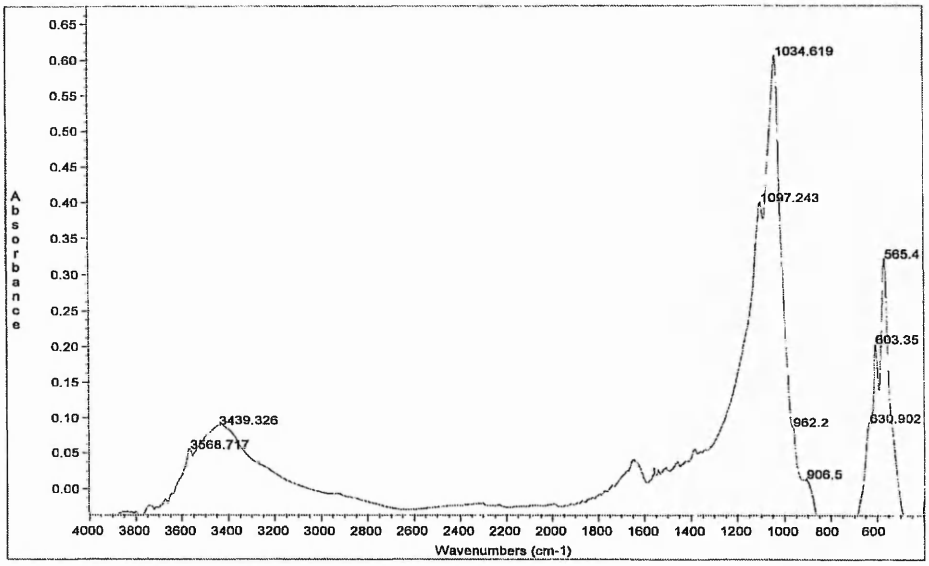

Fig 3.7 FT-IR spectrum of the precipitate formed by mixing 0.242 M an d 0.145 M solutions of calcium nitrate and diammonium hydrogen phosphate at 23 °C and pH=7.4 after drying at 250°C for 1h.

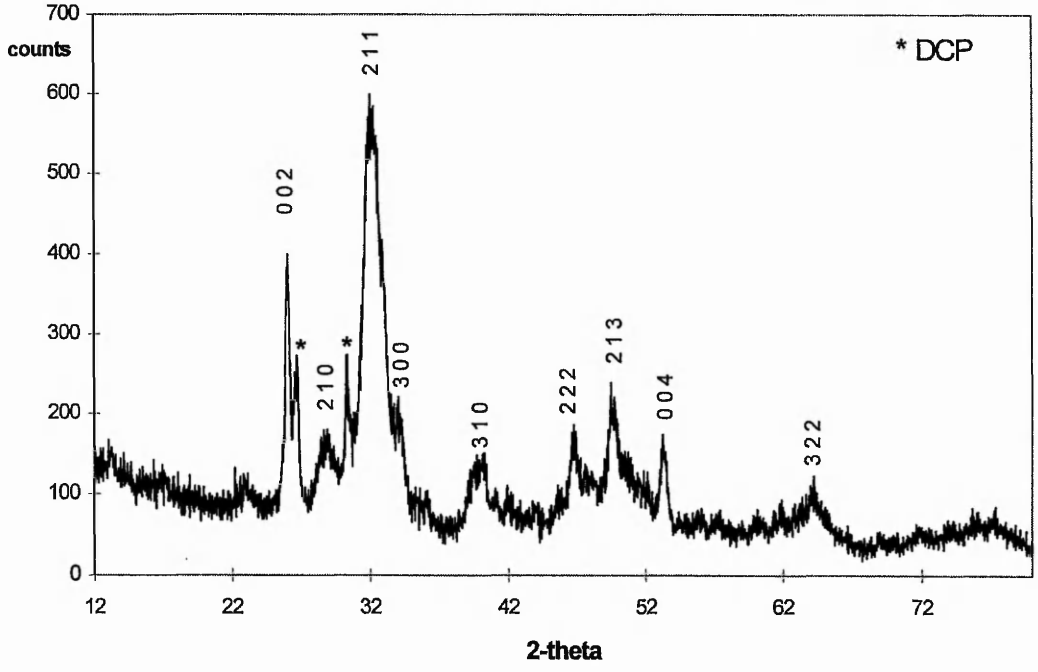

Fig 3.8 XRD pattern of the precipitate formed by mixing 0.242 M an d 0.145 M solutions of calcium nitrate and diammonium hydrogen phosphate at 23 °C and pH=7.4 after drying at 250°C for 1h.

The broad reflections observed in the XRD spectrum (fig. 3.8) indicated that the crystals were poorly crystalline and very hydrated. The XRD analysis showed the presence of DCP

in the precipitate with reflections at ca 26 2-theta degrees and 30 2-theta degrees being observed.

3.3.3 Effect of concentration

The main calcium phosphate phase detected after heating the precipitate at 250°C for 1h to remove ammonium salts for reactions carried out at 23°C from 0.242M Ca^{2+} and 0.145M HPO_4^{2-} and at 10 mM Ca^{2+} and 6 mM HPO_4^{2-} was DCP. However the proportion of apatite in the final precipitate increased with a decrease in the calcium and phosphate concentration (fig. 3.9 and fig. 3.10). The FT-IR spectrum of the precipitate formed at 0.242M Ca^{2+} and 0.145M HPO_4^{2-} corresponded to that of DCP (fig 3.9a). The FT-IR spectrum of the precipitate formed at 10 mM Ca^{2+} and 6 mM HPO_4^{2-} showed bands at 1107 cm^{-1}, 1076 cm^{-1} and 905 cm^{-1} attributable to the presence of OCP (fig 3.9b). Finally the FT-IR spectrum of the precipitate formed at 6 mM Ca^{2+} and 3.2 mM HPO_4^{2-} showed a spectrum typical of apatite (fig 3.9c).

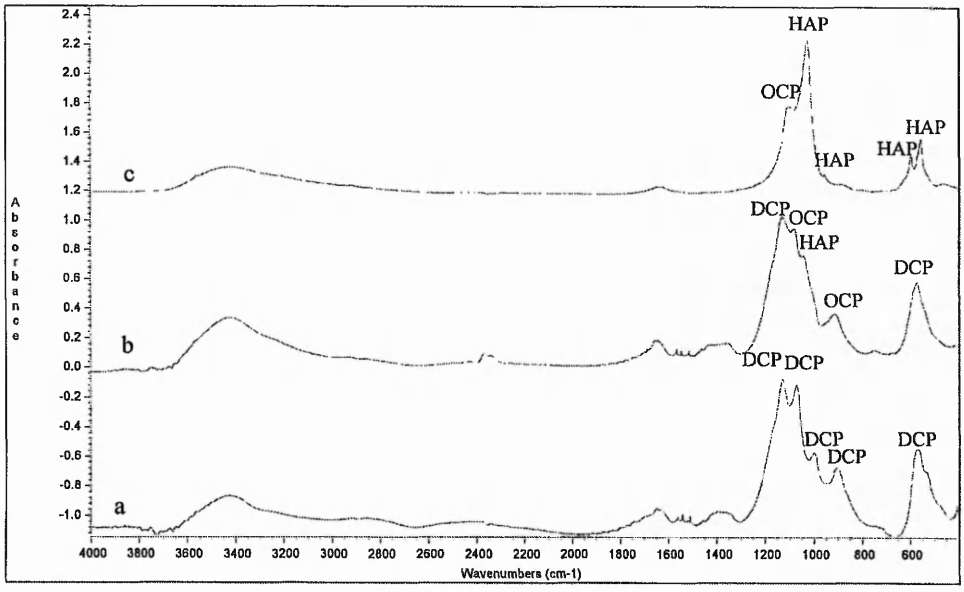

Fig 3.9 FT-IR spectra of precipitate formed at 23°C from solution containing a) 0.242M $Ca(NO_3)_2$ and 0.145M $(NH_4)_2HPO_4$, b) 10 mM $Ca(NO_3)_2$ and 6mM $(NH_4)_2HPO_4$, and c) 6 mM $Ca(NO_3)_2$ and 3.2 mM $(NH_4)_2HPO_4$ after drying at 250°C for 1h.

The XRD patterns of the precipitates also showed an increase in the reflections due to the apatite phase with decreasing concentrations of the precursors (fig 3.10). The XRD pattern for the precipitate formed using 0.242M Ca^{2+} and 0.145M HPO_4^{2-} corresponded to DCP (fig 3.10a). The presence of apatite even in this sample could not be excluded due to the likely difference in crystal size (TEM data see later). The DCP crystals were much bigger than the apatite crystals which were not only small but poorly crystalline and gave broad and low intensity reflections compared to the DCP, crystals, whose reflections were narrow and of high intensity. When 10 mM Ca^{2+} and 6 mM HPO_4^{2-} were used to precipitate calcium phosphate, the XRD pattern showed the presence of apatite via a peak at ca. 32 2-theta degrees (fig. 3.10b). When 6 mM Ca^{2+} and 3.2 mM HPO_4^{2-} were used, the XRD pattern corresponded to very poorly crystalline apatite (fig 3.10c), still with some DCP present.

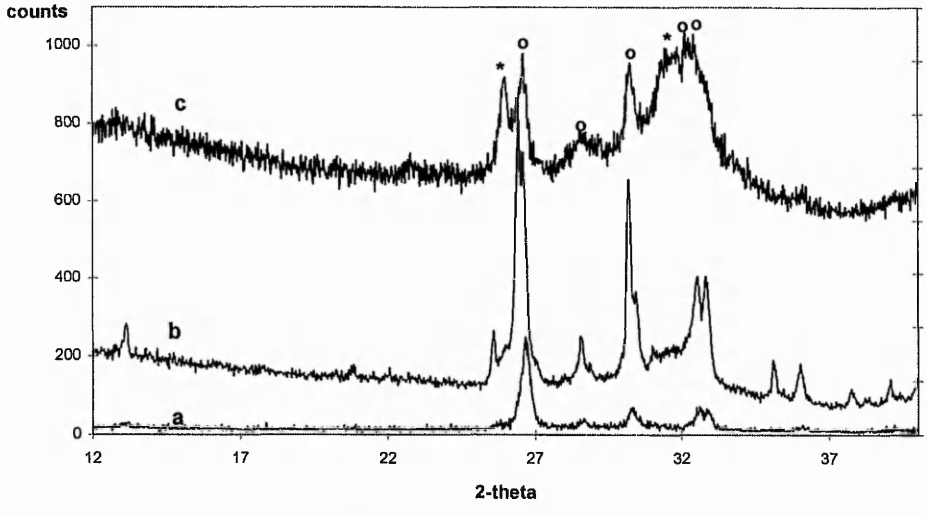

Fig 3.10 XRD patterns of precipitate formed at 23°C from solution containing a) 0.242M $Ca(NO_3)_2$ and 0.145M $(NH_4)_2HPO_4$, b) 10 mM $Ca(NO_3)_2$ and 6mM $(NH_4)_2HPO_4$, and c) 6 mM $Ca(NO_3)_2$ and 3.2 mM $(NH_4)_2HPO_4$ after drying at 250°C for 1h. * HAP, °DCP.

For reactions performed at 37°C, DCP was formed at the highest concentration of calcium and phosphate as shown by XRD analysis (fig 3.11a). The spectrum showed the main reflections for DCP at ca. 26 2-theta and 30 2-theta degrees. The reflections at ca. 25.5 2-theta and 32 2-theta degrees corresponded to HAP. At the remaining concentrations the main product was apatite (fig 3.11b and 3.11c). With decreasing concentrations of precursors, the spectra showed a decrease in crystallinity.

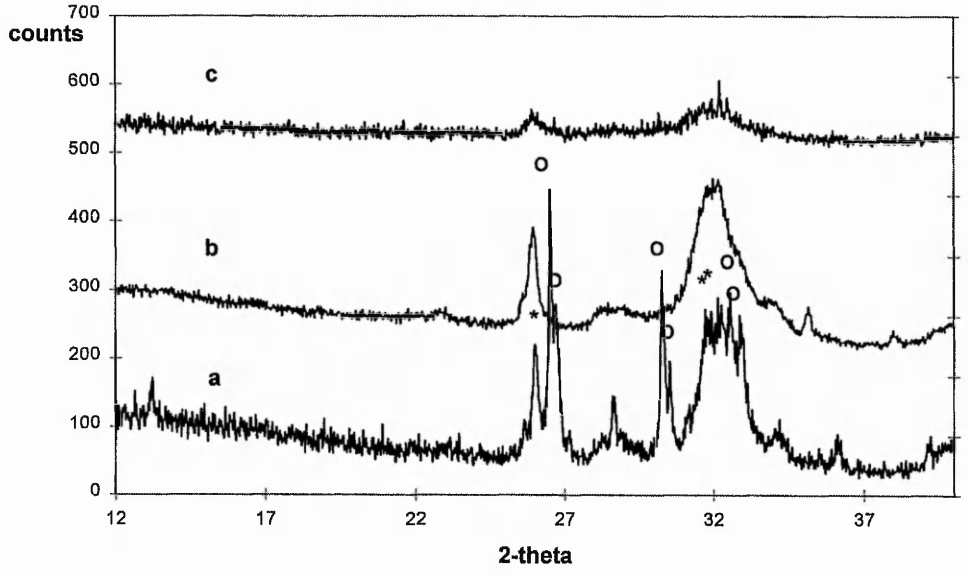

Fig 3.11 XRD patterns of precipitate formed at 37°C from solution containing a) 0.242M $Ca(NO_3)_2$ and 0.145M $(NH_4)_2HPO_4$, b) 10 mM $Ca(NO_3)_2$ and 6mM $(NH_4)_2HPO_4$, and c) 6 mM $Ca(NO_3)_2$ and 3.2 mM $(NH_4)_2HPO_4$,. °DCP, *HAP.

3.3.4 Effect of precursors

For precipitations carried out at 37°C and at 0.242M Ca^{2+} and 0.145M HPO_4^{2-}, the use of different precursors affected the calcium phosphate phase precipitated and the yield. Table 3.4 show the weights of precipitate obtained.

	23 °C		37 °C	
	$CaCl_2.2H_2O$/ $NaH_2PO_4.2H_2O$	$Ca(NO_3)_2$/ $(NH_4)_2HPO_4$	$CaCl_2.2H_2O$/ $NaH_2PO_4.2H_2O$	$Ca(NO_3)_2$/ $(NH_4)_2HPO_4$
no pHc	1.0683	0.8325*	0.9189	0.6447*

Table 3.4 Weights (g) of precipitate formed from solutions containing 0.242M Ca^{2+} and 0.145M HPO_4^{2-} and then dried at 250°C for 1h, (* $p<0.05$ compared to precipitates formed from $CaCl_2.2H_2O/NaH_2PO_4.2H_2O$).

The XRD patterns obtained from the precipitate formed at 37 °C (fig 3.12) showed the formation of two calcium phosphate phases, DCP and HAP. The precipitate formed from NaH_2PO_4 showed a higher content of DCP than the precipitate formed from $(NH_4)_2HPO_4$.

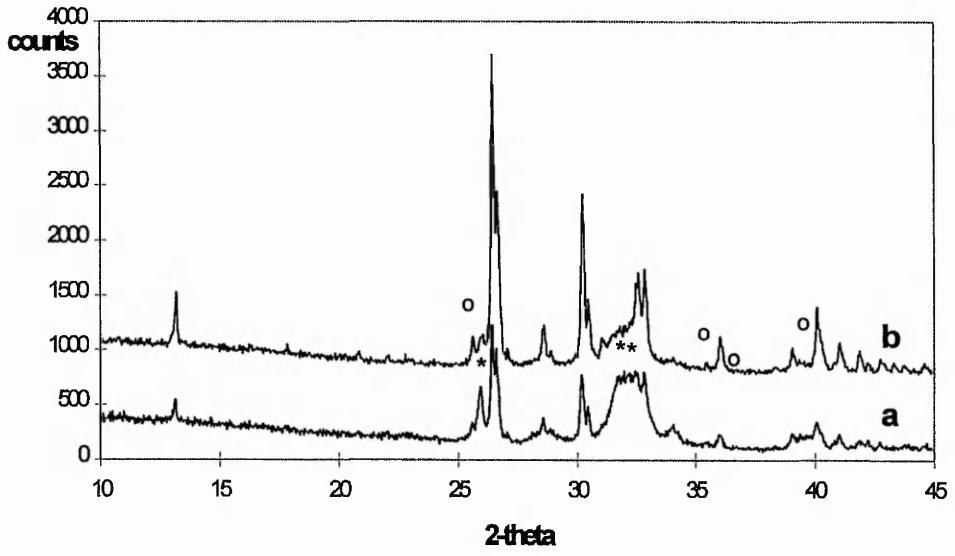

Fig 3.12 XRD spectra of precipitate formed at 37°C from solution containing a) 0.242M $Ca(NO_3)_2$ and 0.145M $(NH_4)_2HPO4$ and b) 0.242M $CaCl_2$ and 0.145M NaH_2PO_4 after drying at 250°C for 1h.* HAP, °SRM.

The DCP crystals synthesised at 23 °C using NaH_2PO_4 as precursor showed interpenetrating growth[38] (Fig 3.13).

Fig 3.13 SEM micrograph of precipitate formed at 23 °C and using as precursor 0.242M NaH_2PO_4 and 0.145M $CaCl_2$ after drying at 250°C and 1h.

The different precursors appeared to affect the crystal differently in different directions. The reflection at ca. 30 2-theta degrees corresponding to the Miller Index (-1 1 2) (JCPDS 9-80), for the material precipitated at 23°C using $(NH_4)_2HPO_4$ as precursor, showed a decrease in intensity (fig. 3.14a) compared to the material precipitated using NaH_2PO_4 as precursor (fig. 3.14b).

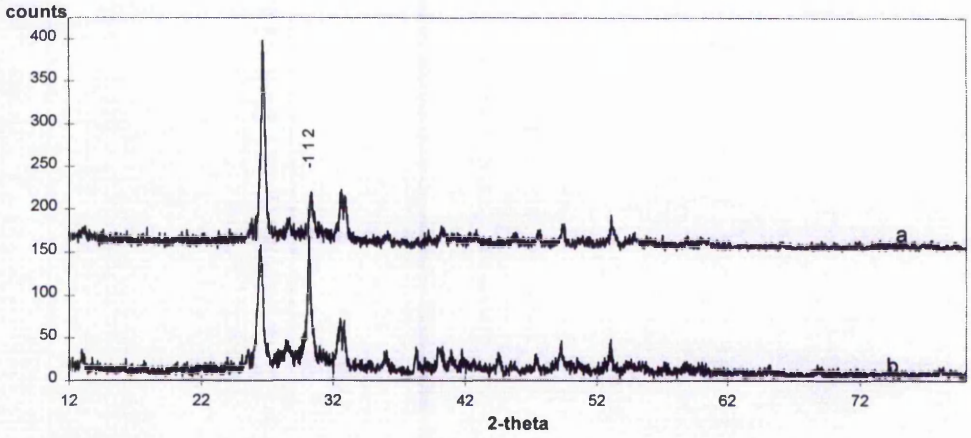

Fig 3.14 XRD patterns of precipitate formed at 23°C from solution containing a) 0.242 M $Ca(NO_3)_2$ and 0.145 M $(NH_4)_2PO_4$ and b) 0.242 M $CaCl_2$ and 0.145 M NaH_2PO_4 after drying at 250°C for 1h.

Table 3.5 shows the crystalline sizes for the precipitate formed at 23°C and 37°C calculated using the Debye-Scherrer equation[39]. The crystal size varied depending on the axis-direction. There was not any crystal size change for the (0 2 0) direction indicating that the crystal grow in the b-axis was not affected by the use of different precursors. Since there was not much change in the measured crystallite size for the (-2 2 0) and (-2 3 0) directions, the crystal grow in the a-axis was not affected either. However, for the (-1 1 2) direction, the crystallite size was much smaller for the DCP crystals precipitated at both 23°C and 37°C degrees using $(NH_4)_2HPO_4$ as the precursor. This indicated that the c-axis was affected by the use of the different precursors. The crystal size calculated by the Scherrer equation corresponded to the sub-domains which formed the DCP crystal. The use of NaH_2PO_4 appeared to affect the c-axis direction of these sub-domains (see fig. 3.6b).

T	DCP				HAP
	(0 2 0)	**(-2 2 0)**	**(-1 1 2)**	**(-2 3 0)**	**(0 0 2)**
23°C					
$CaCl_2$/ NaH_2PO_4	-	166	327	192	-
$Ca(NO_3)_2$/$(NH_4)_2HPO_4$	-	271*	198*	248*	-
37°C					
$CaCl_2$/ NaH_2PO_4	690	556	603	-	-
$Ca(NO_3)_2$/$(NH_4)_2HPO_4$	649	612*	494*	-	225

Table 3.5. Crystalline sizes (Å) for the precipitate formed at 23°C and 37°C using 0.242 M Ca^{2+} and 0.145 M $HPO_4^{2-}/H_2PO_4^-$ after drying at 250°C for 1h, (* $p<0.05$ compared to control).

3.3.5 Heat treatment

Samples of the precipitates formed from 0.242M $Ca(NO_3)_2/CaCl_2$ and 0.145M $(NH_4)_2HPO_4/NaH_2PO_4$ at 23°C were calcined at 600°C and 1000°C for 10h. The FT-IR spectrum of the precipitate formed at 23 °C and calcined at 600 °C for 10 h showed that there was some transformation of DCP into β-$Ca_2P_2O_7$ (β-CPP) (Fig 3.15b). This was

confirmed by XRD analysis (Fig 3.16b) (JCDPS 9-346). The FT-IR spectrum of the precipitate calcined at 1000 °C corresponded to β-$Ca_2P_2O_7$ (Fig 3.15c). It was also confirmed by XRD analysis (Fig 3.16c). EDX analysis of the precipitate gave a Ca/P=1.01 ± 0.01.

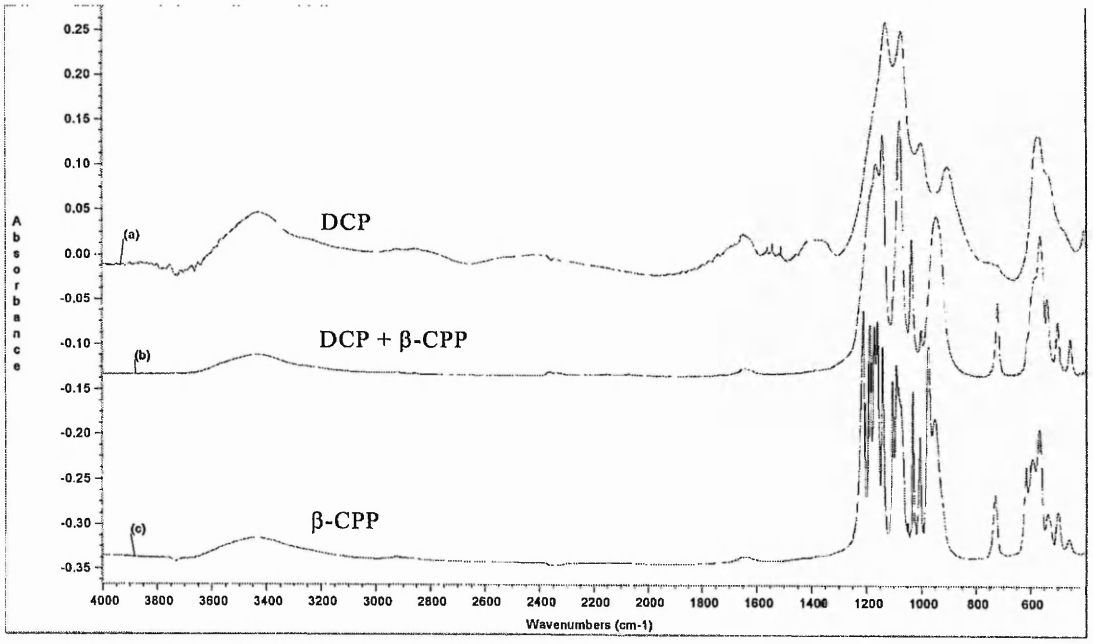

Fig 3.15. FT-IR spectra of precipitate synthesised at 23 °C from 0.242M $Ca(NO_3)_2$ and 0.145M $(NH_4)_2HPO_4$ and then dried at (a) 250 °C for 1h and calcined at (b) 600 °C for 10h and (c) 1000 °C for 10h. (see appendix (I) for the FT-IR spectrum of β-$Ca_2P_2O_7$ used as a standard).

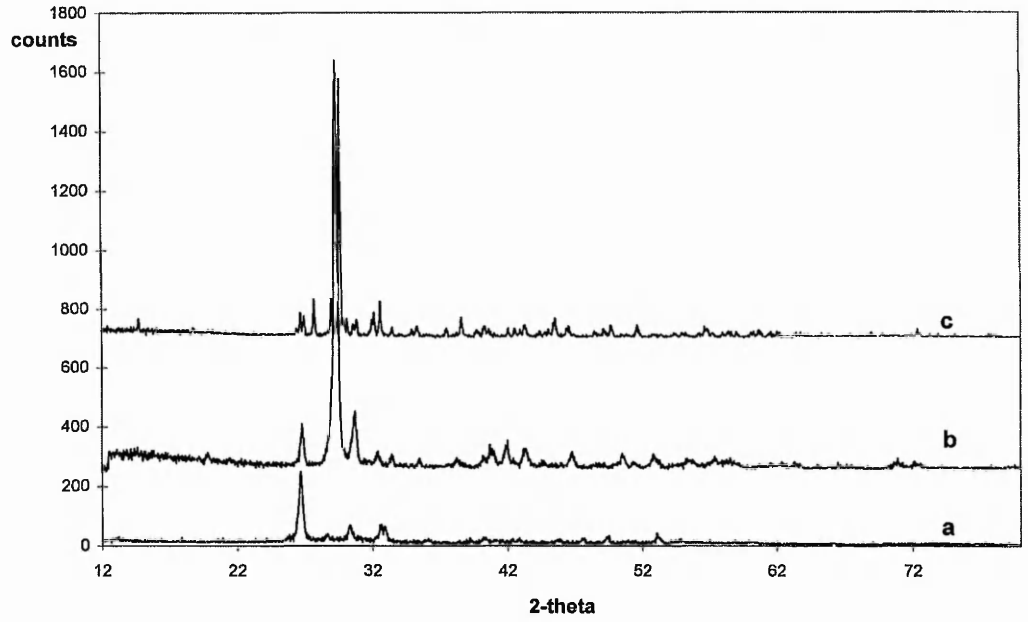

Fig 3.16. XRD patterns of precipitates synthesised at 23 °C from 0.242M $Ca(NO_3)_2$ and 0.145M $(NH_4)_2HPO_4$ and then dried at (a) 250 °C for 1h and calcined at (b) 600 °C for 10h and (c) 1000 °C for 10h. (see appendix (I) for the XRD of β-$Ca_2P_2O_7$ used as a standard for identification).

Samples of the precipitate formed from 0.242M $Ca(NO_3)_2/CaCl_2$ and 0.145M $(NH_4)_2HPO_4/NaH_2PO_4$ at 37 °C were calcined at 600 °C and 1000 °C for 10h. The FT-IR spectrum of the precipitate calcined at 600 °C showed the transformation of the precipitate into β-$Ca_3(PO_4)_2$ (β-TCP) (Fig 3.17b). At 1000 °C, the precipitate had transformed into β-$Ca_3(PO_4)_2$ as its FT-IR spectrum showed (Fig 3.17c). There was also the presence of some β-$Ca_2P_2O_7$.

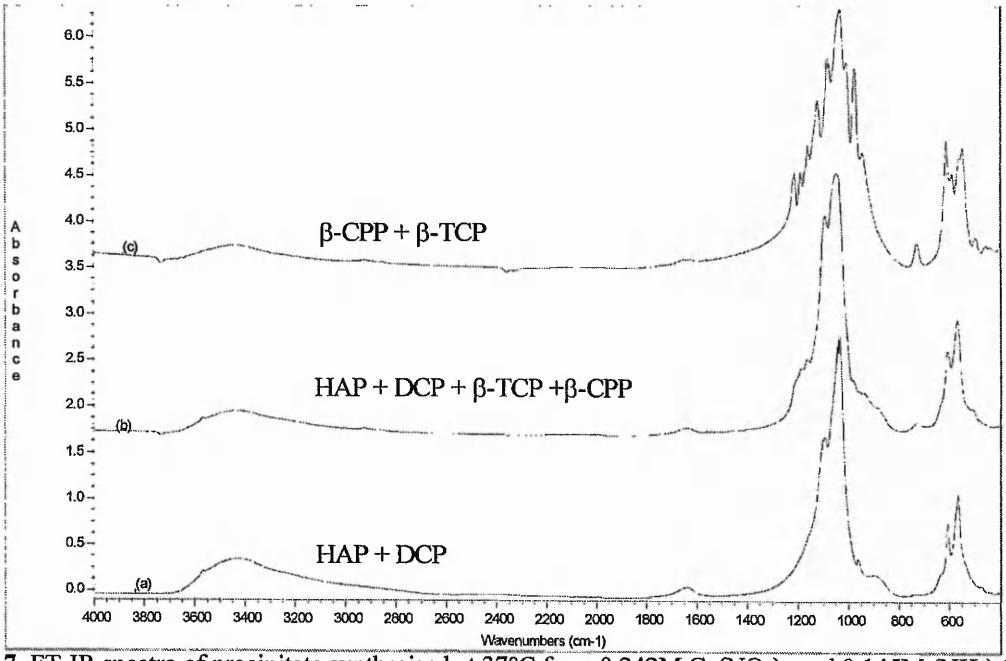

Fig 3.17. FT-IR spectra of precipitate synthesised at 37°C from 0.242M $Ca(NO_3)_2$ and 0.145M $(NH_4)_2HPO_4$ and then dried at (a) 250 °C for 1h and calcined at (b) 600 °C for 10h and (c) 1000 °C for 10h. (see appendix (I) for the FT-IR and XRD of the β-$Ca_2P_2O_7$ and β-$Ca_3(PO_4)_2$ used as a standard for identification).

XRD analysis confirmed the transformation of DCP and apatite crystals into β- $Ca_3(PO_4)_2$ and β-$Ca_2P_2O_7$ (fig. 3.18).

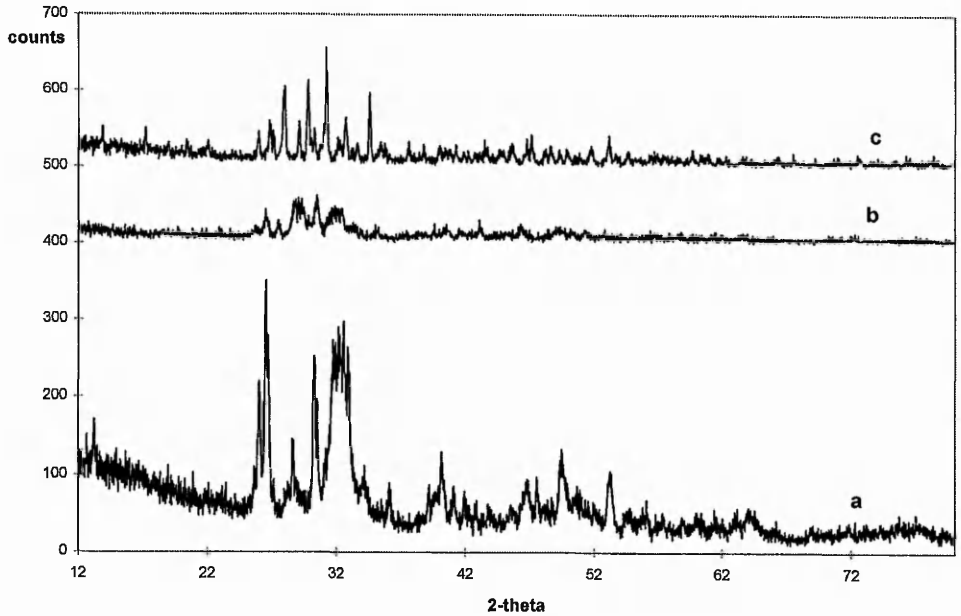

Fig 3.18. XRD spectra of precipitate synthesised at 37°C from 0.242M $Ca(NO_3)_2$ and 0.145M $(NH_4)_2HPO_4$ and then dried at (a) 250 °C for 1h and calcined at (b) 600 °C for 10h and (c) 1000 °C for 10h. (see appendix (I) for the FT-IR and XRD of the β-$Ca_2P_2O_7$ and β-$Ca_3(PO_4)_2$ used as a standards for identification).

EDX analysis gave a Ca/P=1.59 ± 0.16 for β-$Ca_3(PO_4)_2$ and Ca/P=1.05 ± 0.15 for β-$Ca_2P_2O_7$.

Table 3.6 lists the d-spacings and Miller indices obtained from electron diffraction for the precipitate calcined at 1000 °C which corresponds to β-$Ca_2P_2O_7$ and β- $Ca_3(PO_4)_2$ (JCPDS 9-346 and 9-169).

d-spacings	**Miller indices (β-$Ca_2P_2O_7$ JCPDS 9-346, β-$Ca_3(PO_4)_2$ JCPDS 9-169)**	
3.753	(1 1 4)	β-$Ca_2P_2O_{7(w)}$
3.042	(0 0 8)	β-$Ca_2P_2O_{7(s)}$
2.953	(2 1 1)	β-$Ca_2P_2O_{7(m)}$
2.404	(2 1 6)	β-$Ca_2P_2O_{7(m)}$
	(1 2 11)	β- $Ca_3(PO_4)_{2(m)}$
1.859	(3 2 0)	β-$Ca_2P_2O_{7(m)}$
1.793	(3 0 8)	β-$Ca_2P_2O_{7(w)}$
	(5 0 2)	β- $Ca_3(PO_4)_{2(m)}$
1.545	(5 1 7)	β- $Ca_3(PO_4)_{2(m)}$
1.460	(1 5 11)	β- $Ca_3(PO_4)_{2(w)}$

Table 3.6 d-spaces (Å) and Miller indices for the material precipitated from 0.242M $Ca(NO_3)_2$ and 0.145M $(NH_4)_2HPO_4$ at 23 °C and calcined at 1000 °C for 10h. (s) strong, (m) medium, (w) weak.

3.3.6 The formation and transformation of calcium phosphate crystals

The formation and transformation of calcium phosphates *in vitro* occurs in several distinct steps which can be followed by monitoring pH changes as a function of time. Figure 3.19

shows the pH changes with time during the precipitation reactions from solutions containing 10 mM $Ca(NO_3)_2$ and 6 mM $(NH_4)_2HPO_4$ at 23°C and 37°C.

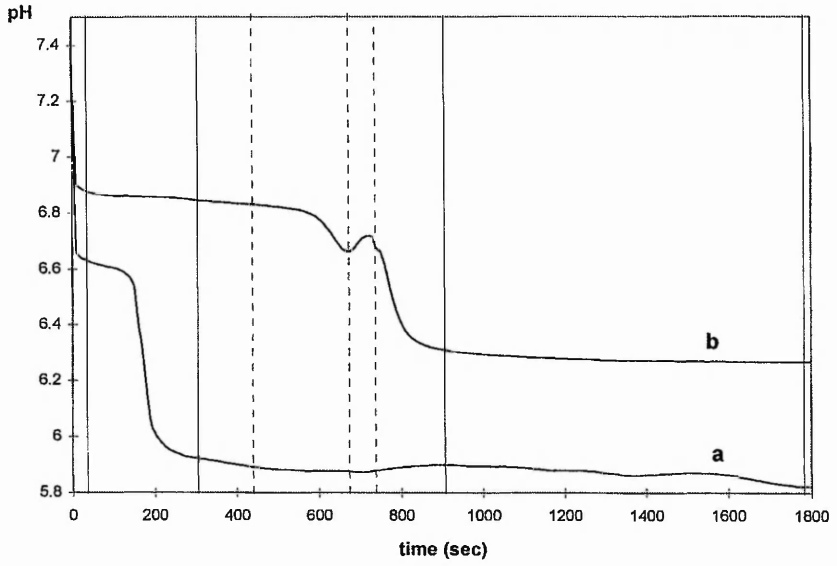

Fig 3.19 pH changes with time during precipitation reactions from solutions containing 10 mM $Ca(NO_3)_2$ and 6 mM $(NH_4)_2HPO_4$ at a) 37°C and b) 23°C (····· time when samples were taken for XRD and FT-IR analysis only, ——— time when samples were taken for XRD, FT-IR and TEM analysis).

At 23°C, after the first sharp pH drop due to the addition of the calcium solution, there was a period of more or less constant pH. During this time nucleation and formation of the precursors occurred. Samples taken after ca.1 min of reaction showed the presence of spherical particles of ca. 100 nm diameter and Ca/P =1.1 ± 0.4 (fig 3.20a). The structures which grew, forming colloidal chains, were amorphous as they did not give electron diffraction patterns. After 5 min, the particles had a flake-like structure (fig 3.20b). They grew in clusters forming aggregates. The structure gave a weak polycrystalline electron diffraction pattern and had a Ca/P =1.4 ± 0.2. FT-IR and XRD analysis of these samples were characteristic of a poorly crystalline apatitic calcium phosphate phase (fig 3.21a) and fig 3.22a). After ca. 10 min of constant pH, there was a pH drop and two different types of

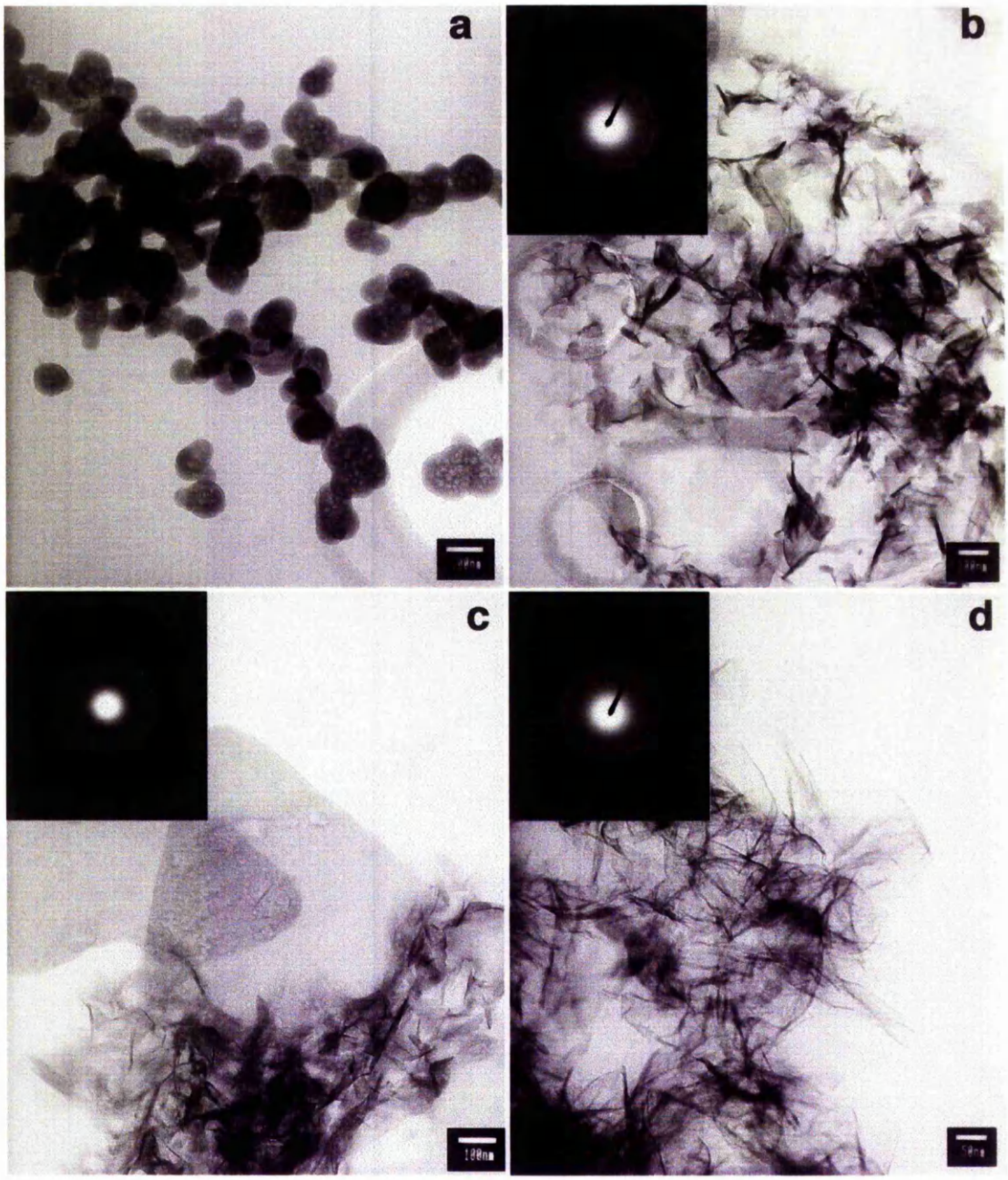

Figure 3.20 Calcium phosphate was precipitated from a solution containing 10 mM $Ca(NO_3)_2$ and 6 mM $(NH_4)_2HPO_4$ at 23°C. During the precipitation reaction samples were taken for TEM analysis at a) 1 min, b) 5 min, c) 15 min and d) 30 min of reaction. The d-spacings obtained for b and d were ca. 2.78 Å and 3.46 Å corresponding to the HAP Miller Indices (1 1 2) and (0 0 2) (JCPDS 9-432). The electron diffraction at c corresponds to the plate-like structure and the d-spacings obtained were attributed to the DCP Miller Indices (-1 1 2) and (2 -1 1) (JCPDS 9-80).

plate-like crystals corresponding to dicalcium phosphate (Ca/P 1.03) and OCP (Ca/P 1.6 ± 0.3) (fig 3.20c) were observed in the TEM. FT-IR and XRD analysis of samples extracted at this time confirmed the formation of this phase (fig 3.22a and fig 3.22b) Then there was an increase of pH due to the partial dissolution of OCP and apatite crystals which were less stable at that pH than DCP[41]. The crystals at this point were less crystalline than in the early stage as evidenced by the FT-IR spectrum of the precipitate which presented shifts in the main reflections due to the loss of crystallinity (fig 3.21c) and the XRD pattern corresponded to a less crystalline precipitate (fig 3.22c). Finally, there was a last pH drop attributed to the recrystallisation of the main phase, dicalcium phosphate. Non-stoichiometric hydroxyapatite (Ca/P 1.3 ± 0.3) was also detected in the final precipitated (fig 3.20d).

FT-IR analysis of the final precipitate showed shifts of the bands attributed to the HPO_4^{2-} stretching modes of DCP to lower wavelength values (1107 cm^{-1}, 1076 cm^{-1} and 905 cm^{-1}) due to the contribution of the apatite presence in the precipitate (fig 3.21d).

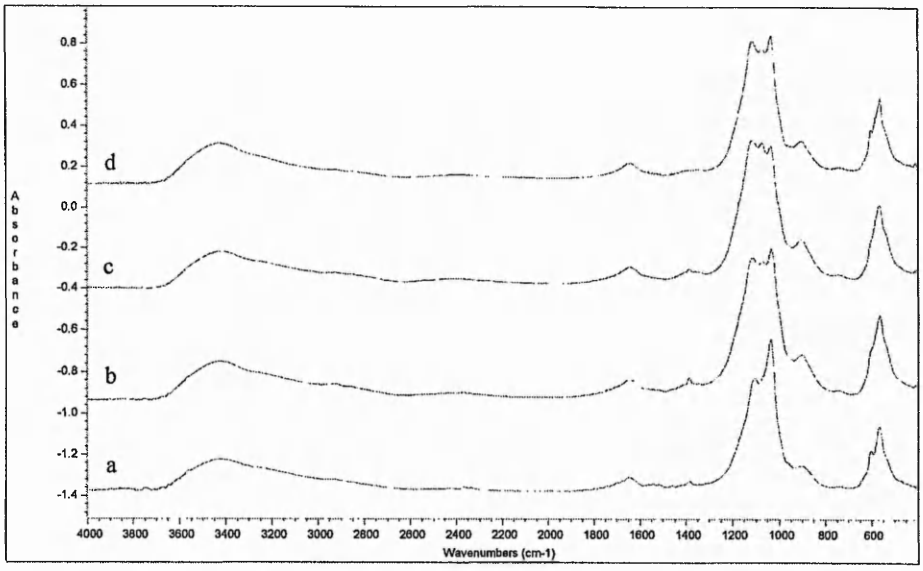

Fig 3.21 FT-IR spectra of the precipitate formed at 23°C from 10mM $Ca(NO_3)_2$ and 6 mM $(NH_4)_2HPO_4$ at a) 5 min, b) 11 min, c) 12 min, and d) 30 min.

The XRD spectrum showed the presence of apatite in the area to the low 2-theta side of the reflections at around 33° two-theta and to the low two-theta side of the reflection at ca. 27° two-theta (fig 22d).

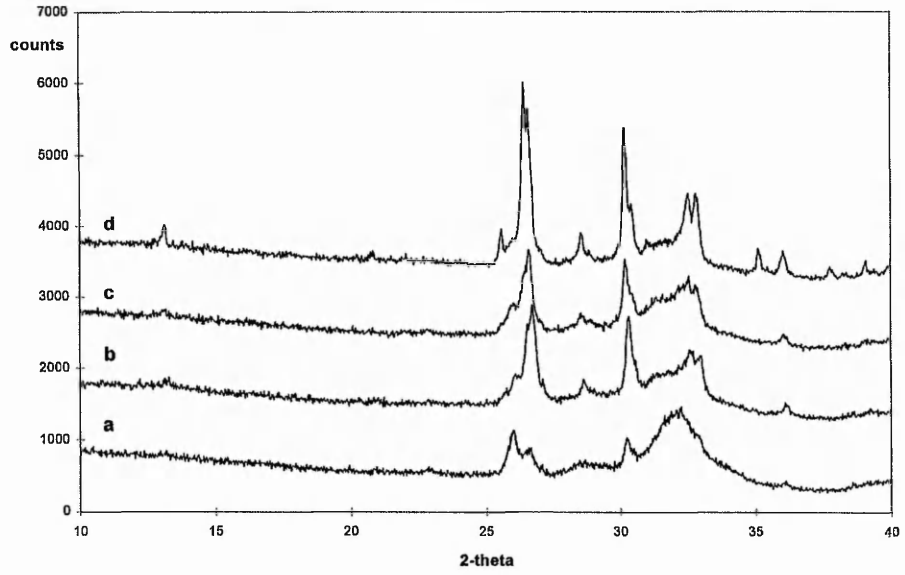

Fig 3.22 XRD patterns of the precipitate formed at 23°C from a solution containing 10 mM $Ca(NO_3)_2$ and 6 mM $(NH_4)_2HPO_4$ at a) 5 min, b) 11 min, c) 12 min, and d) 30 min.

Fig 3.19b also shows the pH changes with time during reaction at 37°C. The crystallisation process was speeded up with the increase of temperature and for samples taken at the early stages, OCP plates (Ca/P 1.6 ± 0.3), flakes and needles (1.6 ± 0.1) were detected (1 min) (fig. 3.23a). DCPD was not detected during electron microscopy studies. After 5 min the flakes (Ca/P 1.78 ± 0.28) gave an electron diffraction pattern showing a preferential orientation corresponding to the crystal growth direction (fig. 3.23b). The d-spacing values obtained from the electron diffraction patterns were ca. 2.87 Å which could be attributed to OCP (JCPDS 26-1056) and 3.44 Å which could be attributed to OCP and HAP (JCPDS 9-432). After 15 min plate-like OCP, needles and flakes were observed, although the

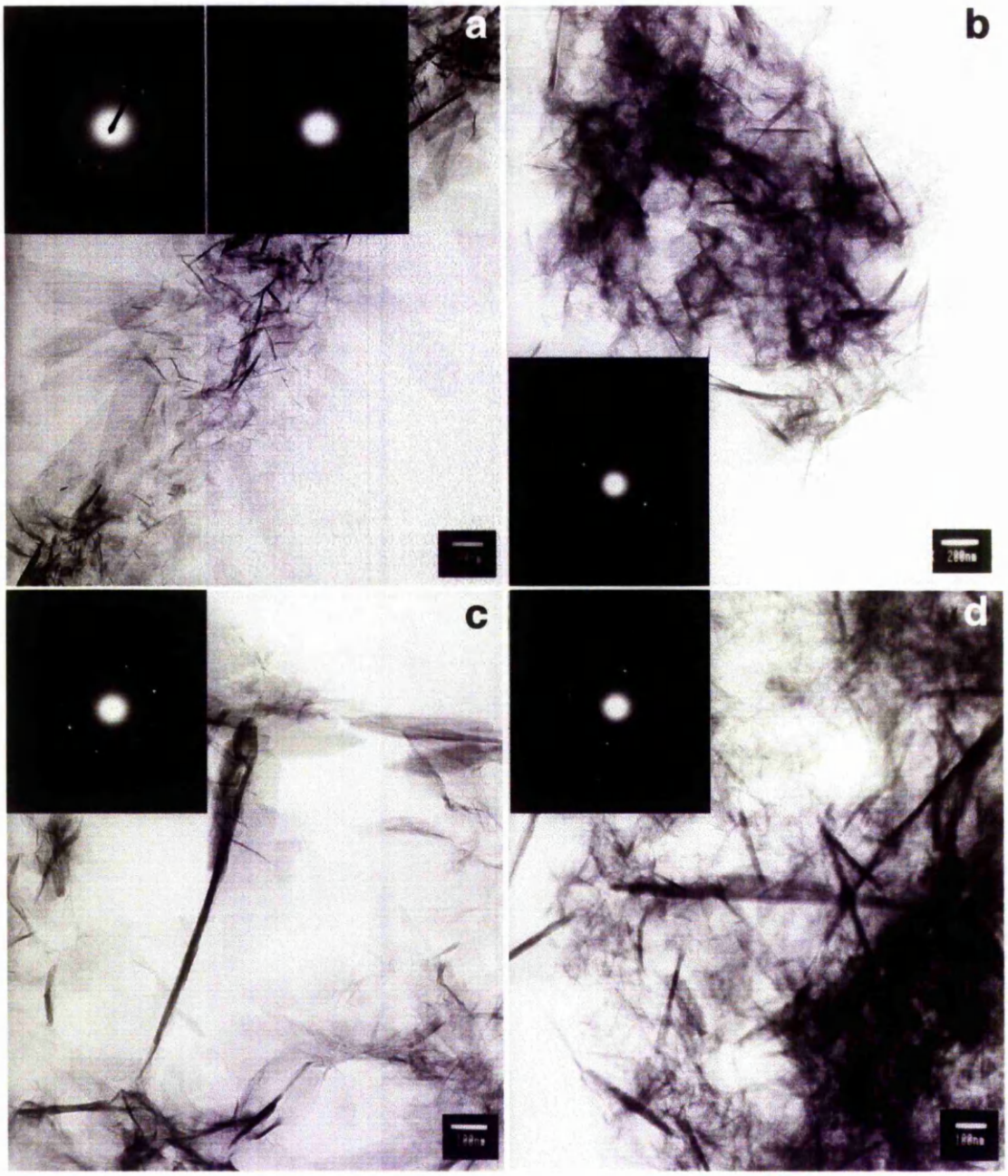

Figure 3.23 Calcium phosphate was precipitated from a solution containing 10 mM $Ca(NO_3)_2$ and 6 mM $(NH_4)_2HPO_4$ at 37°C. During precipitation reaction samples were taken for TEM analysis at a) 1 min, b) 5 min, c) 15 min and d) 30 min of reaction. a) The top left electron diffraction pattern was obtained from the needles and the top right electron diffraction was obtained from the plate-like OCP crystals, (see table 3.7 for d-spacings).

needles were observed more often (fig. 3.23c,d). The Ca/P ratio for these structures varied little and were 1.5 ± 0.2 for the plates and flakes, and 1.6 ± 0.1 for the needles.

Table 3.7 shows the d-spacings calculated from electron diffraction data for the different structures during the precipitation process.

time (min)	plate	needle	flakes	OCP (JCPDS-26-1056)	HAP (JCPDS-9-432)
1	9.219			9.360	
	5.431			5.417	
	3.945			3.919	
		3.887		3.879	3.88
	3.644			3.660	
	3.508	3.539	3.539		3.51
	3.478	3.478		3.492(s)	
	3.447	3.447		3.441	3.44(s)
	3.331	3.418		3.311	
	3.223			3.209	
	3.122	3.171			3.17
	2.893	3.097		3.117	3.08
	2.873		2.852	2.873	
	2.832	2.832		2.833(s)	2.814(s)
	2.812	2.812			
		2.753		2.745	2.778(s)
		2.661			2.631(s)
	2.574			2.567	2.296
	2.292				
	2. 278			2.271	
		2.265		2.265	2.262(s)
		2.166		2.158	
			1.924		
	1.982			1.990	
	1.870				1.871
	1.861	1.861			1.754
	1.746	1.762		1.745	
		1.724			
	1.408				1.722
					1.407
5		4.719			4.72
		3.964		3.919	4.07
	3.478			3.492	3.51
		3.447	3. 447	3.441(s)	3.44(s)
	2.852		3.418	3.424(s)	
			2.873	2.873	
		2.812			2.814(s)
		2.802		2.779(s)	2.778(s)
		2.292			2.296
		1.982		1.990	
			1.924	1.929	
	1.739			1.743	1.722

Table 3.7. d-spacings (Å) for the different crystal morphologies from the precipitate formed during reaction between 1-30 min at 37°C and d-spacings for OCP (JCPDS 26-1056) and HAP (JCPDS 9-432).

time (min)	plate	needle	flakes	OCP (JCPDS-26-1056)	HAP (JCPDS-9-432)
15		3.508		3.492	2.51
	3.478	3.478	3.478		
	3.447			3.441(s)	3.44(s)
	3.097				3.08
	2.852		2.873	2.873	
	2.832		2.832	2.833(s)	
		2.792	2.812		2.814(s)
			2.792	2.779(s)	2.778(s)
	2.625				2.631(s)
			2.265		2.262(s)
	2.002				2.000
			1.972		
		1.835	1.879		1.871
				1.837	
	1.827	1.746		1.832	
		1.724		1.745	
				1.722	
	1.709				
30	8.435				8.17
		3.508			3.51
		3.478		3.492	
	3.417			3.424(s)	
	3.388			3.378	
		3.197		3.180	3.17
	3.146	3.146		3.132	
		2.873		2.873	
		2.832		2.833(s)	
	2.792				2.814(s)
	2.772			2.779(s)	2.778(s)
	2.697			2.707	
	2.679			2.671(s)	
	2.660				
	2.558			2.567	
	2.332	2.332		2.335	
		1.934		1.936	
		1.915		1.914	
		1.870			1.871
	1.853				1.841(s)
		1.754			1.754

continuation Table 3.7. d-spacings (Å) for the different crystal morphologies from the precipitate formed during reaction between 1-30 min at 37°C and d-spacings for OCP (JCPDS 26-1056) and HAP (JCPDS 9-432).

The d-spacings obtained from the plate-like structure after 1 and 5 min were attributable to OCP (JCPDS 26-1056). The d-spacings obtained for the needle and flake-like structures were attributable to both OCP(JCPDS 26-1056) and HAP (JCPDS 9-432). After 15 min,

the flake-like crystals exhibited d-spacings which corresponded to HAP. After 30 min, the plate-like crystals showed d-spacings which could be attributed to OCP and the needle-like crystals showed d-spacings attributable to both OCP and HAP. The polycrystalline electron diffraction ring patterns obtained for the flakes after 30 min were very diffuse indicating low crystallinity.

3.4 Discussion

The nature of the calcium phosphate phase which forms during precipitation from aqueous solution is markedly dependent upon the calcium and phosphate concentration, pH, T, ionic strength. Some of these factors, such as pH, temperature, type and concentration of starting materials have been studied. Changes in any of these factors will affect preferentially the rates of one or more processes involved (nucleation, transformation and crystal growth), thus changing the properties of the precipitate.

At very low pH (pH<4.0) the system is governed by the solubility of $Ca(H_2PO_4)_2 \cdot H_2O$. At a higher pH (up to 6.00) the system is governed by the solubility of $CaHPO_4 \cdot 2H_2O$. Above pH 6.2, $CaHPO_4 \cdot 2H_2O$ is unstable and undergoes spontaneous hydrolysis[40]. It has been reported that the hydrolysis product exhibits the crystal structure of hydroxyapatite which shows a variable composition and forms very small crystals[40]. At near-neutral or slightly alkaline pH's, HAP is the least soluble phase and in the absence of kinetic complications it should be the thermodynamically most stable phase[31].

For experiments where the pH was held at 7.4, the main calcium phosphate phase precipitated was apatitic in nature. The product was non stoichiometric and exhibited low crystallinity, characteristics of calcium phosphates obtained by precipitation synthesis. It has been suggested that these characteristics are mainly due to the fact that amorphous

calcium phosphate (ACP) with low Ca/P ratio precipitates as a gel-like precursor and with much water being incorporated[40].

When precipitation was carried out at high supersaturation (0.242M Ca^{2+} and 0.145M $H_2PO_4^-$/ HPO_4^{2-}) , there was no difference in the main calcium phosphate phases formed at 23 °C irrespective of the precursors used in the precipitation reaction. However, at 37 °C, the proportion of calcium phosphate dibasic present in the final precipitate was much higher compared to the precipitate obtained from the moderate supersaturation experiments (10 mM Ca^{2+} and 6 mM HPO_4^{2-}).

When precipitation was carried out at 23°C using 10 mM and 6 mM concentration of calcium and phosphate concentrations, despite the main phase precipitated being DCP (as detected by XRD analysis), DCP was difficult to detect by infrared spectroscopy. The infrared spectrum presented bands attributable to the presence of an apatitic material. The material precipitated at 37° C from the highest concentration of calcium and phosphate ions had DCP and apatite crystals. The presence of DCP crystals shifted the values expected for apatite and the appearance of a shoulder at around 900-870 cm^{-1} corresponding to HPO_4^{2-} found in DCP and non-stoichiometric hydroxyapatite. The presence of DCP was confirmed by XRD analysis.

When precipitation was carried out at 37 °C using 10 mM Ca^{2+} and 6 mM $(NH_4)_2HPO_4$, an apatitic calcium phosphate phase was formed. In addition to the absorption bands assigned to apatite, the FT-IR spectra also exhibited a band at approximately 900 cm^{-1} indicating the presence of HPO_4^{2-} from non-stoichiometric apatite. The need for several techniques to identify the crystal phases present in the final product was obvious from these studies.

When the precipitate formed at 23°C was heated at 600 °C and 1000 °C it transformed into β-$Ca_2P_2O_7$. This agreed with the results obtained by Berry *et al.* (1967) who reported that the pyrolysis of HPO_4^{2-} groups to pyrophosphate ($P_2O_7^{4-}$) occurs according to the reaction:

$$2\ HPO_4^{2-} \rightarrow P_2O_7^{4-} + H_2O.$$

Gravimetric analysis has shown that DCPD changes in air to β-$Ca_2P_2O_7$ when it is heated at 500-750 °C[29].

When the precipitated formed at 37°C was heated at 600 °C and 1000 °C it transformed into β-$Ca_3(PO_4)_2$ and β-$Ca_2P_2O_7$. Jarcho *et al.* have reported that both amorphous calcium phosphate and calcium deficient hydroxyapatite serve as thermochemical precursors for the formation of β-$Ca_3(PO_4)_2$[41]. The presence of β-$Ca_2P_2O_7$ in the material heated to such a temperature, again indicated the presence of calcium phosphate dibasic in the pre-calcined precipitate for the precipitated obtained from solutions containing the highest concentrations of calcium and phosphate, 0.242M and 0.145M respectively.

When NaH_2PO_4 was used as the phosphate precursor, at moderate supersaturation the main phase precipitated which was detected by XRD analysis was apatite but at high supersaturation both calcium phosphate dibasic and apatite were detected. Termine *et al.* (1970) found that Na^+, K^+ and citrate did not affect the transformation of ACP to HAP but Mg^{2+}, CO_3^{2-}, $P_2O_7^{4-}$ were effective stabilisers of ACP even when used at very low concentrations[42]. In this study Na^+ seemed to stabilise calcium phosphate dibasic at both room temperature and 37 °C when used together with high concentrations of calcium and phosphate ions.

The precipitation process proceeded in two distinct stages (see fig 3.20). Brecevic *et al.* (1972) obtained similar results by electron microscopy studies when precipitating

calcium phosphate at moderate supersaturation[19]. The first stage corresponded to the formation of an initial precipitate consisting of amorphous colloidal particles which showed chain-like agglomerates. In the second stage a crystalline precipitate formed. This precipitate was calcium phosphate dibasic which was insoluble at pH ≈ 5. Similar results were also obtained by Christoffersen *et al.* (1989) who investigated the formation of calcium phosphate at 15, 30 and 42 °C by electron microscopy[22]. They found that at 15 °C, DCPD nucleated and formed soon after mixing. At 30 and 42 °C the final product was a deficient form of calcium hydroxyapatite that they called d-HA. d-HA was preceded by an initial precipitation of an amorphous calcium phosphate phase called ACP1 which transformed into another amorphous calcium phosphate phase called ACP2 after which OCP and d-HA crystallised. They found that these transformations occurred faster the higher the temperature. ACP2 was considered necessary for the development of OCP and d-HA. However, at 30 °C if ACP1 was filtered off from the reaction mixture DCPD would only precipitate. They also reported that DCPD did not transform into HA. Gregory *et al.* (1970) found that through the pH range 4.0-6.4 the solubility of DCPD decreased significantly with increase in temperature[43]. The results obtained from this study corroborate the findings of Christoffersen *et al.* (1989)[19] findings and disagree with the findings of Tsuge *et al.* (1996)[25] who reported that at 25°C ACP transformed into DCPD. In the experimental conditions used in the current study initially ACP and DCPD formed. Then as ACP disappeared, OCP and apatite crystals appeared and DCPD crystals grew in size. ACP transformed into OCP and apatite but not into DCP, which formed independently from ACP.

There is no doubt in the existence of ACP as a first precursor in the formation of apatite crystals. In this study, ACP had a Ca/P slightly lower (1.1) than the Ca/P reported by others

researchers (1.4)[2]. The next precursor observed in this present study and the precursors described previously as an "OCP-like phase"[15] and as a "separate amorphous phase" ACP2[19] seemed to be the same calcium phosphate phase taken at different time points in the transformation process (fig 3.23b). It grows in clusters and consists of flake-like structures that presented both apatite and OCP structural characteristics as evidenced by electron diffraction data.

The classical formulation of the nucleation process has been used by many researchers to explain the nucleation of calcium phosphate at physiological conditions. Walton *et al.* (1967) reported that the stoichiometry of the initial phase in calcium phosphate precipitation at physiological pH was approximately 1.5 and it was thus similar to tricalcium phosphate $Ca_3(PO_4)_2$[44]. The product was metastable, since hydroxyapatite was known to be the stable phase under these conditions. The stoichiometry of a product $Ca_3(PO_4)_2$ represents the minimum number of ions in a neutral molecule and may therefore have a low entropy of formation. However although the stoichiometry is the same as tricalcium phosphate, the crystalline arrangement is unlikely to resemble that of the latter compound. Boskey *et al.* (1976) precipitated apatitic calcium phosphate in nature from low supersaturating solutions[11]. HAP formed without an amorphous precursor phase when the solution was sufficiently dilute and the crystals grew in only one dimension, the hydroxyapatite c-axis, as a function of time. The growth of hydroxyapatite appeared to occur by a ripening process. In contrast, Koutsoukos *et al.* (1980) prepared stoichiometric hydroxyapatite from solutions at physiological concentrations at 37 °C[45]. Feenstra *et al.* (1979) found OCP when moderate supersaturation (0.2-1.15M calcium / 0.12-0.74M phosphate) was used to precipitate calcium phosphate[21]. They reported the heterogeneous nucleation of ACP and proposed OCP as an intermediate in the conversion of ACP to an

apatitic calcium phosphate. Eanes *et al.* (1965) reported the formation of an ACP when precipitation was carried out at pH=10.5-9.8 and 30.5 °C[13]. They applied Ostwald ripening theory to discuss the growth of the precipitate in their system. ACP formed immediately after mixing. After a progressive transformation ACP totally converted to HAP.

In this system, the crystals seem to grow following the same rules. The pH rise observed between the two pH drops for the materials precipitated at 23 °C can be attributed to the partial dissolution of the flakes and OCP crystals which became less stable and more soluble as the pH decreased. At 37 °C, after 5 min of reaction, the OCP plates become so thin that sometimes they were difficult to detect in the electron microscope due to the lack of imaging contrast. OCP was more stable at 37°C than at 23 °C. The flakes had d-spacings, as measured by electron diffraction, that could be attributed to HAP or OCP and some measured d-spacings had values in between the values of the two structures. It seems that this precursor might have the ability to convert to HAP or OCP depending on the surrounding conditions. At very low concentration of calcium and phosphate, they could develop into HAP, but as the concentration of the solution increased and the kinetics then became more important the flakes converted into OCP which later transformed to HAP.

In conclusion, the nature of the calcium phosphate phase which forms during precipitation from aqueous solution is markedly dependent upon the calcium and phosphate concentration, pH, T, ionic strength. Na^+ favoured the formation of DCPD over HAP when high concentrations of calcium and phosphate were used. The transformation of ACP to HAP occurred by the Ostwald ripening process. At very low concentrations of calcium and phosphate ACP may develop directly into HAP but as the concentrations of calcium and phosphate in the solution increase, ACP transforms to HAP through the OCP intermediate.

3.5 References

1. Posner, A.S. (1969). Crystal Chemistry of Bone Mineral. *Physiol. Rev.* **49**:760.
2. Nancollas, G.H. and Mohan, M.S. (1970). The Growth of Hydroxyapatite Crystals. *Arch. Oral Biol.*, **15**:1970.
3. Meyer, J.L., Eick, J.D., Nancollas, G.H. and Johnson, L.N. (1972). A Scanning Electron Microscopic Study of the Growth of Hydroxyapatite Crystals. *Calcif. Tiss. Res.*, **10**:91.
4. Meyer, J.L. and Nancollas, G.H. (1973). The Influence of Multidentate Organic Phosphonates on the Crystal Growth of Hydroxyapatite. *Calcif. Tiss. Res.* **13**:295.
5. Meyer, J.L., McCall, J.T., Smith, L.H. (1974). Inhibition of Calcium Phosphate Crystallisation by Nucleoside Phosphate. *Calcif. Tiss. Res.* **15**:287.
6. Nancollas, G.H. and Wefel, J.S. (1976). Seeded Growth of Calcium Phosphates: Effect of Different Calcium Phosphate Seed Material. *J. Dent. Res.*, **55**(4):617.
7. Nancollas, G.H. and Tomazic, B. (1974). Growth of Calcium Phosphate on Hydroxyapatite Crystals. Effect of Supersaturation and Ionic Medium. *J. Phys. Chem.*, **78**(22):2218.
8. Eanes, E.D. (1976). The Interaction of Supersaturated Calcium Phosphate Solutions with Apatitic Substrates. *Calcif. Tiss. Res.*, **20**:75.
9. Eanes, E.D., and Meyer, J.L. (1977). The Maduration of Crystalline Calcium Phosphates in Aqueous Suspensions at Physiologic pH. *Calcif. Tiss. Res.*, **23**:259.
10. Nelson, D.G.A., Salimi, H. and Nancollas, G.H. (1986). Octacalcium Phosphate and Apatite Overgrowths: A Crystallographic and Kinetic Study. *J. Colloid Interf. Science*, **110**(1):32.
11. Robinson, R.A. (1952). An Electron-Microscopic Study of the Crystalline Inorganic Component of Bone and its Relationship to the Organic Matrix. *J. Bone & Joint Surg.*, **34A**:389.
12. Boskey, A.L. and Posner, A.S. (1976). Formation of Hydroxyapatite at Low Supersaturation. *J. Phys. Chem.*, **80**(1):40.
13. Eanes, E.D., Gillessen, I.H. and Posner, A.S. (1965). Intermediate States in the Precipitation of Hydroxyapatite. *Nature*, **208**:365.

14.Boskey, A.L. and Posner, A.S. (1973). Conversion of Amorphous Calcium Phosphate to Microcrystalline Hydroxyapatite. A pH-Dependent, Solution-Mediated, Solid-Solid Conversion. *J. Phys. Chem.*, **77**(19):2313.

15.Eanes, E.D., Termine, J.D. and Nylen, M.U. (1973). An Electron Microscopic Study of the Formation of Amorphous Calcium Phosphate and its Transformation to Crystalline Apatite. *Calcif. Tiss. Res.*, **12**:143.

16.Posner, A.S. (1973). Amorphous Calcium Phosphate in Hard Tissue. Particle Growth in Suspensions. Edited by A.L. Smith. Academic Press INC. London.

17.Posner, A.S. and Betts, F. (1975). Synthetic Amorphous Calcium Phosphate and its Relation to Bone Mineral Structure. *Acc. Chem. Res.*, **8**:273.

18.Blumenthal, N.C., Betts, F. and Posner, A.S. (1981). Formation and Structure of Ca-Deficient Hydroxyapatite. *Calcif. Tiss. Int.*, **33:**111.

19.Brecevic, L.J. and Füredi-Milhofer, H. (1972). Precipitation of Calcium Phosphates from Electrolyte Solutions. II The Formation and Transformation of the Precipitates. *Calcif. Tiss. Res.*, **10**:82.

20.Eanes, E.D., and Meyer, J.L. (1977). The Maduration of Crystalline Calcium Phosphate in Aqueous Suspensions at Physiological pH. *Calcif. Tiss. Res.* **23**:259.

21.Feenstra, T.P. and de Bruyn, P.L. (1979). Formation of Calcium Phosphates in Moderately Supersaturated Solutions. *J. Phys. Chem.*, **83**(4):475.

22.Christoffersen, J., Christoffersen, M.R., Kibalczyc, W., and Andersen, F.A. (1989). A Contribution to the Understanding of the Formation of Calcium Phosphates. *J. Cryst. Growth*, **94**:767.

23.Lazic, S. (1995). Microcrystalline Hydroxyapatite Formation from Alkaline Solutions. *J. Cryst. Growth,* **147**(1-2):147.

24.Graham, S. and Brown, P.W. (1996). Reactions of Octacalcium Phosphate to Form Hydroxyapatite. *J. Cryst. Growth*, **165**:(1-2):106.

25.Tsuge, H. Yoshizawa, S. and Tsuzuki, M. (1996). Reactive Crystallisation of Calcium Phosphate. *Trans IChemE*, **74**(A):797.

26.Francis, M.D. and Webb, W.C. (1967).Hydroxyapatite Formation from a Hydrated Calcium Monohydrogen Phosphate Precursor. *Calcif. Tiss. Res.*, **6**(4):335.

27.Brown, W.E. (1965). A Mechanism for Growth of Apatitic Crystal. In Tooth Enamel. Edited by Stack, M.V. and Fearnhead. Wright & Sons. Bristol.

28.Posner, A.S., Blumenthal, N.C. and Betts, F. (1980). Formation and Structure of Chemically Precipitated Hydroxyapatites. Proceedings of the 2nd International Congress on Phosphorous Compounds, pp. 25. Boston.

29.Berry, E.E. (1967). The Structure and Composition of Some Calcium-Deficient Apatites. *J Inorg. Nuc. Chem.*, **29**:317.

30.Füredi-Milhofer, H., Brecevic, L.J., Oljica, E., Purgaric, B., Gass, Z. and Perovic, G. (1971). The Influence of Precipitation Conditions on the Formation and Transformation of Calcium Phosphate Precipitates. Tooth Enamel II, pp 109. Edited by Fearnhead, R.W. & Stack, M.V. John Wright&Sons.

31.Nancollas, G.H. (1980). The Precipitation of Calcium Phosphates. Thermodynamic and Kinetics Considerations. Proceedings of the 2nd International Congress on Phosphorous Compounds, pp. 11. Boston.

32.Cheng, P.T. and Pritzker, K.P.H. (1983). Solution Ca/P Ratio Affects Calcium Phosphate Crystal Phases. *Calcif. Tiss. Int.*, **35**:596.

33. Hidaka, S., Abe, K. and Liu, S.Y. (1991). A New Method For the Study of the Formation and Transformtaion of Calcium Phosphate Precipitates: Effects of Several Chemical Agent and Chinese Folk Medicines. *Archs. Oral Biol.* **36**(1):49.

34.Berry, E.E. and Baddiel, C.B. (1967). The Infra-red Spectrum of Dicalcium Phosphate Dihydrated (Brushite). *Spectrochim. Acta* **23A**:2089.

35.Rey, C., Shimizu, M., Collins, B., and Glimcher, M.J. (1991). Resolution-Enhanced Fourier-Transform Infrared-Spectroscopy Study of the Environment of Phosphate Ions in the Early Deposits of a Solid-Phase of Calcium Phosphate in Bone and Enamel and their Evolution with age. I. Investigations in the ν_4 PO_4 domain. *Calcif. Tiss. Int.* **46**:384.

36.Rey, C., Shimizu, M., Collins, B., and Glimcher, M.J.(1991). Resolution-Enhanced Fourier-Transform Infrared-Spectroscopy Study of the Environment of Phosphate Ions in the Early Deposits of a Solid-Phase of Calcium Phosphate in Bone and Enamel and their Evolution with age. II. Investigations in the ν_3 PO_4 domain. *Calcif. Tiss. Int.* **49**:383.

37.Gadaleta, S.J., Paschalis, E.P., Betts, F., Mendelsohn, R. and Boskey, A.L.(1996). Fourier Transform Infrared Spectroscopy of the Solution-Mediated Conversion of

Amorphous Calcium Phosphate to Hydroxyapatite: New Correlations Between X-ray Diffraction and Infrared Data. *Calcif. Tiss. Int.* **58**:9.

38.Mullin, J.W. (1993). Crystallization. 3rd Edition. Butterworth-Heinamann. Sulfok.

39.Cullity, B.D. (1978). Elements of X-Ray Diffraction, 2nd ed., Addison-Wesley, Massachusetts.

40.Kanazawa, T. (1989). Materials Science Monographs, 52: Inorganic Phosphate Materials, Elsevier.

41.Jarcho, M., Bolen, C.H., Thomas, M.B., Bobick, J., Kay, J.F. and Doremus, R. H. (1976). Hydroxyapatite Synthesis and Characterisation in Dense Polycrystalline Form. *J. Mater. Science*, **11**:2027.

42.Termine, J.D., Peckauskas, R.A., Posner, A.S. (1970). Calcium Phosphate Formation *in vitro* II. Effect of Environment on Amorphous-Crystalline Transformation. *Arch. Biochem. Biophys.* **140**:318.

43.Gregory, T.M., Moreno, E.C. and Brown, W.E. (1970). Solubility of $CaHPO_4 \cdot 2H_2O$ in the System $Ca(OH)_2$-H_3PO_4-H_2O at 5, 15,25 and 37.5°C. *J. Res. Nat. Bureau Stard.*, **74**:461.

44.Walton, A.G., Bodin, W.J. Bodin, Füredi, H. and Schwartz, A. (1967). Nucleation of Calcium Phosphate from Solution. *Canadian J. Chem.*, **45**:2695.

45.Koutsoukos, P. Amjad, Z., Tomson, M.B. and Nancollas, G.H. (1980). Crystallisation of Calcium Phosphates. A Constant Composition Study. *J. Am. Chem. Soc.*, **102**(5):1553.

CHAPTER 4: EFFECT OF SOLUBLE SILICON SPECIES ON CALCIUM PHOSPHATE PRECIPITATION

4.1 Introduction

Silicon is the second most abundant element in the earth's crust after oxygen and it is an element required in trace amounts for life. The human ingestion of silicon in its most bioavailable form, silicic acid, has been estimated to be 30 mg Si per day with 60% of this from cereals and 20% from water and drinks[1]. The normal human serum silicon concentration is ca. 50 μg/dl[2]. The silicon is present almost entirely as free soluble monosilicic acid. The involvement of silica in osteogenesis and connective tissue metabolism is well-established. The level of silica in connective tissues (100 ppm) and in regions of active calcification is approximately 100 times higher than most other tissues (1-2 ppm)[3]. In the early 70's Carlisle reported that silicon might be essential for normal bone growth and development[4-6]. Experiments with chicks showed that birds on a silicon-deficient diet presented small and flexible bone structures. Their femura and tibiae fractured more easily under pressure than those birds on a silicon-supplemented diet[7]. Shwarz and Milne, (1972), also reported that silicon had growth promoting effects in rats. Rats maintained on low silicon diets showed skull and pigmentation abnormalities[8]. Silicon effects appear to be primarily on the synthesis of organic matrix components of bone and cartilage[2], but also on the incorporation of mineral itself. Silicon and silica-containing particles have also been found in the heart and tongue of mice and supragingival dental calculus from humans and Japanese Monkeys[9-11]. Damen *et al.,* (1989), reported that silica acts as an heterogeneous nucleation substrate with the formation of HAP nuclei favoured over the formation of other calcium phosphate (CP) nuclei[12]. It has been proposed that

silicate ions might play an important role in the formation of apatite nuclei[12]. Other recent studies have shown that silica and silicate ions promote calcification[13]. Tanizawa *et al.*, (1995), proposed that ACP is formed in an early stage followed by formation of DCPD and HAP[14]. They reported that the transformation was enhanced by the presence of silica. Table 4.1 summarises the studies of the effect of silicon species on calcium phosphate precipitation over the last few years.

silicon species	experimental conditions	results	researchers
silicic acid	T=17°C, pH=7.4 1 mM $[Ca^{2+}]$=2.5mM $[H_2PO_4^-]$=6.6 mM	No inhibition of initial precipitation of calcium phosphate. No alteration of phase composition or microstructure	Birchall *et al.*, (1986)
silicic acid polysilicic acid silica gel	T=37 °C, pH=7.2 0-5 mM $[Ca^{2+}]$=1mM $[H_2PO_4^-]$=7.5mM	Stimulation of CP precipitation associated with polymerized rather than monomeric silicic acid	Damen *et al.* (1989)
silicic acid silica gel	T=37 °C, pH=7.4 0-30 mM, 0.05-10 mg/ml $[Ca^{2+}]$=3mM $[H_2PO_4^-]$=3mM	Stimulation of CP precipitation associated with polysilicic acids at low levels (0.01-0.1 mM) Inhibitory effect at 3.0-30 mM of silicic acid and 10 mg/ml silica Silica gel stimulated the rate of HA transformation (0.05-1.5 mg/ml)	Hidaka *et al.* (1993)
silicate ions silica gel	T=25 °C, pH=7.25 0-4.4 mM $[Ca^{2+}]$=6mM $[H_2PO_4^-]$=3.2mM	Silicate ions stabilised DCPD Silica was a substrate for ACP and DCPD nucleation	Tanizawa *et al.* (1995)

Table 4.1 Summary of studies of the effect of silica on the precipitation of calcium phosphate crystals.

Although other authors found that the stimulating effect seemed to be associated to polymerised rather than monomeric silicic acid (table 4.1), the current study is about the effects of orthosilicic acid on calcium phosphate nucleation and transformation. Electron microscopic studies on nucleation and crystal growth during the formation of calcium phosphate crystals in the presence of orthosilicic acid have been performed.

4.2 Materials and Methods

Materials

Diammonium phosphate dibasic 99% ($(NH_4)_2HPO_4$) from Sigma Chemical Co.

Calcium nitrate anhydrous 98+% ($Ca(NO_3)_2$ from Avocado Research Chemicals Ltd.

Silicate standard solution (1000 ppm as SiO_2) from BDH.

Sodium Chloride 99% (NaCl) from BDH. Ultrapur nitric acid from Prolabo.

Method

Calcium phosphate powders were made as described in chapter 2. The effect of orthosilicic acid was studied in the precipitation of calcium phosphate using a final concentration of 0.242 M and 0.145 M of calcium nitrate and diammonium hydrogen phosphate solutions respectively. In experiment 1 the pH was kept constant at 7.4 during precipitation. A second experiment was carried out with the same conditions as experiment 1 but there was no further pH control after adjusting the pH of the phosphate solution to 7.4. Finally a third experiment (experiment 3) was carried out using concentrations of 10 mM and 6mM of calcium and phosphate solutions respectively. The Ca/P ratio was 1.67. In the three experiments, 0, 0.082, 0.164, 0.409, and 0.818 mM of orthosilicic acid were added to the phosphate solution prior adjusting the pH to 7.4 and prior to adding the calcium nitrate solution except for experiment 1 where orthosilicic acid was added to the calcium solution to study the effects of silicic acid on the precipitate depending upon which solution the silicic acid was added to. $Ca(NO_3)_2$ and $(NH_4)_2HPO_4$ were used as precursors. The final concentrations of orthosilicic acid were 0, 0.041, 0.082, 0.204 and 0.409 mM. In experiment 3, NaCl was used as a electrolyte to keep the ionic strength constant at 0.165M. The pH was monitored during the precipitation process and samples were taken for TEM

analysis as described in chapter 2. After 30 min, the precipitate formed was filtered and washed with deionized distilled H_2O. The samples were dried at 250 °C for 1h and then analysed by FT-IR, XRD, EDX and TEM (see chapter 2).

Statistics

The mean ± standard deviation was calculated from four/eight experiments using the t- test Student. Statistical comparisons were made by the F-distribution test. The difference was considered significant at $p < 0.05$.

4.3 Results

Experiment 1

This experiment was designed to assess the effect of silicic acid in either the phosphate solution or the calcium solution on the nature of the precipitate formed. 0.242 M $Ca(NO_3)_2$ and 0.145 M $(NH_4)_2HPO_4$ solutions were used and the pH was kept at 7.4 during precipitation by addition of 1M HNO_3. The calcium phosphate phase precipitated was apatite (see chapter 3). The effect of orthosilicic acid was independent of the solution in which it was initially added.

precursor solution (expt. 1)	**0 mM $Si(OH)_4$**	**0.082 mM $Si(OH)_4$**	**0.204 mM $Si(OH)_4$**	**0.409 mM $Si(OH)_4$**
$Ca(NO_3)_2$	0.864 ± 0.197	0.916 ± 0.117	1.039 ± 0.012	1.048 ± 0.027
$(NH_4)_2HPO_4$		1.035 ± 0.005	1.017 ± 0.005	1.046 ± 0.011

Table 4.1 Weights of precipitate in g for n=2 for precipitate formed at 23°C and pH=7.4 after drying at 250°C for 1h,(* $p<0.05$).

There was no significant difference between the yields obtained from samples precipitated in the absence or presence of orthosilicic acid.

FT-IR spectrum of the precipitate formed in the presence of orthosilicic acid showed a shift in the band at ca. 1095 cm^{-1} (control) to higher wavelength, 1109 cm^{-1}, indicating the presence of HPO_4^{2-} in the apatite structure. The bands at 960 cm^{-1} and 3570 cm^{-1} corresponding to OH^- vibration modes from hydroxyapatite disappear when increasing the concentration of orthosilicic acid present during precipitation and it seemed to be independent of which solution the silicic acid was initially present in (fig.4.1).

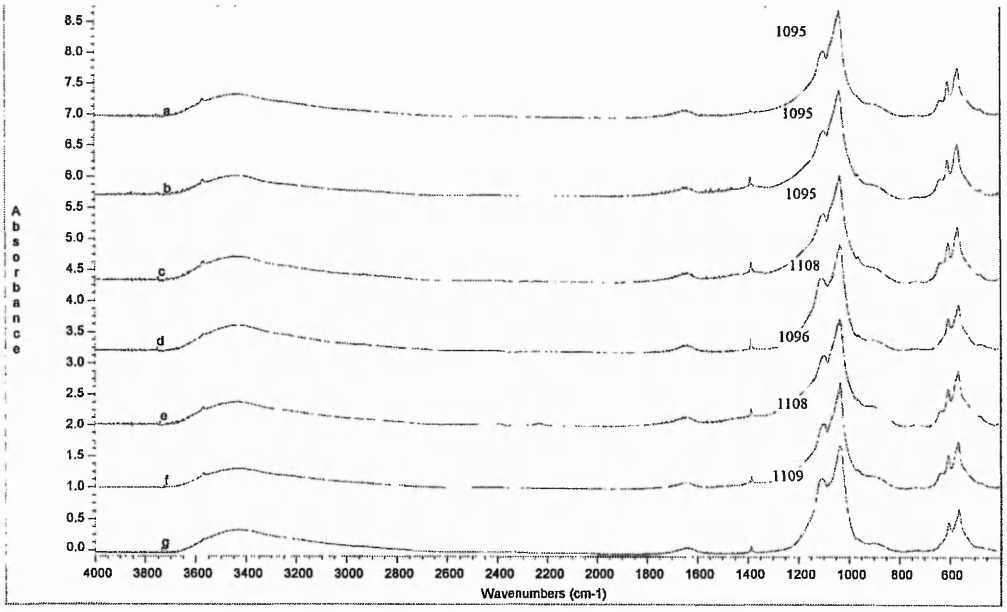

Figure 4.1 FT-IR spectra for the precipitate formed at 23°C and pH=7.4 in the presence of a) 0, b) 0.082 mM of $Si(OH)_4$ in the HPO_4^{2-} solution, c) 0.082 mM of $Si(OH)_4$ in the Ca^{2+} solution, d) 0.204 mM of $Si(OH)_4$ in the HPO_4^{2-} solution, e) 0.204 mM of $Si(OH)_4$ in the Ca^{2+} solution, f) 0.409 mM of $Si(OH)_4$ in the HPO_4^{2-} solution and g) 0.409 mM of $Si(OH)_4$ in the Ca^{2+} solution, after drying at 250°C for 1h.

XRD analysis showed that the shift observed in the FT-IR spectrum from the precipitate formed in the presence of orthosilicic acid was due to the formation of DCP (fig 4.2). The XRD patterns of the precipitate formed in the presence of orthosilicic acid showed

reflections at ca. 26 and 30 2-theta degrees corresponding to the Miller Indexes (-2 2 0) and (-1 1 2) (JCPDS 9-80) respectively. When orthosilicic acid was added in the HPO_4^{2-} solution, the effect seemed to be more pronounced (fig 4.2d and 4.2f) than when silicic acid had been added to the Ca^{2+} solution (fig. 4.2e and 4.2g).

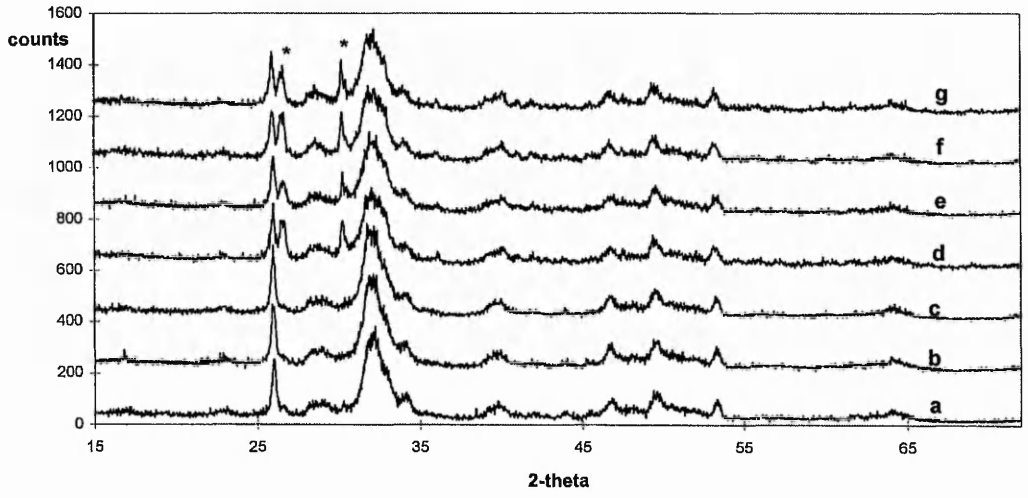

Figure 4.2 XRD patterns for the precipitates formed at 23°C and pH=7.4 in the presence of a) 0, b) 0.082 mM of $Si(OH)_4$ in the HPO_4^{2-} solution, c) 0.082 mM of $Si(OH)_4$ in the Ca^{2+} solution, d) 0.204 mM of $Si(OH)_4$ in the HPO_4^{2-} solution, e) 0.204 mM of $Si(OH)_4$ in the Ca^{2+} solution, f) 0.409 mM of $Si(OH)_4$ in the HPO_4^{2-} solution and g) 0.409 mM of $Si(OH)_4$ in the Ca^{2+} solution, after drying at 250°C for 1h. * DCP.

The average size of the crystals calculated from x-ray broadening analysis showed that the crystals precipitated in the presence of orthosilicic acid were smaller than in its absence for the apatite phase, (table 4.2). DCP crystals showed an increment in crystallite size for the direction (-1 1 2) with increasing concentration of $Si(OH)_4$ present in the precipitating solution.

$Si(OH)_4$ (mM)	HAP	DCP	
	(0 0 2)	(-2 2 0)	(-1 1 2)
0	293	-	-
0.082 in HPO_4^{2-}	272*	-	-
0.082 in Ca^{2+}	262*	-	-
0.204 in HPO_4^{2-}	280	184*	308*
0.204 in Ca^{2+}	262*	147*	360*
0.409 in HPO_4^{2-}	198*	148*	389*
0.409 in Ca^{2+}	221*	160*	576*

Table 4.2 Crystallite sizes (Å) for the DCP and apatite crystals precipitated from 0.242M $Ca(NO_3)_2$ and 0.145M $(NH_4)_2HPO_4$ at 23°C and pH=7.4 after drying at 250°C for 1h. (*$p<0.05$ compared to control).

Although the crystallite sizes calculated from x-ray diffraction data indicated that the apatite crystals precipitated in the presence of orthosilicic acid were smaller than the control, electron microscopy analysis of the precipitates showed that the apatite crystals formed in the presence of orthosilicic acid appeared to be more crystalline (fig. 4.3b,c,d,e,f,g) compared to the material precipitate in the absence of orthosilicic acid (fig.4.3a). The polycrystalline electron diffraction patterns obtained for the precipitates were characteristic of non-stoichiometric hydroxyapatite (see chapter 3) with d-spacings ca. 2.80 Å and 3.45 Å corresponding to the HAP Miller Indexes (2 1 1) and (0 0 2) respectively. The Ca/P ratios for the apatite crystals formed in the presence of orthosilicic acid (Ca/P 1.48 ± 0.05) were slightly higher than the Ca/P ratios of the precipitate formed in the absence of orthosilicic acid (Ca/P 1.42 ± 0.18).

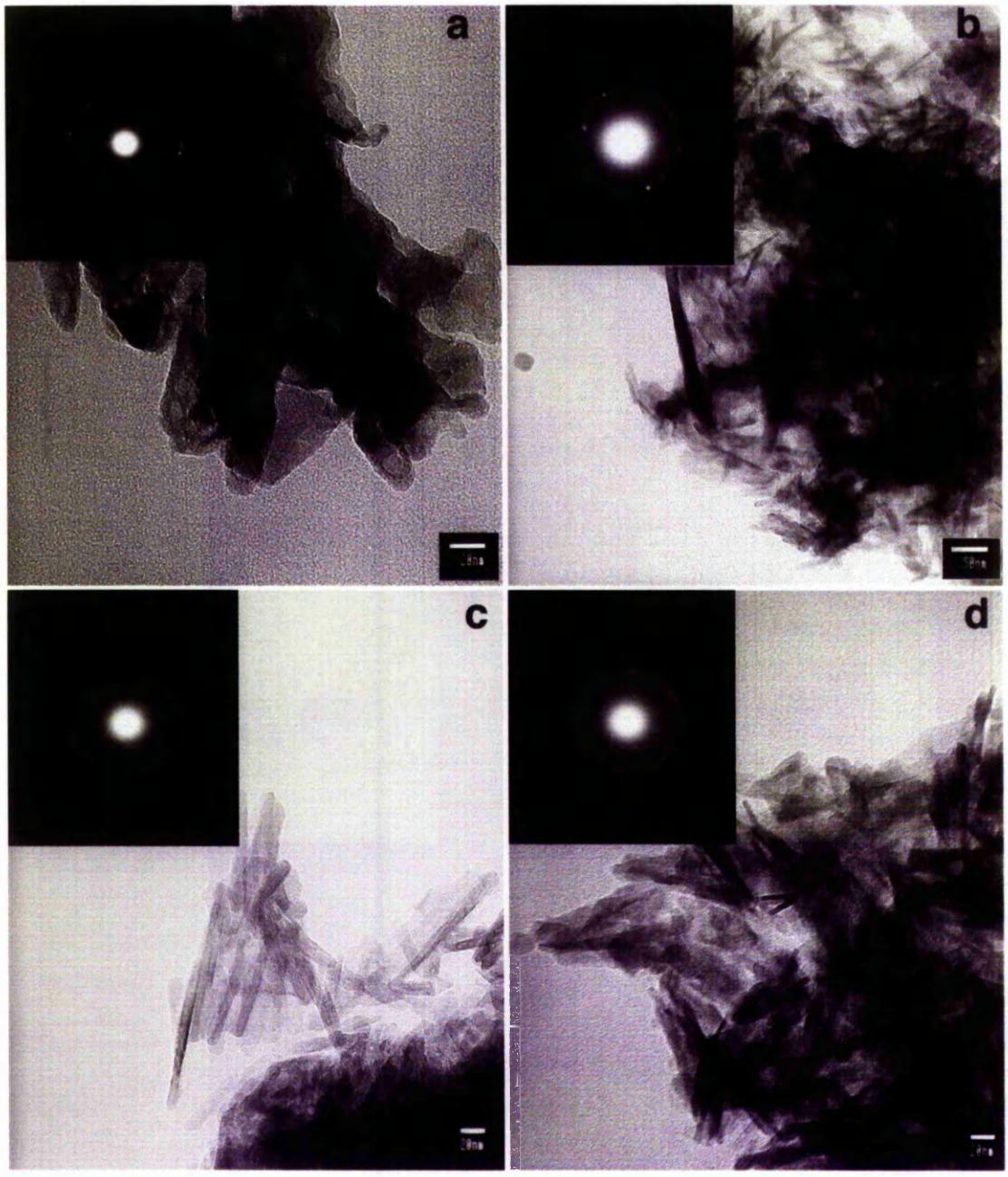

Figure 4.3 Calcium phosphate was precipitated from a solution containing 0.242 M $Ca(NO_3)_2$ and 0.145 M $(NH_4)_2HPO_4$ at 23°C and pH=7.4 in the presence of a)0, b) 0.082 mM, c) 0.204 mM and d) 0.409 mM Si(OH)4. The d-spacings obtained from the electron diffraction patterns were ca. 2.78 Å and 3.46 Å corresponding to the HAP Miller Indices (1 1 2) and (0 0 2) (JCPDS 9-432).

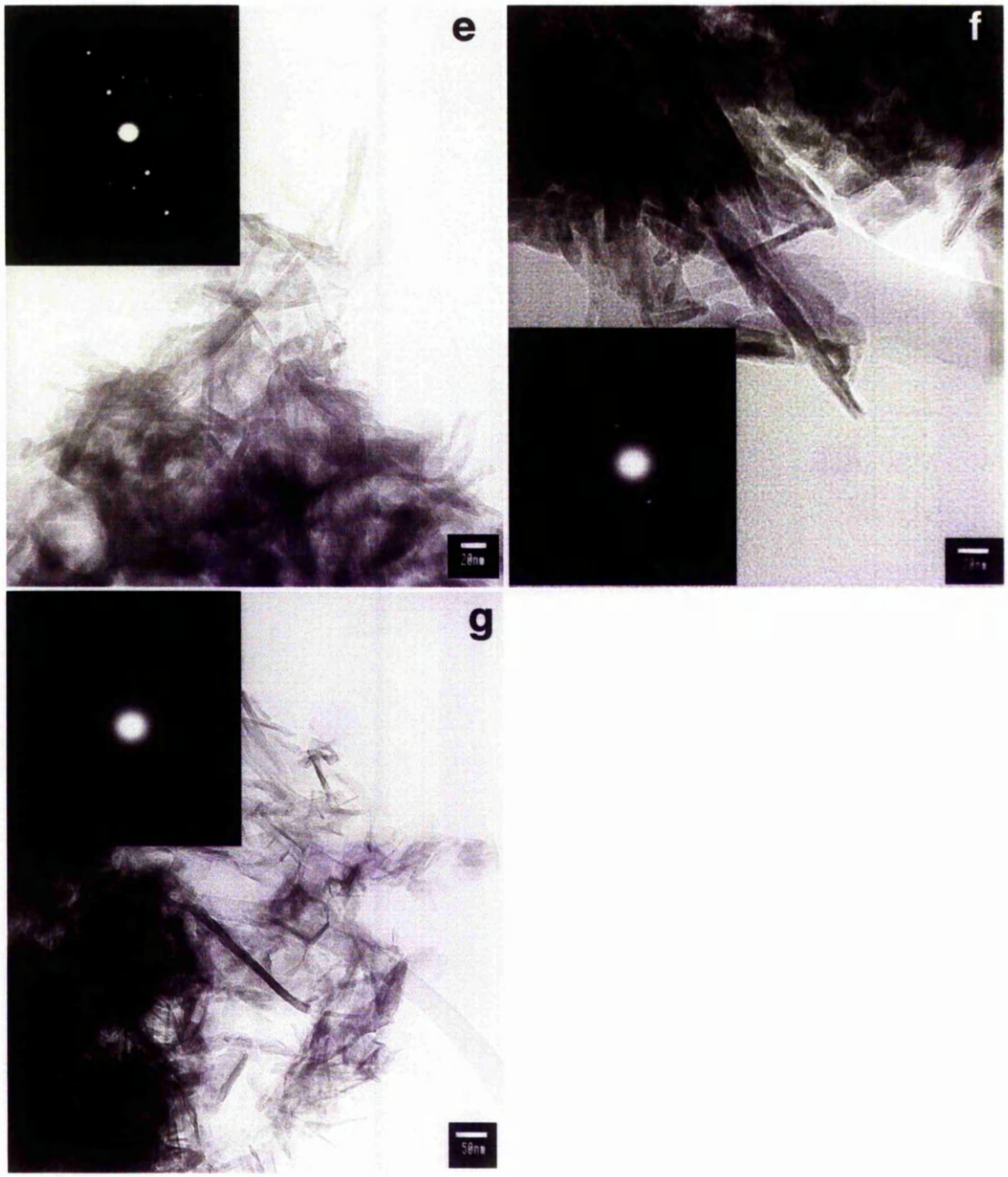

Continuation Figure 4.3 Calcium phosphate was precipitated from a solution containing 0.242 M $CaCl_2$ and 0.145 M NaH_2PO_4 at 23°C and pH=7.4 in the presence of a)0.082 mM, b) 0.204 mM and c) 0.409 mM $Si(OH)_4$. The d-spacings obtained from the electron diffraction patterns were ca. 2.78 Å and 3.46 Å corresponding to the HAP Miller Indices (1 1 2) and (0 0 2) (JCPDS 9-432).

Experiment 2

Calcium phosphate was precipitated in the presence of silica at 23°C and 37°C. The final calcium concentration was 0.242M and the final phosphate concentration was 0.145M in a total volume of 100 ml. After drying and weighing the precipitates, the yield of the product formed in the presence of silica was slightly higher (table 4.3). The addition of orthosilicic acid appeared to stimulate calcium precipitation.

precursors	T (°C)	0	0.082 mM $Si(OH)_4$	0.204 mM $Si(OH)_4$	0.409 mM $Si(OH)_4$
$(NH_4)_2HPO_4/Ca(NO_3)_2$	23	0.8325	0.8460	0.8544	0.8695
	37	0.6447	0.7104	0.6995	0.6954

Table 4.3 Weights of precipitate in g for n=1.

The FT-IR. spectra of the precipitate formed at 23 °C showed that the calcium phosphate precipitate in the presence of silica did not differ from the control (fig 4.4). The main phase was DCP (see chapter 3).

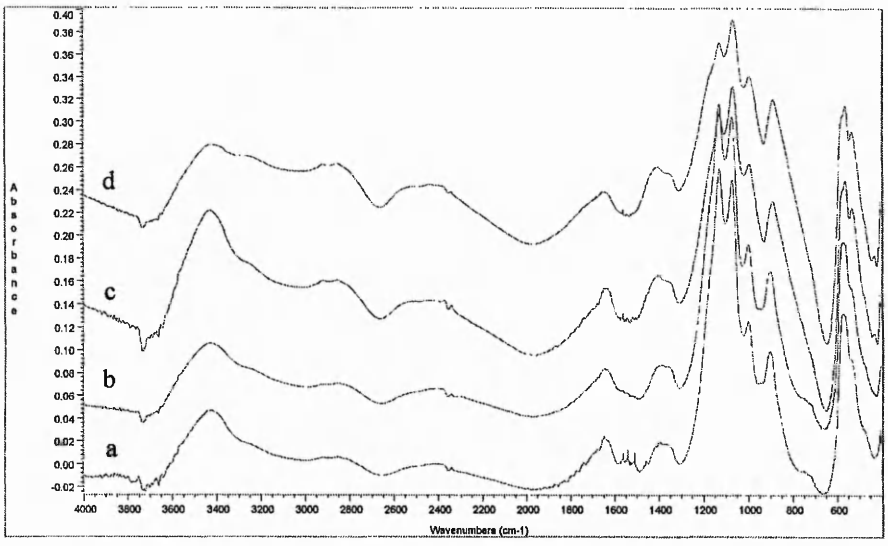

Figure 4.5 FT-IR spectra for the precipitates formed at 23°C from a solution containing 0.242M $Ca(NO_3)_2$ and 0.145M $(NH_4)_2HPO_4$ in the presence of a) 0, b) 0.082 mM of $Si(OH)_4$, c) 0.204 mM of $Si(OH)_4$, d) 0.409 mM of $Si(OH)_4$, after drying at 250°C for 1h.

However, the XRD patterns from the precipitate formed in the presence of silica showed an apparent increase of crystallinity when silica was present in the reagent solution as evidenced by a decrease in the broadening of the reflections on the XRD patterns (fig 4.6).

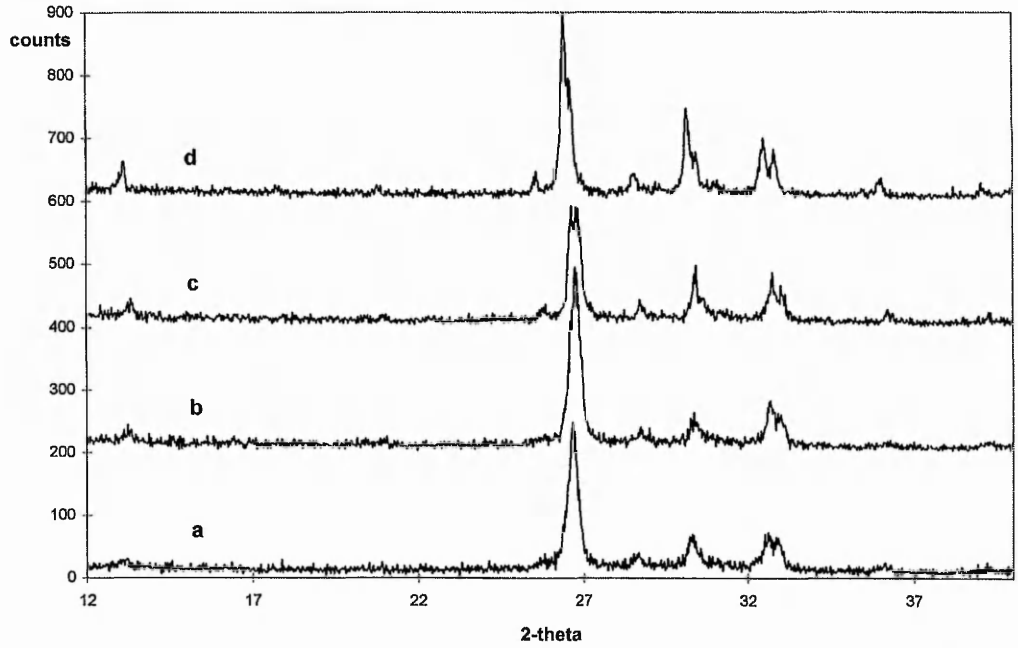

Figure 4.6 XRD patterns of the precipitates formed at 23°C from a solution containing 0.242M $Ca(NO_3)_2$ and 0.145M $(NH_4)_2HPO_4$ in the presence of a) 0, b) 0.082 mM of $Si(OH)_4$, c) 0.204 mM of $Si(OH)_4$, d) 0.409 mM of $Si(OH)_4$, after drying at 250°C for 1h.

The average crystalline size of the apatite crystals, obtained from an x-ray broadening analysis and particle size determination based on the Debye-Scherrer equation[15], increased when silica was present during the precipitation reaction at 23 °C (table 4.4). Crystallinity increased for calcium phosphate dibasic precipitated at 23 °C. The widths of the lathe-like crystals which form the DCPD crystals (see chapter 3) were calculated from the TEM micrographs for comparison to the crystalline size calculated from the x-ray broadening analysis. The observed effect of orthosilicic acid on the crystal size was not linear.

silica (mM)	crystalline size (Å)						
	(0 1 0)	(0 2 0)	(-2 2 0)	(-1-1 1)	(-1 1 2)	(-2 3 0)	TEM
0	210	-	246	382	240	207	520
0.082	373*	-	256	531*	267*	284*	-
0.204	477*	649*	424*	574*	533*	268*	690*
0.409	449*	649*	556*	624*	514*	348*	549

Table 4.4 Crystalline size (Å) of DCPD crystal precipitates formed from a solution containing 0.242M $Ca(NO_3)_2$ and 0.145M $(NH_4)_2HPO_4$ at 23 °C (* $p<0.05$, compared to control).

When the precipitation was carried out at 37 °C, the presence of silica appeared to promote calcium phosphate dibasic formation over apatite formation. The XRD pattern of the precipitate showed the presence of both calcium phosphate phases (fig 4.7). The reflections in the area at ca. 32 2-theta degrees corresponding to HAP showed a decrease in intensity. The XRD spectra not only showed increment of one phase over the other but an increase in crystallinity.

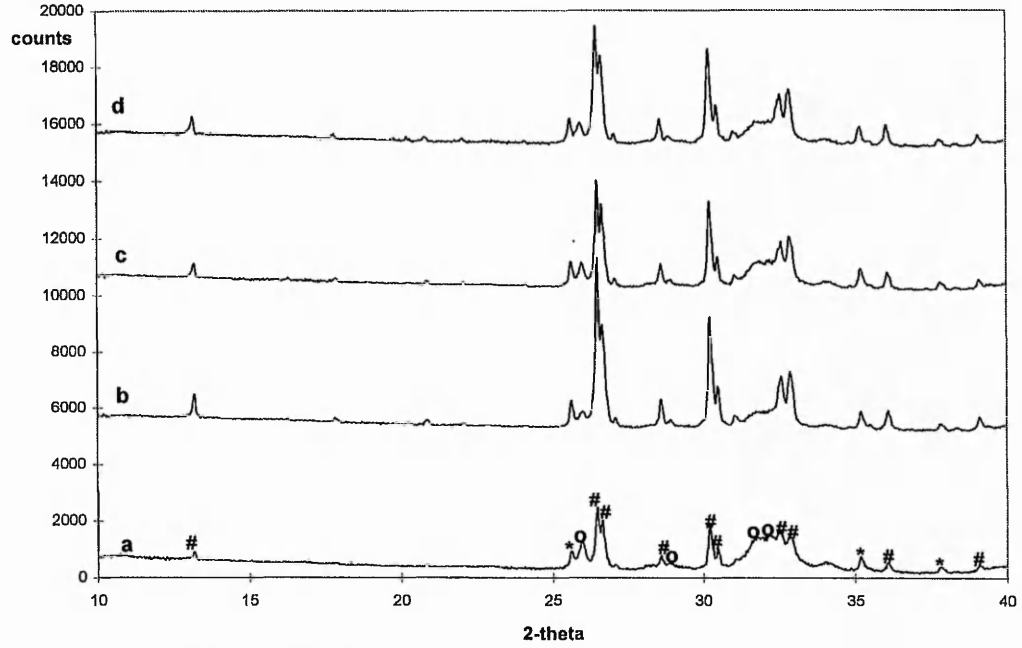

Figure 4.7 XRD patterns of the precipitates formed at 37°C from a solution containing 0.242M $Ca(NO_3)_2$ and 0.145M $(NH_4)_2HPO_4$ in the presence of a) 0, b) 0.082 mM of $Si(OH)_4$, c) 0.204 mM of $Si(OH)_4$, d) 0.409 mM of $Si(OH)_4$, after drying at 250°C for 1h. *SRM, °HAP, #DCP.

The XRD analysis not only showed increment of one phase over the other but an increase in crystallinity of both phases. Table 4.5 shows the average crystallite size of the DCP and apatite crystals. Crystal size increased with increasing concentrations of silica.

silica (ppm)	**crystalline size (Å)**						
	(apatite)	**(DCP)**					
	(0 0 2)	**(01 0)**	**(0 2 0)**	**(-2 2 0)**	**(-1-1 1)**	**(-1 1 2)**	**(-2 3 0)**
0	245	-	571	595	339	600	-
0.082	570*	672*	680*	612	754*	664*	314*
0.204	629*	839*	751*	808*	598*	686*	-
0.409	455*	750*	639*	522*	589*	664*	378*

Table 4.5 Crystalline size (Å) of apatite and DCP crystal precipitates at 23°C (* $p<0.05$ compared to control).

EDX analysis of the samples showed an increase in the Ca/P ratio of the precipitate formed in the presence of silica although there was not a trend (Table 4.6).

	silica (mM)			
T	**0**	**0.082**	**0.204**	**0.409**
23°C (DCP)	0.86 ± 0.19	0.86 ± 0.17	0.62 ± 0.03	1.09 ± 0.34
37°C (apatite)	1.56 ± 0.22	1.50 ± 0.26	1.64 ± 0.16	1.64 ± 1.64

Table 4.6 Ca/P of the precipitate formed at 23°C and 37°C. (mean ± SD, n=10).

Figure 4.10 shows TEM images of the apatite crystals precipitate in the absence and presence of silicic acid. The polycrystalline electron diffraction patterns were typical of non-stoichiometric hydroxyapatite (see chapter 3) for the crystals precipitate in the absence and presence of silicic acid. The crystals precipitate in the presence of orthosilicic acid seemed to be more perfect (fig. 4.10b,c,d) and less beam sensitive.

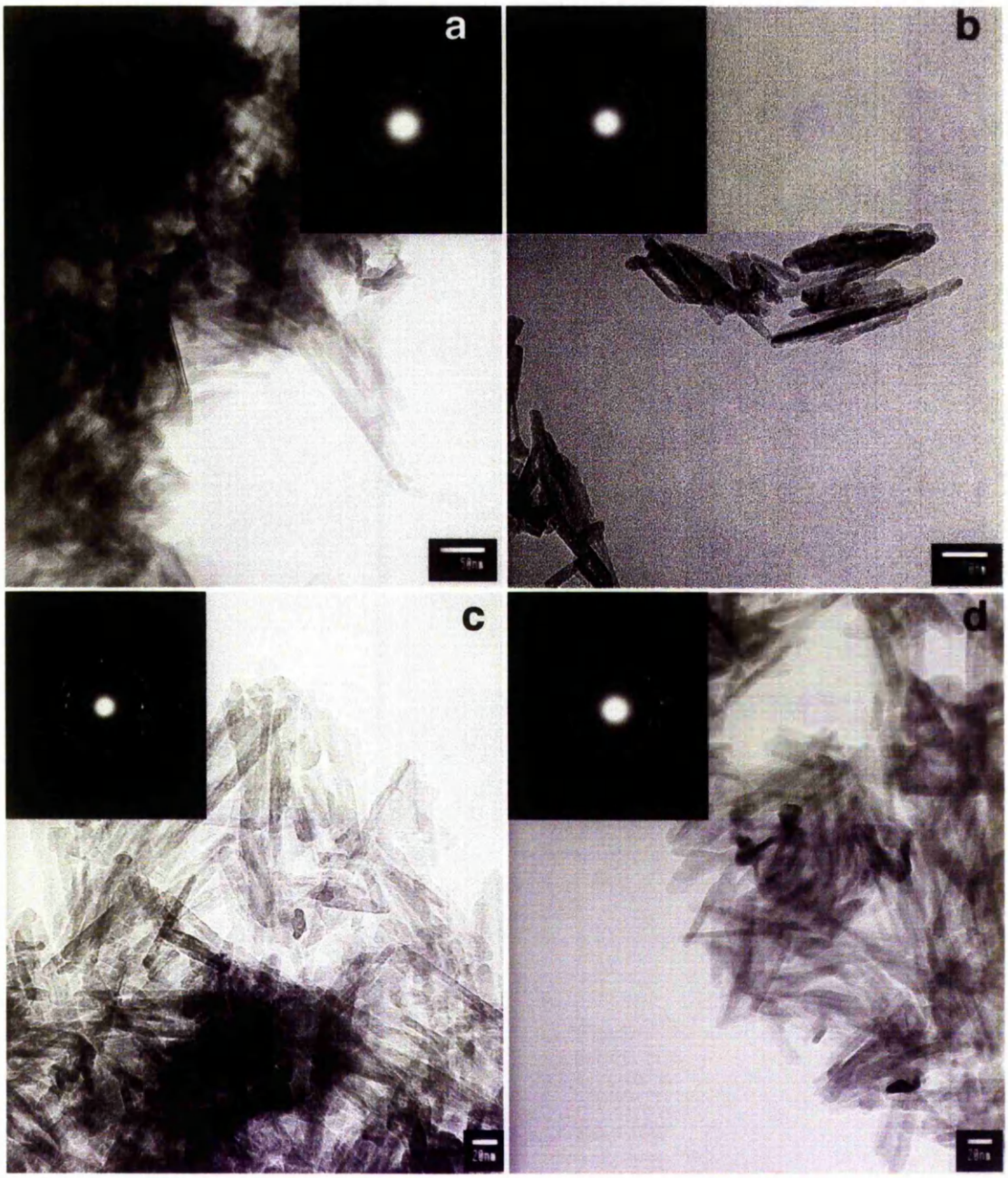

Figure 4.10 Calcium phosphate was precipitated from a solution containing 0.242 M $Ca(NO_3)_2$ and 0.145 M $(NH_4)_2HPO_4$ at 37°C in the presence of a) 0, b) 0.082 mM, c) 0.204 mM and d) 0.409 mM $Si(OH)_4$. The d-spacings obtained from the electron diffraction patterns were ca. 3.44 Å and 2.80 Å attributed to the HAP Miller Indices (0 0 2) and (2 1 1) (JCPDS 9-432).

For the precipitate formed at 37 °C, the lattice parameters were calculated from TEM and XRD data using the same method (appendix II) due to the lack of (h k l) values to apply Cohen's method[15]. The crystal structure of HAP belongs to the space group $P6_3/m$ in the hexagonal system. Its lattice parameters are a(=b)=9.432 Å and c=6.881 Å. As the apatite crystals presented the same morphology and diffraction pattern as hydroxyapatite, the equation for the hexagonal system which relates d-spacing and lattice parameters was used to calculate a,b and c from the x-ray diffraction data (table 4.7) and electron diffraction data (table 4.8) to study the effect of silica on the lattice unit (appendix II).

silica (mM)	Unit cell parameters (Å) 37 °C	
	a=b	c
0	9.4241	6.8484
0.082	9.3978	6.8368
0.204	9.4116	6.8356
0.409	9.4296	6.8576

Table 4.7 Unit cell parameters (Å) of apatite crystal precipitated at 37°C from XRD data.

silica (mM)	Unit cell parameters (Å) 37 °C	
	a=b	c
0	9.4997	6.9022
0.082	9.5459	6.8470
0.204	9.5060	6.8116
0.409	9.5714	6.7974

Table 4.8 Unit cell parameters (Å) of apatite crystal precipitates at 37°C from TEM data.

The apatite crystals precipitated at 37°C were very small and highly hydrated. The x-ray diffraction pattern of the material had very broad reflections and noisy background and therefore the x-ray method was relatively insensitive. Although, symmetry-true, indexable single-crystal diffraction patterns can be obtained with electrons from very minute crystals and

be analysed very thoroughly for crystalline components present in minor amounts, the electron diffraction pattern obtained for the apatite phase precipitated was polycrystalline due to the agglomeration of the crystals and only some of the (h k l) Miller indices could be assigned. The dimensions of the apatite crystals measured from the TEM micrographs showed that silica affects the length of the crystals (table 4.9). Two different values were obtained when measuring the width/depth of the crystals, depending on the way the crystals lay on the grid. Non-stoichiometric hydroxyapatite has a hexagonal symmetry. The equation for the hexagonal system relates d-spacing and the a and c lattice parameters (see appendix (II)). Thus the changes in the c parameter also affected a(=b) and changes in the width/depth of the crystals (table 4.9).

silica (ppm)	**crystal dimension (Å)**		
		37 °C	
	length	**width/depth**	
0	1205.1	115.4	76.9
0.082	1548.0	145.2	47.0
0.204	1113.2	115.4	53.3
0.409	778.2	127.2	53.3

Table 4.9 Crystal dimensions (Å) of apatite crystal precipitates at 37 °C after drying at 250°C for 1h.

Experiment 3

Figure 4.11 shows the pH changes with time during the reaction at 23 °C in the presence of a final concentration of orthosilicic acid of 0.041, 0.082, 0.204 and 0.409 mM. In the presence of orthosilicic acid, the induction time decreased at a very slow rate compared to the control which remained more or less constant. The induction time was also slightly shorter than the induction time for the control. An inflexion point during the induction time

was observed for precipitations carried out in the presence of 0.204 mM and 0.409 mM orthosilicic acid. After the first pH drop, the pH rose. The rate in which the pH rose appeared to decrease with increasing concentration of orthosilicic acid. Then the pH dropped and stabilised to the same value for the control solution and solutions containing silicic acid.

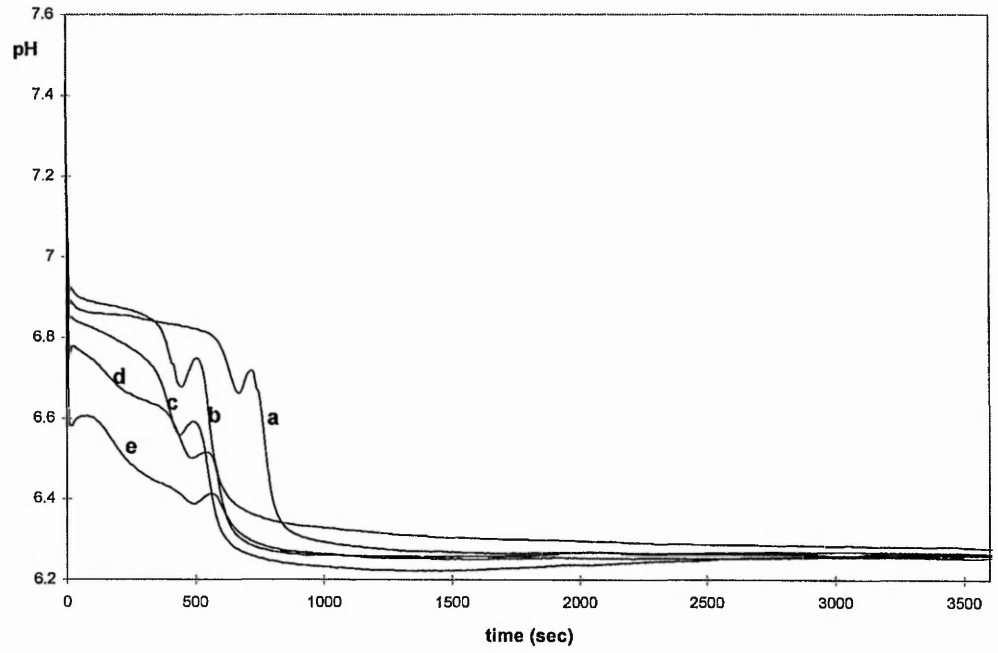

Fig. 4.11 pH changes with time in the presence of a) 0 mM, b) 0.041 mM, c) 0.082 mM, d) 0.204 mM, and e) 0.409 mM orthosilicic acid at 23 °C.

At 37 °C the pH curves did not show any difference for the precipitations carried out in the presence of silicic acid for the lowest concentrations of orthosilicic acid. In the presence of 0.204 mM and 0.409 mM of orthosilicic acid, the pH slowly decreased during the induction time compared to the control.

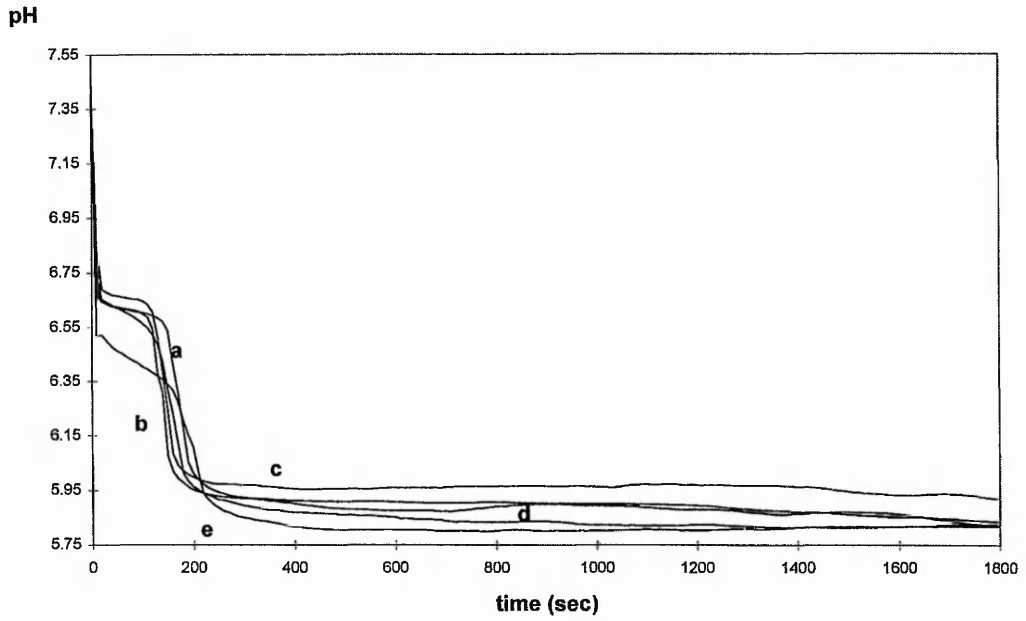

Fig 4.12 pH changes with time in the presence of a) 0 mM, b) 0.041 mM, c) 0.082 mM, d) 0.204 mM, and e) 0.409 mM orthosilicic acid at 37°C.

Table 4.10 shows the yield of precipitate formed in the presence of orthosilicic acid at 23°C and 37°C.

T (°C)	0 mM	0.041 mM	0.082 mM	0.204 mM	0.409 mM
23	39.23	40.06	40.86	41.26*	42.3*
37	37.27	34.66*	35.8	37.93	38.66

Table 4.10 Weights of precipitate formed at 23°C in mg (*$p<0.05$, compared to control).

The XRD patterns for the precipitate formed in the presence of orthosilicic acid at 23°C showed the appearance of a reflection at $2\theta=26°$ corresponding to the presence of apatite crystals. More difficult to assign, it was possible to observe changes in the area ca. $2\theta=31°$ corresponding also to the presence of apatitic crystals in the precipitate and at ca. $2\theta=13°$

the reflection corresponding to the Miller Index (0 1 0) for DCP phase seems to broaden indicating smaller/less crystalline crystals (table 4.11).

	crystalline size (Å)	
silica (mM)	**(-2 2 0)**	**(-1 1 2)**
0	180 ± 33	258 ± 24
0.041	160 ± 14	161* ± 56
0.082	140 ± 32	201 ± 74
0.204	148 ± 22	194* ± 3
0.409	152 ± 12	211 ± 36

Table 4.11 . Crystal dimensions (Å) of crystal precipitated at 23 °C after drying at 250°C for 1h (*p<0.05 compared to control, n=4).

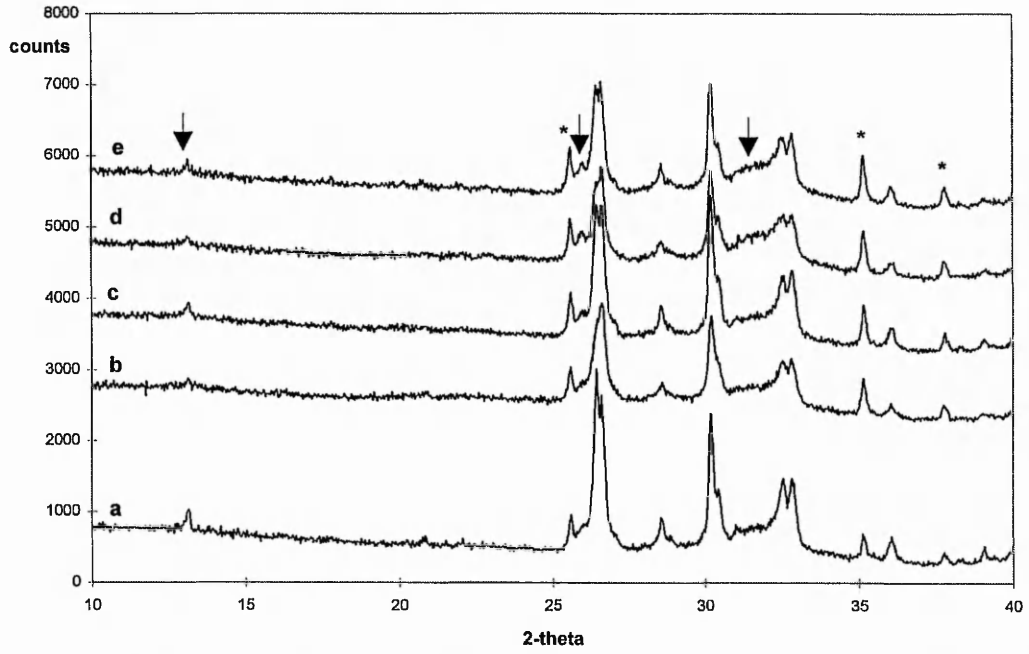

Fig. 4.13 XRD spectra of the precipitate formed at 23 °C in the presence of a) 0 mM, b) 0.041 mM, c) 0.082 mM, d) 0.204 mM, and e) 0.409 mM orthosilicic acid after drying at 250°C for 1h. * standard reference material.

The FT-IR spectra for the precipitate formed at 23 °C in the presence of orthosilicic acid did not show any difference in crystal phases from the control. The FT-IR spectra showed the characteristic bands corresponding to the HPO_4^{2-} and PO_4^{2-} vibration and bending modes for DCP, OCP and apatite (see chapter 3). There was a shift to higher wavenumber of the band at 3420 cm^{-1} (control) to 3425 cm^{-1} (orthosilicic acid) attributable to absorbed water.

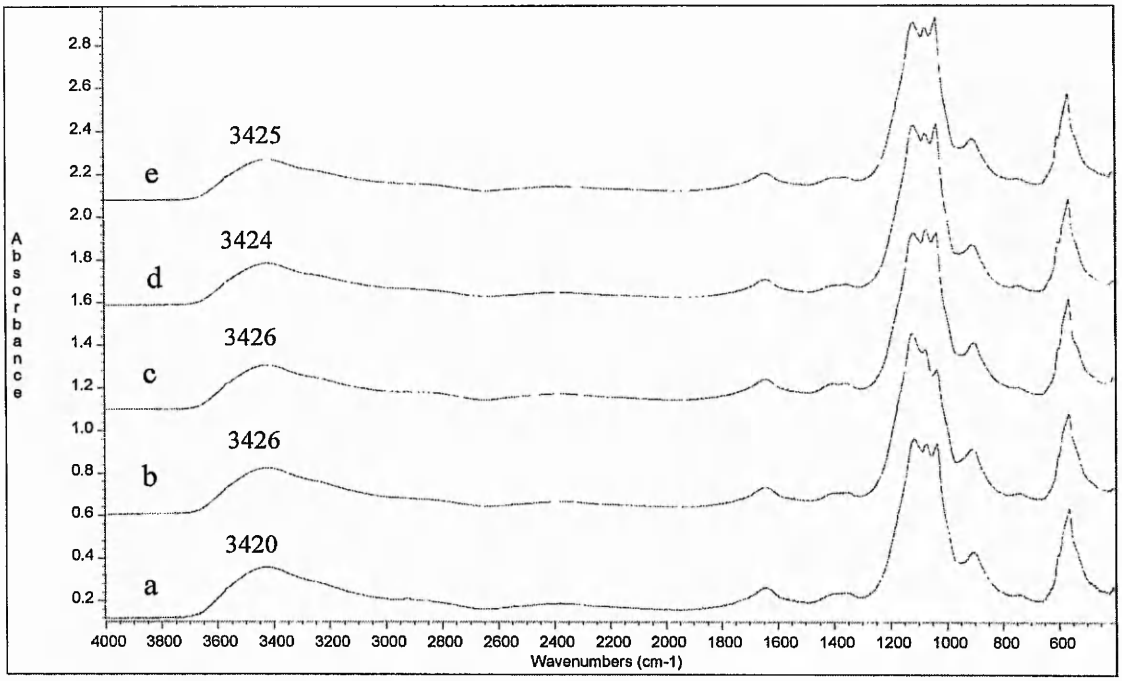

Fig. 4.14 FT-IR spectra of the precipitate formed at 23 °C in the presence of a) 0 mM, b) 0.041 mM, c) 0.082 mM, d) 0.204 mM, and e) 0.409 mM orthosilicic acid after drying at 250°C for 1h.

The XRD patterns for the precipitates prepared at 37 °C showed the presence of apatite. The patterns of the precipitate formed in the presence of orthosilicic acid did not differ from the control although a slight increase in crystallinity was shown for some reflections which could correspond to hydroxyapatite and/or OCP crystals (fig. 4.15).

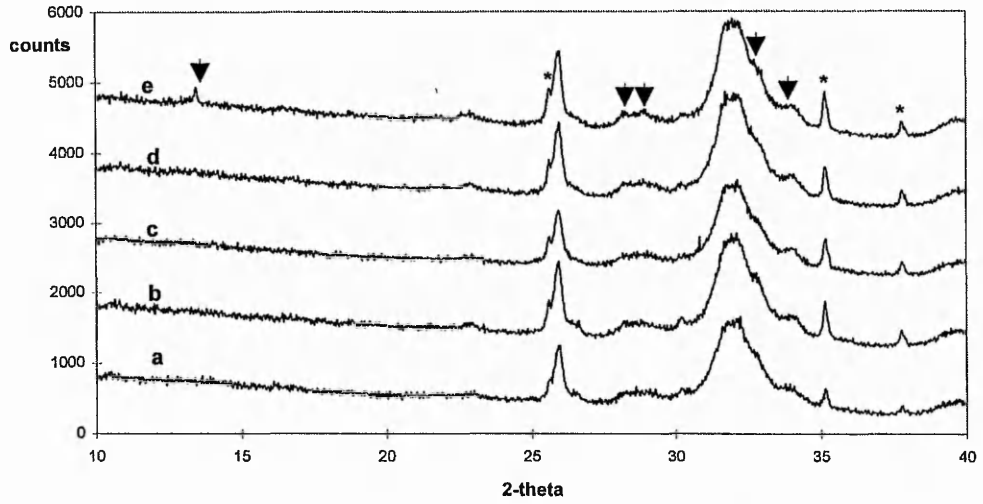

Fig. 4.15 XRD spectra of the precipitate formed at 37°C in the presence of a) 0 mM, b) 0.041 mM, c) 0.082 mM, d) 0.204 mM, and e) 0.409 mM orthosilicic acid after drying at 250°C for 1h. *standard reference material, arrows shows the reflections which could correspond to hydroxyapatite and/or OCP crystals.

The crystallite size was calculated by x-ray broadening analysis of the most intense reflections (table 4.12).

	crystalline size (Å)	
silica (mM)	**(0 0 2)**	**(2 1 1)**
0	194 ± 14	44 ± 3
0.041	190 ± 28	52* ± 5
0.082	168 ± 13	57* ± 1
0.204	176 ± 19	58* ± 4
0.409	191 ± 16	61* ± 7

Table 4.12 . Crystal dimensions (Å) of crystal precipitated at 37 °C after drying at 250°C for 1h calculated by x-ray broadening analysis (*p < 0.05 compared to control, n=4).

The FT-IR spectra for the precipitate formed at 37°C also showed a shift to higher wavenumber of the band at 3423 cm^{-1} (control) to 3428 cm^{-1} (orthosilicic acid) corresponding to the -OH of the absorbed water (fig. 4.16). The spectra were characteristic of non-stoichiometric hydroxyapatite (see chapter 3).

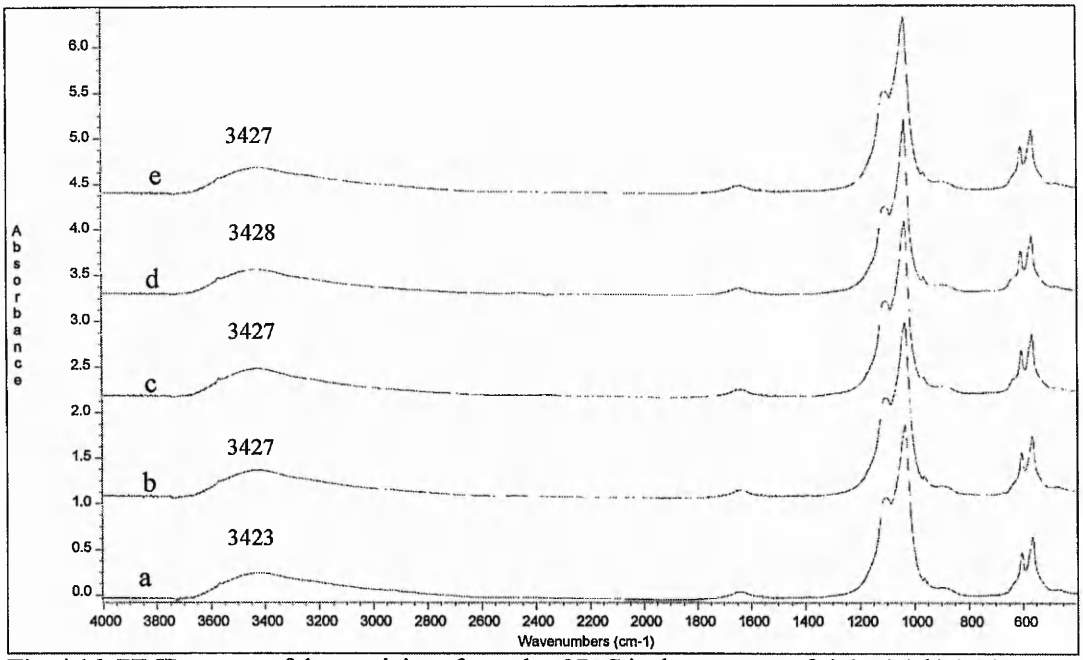

Fig. 4.16 FT-IR spectra of the precipitate formed at 37 °C in the presence of a) 0 mM, b) 0.041 mM, c) 0.082 mM, d) 0.204 mM, and e) 0.409 mM orthosilicic acid.

Transmission electron microscopy was used to investigate the structure, morphology and composition of precipitates formed in the presence of orthosilicic acid (for control see chapter 3). For precipitations carried out at 23 °C in the presence of 0.041 and 0.082 mM orthosilicic acid round spheres, OCP plates and flakes were already observed at 1 min of reaction (fig.4.17a, fig 4.18a-c). For higher concentrations of orthosilicic acid (0.240 and 0.409 mM) only round spheres were observed (fig. 4.19a, 4.20b). After 5 min the rough spheres were still detected for 0.041 mM orthosilicic acid (fig. 4.17b). With increasing concentrations of orthosilicic acid, the spheres showed a higher Ca/P (table 4.13). After 15 min, OCP plate-like crystals and needles were observed for all concentrations of orthosilicic acid (fig. 4.17c, fig. 4.18d-f, fig. 4.19d-g, fig. 4.20d, f-g). After 30 min reaction DCPD crystals were detected for 0.041 and 0.082 mM orthosilicic acid (fig. 4.17d, fig. 4.18g). For 0.204 and 0.409 mM orthosilicic acid DCPD like crystals were detected after

15 min of reaction (fig. 4.19c, fig. 4.20c,e). EDX analysis detected some Si in the plate-like and flake crystal structures at these concentrations (table 4.13).

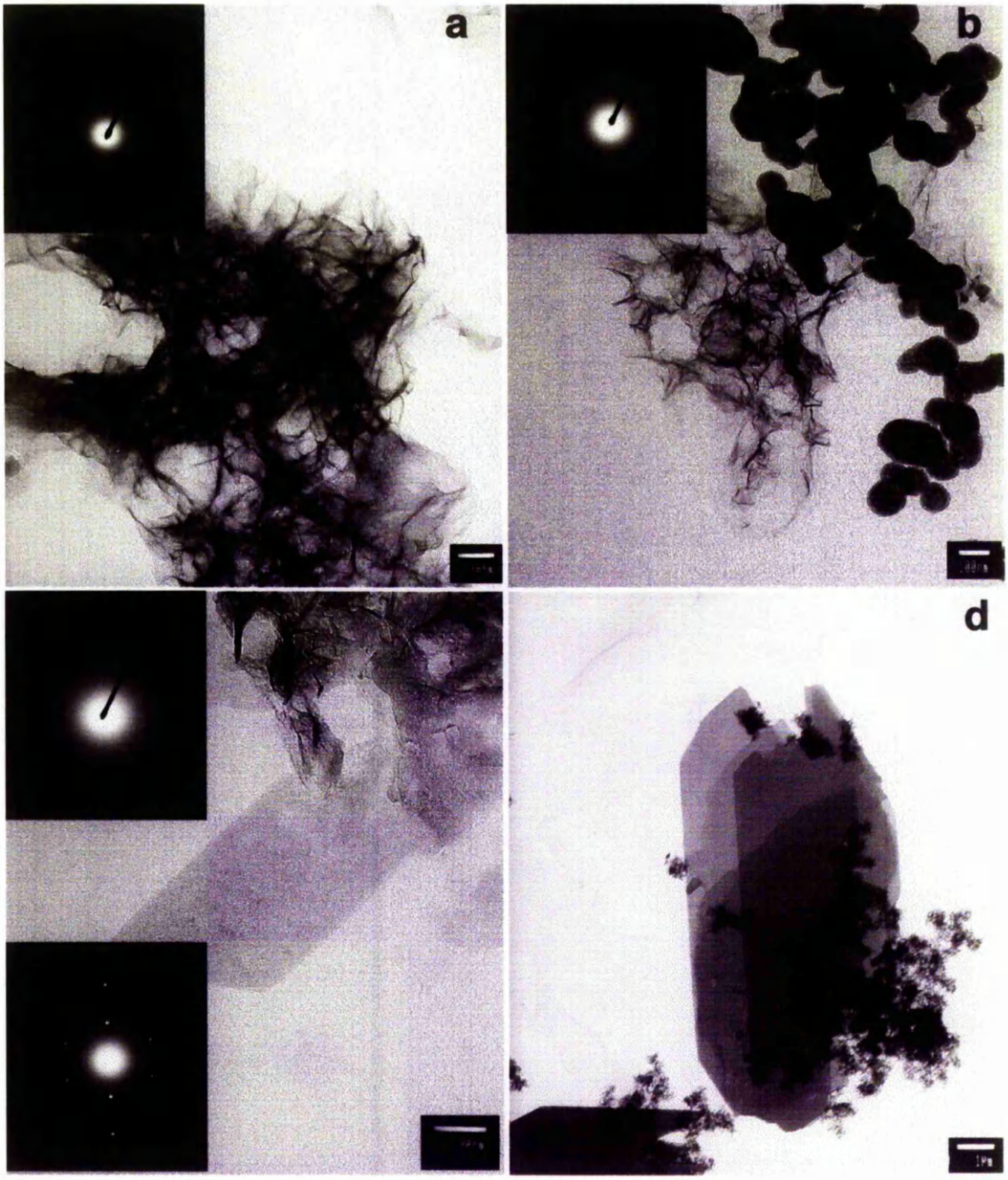

Figure 4.17 Calcium phosphate was precipitated from a solution containing 10 mM $Ca(NO_3)_2$ and 6 mM $(NH_4)_2HPO_4$ at 23°C in the presence of 0.041 mM $Si(OH)_4$. During precipitation reaction samples were taken for TEM analysis at a) 1 min, b) 5 min, c) 15 min and d) 30 min of reaction (see appendix III for d-spacings values calculated from the electron diffraction data).

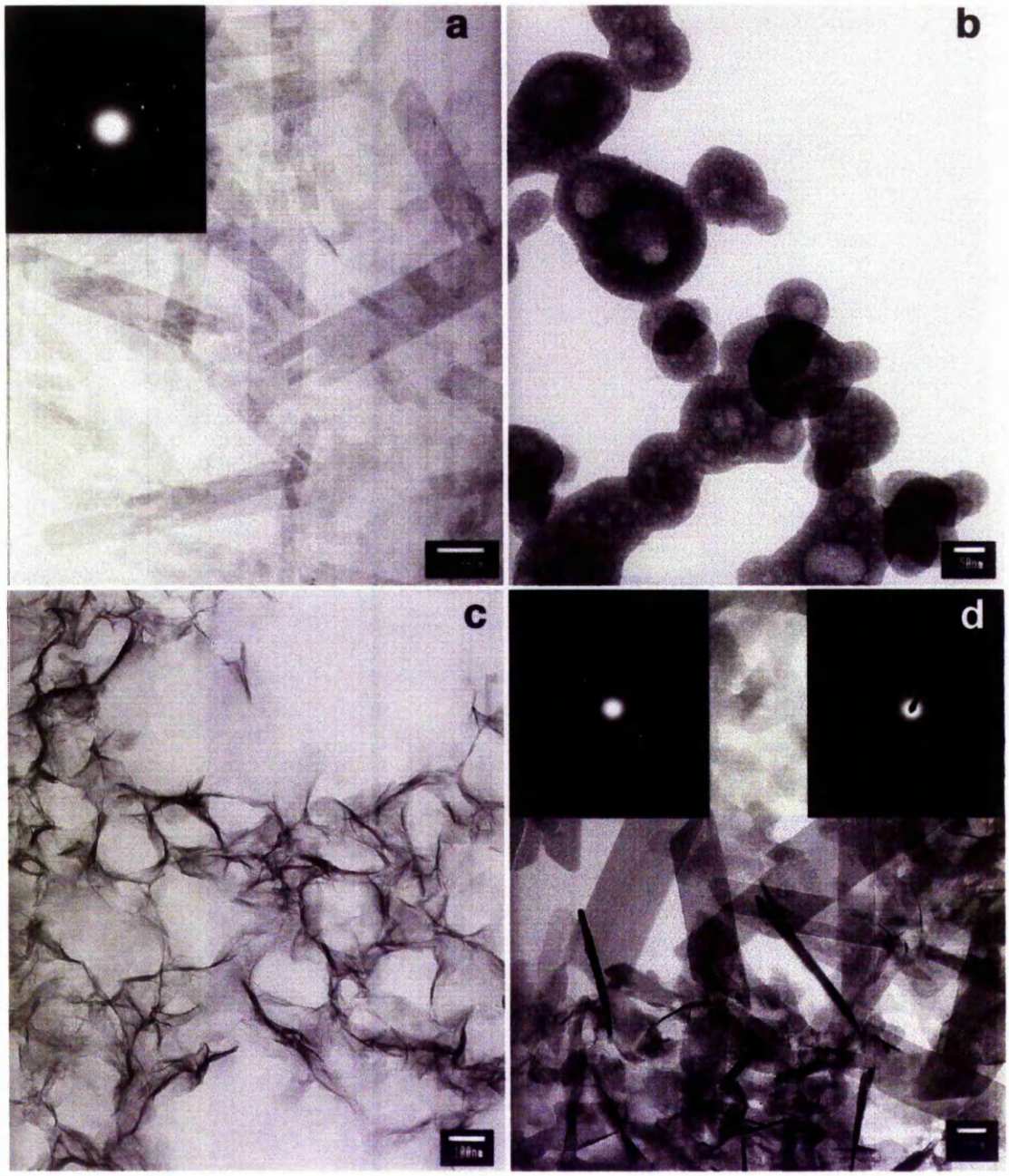

Figure 4.18 Calcium phosphate was precipitated from a solution containing 10 mM $Ca(NO_3)_2$ and 6 mM $(NH_4)_2HPO_4$ at 23°C in the presence of 0.082 mM $Si(OH)_4$. During precipitation reaction samples were taken for TEM analysis at a) and b) 1 min, c) and d) 5 min (see appendix III for d-spacings values calculated from the electron diffraction data).

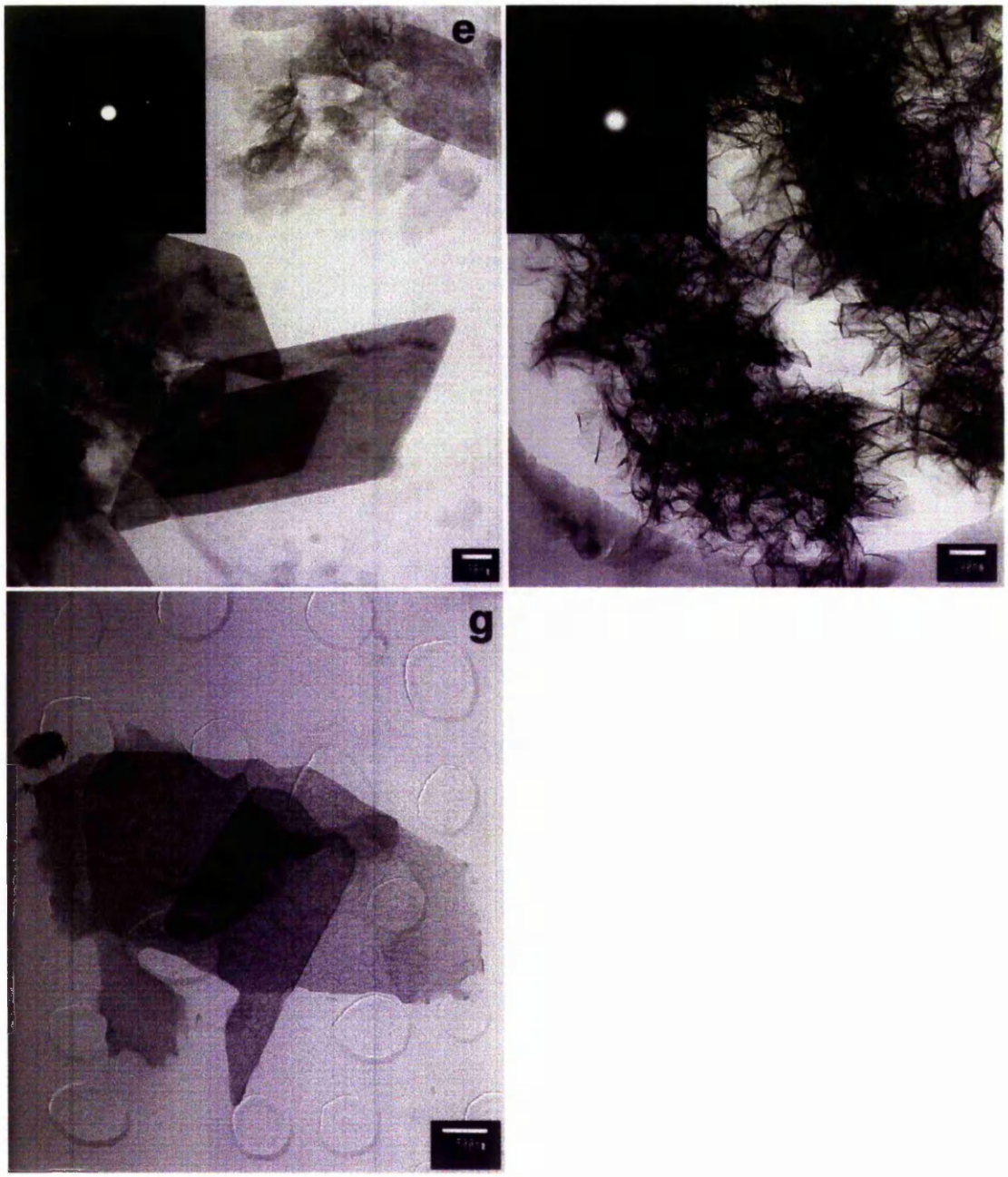

Continuation Figure 4.18 e) 15 min and f) and g) 30 min of reaction (see appendix III for d-spacings values calculated from the electron diffraction data).

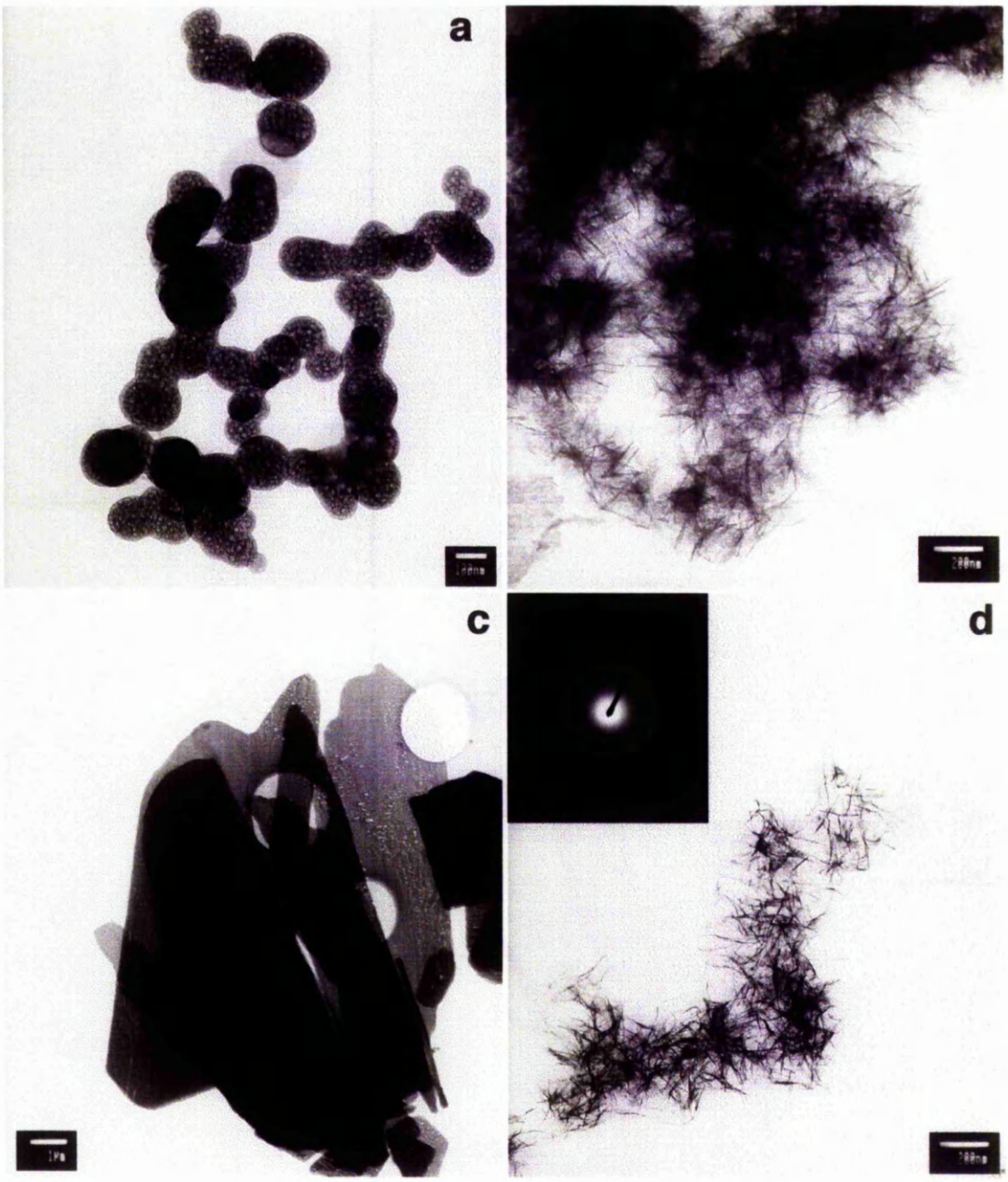

Figure 4.19 Calcium phosphate was precipitated from a solution containing 10 mM $Ca(NO_3)_2$ and 6 mM $(NH_4)_2HPO_4$ at 23°C in the presence of 0.204 mM $Si(OH)_4$. During precipitation reaction samples were taken for TEM analysis at a) and b) 1 min, c) and d) 5 min (see appendix III for d-spacings values calculated from the electron diffraction data).

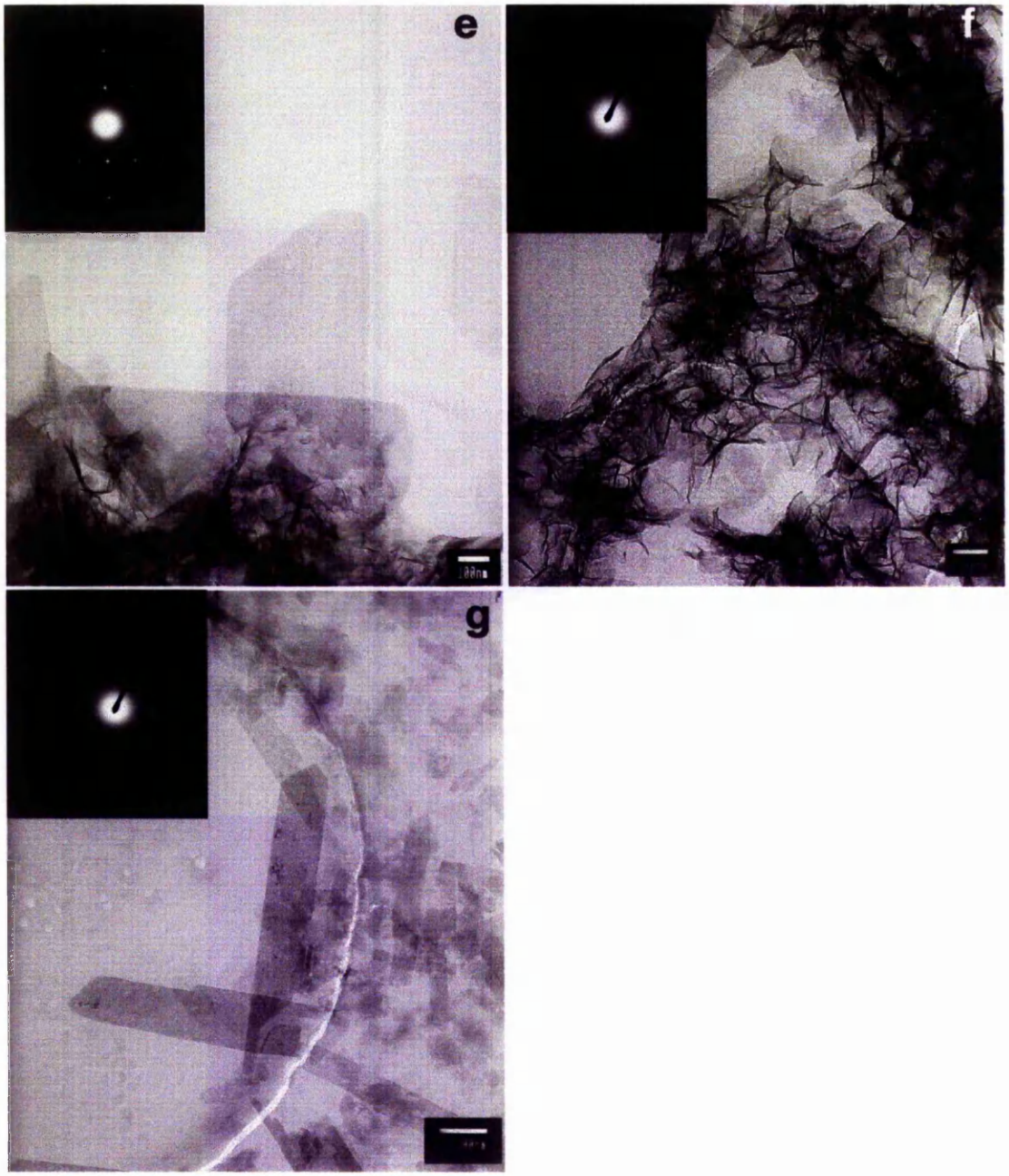

Continuation Figure 4.19 e) 15 min and f) and g) 30 min of reaction (see appendix III for d-spacings values calculated from the electron diffraction data).

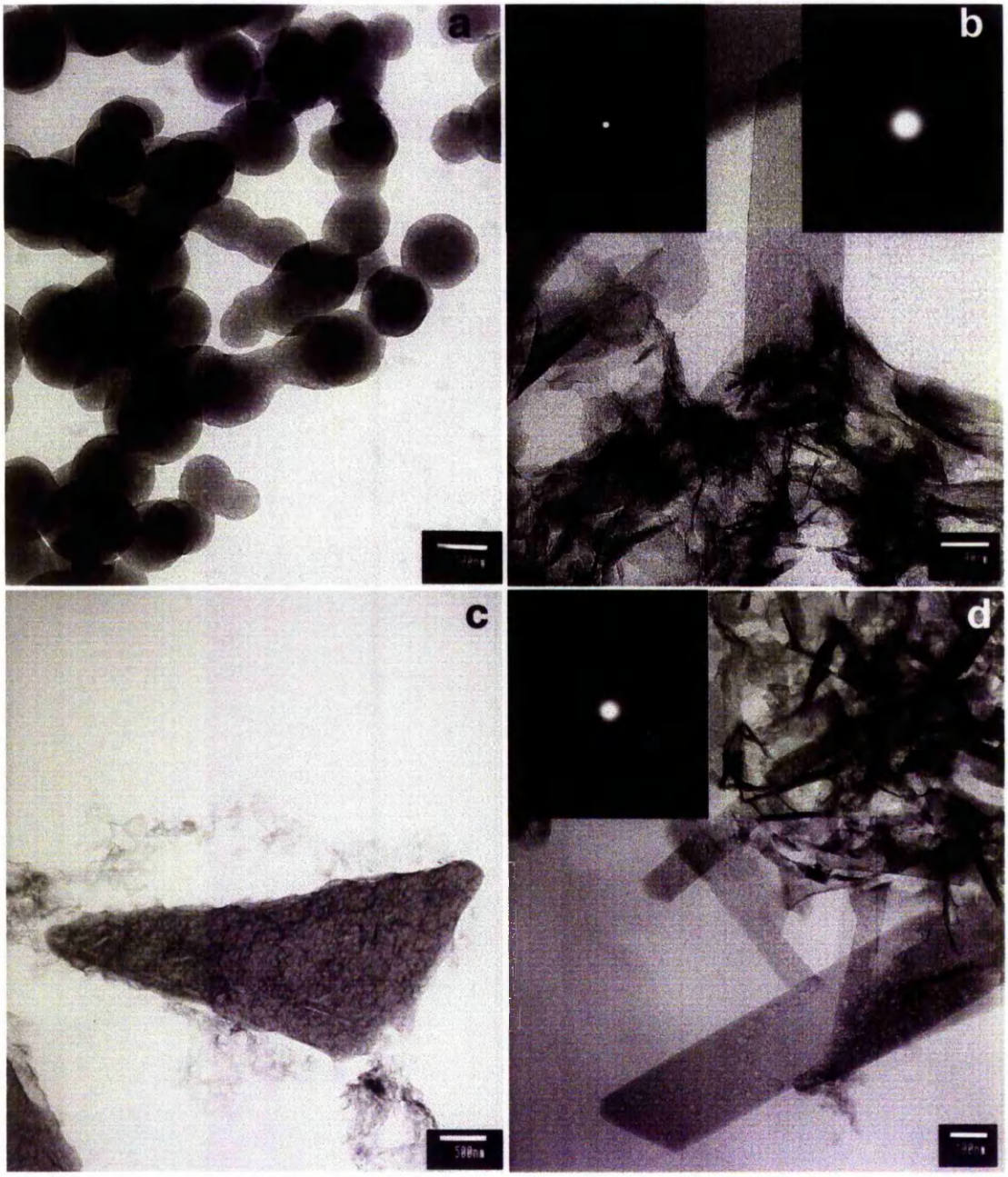

Figure 4.20 Calcium phosphate was precipitated from a solution containing 10 mM $Ca(NO_3)_2$ and 6 mM $(NH_4)_2HPO_4$ at 23°C in the presence of 0.409 mM $Si(OH)_4$. During precipitation reaction samples were taken for TEM analysis at a) 1 min, b) 5 min, c) and d) 15 min (see appendix III for d-spacings values calculated from the electron diffraction data).

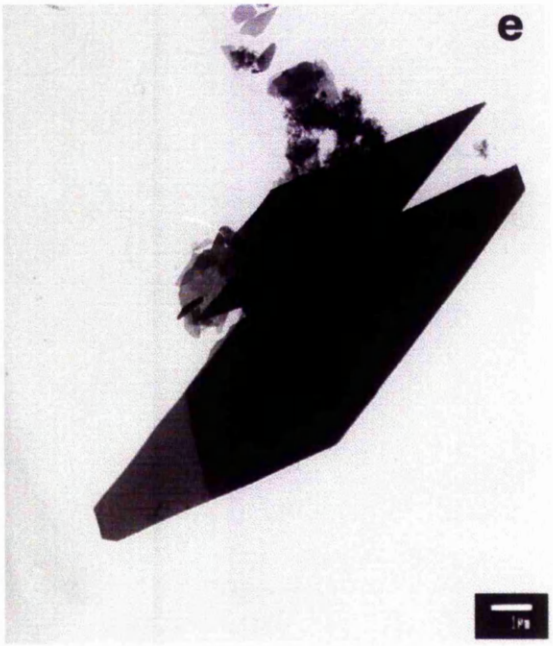

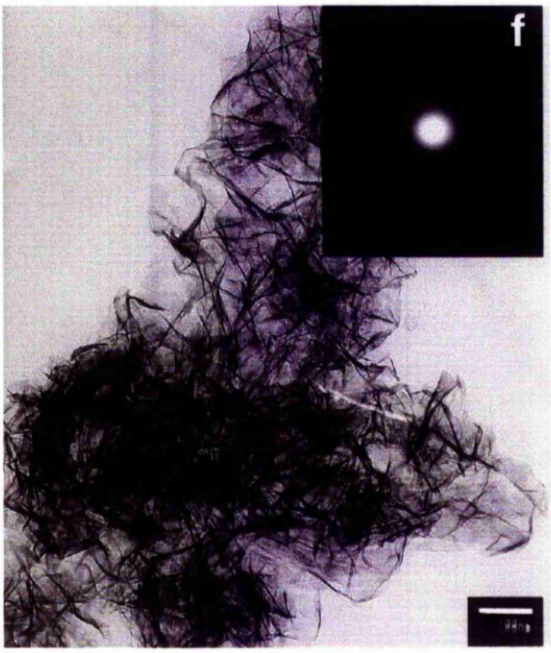

Continuation Figure 4.20 e) and f) 30 min of reaction (see appendix III for d-spacings values calculated from the electron diffraction data).

Table 4.13 shows the variation of the Ca/P and Si/P ratios for the different morphologies observed during precipitation reactions performed at 23 °C.

	spheres		flakes		plates-like OCP		plates-like DCPD	
time (min) $Si(OH)_4$ (mM)	**Ca/P**	**Si/P**	**Ca/P**	**Si/P**	**Ca/P**	**Si/P**	**Ca/P**	**Si/P**
1								
0	1.09 ±0.35	-	-	-	-	-	-	-
0.082	1.03 ±0.07	-	1.79 ±0.17	-	-	-	-	-
0.204	-	-	1.32 ±0.16	-	1.32 ±0.15	-	-	-
0.409	1.03 ±0.37	-	1.64 ±0.33	-	1.53 ±0.08	-	-	-
5								
0	-	-	1.39 ±0.23	-	1.35 ±0.04	-	-	-
0.082	1.00 ±0.17	-	-	-	-	-	-	-
0.204	1.33 ±0.26	-	1.59 ±0.34	-	1.36 ±0.11	-	-	-
0.409	1.30 ±0.20	-	1.12 ±0.29	-	1.37 ±0.13	-	0.91 ±0.05	-
15								
0	-	-	1.46 ±0.20	-	1.62 ±0.26	-	1.03	-
0.082	1.3	-	1.60 ±0.17	0.03 ±0.03	-	-	1.02 ±0.19	-
0.204	1.46 ±0.22	0.12 ±0.09	1.46 ±0.22	-	-	-	0.85 ±0.09	-
0.409	-	-	1.16 ±0.24	-	-	-	0.93 ±0.01	-
30								
0	-	-	1.56 ±0.06	-	1.53 ±0.02	-	0.90 ±0.12	-
0.082	-	-	1.14 ±0.21	-	-	-	0.89 ±0.15	-
0.204	-	-	1.12 ±0.23	-	-	-	0.85 ±0.09	-
0.409	-	-	1.26 ±0.12	-	-	-	0.88 ±0.27	-

Table 4.13 Ca/P and Si/P ratio of the crystal phases present during precipitation at 23 °C (mean± SD, n=1-10).

Silicon was detected occasionally in the sphere and flake structures. Silicon was not detected in the plate-like DCPD crystals.

At 37°C, for the control (for control see chapter 3) and precipitates formed in the presence of orthosilicic acid, spheres, plates, flakes and needles were detected from 1 min (fig.4.21a-c, 4.22a-c, fig. 4.23a-c). The electron diffraction patterns obtained for the plates were attributable to OCP and those obtained for the needles and flakes were typical of non-stoichiometric hydroxyapatite (see chapter 3). After 15 min OCP plates and needles were observed for precipitates formed in the presence of orthosilicic acid (fig. 4.21d, fig. 4.22d, fig. 4.23d). After 30 min needles were observed at all concentrations of orthosilicic acid (fig. 4.21e, fig. 4.22e, fig. 4.23e). In the presence of orthosilicic acid the Ca/P ratio of the observed crystal phases were higher than those in the control (table 4.14). The Si detected by EDX was also higher for the plate-like OCP crystals and needles (table 4.14).

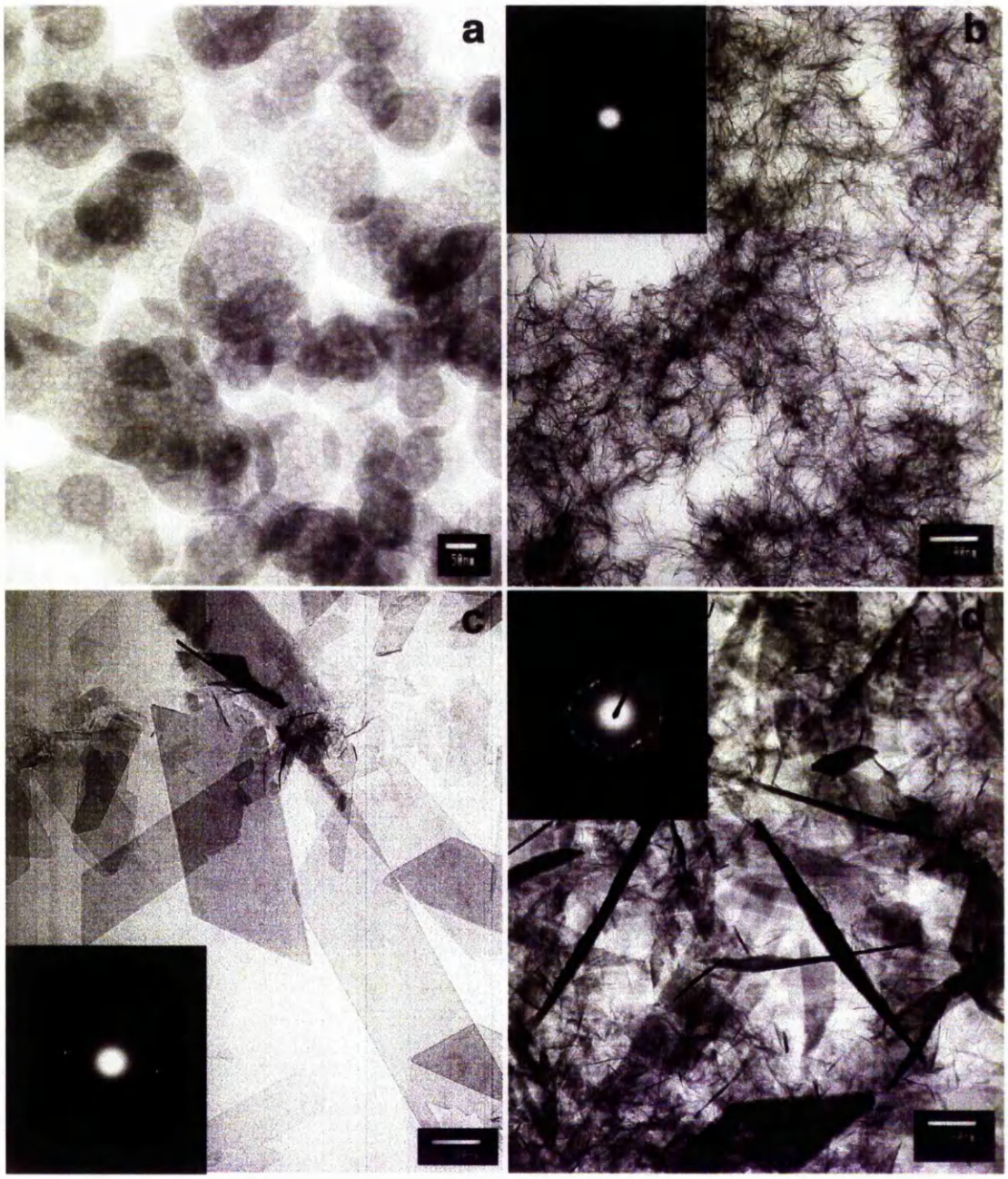

Figure 4.21 Calcium phosphate was precipitated from a solution containing 10 mM $Ca(NO_3)_2$ and 6 mM $(NH_4)_2HPO_4$ at 37°C in the presence of 0.082 mM $Si(OH)_4$. During precipitation reaction samples were taken for TEM analysis at a), b) and c) 1 min, d) 5 min (see appendix III for d-spacings values calculated from the electron diffraction data).

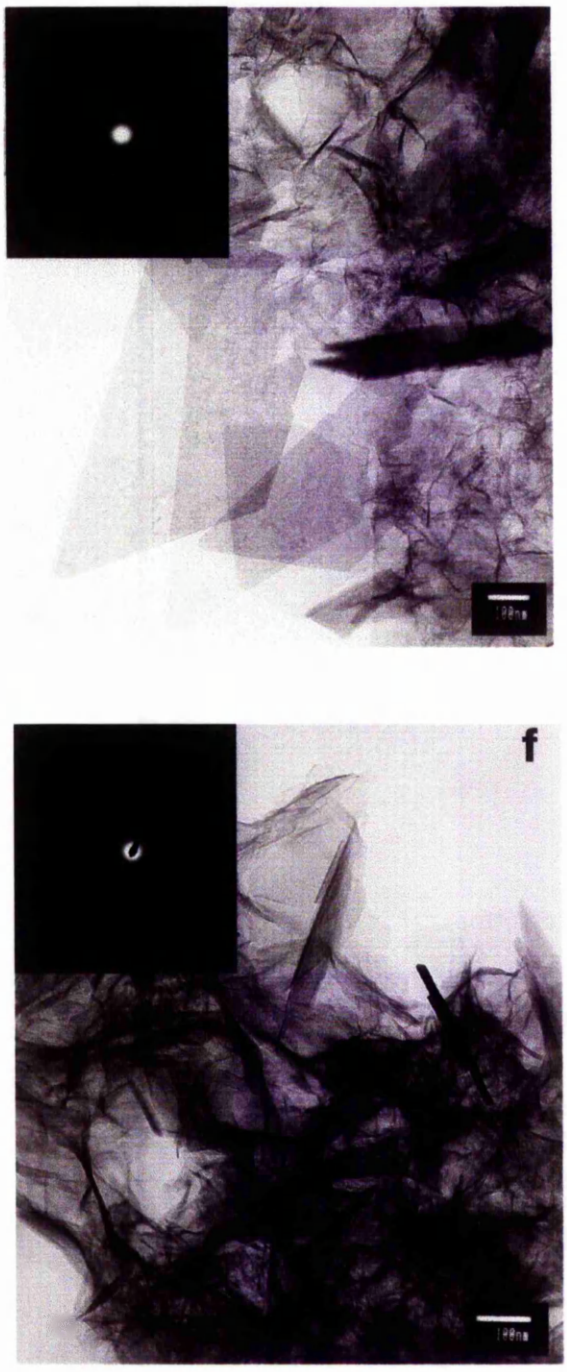

Continuation Figure 4.21 e) 15 min and f) 30 min of reaction (see appendix III for d-spacings values calculated from the electron diffraction data).

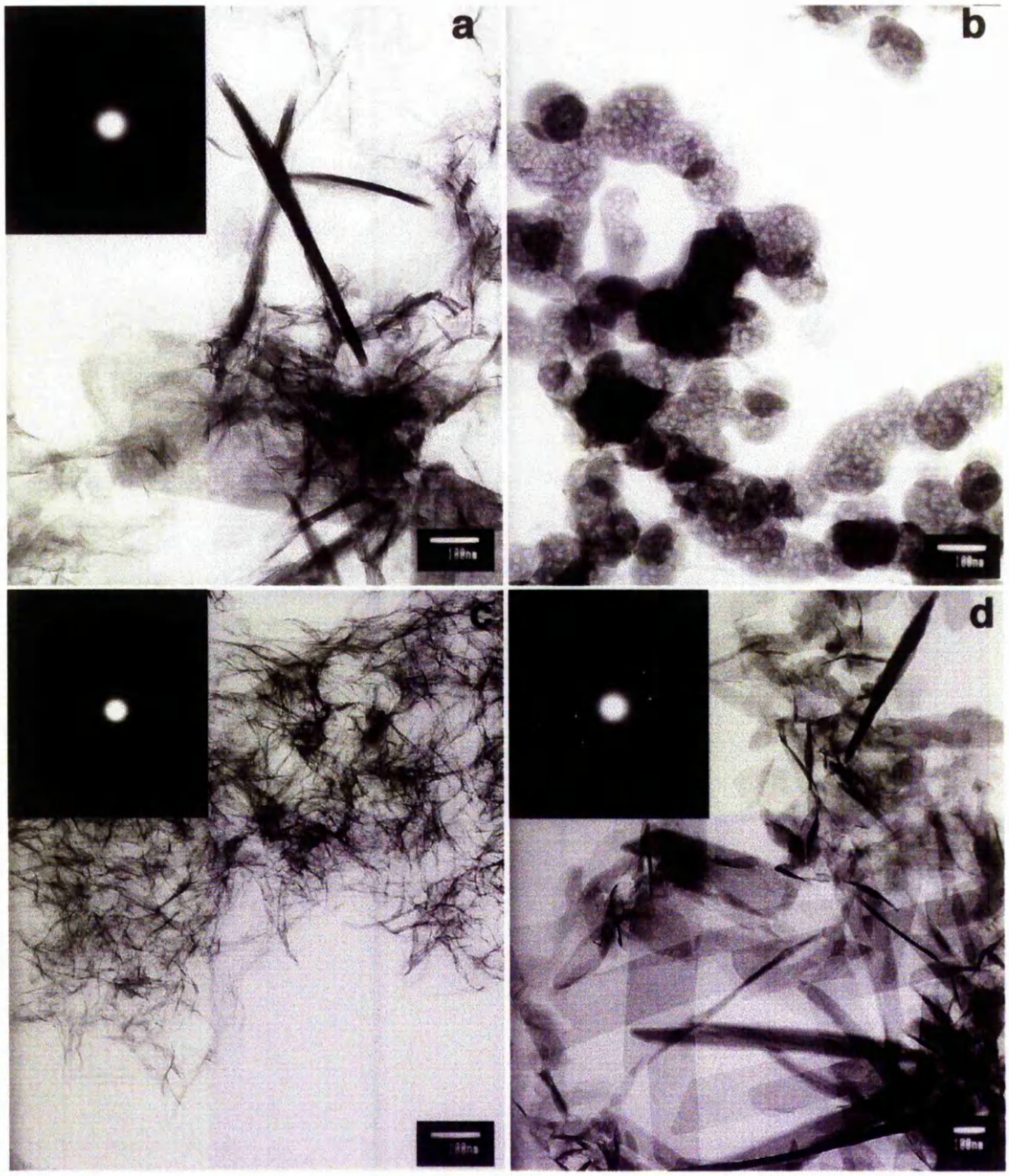

Figure 4.22 Calcium phosphate was precipitated from a solution containing 10 mM $Ca(NO_3)_2$ and 6 mM$(NH_4)_2HPO_4$ at 37°C in the presence of 0.204 mM $Si(OH)_4$. During precipitation reaction samples were taken for TEM analysis at a), b) and c) 1 min, d) 5 min (see appendix III for d-spacings values calculated from the electron diffraction data).

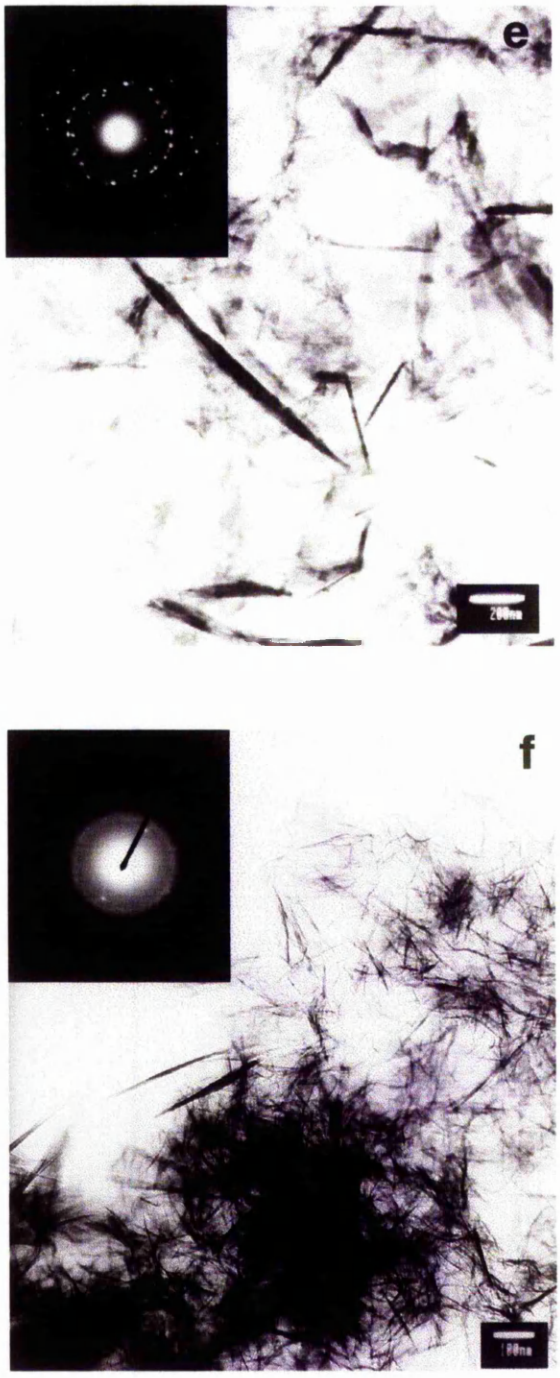

Continuation Figure 4.22 e) 15 min and f) 30 min of reaction (see appendix III for d-spacings values calculated from the electron diffraction data).

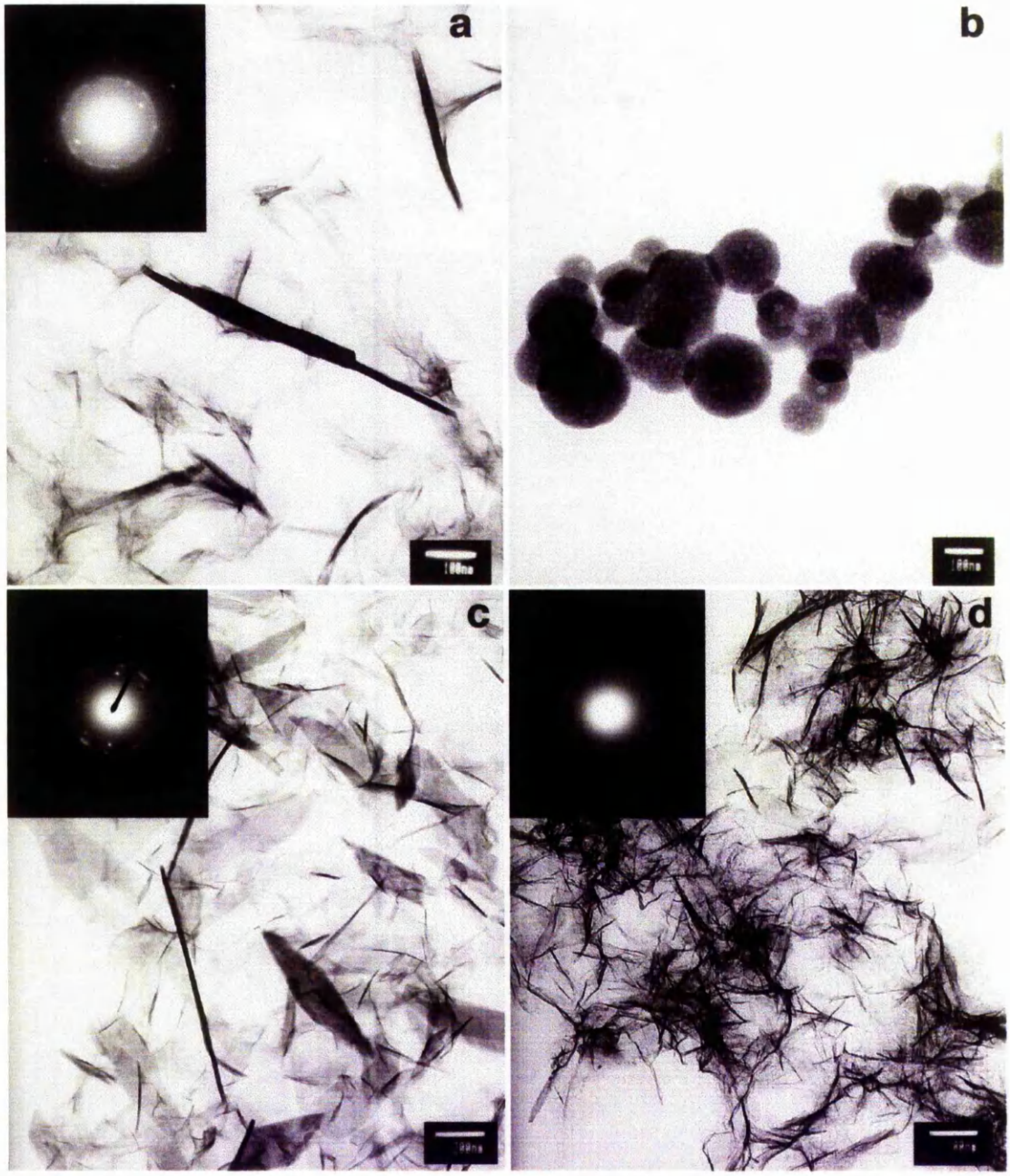

Figure 4.23 Calcium phosphate was precipitated from a solution containing 10 mM $Ca(NO_3)_2$ and 6 mM $(NH_4)_2HPO_4$ at 37°C in the presence of 0.409 mM $Si(OH)_4$. During precipitation reaction samples were taken for TEM analysis at a), b) and c) 1 min, d) 5 min (see appendix III for d-spacings values calculated from the electron diffraction data).

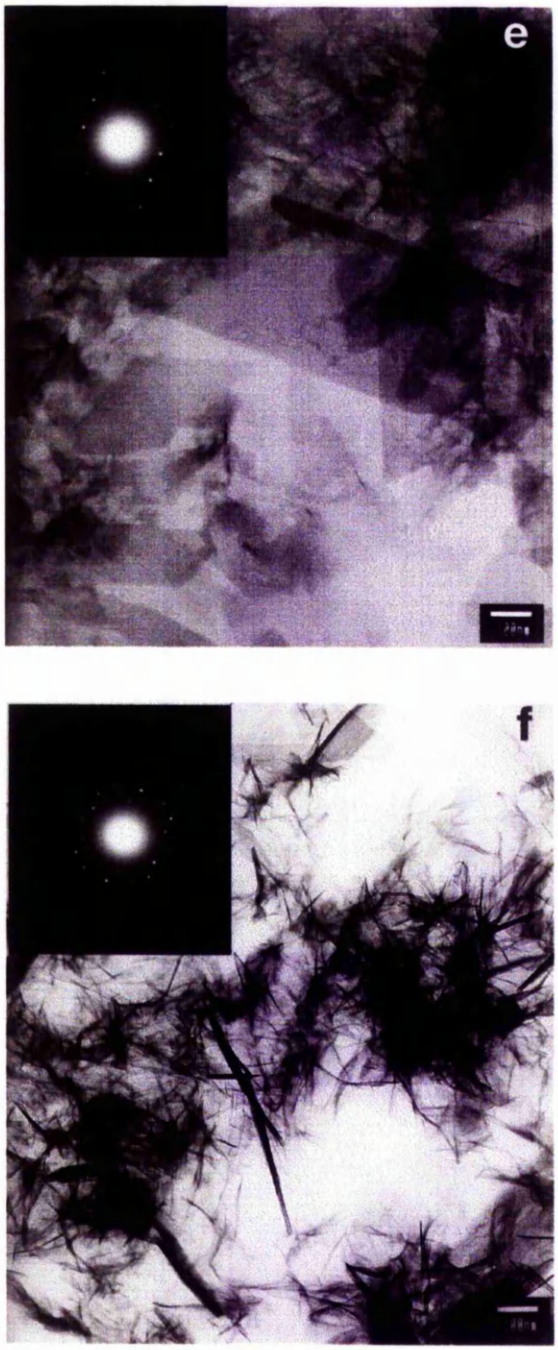

Continuation Figure 4.23 e) 15 min and f) 30 min of reaction (see appendix III for d-spacings values calculated from the electron diffraction data).

Table 4.14 shows the variation of the Ca/P and Si/P ratios for the different morphologies detected during the precipitation at 37°C.

	spheres		flakes		plate-like OCP		needles	
time (min) $[Si(OH)_4]$(mM)	**Ca/P**	**Si/P**	**Ca/P**	**Si/P**	**Ca/P**	**Si/P**	**Ca/P**	**Si/P**
1								
0	-	-	-	-	1.63 ±0.34	-	1.58 ±0.11	-
0.082	-	-	-	-	1.20 ±0.18	0.15 ±0.14	1.69 ±0.17	0.15 ±0.14
0.204	1.20 ±0.07	0.10 ±0.13	1.34 ±0.12	0.16 ±0.09	1.67 ±0.31	0.35 ±0.20	-	-
0.409	1.11 ±0.10	0.02 ±0.002	-	-	1.53 ±0.21	0.44 ±0.55	1.21 ±0.14	0.14 ±0.14
5								
0	-	-	1.42 ±0.28	-	1.69 ±0.27	-	1.65 ±0.32	-
0.082	-	-	-	-	1.66 ±0.10	0.16 ±0.18	1.62 ±0.14	0.16 ±0.15
0.204	-	-	-	-	1.57 ±0.17	0.20 ±0.23	1.54 ±0.16	0.20 ±0.23
0.409	-	-	-	-	1.53 ±0.28	0.20 ±0.06	1.48 ±0.29	0.20 ±0.06
15								
0	-	-	1.50 ±0.12	-	1.56 ±0.29	-	1.59 ±0.34	-
0.082	-	-	1.54 ±0.19	0.11 ±0.09	1.87 ±0.14	0.45 ±0.12	-	-
0.204	-	-	-	-	1.49 ±0.12	0.15 ±0.07	1.39 ±0.16	0.15 ±0.11
0.409	-	-	-	-	1.73 ±0.16	0.43 ±0.16	1.47 ±0.15	0.21 ±0.09
30								
0	-	-	-	-	1.56 ±0.18	-	1.90 ±0.29	-
0.082	-	-	-	-	1.61 ±0.12	0.08 ±0.06	1.57 ±0.12	0.12 ±0.05
0.204	-	-	-	-	1.34 ±0.13	0.44 ±0.23	1.37 ±0.14	0.09 ±0.01
0.409	-	-	-	-	1.76 ±0.26	0.19 ±0.11	-	-

Table 4.14 Ca/P and Si/P ratio of the crystal phases present during precipitation at 37°C (mean ± SD, n=1-10).

Silicon was detected in the plate-like OCP, flake-like and apatite crystals. Sometimes when silicon was detected the Ca/P molar ratio increased indicating the possibility of substitution of PO_4^{2-} for $Si(OH)_4$. However, sometimes the detection of silicon was not accompanied by

a decrease in Ca/P molar ratio. Silicon could have only been adsorbed onto the crystal surface.

Electron diffraction data for the crystal phases detected during precipitation in the presence of orthosilicic did not differ from the control (appendix III).

Samples of the material dried at 250°C for 1h were dissolved in ultrapure nitric acid and filtered through a 0.45 μm filter. Samples were sent to Manchester University for silicon analysis. No silicon was detected. The sensitivity of the technique was 1 ppm.

4.4 Discussion

The effect of orthosilicic acid on calcium phosphate formation and transformation has been studied. The data presented in this study show that orthosilicic acid has an effect depending on the initial Ca-P/Si ratio in solution. When orthosilicic acid was present in the reacting solution with a concentration of 0.242M of calcium and 0.145M of phosphate there was a slight increase in the product yield, which could suggest that silicic acid at concentrations as low as 0.041 mM stimulated the precipitation of calcium phosphate. However, when lower concentrations of calcium (10mM) and phosphate (6 mM) were used, the stimulating effect only appeared to be present for the precipitations carried out at 23°C (table 4.10).

Tanizawa *et al.* 1995, proposed the following mechanism for hydroxyapatite formation:

$$3Ca^{2+} + 2H_2PO_4^- + 4OH^- + (x-4)H_2O \rightarrow Ca_3(PO_4)_2.xH_2O \quad (1)$$

$$Ca^{2+} + H_2PO_4^- + 4OH^- + H_2O \rightarrow CaHPO_4.2H_2O \quad (2)$$

$$10[Ca_3(PO_4)_2.xH_2O] + 2OH^- \rightarrow 3Ca_{10}(PO_4)_6(OH)_2 + 2H_2PO_4^- + (10x-4)H_2O \quad (3)$$

$$10[CaHPO_4.2H_2O] + 4OH^- \rightarrow Ca_{10}(PO_4)_6(OH)_2 + 4H_2PO_4^- + H_2O \quad (4)$$

They stated that silicate ions (SiO_4^{4-}) slowed the four reactions only at low concentrations (0.44-0.88 mM) and inhibited the transformation of DCPD to HAP which can occur easily in wet conditions[14]. They did not identify any calcium-silicate containing precipitates by x-ray analysis. They also reported that the Ca/P ratio increased with an increase in silica concentration. They suggested that silica could provide favourable sites for ACP or DCPD nucleation and that a large amount of precipitate forms as a result. The incorporated SiO_4^{4-} had an stabilising effect on DCPD. Damen *et al.* (1989) also reported that small amounts of silica stimulate the spontaneous precipitation of calcium phosphate from supersaturated solutions[12]. They investigated a wide range of calcium to phosphate molar ratios and metastable solutions with a calcium phosphate concentration product as low as 1.88 mM^2. A proposed mechanism to explain this effect was proposed by Hidaka *et al.* 1996 when they studied the effects of indium and ferric ions on the precipitation of calcium phosphate[16]. They observed that these ions could behave similarly to silica. They suggested that at pH=7.4 indium and ferric ion solubilised and then the metal hydroxide [$M(OH)_3$] formed would polymerise. In the case of silica, it would be present as $Si(OH)_4$. It has been suggested that each Ca^{2+} can link approximately to one $Si(OH)_4$ group[17]:

$$Si_s(OH) + Ca^{2+} \rightarrow Si_sOCa^{2+} + H^+$$

Rølla *et al.* (1989) had already proposed that the calcium-binding capacity of the polymerised silicic acid may stimulate the spontaneous precipitation of calcium phosphate *in vitro*[10]. However, they found that concentrations of 3.0-30 mM of silicic acid and 10 mg/ml of silica inhibited calcium phosphate precipitation. They found that stimulation occurred at concentrations where the effects of chelating capacity of the polysilicic acid and silica were not significant. Therefore, when polysilicic acid and silica were in high concentration, the degree of supersaturation of calcium ions was reduced by chelation and

the formation of calcium phosphate precipitates was suppressed. Silica-gel particles have been found to stimulate the rate of hydroxyapatite formation at a concentration range of 0.05-1.5 mg/ml[17]. However, silicic acid, being a weak acid (pk_i=9.8) interacts only with basic metal ions, therefore, at physiological pH, calcium and magnesium are excluded[18]. A calcium silicate nucleating agent was proposed by Iler (1979)[3], but at pH< 9 such species are not predicted. The mechanism proposed by Hidaka *et al.* (1996) would not be valid *in vivo*[16].

Another hypothesis to explain the stimulatory-precipitation effect of silica on calcium phosphate was proposed by Karlsson *et al.* (1989)[19]. They suggested that [≡Si—O—] pairs form chelates with phosphate ions, and that this was an essential step in apatite formation. Other mechanisms proposed for the stimulatory-precipitation effect of silica on calcium phosphate are based upon silica surfaces and polymeric silica species[13]. Pereira and Hench (1996) in their review discussed the possible role of soluble silicon species[13]. They concluded that the precipitation of hydroxyapatite involved the surface of silica or oligomers of hydrated silica, rather than soluble monomeric silicate species. They reported that the physical aspects of the silica surface, the negative surface charge and the presence of nm scale porosity would be directly responsible for hydroxyapatite precipitation. They did not support the involvement of silanol groups in the nucleation process, although they did not deny the possibility.

The concentration of silica used in this study was lower than 0.5 mM, a concentration above which polymerisation of silicic acid occurs in the presence of ammonium species[20]. In the current experiments, silicon was present as a soluble species, there were not a significant concentration of polymers, no negative surface charges, and no pores to which one could attribute the stimulatory effect of silicon on calcium phosphate formation and

transformation. However, monomolecular silicon species have associated with it four hydroxyl groups and therefore, it may be possible that the silanol groups were involved in the nucleation process. The addition of orthosilicic acid to the calcium solution did not show a different effect from the addition of the orthosilicic acid to the phosphate solution prior to mixing of the two solutions. This suggests that the mechanism by which orthosilicic acid affects the nucleation is the same independent of the solution to which the orthosilicic acid had been added. As Karlsson *et al.* (1989) suggested, the orthosilicic acid could interact with the phosphate ions (fig. 4.24)

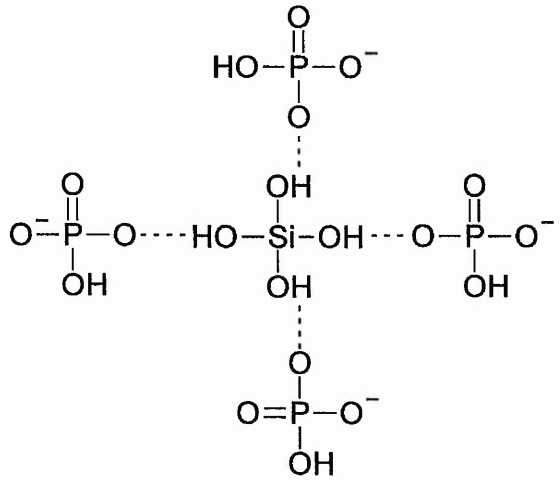

Figure 4.24 Proposed mechaninsm for complexation of silicic acid by phosphate ions.

When the concentration of phosphate was 0.242 M, the silicic acid might be able to bind at least 4 HPO_4^{2-}. The Ca^{2+} ions would be attracted by the negative charge of the phosphate groups and then calcium phosphate would form. When the pH decreases, the interaction between orthosilicic acid and phosphate would weaken and the complex would break

down. When the concentration of phosphate is lower, the degree of supersaturation would be reduced by interaction of the silicon hydroxyl groups and phosphate ions and the formation of amorphous products, (e.g. ACP) would increase. ACP would then transform in time into OCP or HAP depending on the solution conditions. As a consequence, the orthosilicic acid would provide more nucleating sites which would favour the formation of apatite. This could explain why ACP spheres were still observed after 5 min of precipitation in the presence of orthosilicic acid. Although the flake-like, plate-like OCP and needle structures were detected soon after mixing (1 min), the ACP (spheres) were still detected after 5 min indicating that silicic acid was still stimulating the nucleation of new particles. The results from this study are contrary to the results obtained by Birchall, 1986 who studied the effect of silicic acid on the precipitation and ageing of calcium phosphates[8]. He found that the addition of 1mM silicic acid did not alter the phase composition or microstructure as seen by electron microscopy when compared to the control.

The Ca/P ratios of the calcium phosphate phases present in this experiment during precipitation increased when orthosilicic acid was present in the reaction solution. Occasionally, the increase in the Ca/P ratio coincided with the detection of silicon in the structure. Although no silicon was detected in the bulk sample by atomic emission spectroscopy (AES) (detection limit is 1 ppm Si), EDX analysis detected some amounts of silicon present in the early stages of the precipitation process (table 4.14). Carlisle (1972) found that in the early stages of active calcification in young bone, when the calcium content of the preosseous tissue is very low, there is a direct relationship between silicon and calcium[21, 22].

When a crystal grows from a solution containing an additive (in this case orthosilicic acid), it will generally reject it if it is less soluble in the crystal than in the solution[23]. When the smaller crystals dissolve, larger crystals will grow (Ostwald ripening). The new growth on the latter, taking place slowly, will be purer than the dissolved crystals. Some silicon was detected in the spheres formed soon after mixing the calcium and phosphate solutions (1 min) for precipitations carried out at 37°C. As precipitation carried on, the spheres dissolved and larger crystals formed (flakes). During precipitation the solution pH decreased, and consequently the orthosilicic acid would be less strongly adsorbed onto the crystal surface. It would desorb. Therefore no incorporation of orthosilicic acid into the crystal would occur. However, if orthosilicic acid was strongly adsorbed to the crystals, and if it was sufficiently mobile, it might segregate within the crystal lattice, on dislocation lines or at the surface. If its distribution was anisotropic changes in one of the crystal lattice dimensions or habit modifications would be observed. TEM analysis showed that silica affected the length of the apatite crystals formed at 23°C. Non-stoichiometric hydroxyapatite has a hexagonal symmetry and the crystal growth direction is along the c-axis. The apatite crystals precipitated in the presence of orthosilicic acid were longer compared to those precipitated in the absence of orthosilicic acid. However, only the apatite crystals precipitated in the presence of 0.082 mM orthosilicic acid at 37°C were longer compared to those precipitated in the absence of orthosilicic acid. A change in the c unit cell parameter would be expected. Changes in the c unit cell parameter would also affect the a(=b) since the hexagonal system relates d-spacing and the a and c parameters (see appendix (II)). The x-ray data showed a decrease in the c lattice and an increase in the a(=b) lattice parameters compared to the control for the apatite crystals precipitated in the presence of orthosilicic acid at 37°C. Substitutions of Ca^{2+} with Sr^{2+}, Ba^{2+}, Cd^{2+}, and Pb^{2+}

have been obtained[24, 25]. The a(=b) and c lattice parameters of Ca^{2+}-substituted HAP vary with the substituting cationic radius: barium hydroxyapatite gives the maximum values of a=10.178 Å and c=7.730 Å[24]. Both lattice parameters increase with the cationic substitutions. The anion groups OH^- and PO_4^{3-} are, respectively, substituted with the halogen ions and CO_3^{2-}. In chloroapatite, a increases to 9.634 Å and c decreases to 6.778 Å[25].

When 10 mM Ca^{2+} and 6 mM HPO_4^{2-} were used to precipitate calcium phosphate crystals in the presence of orthosilicic acid, the formation of more than one calcium phosphate crystal phase made it impossible to analyse the unit cell parameters using the XRD data. The electron diffraction data obtained for apatite were also polycrystalline patterns and the data was not reliable enough to calculate the unit cell parameters for the apatite crystals. A fine detail single crystal analysis should be done to determine on which sites silica as orthosilicic acid is affecting the apatite structure.

Waterglass-derived silica, a number of industrial silicas and silica used in toothpaste, all reduced the induction time of calcium phosphate precipitation from supersaturated solutions to a similar extent. Waterglass when diluted at physiological pH, results in the formation of the soluble monosilicic acid[12]. Damen *et al.* (1989) found that silicic acid reduced the induction time ca. 60% at concentrations of 0.5 mM diluted from a 2mM stock solution[12]. They also found that silica could reduce the induction time in the presence of cultured oral bacteria and counteract the increase of the induction time caused by inhibitors derived from these bacteria[26]. These results supported the idea that silica when incorporated into dental plaque, may stimulate calculus formation[27]

When certain organic substances and ions inhibit the formation of calcium phosphate precipitates, a decrease in the rate of hydroxyapatite transformation usually accompanies the elongation of the induction time[28]. If agents accelerate the reaction, e.g. sodium lauryl

sulphate, an increase in hydroxyapatite transformation is associated with a shortening of the induction time[29].

Hidaka *et al.*, 1993 reported that silicates and clay-minerals regulate calcium phosphate precipitation *in vitro*[30]. Silicic acid, silica, kaolin and talc stimulate, but mica inhibited the rate of hydroxyapatite transformation without changing the induction time. Silicic acid at a concentration between 0.01 to 0.1 mM was found to stimulate the rate of hydroxyapatite transformation in the formation of calcium phosphate precipitated. They found that its effect was related to its state of polymerisation. The data from this study have shown that the induction time was shortened in the presence of orthosilicic up to a concentration of 0.082 mM for reactions carried out a 23°C. Orthosilicic acid accelerated the precipitation process and at the higher concentrations of 0.204 mM and 0.409 mM although the process was slowed down, it was still faster than the control.

The effect of orthosilicic acid on calcium phosphate precipitation *in vitro* depends on the experimental conditions, such as concentration, temperature, etc. In this study at high concentrations of calcium (0.242M) and phosphate (0.145M), orthosilicic acid increased the crystallinity of the calcium phosphate crystal phases formed at both 23°C and 37°C. When lower concentrations of calcium (10 mM) and phosphate (6mM) were used, the presence of orthosilicic acid seemed to favour the formation of apatite over DCP. At physiological concentrations this effect could be higher. Orthosilicic acid also shortened the induction time accelerating the precipitation process. Orthosilicic acid seemed to affect the crystal growth of apatite in an anisotropic way although a fine detail single crystal study would be necessary to identify how orthosilicic acid affects the crystal structure at the molecular level.

4.5 References

1. Birchall, J.D. (1995). The Essentiality of Silicon in Biology. *Chem. Soc. Rew.* **24**(5):351.
2. Carlisle, E.M. (1986). Silicon as an Essential Trace Element in Animal Nutrition. *Ciba Foundation Symposium* 121, pp 123. Silicon Biochemistry. Wiley, Chichester.
3. Iler, R.K. (1970). The Chemistry of Silica. Edited by John Wiley&Sons. Wiley-Interscience. New York.
4. Carlisle, E.M. (1970). Silicon: a possible factor in bone calcification. *Science*, **167:**179.
5. Carlisle, E.M. (1971). A Relationship Between Silicon, Magnesium and Fluorine in Bone Formation in the Chick. *Fed. Proc.*, **30**:462.
6. Carlisle, E.M. (1972). Silicon an essential element for the chick. *Science*, **178:**619.
7. Carlisle, E.M. (1974) Silicon as an essential element. *Fed. Proc.*, **33**:1758.
8. Shwarz, K. and Milne, D. B. (1972). Growth-Promoting Effects of Silicon in Rats. *Nature*, **239**:333.
9. Hidaka, S., Okamoto, Y., Abe K.B., Miyazaki, K., Suekawa, M. and Liu, S.Y. (1995). The Occurrence of Silicon-Containing Particles in Calcified Lesions of DBA/2NCrj Mice. *Archs. Oral Biol.,* **40**(8):765.
10. Rølla, G., Guggenheim, B. and Schmid, R. (1989). The Effect of Silicon on Dental Calculus Formation in the Rat. In Recent Advances in the Study of Dental Calculus, pp.97. Edited by Ten Cate. Oxford University Press, Oxford.
11. Hidaka, S., Okamoto, Y., Oga, Y., Hirose, T., and Abe, K. (1994). Localized Silicon Distribution in Supragingival Calculus From Japanese Monkeys. (*Macaca Fuscata*). *Archs. Oral Biol.,* **39**(7):595.
12. Damen, J.J.M. and Ten Cate, J.M. (1989). The effect of Silicic Acid on Calcium Phosphate Precipitation. *J. Dent. Res.*, **68**(9):1355.
13. Pereira, M.M. and Hench, L.L. (1996). Mechanisms of Hydroxyapatite Formation on Porous Gel-Silica Substrates. *J.Sol-Gel Sci. Techn.,* **7**:59.
14. Tanizawa, Y. and Suzuki, T. (1995). Effects of Silicate Ions on the Formation and Transformation of Calcium Phosphates in Neutral Aqueous Solutions. *J. Chem. Soc. Faraday Trans.,* **91**(19):3499.

15.Cullity, B.D. (1978). Elements of X-Ray Diffraction, 2nd ed., Addison-Wesley. Massachusetts.

16.Hidaka, S., Okamoto, Y., Abe K.B, and Miyazaki, K. (1996). Effects of Indium and Iron Ions on *in vitro* Calcium Phosphate Precipitation and Crystallinity. *J. Biomed. Mater. Res.*, **31**:11.

17.Birchall, J.D. and Espie, A.W. (1986). Biological Implications of the Interaction (via silanol groups) of Silicon with Metal Ions. *Ciba Foundation Symposium* 121, pp 140. Silicon Biochemistry. Wiley, Chichester.

18.Williams, R.J.P. (1986). Introduction to Silicon Chemistry and Biochemistry. *CIBA Foundation Symposium 121*, pp.24. Silicon Biochemistry. Wiley, Chichester.

19.Karlsson, K.H., Froberg, K. and Ringborn, T. (1989). A structural Approach to Bone Adhering of Bioactive Glasses. *J. Non Cryst. Solids*, **112**:69.

20.Perry, C.C. and Keeling-Tucker, T. (1998). Aspects of Bioinorganic Chemistry of Silicon in Conjunction with the Biometals Calcium, Iron and Aluminium. *J. Inorg. Biochem.*, **69**:181.

21.Carlisle, E.M. (1969). Silicon Localisation and Calcification in Developing Bone. *Fed. Proc.*, **28**:374.

22.Carlisle, E.M. (1970). A Relationship between Silicon and Calcium in Bone Formation. *Fed. Proc.*, **27**:565.

23.Walton, A.G. (1967). The Formation and Properties of Precipitates. Edited by Interscience Publishers. New York.

24.Gonzalez-Diaz, P.F. and Santos, M. (1977). On the Hydroxyl Ions in Apatites. *J. Solid State Chem.*, **22**:193.

25.Maiti, G.C. and Freund, F. (1981). Influence of Fluorine Substitution on the Proton Conductivity of Hydroxyapatite. *J. Am. Chem. Soc. Dalton Trans .*, **4**:949.

26.Damen, J.J.M. and Ten Cate, J.M. (1991). Silica-induced Precipitation of Calcium Phosphate in the presence of Inhibitors of Hydroxyapaptite Formation. *J. Dent. Res.*, **71**(3):453.

27.Rølla, G., Gaare, D., Langmyhr, F.J. and Helgeland, K. (1989). Silicon in Calculus and its Potential Role in Calculus Formation. In Recent Advances in the Study of Dental Calculus, pp.97. Edited by Ten Cate. Oxford University Press, Oxford.

28.Hidaka, S., Abe, K. and Liu, S.Y. (1991). A New Method For the Study of the Formation and Transformation of Calcium Phosphate Precipitates: Effects of Several Chemical Agent and Chinese Folk Medicines. *Archs. Oral Biol.* **36**(1):49.

29.Hidaka, S. and Abe, K. (1992). The Effects of Sodium Lauryl Sulphate and its Oxidative Breakdown Products on Calcium Phosphate Precipitation and Transformation. *Archs. Oral Biol.* **37**:159.

30.Hidaka, S., Okamoto, Y., and Abe, K. (1993). Possible Regulatory Roles of Silicic Acid, Silica and Clay Minerals in The Formation of Calcium Phosphate Precipitates. *Archs. Oral Biol.,* **38**(5):405.

CHAPTER 5: EFFECT OF AL(III) SPECIES ON THE PRECIPITATION OF CALCIUM PHOSPHATE CRYSTALS

5.1 Introduction

Al(III) is believed to be one of the contributing factors to the development of several types of human disorders such as Alzheimer's disease and osteomalacia[1-3]. Long-term haemodialysis patients with renal disease show raised serum Al(III) levels increasing the mortality risk[4]. Some studies have showed that aluminium causes calcium loss and inhibition of intestinal absorption of fluoride[5] and it might play a role in the development of bone fragility[6]. It has also been reported that aluminium inhibits bone mineralisation[7]. Other studies have shown that aluminium inhibits osteoblast proliferation and activity[8, 9]. However the mechanism of aluminium toxicity on bone is still in debate. It is not clear whether the decrease in bone mineralisation may be the result of the effect of aluminium on osteoblast function since they are required for normal matrix calcification or a direct effect of aluminium on the calcification process[10].

In vitro studies have shown that aluminium inhibits the transformation of ACP into HAP[11]. It has also been reported that aluminium and aluminium complexes inhibit the rate of the dissolution and crystal growth of calcium hydroxyapatite at concentrations ca. 1μM[12-14]. However, more recent studies have shown that aluminium did not inhibit the formation and transformation of calcium hydroxyapatite[15].

This study was undertaken to investigate the effect of aluminium on the formation of calcium phosphate crystals. Electron microscope analysis was performed to identify and characterise the calcium phosphate materials formed during the precipitation reactions in the presence of aluminium chloride.

5.2 Materials and Methods

Materials

Ammonium phosphate dibasic 99% ($(NH_4)_2HPO_4$) was purchased from Sigma Chemical Co. Anhydrous calcium nitrate anhydrous 98+% ($Ca(NO_3)_2$ was purchased from Avocado Research Chemicals Ltd. Aluminium Chloride 99% ($AlCl_3 \cdot 6H_2O$) was purchased from Fisher. Standards for use in the x-ray diffraction and FTIR analysis: Calcium phosphate dibasic ($CaHPO_4$), and Hydroxyapatite, $Ca_5(PO_4)_3(OH)$, and Corundum (α-Al_2O_3) were purchased from Sigma Chemical Co. Ultrapur HNO_3 was purchased from Prolabo.

Methods

Calcium phosphate powders were made as described in chapter 2. Prior to adjusting the pH to 7.4 and mixing the calcium and phosphate solutions, aluminium was added to the phosphate solution from a freshly prepared 750 mM stock solution of $AlCl_3 \cdot H_2O$. The final aluminium concentrations were 7.5 μM and 75 μM. $Ca(NO_3)_2$ and $(NH_4)_2HPO_4$ were used as precursors, NaCl was used as the electrolyte to keep the ionic strength constant at 0.165M. The pH was monitored during the precipitation process and samples were taken for TEM analysis (see chapter 2). After 30 min, the precipitate formed was filtered and washed with deionized distilled H_2O. The samples were dried at 250 °C for 1h and then analysed by FT-IR, XRD, EDX and TEM.

Statistics

The mean ± standard deviation was calculated from four/eight experiments using the t-Student test. Statistical comparisons were made by the F-distribution test. The difference was considered significant at $p < .05$.

5.3 Results

Figure 5.1 shows a typical example of the changes of pH changes with time during reaction at 23°C and 37°C in the presence of aluminium ions at 7.5 and 75 μM.

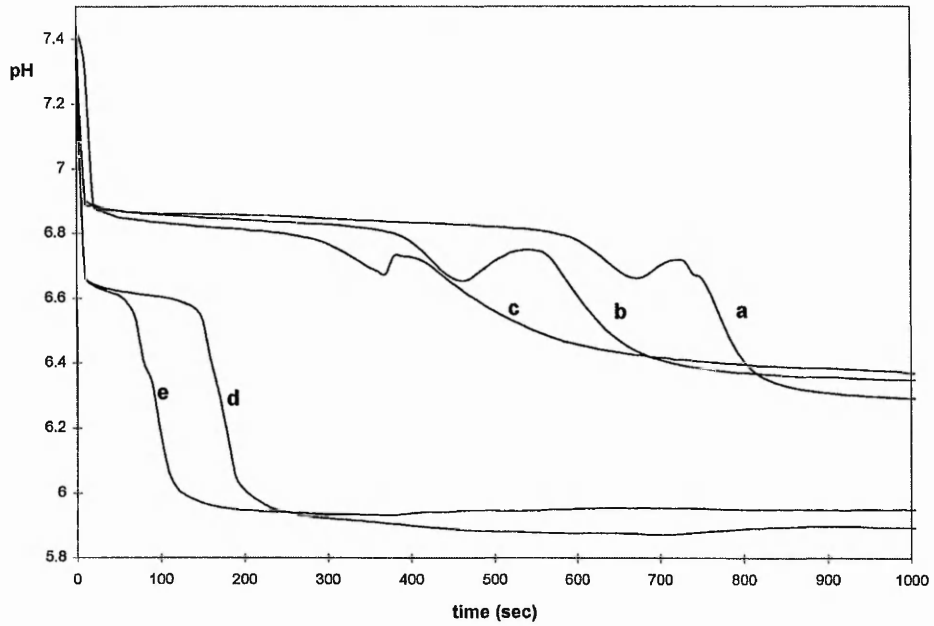

Figure 5.1 pH plotted as a function of time for experiments at 23°C a) control, b) 7.5 μM Al(III), c) 75 μM Al(III) and 37°C d) control, e) 75 μM Al(III).

For reactions run at both temperatures, the initial pH drop corresponds to the nucleation stage[16] and the presence of aluminium had no measurable effect on the pH drop, although different at the two temperatures. Following the initial pH drop due to the addition of the calcium solution to the phosphate solution, there was a period of more or less constant pH followed by a single pH drop for materials prepared at 37°C or by a series of pH changes with a final pH drop for the samples prepared at room temperature. The presence of aluminium ions in the reaction mixture had an effect on the time period for which pH remained virtually constant and on the rate of change of pH referred to as the transformation stage[16]. At 23°C the presence of aluminium reduced the time for which pH remained virtually constant from ca. 12 ± 1 minutes (control) to ca. 8 ± 1.5 minutes (7.5

μM Al) to ca. 10 ± 1 minutes (75μM Al) although the pH of the system was also slightly reduced in the presence of the aluminium ions.

The precipitates formed were analysed for aluminium content by atomic absorption spectrometry (table 5.1). The aluminium content in the sample increased with increasing concentration of aluminium present in the reaction solution.

	Al concentration ($mg.g^{-1}$) Mean ± SD	
	23 °C	**37°C**
control	2.060 ± 0.013	3.055 ± 0.0003
7.5 μM Al(III)	4.838* ± 0.027	-
75 μM Al(III)	28.931* ± 0.366	23.826* ± 0.343

Table 5.1 Concentration of aluminium in precipitates dried at 250 °C for 1h after 30 min of reaction. (*$p < 0.05$ compared to control, n=2).

FT-IR analysis of the precipitates formed at 23°C showed that the bands at ca 1100 cm^{-1} were shifted to higher wavenumber for precipitates prepared in the presence of aluminium (fig. 5.2).

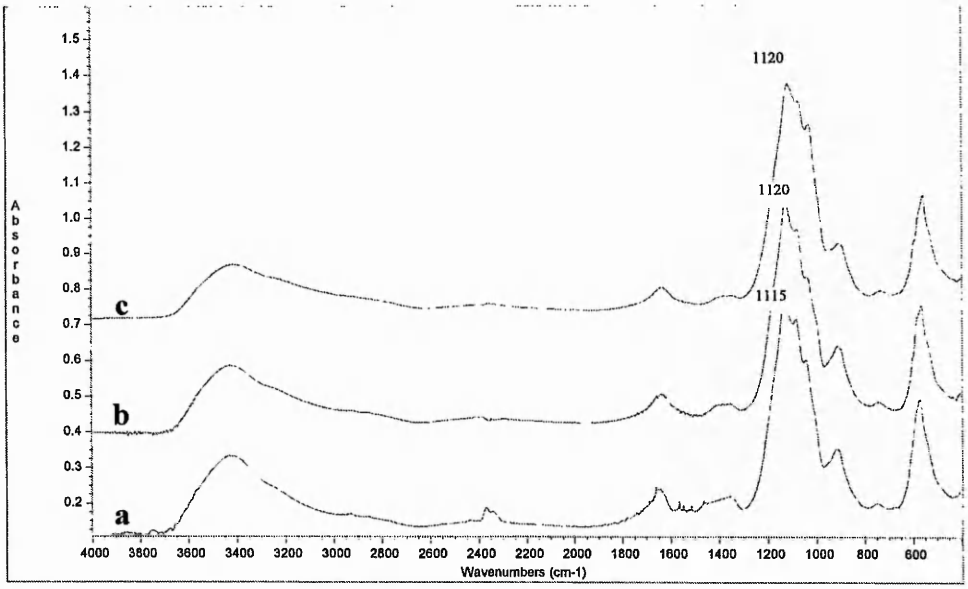

Figure 5.2 FT-IR spectra of the precipitates formed at 23°C in the presence of a) 0, b) 7.5 μM, and c) 75 μM Al(III) after drying at 250°C for 1h.

XRD analysis showed that the shifts observed in the infrared which at first suggested a higher proportion of DCP within the sample, (fig. 5.2b and 5.2c) were due to a decrease in crystallinity of the precipitates when they formed in the presence of aluminium (fig. 5.3).

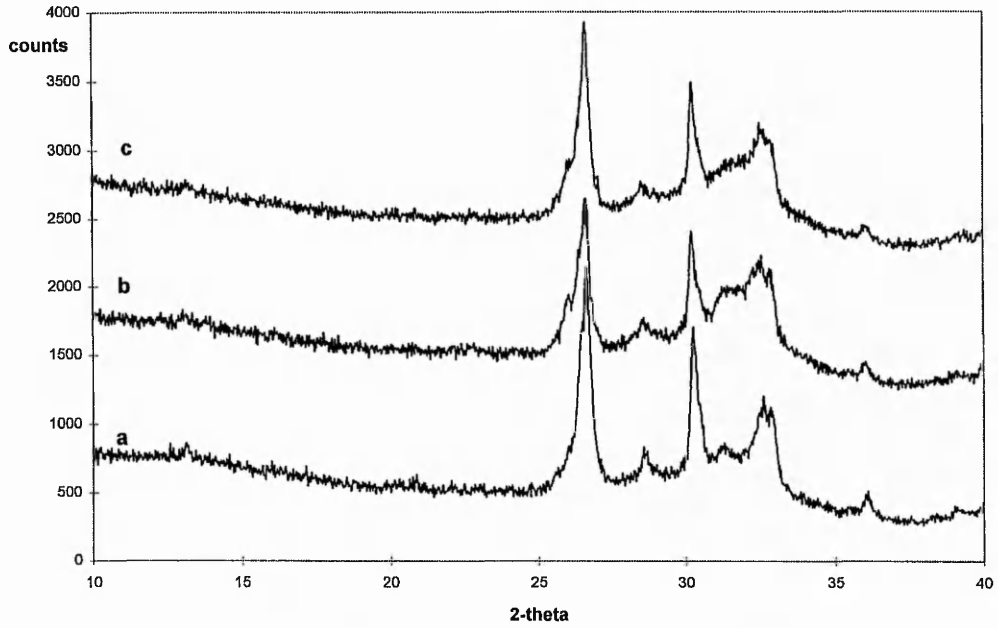

Figure 5.3 XRD patterns of the precipitates formed at 23°C in the presence of a) 0, b) 7.5 μM. c) 75 μM Al(III) after drying at 250°C for 1h.

The precipitates formed at room temperature gave patterns characteristic of DCP (fig. 5.3, see chapter 3) although the area to the low 2-theta side of the reflections at around 33° two-theta and to the low two-theta side of the reflection at ca. 26° two-theta indicated the presence of apatitic material which was later confirmed by electron microscopy analysis. The addition of aluminium to the precipitation mixture resulted in a broadening of the reflections indicating that the DCP crystals formed in the presence of aluminium were less crystalline, (fig. 5.3b and 5.3c).

At 37°C the presence of aluminium in the sample resulted in the reduction or disappearance in the infrared spectra of the band at 634 cm^{-1} and at 3567 cm^{-1} corresponding to the OH librational mode and to the OH stretching mode of HAP respectively and reduction in intensity of the band at 961 cm^{-1}, (fig. 5.4) which was assigned to the PO_4^{3-} stretching mode.

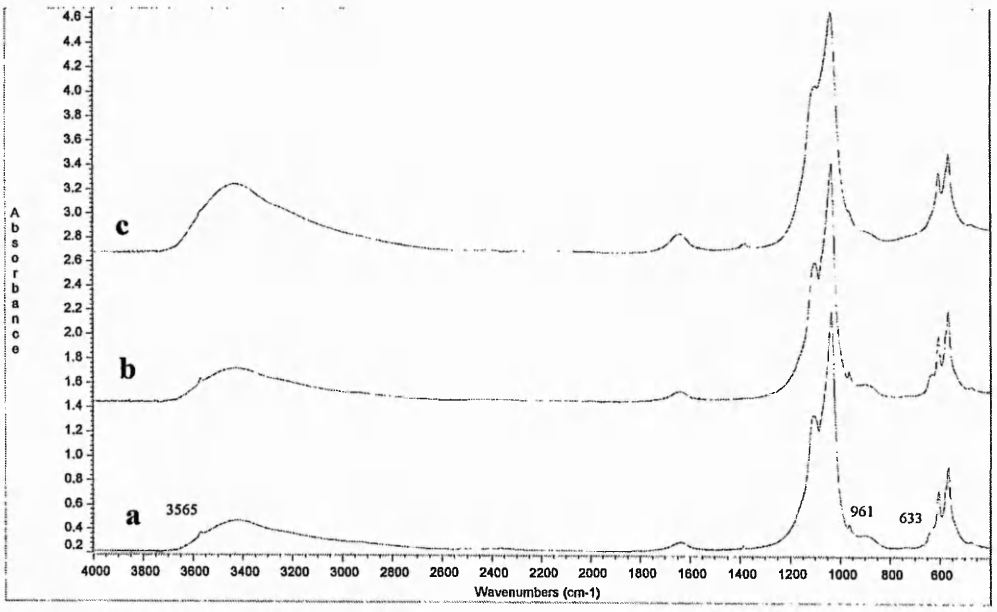

Figure 5.4 FT-IR spectra of the precipitates formed at 37°C in the presence of a) 0, b) 7.5 μM. c) 75 μM Al(III) after drying at 250°C for 1h.

The XRD patterns obtained from the precipitates prepared at 37°C were poorly-crystalline apatite-like crystals, (fig. 5.5) compared to the control.

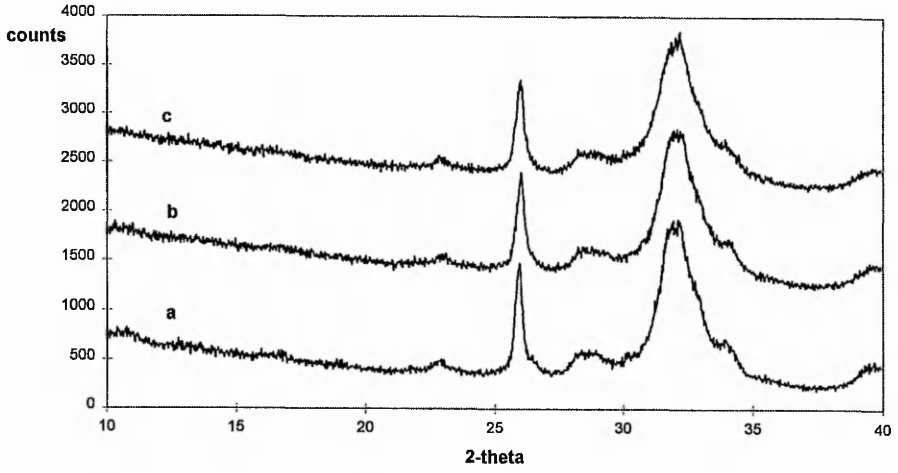

Figure 5.5 XRD patterns of the precipitates formed at 37°C in the presence of a) 0, b) 7.5 μM. c) 75 μM Al(III) after drying at 250°C for 1h.

The XRD data obtained from materials precipitated at both temperatures gave no indication for the presence of aluminium phosphates in the precipitated material (see appendix).

An x-ray broadening analysis and particle size determination based on the Debye-Scherrer equation[17] was performed using the (-220) and (-112) reflections for the precipitate formed at 23°C and (0 0 2) and (2 1 1) for the precipitate formed at 37°C. The presence of aluminium in the precipitation medium produced a systematic decrease in the average crystallite size, table 5.2. However, statistical analysis of the data indicated that there was little difference in the crystallinity of materials precipitated in the absence and presence of aluminium.

	23 °C (DCP)		37 °C (HAP)	
	(-2 2 0)	**(-1 1 2)**	**(0 0 2)**	**(2 1 1)**
control	181 ± 33	259 ± 24	194 ± 14	45 ± 3
7.5 μM Al(III)	150 ± 26	255 ± 50	175 ± 28	44 ± 3
75 μM Al(III)	138 ± 17	200 ± 35	154* ± 8	42 ± 2

Table 5.2. Crystallites sizes (Å) were calculated by the Debye-Scherrer equation. (*$p < 0.05$, n=4).

Electron microscopy studies were able to provide a much fuller picture of the mineral phases present in a given sample and the effects of aluminium on the development of calcium phosphates. Samples were analysed by the dipping method between 1 minute and 30 minutes after the start of the reaction (for the control samples see chapter 3). When aluminium was added to the reaction medium the process of crystallisation was speeded up, (fig. 5.6). At 23°C, in the presence of aluminium, flakes, needles and plates were all detected at 1 minute after the start of the reaction (fig. 5.6b-d). Amorphous aggregates such

as those depicted in figure 5.6a were also observed from 1 minute after the start of the reaction. The aggregate structure contained calcium, aluminium and phosphorous. After 5 minutes of reaction, plates of OCP, some flakes and large plates of DCPD were observed. At 15 minutes the main phase detected was DCPD together with some flakes (fig. 5.6 f-h). The flake-like structures detected in the presence of aluminium were even less well formed than in the absence of aluminium (see chapter 3). Electron diffraction of the flakes formed in the presence of aluminium showed fewer rings than from material with similar appearance prepared in the absence of aluminium (fig. 5.6d).

At 37°C in the presence of aluminium, plates of OCP were only observed at the 1 minute sampling point (fig 5.7b). A few poorly formed needles of HAP were observed at later time points (fig. 5.7c) but the principal morphology observed was flakes of a non-stoichiometric apatitic phase (fig. 5.7e,f). Amorphous aggregates like those observed for reactions carried out at 23°C were also observed at all time points (fig. 5.7d).

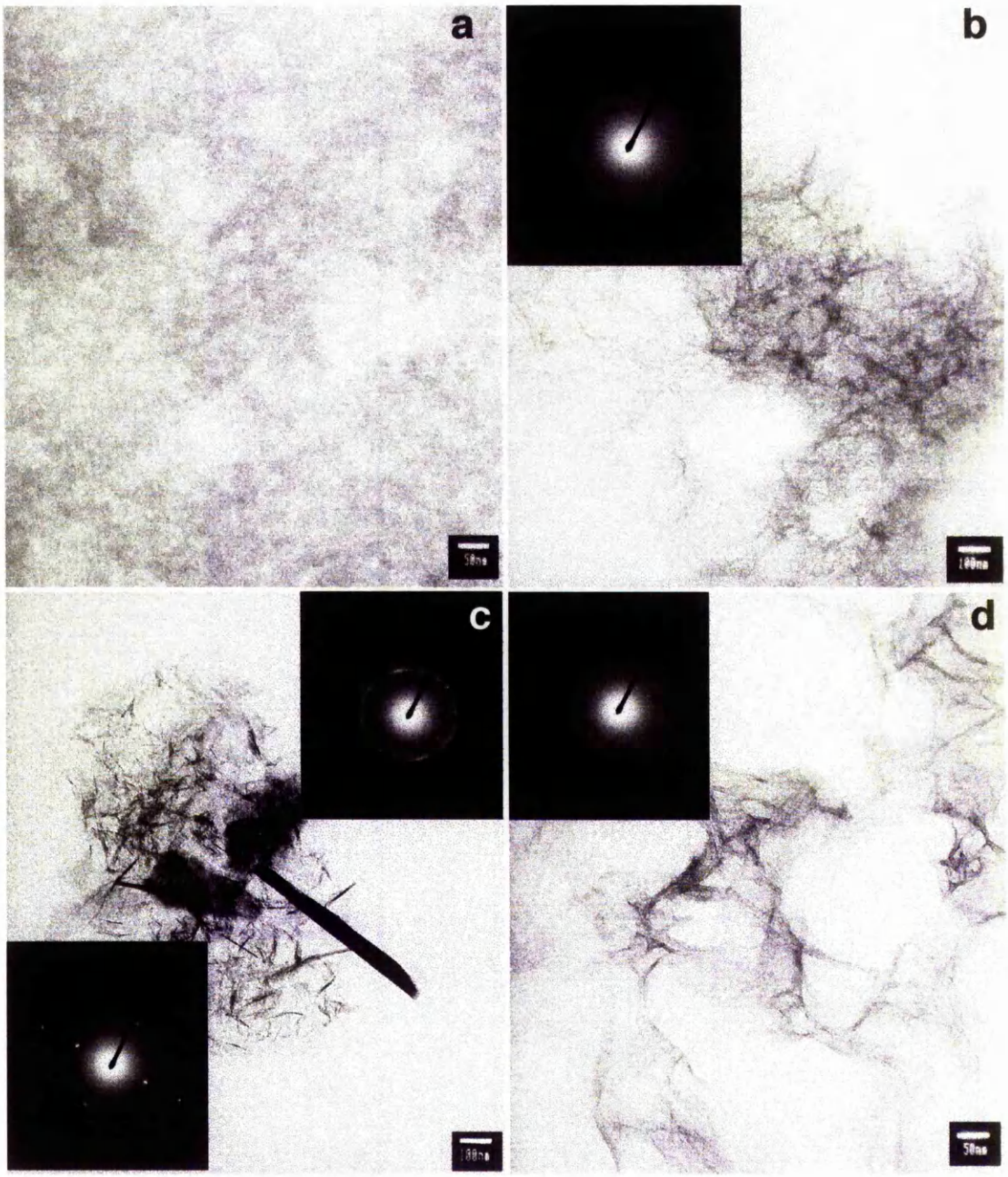

Figure 5.6 Calcium phosphate was precipitated from a solution containing 10 mM $Ca(NO_3)_2$ and 6 mM $(NH_4)_2HPO_4$ at 23°C in the presence of 75 μM Al(III). During precipitation reaction samples were taken for TEM analysis at a) and b) 1 min, c) and d) 5 min (see appendix III for d-spacings values calculated from the electron diffraction data).

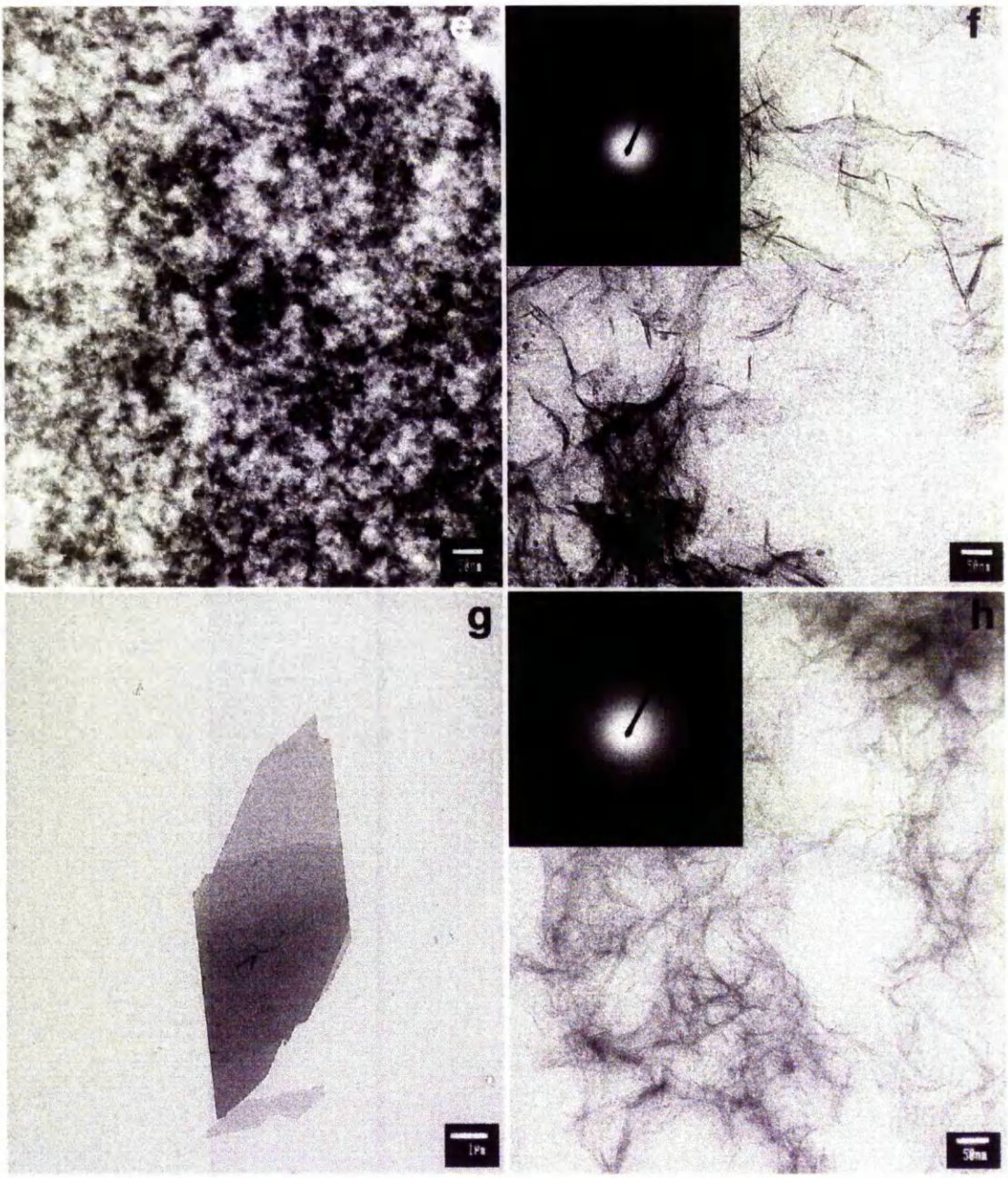

Continuation Figure 5.6 e) and f) 15 min and g) and h) 30 min of reaction (see appendix III for d-spacings values calculated from the electron diffraction data).

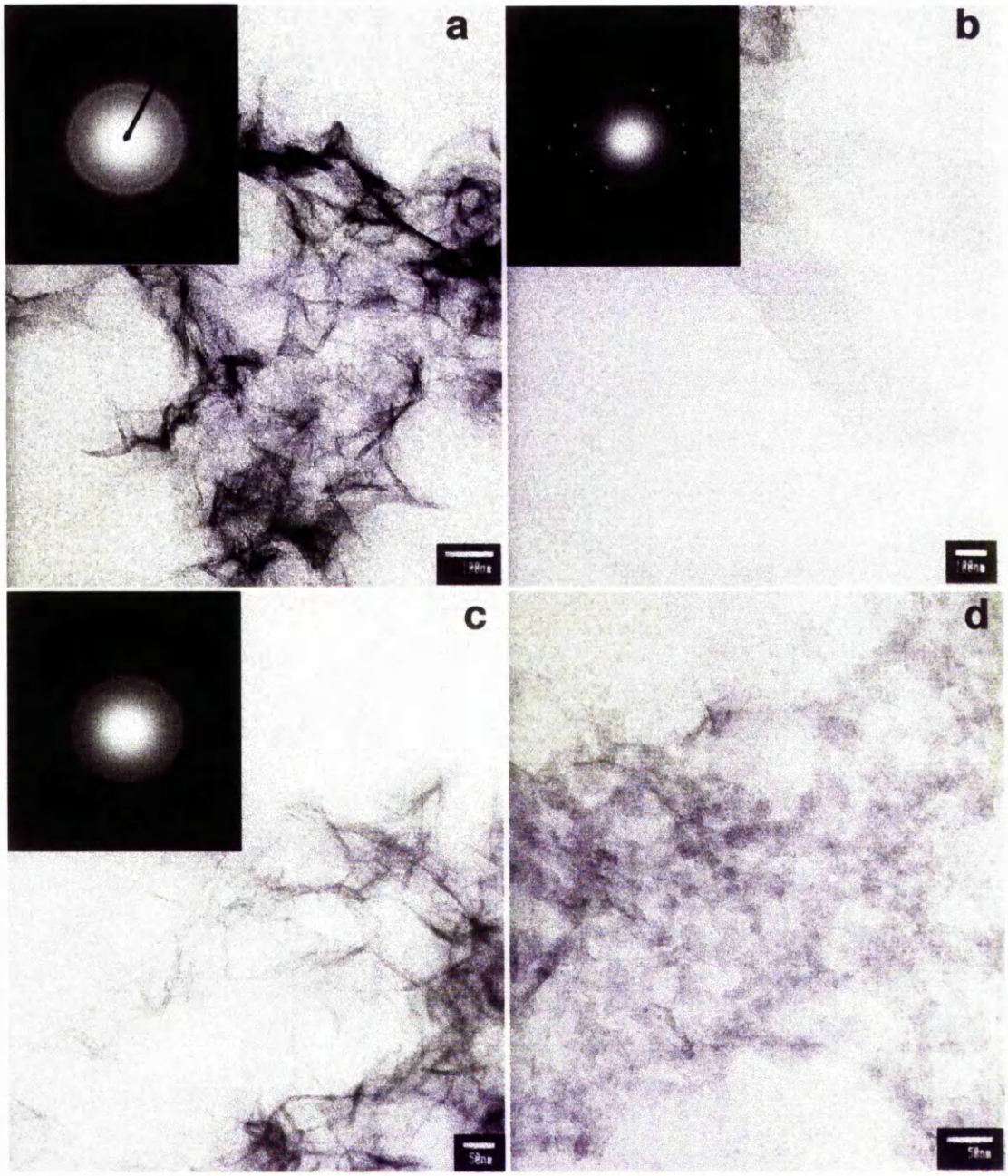

Figure 5.7 Calcium phosphate was precipitated from a solution containing 10 mM $Ca(NO_3)_2$ and 6 mM $(NH_4)_2HPO_4$ at 37°C in the presence of 75 μM Al(III). During precipitation reaction samples were taken for TEM analysis at a)1 min, b) and c) 5 min, d)15 min (see appendix III for d-spacings values calculated from the electron diffraction data).

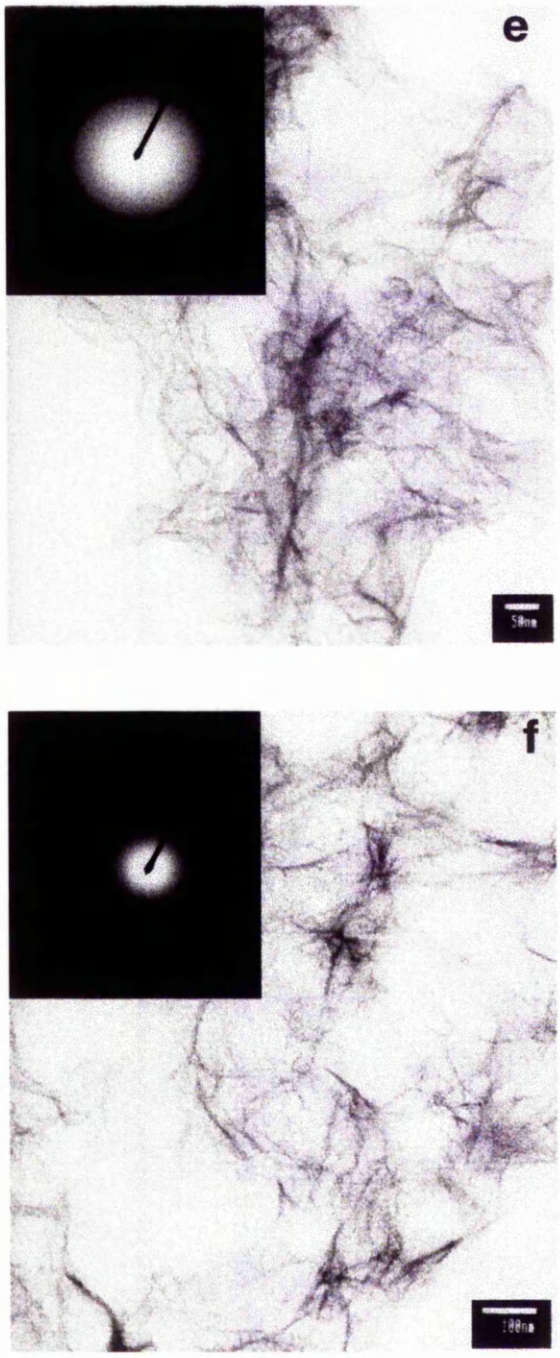

Continuation Figure 5.7 e) 15 min and f) 30 min of reaction (see appendix III for d-spacings values calculated from the electron diffraction data).

Table 5.3 lists the Ca/P and Al/P molar ratios for the precipitates formed at 23°C and 37°C in the presence of 75 μM for the crystal structures observed during the reactions.

T(°C)	amorphous aggregates		flakes		needles		plate-like DCP	
23	**Al/P**	**Ca/P**	**Al/P**	**Ca/P**	**Al/P**	**Ca/P**	**Al/P**	**Ca/P**
1	0.91 ± 0.19	0.57 ± 0.16	0.04 ± 0.01	1.45 ± 0.19	-	-	0.08 ± 0.00	0.87 ± 0.04
5	0.18 ± $1.8x10^{-3}$	0.82 ± 0.27	0.06 ± 0.01	1.45 ± 0.38	-	-	-	1.05 ± 0.16
15	0.60 ± 0.21	1.10 ± 0.48	0.07 ± 0.04	1.24 ± 0.34	-	-	-	0.93 ± 0.20
30	0.63 ± 0.04	0.66 ± 0.02	0.16 ± 0.06	1.12 ± 0.11	-	-	-	0.94 ± 0.04
37								
1			0.02 ± $1.1x10^{-4}$	1.35 ± 0.07	0.04 ± 0.00	1.63 ± 0.02	-	-
5	0.68 ± 0.07	0.63 ± $4x10^{-3}$	0.04 ± 0.02	1.64 ± 0.33	0.06 ± 0.02	1.51 ± 0.22	-	-
15	0.86 ± 0.24	0.53 ± 0.11	0.09 ± 0.02	1.36 ± 0.30	0.29 ± 0.00	1.70 ± 0.52	-	-
30	0.66 ± 0.26	0.68 ± 0.26	0.12 ± 0.04	1.56 ± 0.19	-		-	-

Table 5.3 Al/P ratios for the precipitate formed at 23°C and 37°C in the presence of 75 μM Al(III),(mean ± SD, n=1-10).

The Al/P molar ratio increased during reaction for the flake-like structure precipitated at 23°C. A similar trend was observed for the needle-like crystals formed at 37°C (table 5.3). After 15 min no more needles were observed. The increment in the Al/P molar ratio was accompanied with a decrease in the Ca/P suggesting some substitution of Ca^{2+} by Al^{3+} might have occurred.

5.4 Discussion

For the control material prepared at 23°C two calcium phosphate phases were present, hydrated DCP and an apatite phase. Due to the difference in crystal sizes, the presence of the apatite phase was hidden by the low intensity of its reflections (x-ray diffraction) and the high intensity of the reflections from the DCP crystals which were much larger in size. In contrast, the IR absorbance of the apatite phase was much higher than the absorbance for DCP. This inability to detect phases present at significant levels could lead to confusion when interpreting FT-IR data (FTIR is a technique often used in studies of calcium phosphates) as the presence of DCP causes a shift in the band usually seen at 1091 cm^{-1} and the apearance of a band at ca. 900 cm^{-1} which could also be attributed to non-stoichiometric apatites unless other techniques have been used to confirm their presence or not.

For material prepared at 37°C, OCP, ACP and apatite crystals were all identified by the electron microscopy studies. The XRD pattern obtained from the precipitate was typical of apatite. It was not possible to assign the reflections to any of the other phases present in the system due to the close values of their d-spacings. Infrared spectra also indicated the presence of an apatitic phase but did not allow OCP and ACP phases to be identified.

The human body contains from ca. 2 mmol (extracellular fluids, pH=7.4) to ca 10 (intracellular fluids, pH=6.6) of total phosphate per liter. Aluminium phosphate as $AlPO_4$ cannot form in the human body. Both of the required ions are incompatible in solution at the working pH with PO_4^{3-} ion as the dominant phosphate species only at pH>11.6[18], and Al^{3+} as the dominant Al^{3+} species at pH<5.5[19]. At pH 7.4 values HPO_4^{2-} is the dominant phosphate species[20]. From pH 2 to 6.8 $H_2PO_4^-$ dominates[18]. It has also been reported that

the reduction of phosphate by aluminium phosphate formation does not contribute significantly to the inhibition of HAP formation[21]. At the start of the reaction (pH 7.4) the aluminium was present as the aluminate ion ($Al(OH)_4^-$). Following on from the initial nucleation stage, aluminium seemed to affect the precipitates in the pH range between 6.7-6.4 for materials prepared at 23°C, and ca. pH 6 for materials prepared at 37°C where the concentration levels of the $Al(OH)_2^+$ ion are significant. The $Al(OH)_2^+$ ion may interact with $H_2PO_4^-$ giving $Al(OH)_2 \cdot H_2PO_4$, the solubility of which would limit the free Al^{3+} concentration[18]. There would also be an effect on the equilibrium distribution of $H_2PO_4^-$ and HPO_4^{2-} species which could also modify the calcium phosphate species formed. This shift in equilibrium may also reduce the availability of the HPO_4^{2-} ion to the formation of DCP where aluminium was only detected at the first stages of the precipitation reaction and not detected thereafter. However, the presence of the aluminium still inhibited crystal growth of this phase as evidenced by electron microscopy.

It has been suggested that Al(III) is incorporated into the HAP and OCP crystals probably via a calcium release / aluminium uptake process[21]. Under the experimental conditions employed in this present study, HAP was formed by the transformation of an apatitic flake-like precursor and also by the transformation of the apatitic precursor through an intermediate OCP phase. If the incorporation of Al(III) occurs during the transformation process this could explain the disappearance of OCP after 5 min of the precipitation reaction. The Al(III) species and even the $Al(OH)_2 \cdot H_2PO_4$ may adsorb on the surface of ACP acting as crystal poisons thus preventing the transformation of ACP to HAP. In the case of the ACP to OCP to HAP conversion, the Al(III) species and $Al(OH)_2 \cdot H_2PO_4$ may adsorb to the intermediate phase formed from the dissolution of OCP when it transforms into HAP via the same mechanism.

Birchall, 1986 reported that aluminium could not substitute into the hydroxyapatite lattice and that a mixed Ca/Al phosphate prevented the nucleation, or formation on the surface, of hydroxyapatite and retarded growth[22]. He reported that aluminium had a dramatic effect on the precipitation of calcium phosphate at 17°C from a solution containing 2.5 mM Ca^{2+} and 6.6 mM PO_4^{3-}. He observed that the hydrated DCP was replaced by gelatinous non-crystalline material and this affected the normal progress of crystalline phase development[22].

The AA data showed the presence of Al in the bulk precipitate formed in the presence of Al(III) species. The aluminium content in the sample increased with increasing concentration of aluminium present in the reaction solution. However, the aluminium could come from the amorphous aggregates although the possibility that some $Al(OH)_3$ precipitated could not be rejected. EDX analysis of crystallites also showed the presence of aluminium the level of which varied depending on the crystal type. When a crystal grows from an impure solution (consider Al(III) species as impurities), the impurities may adsorb onto the crystal surface. If the impurity is strongly adsorbed then it will be embedded[23]. The largest crystals are supposed to be the most impure because they nucleate first at high supersaturation. However, in the present system DCP and OCP being the largest crystals showed the lowest aluminium content (see table 5.3). This suggests that aluminium affects the formation of calcium phosphate in the nucleation stage too. Once aluminium has precipitated with Ca and P, it would not redissolve, thereby preventing the growth of the calcium phosphate crystal.

Boskey *et al.*, 1976 who studied the effect of aluminium on the nucleation of hydroxyapatite in dilute solution at pH 7.4, reported similar results[24]. Under their conditions, in a supersaturation range claimed to be similar to that existing *in vivo*,

hydroxyapatite could be formed directly, without an amorphous precursor. Electron microscopy and electron diffraction were used to determine the phase and composition of the very small (5-100 nm) solid particles formed by this method. Particles with hydroxyapatite diffraction spacings and a Ca/P ratio of ca. 1.6 were formed in the control reaction ([Ca] 1.8 mM, [PO_4] 1 mM). However with the addition of 10^{-5} M Al, no hydroxyapatite was produced and the amorphous products were composed of a mixture of phosphates containing both Al and Ca[11]. The electron microscope data obtained from this study suggest that the amorphous aggregates formed in the presence of Al(III) species may be the same as the amorphous products observed by Boskey[11] and the gelatinous non-crystalline material observed by Birchall[22].

In respect of the effect of Al on the mineral component of bone, Meyer&Thomas (1982) had already suggested that Al might seriously interfere with the deposition process[14]. This study agrees with their suggestion. Al(III) seems to stop the transformation of ACP into HAP and the further development of the crystal by precipitating with Ca and P and forming a very insoluble amorphous material. The formation of this complex at the beginning of the reaction could also be the reason for the shortening of the induction time observed in the pH-time curves.

5.5 References

1. Mjöberg, B. (1990). Aluminium May Cause Senile Dementia and Bone Fragility *Calcif. Tiss. Int.* **47**:259.
2. Spencer, H. and Kramer, L. (1985). Osteoporosis: Calcium, Fluoride and Aluminium Interactions. *J. Am. Coll. Nut.* **4**:121.
3. O'Mahony, D. Denton, J., Templar, J., O'Hara., M., Day, J.D., Murphy, S., Walsh, J.B. and Coakley, D. (1995). Bone Aluminium Content in Alzheimer's Disease. *Dementia* **6**:69.

4. Sebert, J.L, Marie, A., Gueris, J., Herve, M.A., Leflon, P., Garabedian, M., Smadja, A., and Fournier, A. (1985). Assessment of the Aluminium Over Load and of its Possible Toxicity in Asymptomatic Uremic Patients: Evidence for a Depressive Effect on Bone Formation. *Bone* **6**:373.
5. Zafar, T., Weaver, C.M., Ashendel, C., and Dunn, M.A. (1997). Effect of Aluminium on Calcium Absorption and Bone Strength. *FASEB J.* **11**(3):3308.
6. Mjöberg, B., Hellquist, E., Mallmin, H., and Lindh, U., (1997). Aluminium, Alzheimer's Disease and Bone Fragility. *Acta Orthop. Scand.* **68**(6):511.
7. Ellis, H.A., McCarthy, J.H., and Herrington, J.J. (1979). Bone Aluminium in Hemodialyzed Patients and in Rats Injected with Aluminium Chloride: Relationship to Impaired Bone Mineralisation. *J. Clin. Pathol.* **32**:834.
8. Zhu, J.M, Huffer, W., and Alfrey, A.C. (1990). Mechanism of Aluminium Induced Bone-Disease. *Kidney Int.* **38**:1141.
9. Rodriguez, M., Felsenfeld, A.J., and Llach, F. (1990). Aluminium Administration in the Rat Separately Affects the Osteoblast and Bone Mineralisation. *J. Bone Min. Res.* **5**(1):59.
10. Quarles, L.D. (1991). Paradoxical Toxic and Trophic Osseous Actions of Aluminium: Potential Explanations. *Mineral Electrolyte Metab.* **17**:233.
11. Posner, A.S., Blumenthal, N.C. and Boskey, A.L. (1986). Model of Aluminium Induced Osteomalacia: Inhibition of Apatite Formation and Growth. *Kidney Int.* **18**:S17.
12. Christoffersen, M.R. and Christoffersen, J. (1985). The Effect of Aluminium on the Rate of Dissolution of Calcium Hydroxyapatite: A Contribution to the Understanding of Aluminium-Induced Bone-Diseases. *Calcif. Tiss. Int.* **37**:673.
13. Christoffersen, M.R. , Thyregod, H.C. and Christoffersen, J. (1987). Effects of Aluminium (III), Chromium (III), and Iron (III) on the Rate of Dissolution of Calcium Phosphate Hydroxyapatite with Absence and Presence of the Chelating Agent Desferrixoamine.*Calcif. Tiss. Int.* **41**:27.
14. Meyer, J.L and Thomas, W.C. (1986). Aluminium and Aluminium Complexes: Effect on Calcium Phosphate Precipitation. *Kidney Int.* **S18**:S20.
15. Okamoto, Y., and S. Hidaka, S. (1994). Studies on Calcium-Phosphate Precipitation: Effects of Metal Ions used in Dental Materials. *J. Biomed. Mater. Res.* **28**:1403.

16. Christoffersen, J., Christoffersen, M.R., Kibalczyc, W., and Andersen, F.A. (1989). A Contribution to the Understanding of the Formation of Calcium Phosphates. *J. Cryst. Growth* **94**:767.

17. Cullity,B.D. (1978). Elements of X-Ray Diffraction, 2nd ed., Addison-Wesley Publishing Company, Massachusetts.

18. Stumm, W., and Morgan, J.J. (1991). Aquatic Chemistry, 2nd ed., John Wiley&Sons, New York.

19. Martin, R.B., (1991). Aluminium in Chemistry Biology and Medicine, Vol. 1. Edited by Nicolini, M., Zatta, P.F. and Corain, B. Cortina International, Verona and Raven Press, New York.

20. Kiss, T., Zatta, P., Corain, B. (1996). Interaction of Aluminium (III) with Phosphate-binding Sites: Biological Aspects and Implications. *Coord. Chem Rev.* **149**:329.

21. Tanizawa, Y., Sawamura, K., and Suzuki, T. (1990). Reactions Characteristic of Dental and Synthetic Apatites with Fe^{2+} and Fe^{3+} Ions. *J. Chem. Soc. Faraday Trans.* **86**:4025.

22. Birchall, J.D. and Espie, A.W. (1986). Biological Implications of the Interaction (via silanol groups) of Silicon with Metal Ions. *Ciba Foundation Symposium* 121, pp 140. Silicon Biochemistry. Wiley, Chichester.

23. Walton, A.G. (1967). The Formation and Properties of Precipitates. Edited by Interscience Publishers. New York.

24. Boskey, A.L. and Posner, A.S. (1976). Formation of Hydroxyapatite at Low Supersaturation. *J. Phys. Chem.*, **80**(1):40.

CHAPTER 6: EFFECT OF SOLUBLE SILICON SPECIES AND AL(III) SPECIES ON THE PRECIPITATION OF CALCIUM PHOSPHATE CRYSTALS

6.1 Introduction

In the early 90's, Birchall hypothesised that silicon species could be involved in a mechanism to protect against aluminium poisoning in a variety of organisms[1,2]. Despite being present at trace amounts in almost all vegetation and animals, even a small elevation in the concentration of aluminium can have devastating effects. The mobilisation of aluminium by acidity in soils, rivers, and lakes is responsible for the toxic effect of 'acid rain' on plants and aquatic life[3]. Aluminium concentrations as low as 5-10μM can be fatal to fish[4]. The use of aluminium-contaminated water in the dialysis of renal failure patients increased plasma aluminium levels resulting in a serious bone disorder in which aluminium accumulates at the growth front of the bone[5,6]. The first experiment to investigate the idea that silicic acid might mitigate the toxic effects of aluminium were carried out on Atlantic young salmon exposed to a toxic aluminium concentration of ca. 7 μM in water at pH 5. In the presence of 100 μM silicic acid all fish remained healthy with gill function intact[4]. The systematic accumulation of aluminium in the fish was inhibited by silicic acid.

Experiments on humans have shown that the presence of silicic acid reduces the gastrointestinal absorption of aluminium[7]. In a recent study on volunteers with good renal function, it was found that silicic acid was not only able to reduce the gastrointestinal absorption of aluminium but also to release and excrete aluminium from the body stores including bone[8]. Based on these and the previous studies where it has been shown that Al(III) species were able to inhibit the transformation of ACP to HAP (see chapter 5), the

ability of silicic acid to ameloriate the effect of aluminium on crystal composition, crystallinity and morphology has been investigated.

6.2 Materials and Methods

Materials

Ammonium phosphate dibasic 99% ($(NH_4)_2HPO_4$) was purchased from Sigma Chemical Co. Anhydrous calcium nitrate anhydrous 98+% ($Ca(NO_3)_2$ was purchased from Avocado Research Chemicals Ltd. Aluminium Chloride 99% ($AlCl_3 \cdot 6H_2O$) was purchased from Fisher. Ultrapur HNO_3 was purchased from Prolabo.

Methods

Experiments were carried out by mixing 50 ml of each of 20 mM $Ca(NO_3)_2$ and 12 mM $(NH_4)_2HPO_4$ solutions at 23°C and 37°C. Prior to mixing, aluminium and orthosilicic acid were added to the phosphate solution from a freshly prepared 75 mM stock solution of $AlCl_3 \cdot H_2O$ and standard silica solution (as Na_3SiO_2). The final aluminium concentration was 75 μM and 0.082, 0.204 and 0.409 mM of orthosilicic acid. The pH of the phosphate solution was adjusted to pH 7.4 by addition of 1M HCl after addition of the aluminium chloride and orthosilicic acid and before mixing with the calcium ion containing solution. The solutions were prepared at a constant ionic strength (0.165M) using NaCl as the electrolyte. During precipitation, the reaction mixture was continuously stirred and the pH monitored using a pH93 reference pH meter (Radiometer Copenhagen). Specimens for transmission electron microscopy study were prepared by placing drops of the suspension directly on holey-carbon FORMVAR-coated copper grids at 1, 5, 15, and 30 min of reaction. After 30 min, the reaction mixture was filtered by suction, rinsed with distilled

deionised H_2O and dried at 250°C for 1h. Samples were analysed by TEM, EDXA, XRD and FT-IR (see chapter 2).

Total aluminium sample concentrations were obtained using a Perkin-Elmer AAnalyst100 graphite furnace HGA 700 furnace atomic absorption spectrophotometer at Manchester University. Total silicon sample concentrations were obtained using a Fisons Horizon Sequential ICP-OES. Ultrapur HNO_3 was used for the AA and ES analysis.

6.3. RESULTS

The formation and transformation of calcium phosphate in the presence of aluminium and both aluminium and orthosilicic acid was followed by monitoring the pH changes as a function of time. Figure 6.1 shows the pH changes with time during reaction at 23°C in the presence of aluminium and both aluminium and orthosilicic acid. The first sharp pH drop corresponds to the nucleation stage. In the presence of aluminium the pH dropped to the same value as the control (6.9). When orthosilicic acid was presence the pH dropped to ca. 6.8, 6.7 and 6.68 for 0.082, 0.204 and 0.409 mM of orthosilicic acid respectively. However the time taken for the pH drop to occur in the presence of aluminium and also in the presence of both aluminium and 0.409 mM of orthosilicic acid was more than doubled. Followed the initial pH drop there was a period of more or less constant pH followed by a series of pH changes. The presence of aluminium in the reaction mixture reduced the time for which pH remained virtually constant from ca. 10 min (control) to ca. 5 min (75 μM Al(III)). Then there was an increase in pH due to the dissolution of the crystals (see chapter 3) followed by another pH drop. When orthosilicic acid was added to the reaction mixture the time for which the pH remained constant was reduced to ca. 6.5 min (0.082 mM), 6.8 min (0.204 mM) and 7 min (0.409 mM). There was also a second pH drop for the reactions

containing 0.082 and 0.204 mM orthosilicic acid but for the solution containing 0.409 mM orthosilicic acid the pH which remained after the drop.

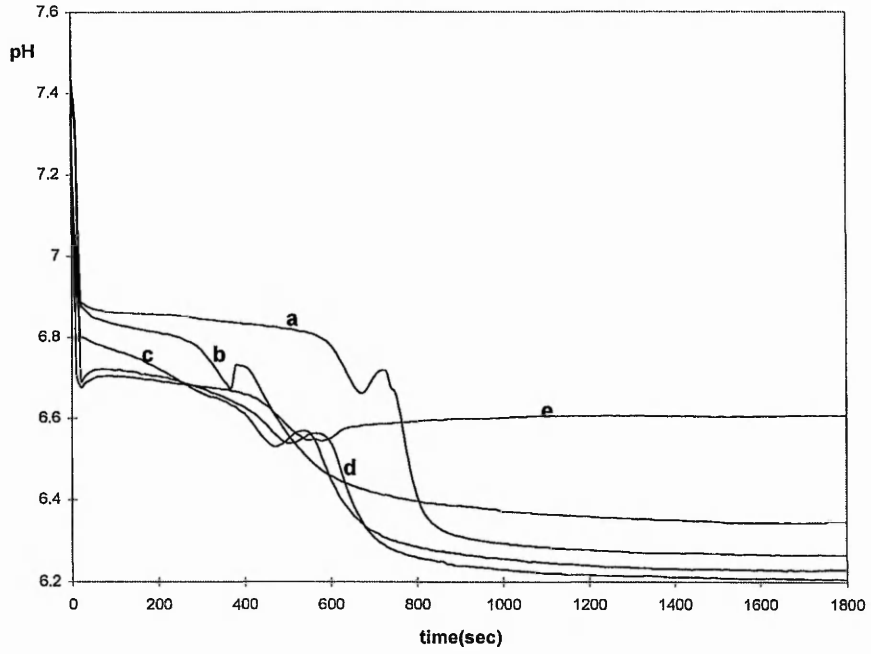

Figure 6.1 Changes in pH with time for reaction carried out at 23°C in the presence of a) 0, b) 75 μM Al(III), c) 75 μM Al(III) and 0.082 mM $Si(OH)_4$, d) 75 μM Al(III) and 0.204 mM $Si(OH)_4$, and e) 75 μM Al(III) and 0.409 mM $Si(OH)_4$.

Figure 6.2 shows the pH changes with time during reaction at 37°C. After the first pH drop due to the nucleation, there was only a second pH drop after ca. 2.5 min (control). The time taken for the second pH drop to occur in the presence of aluminium was ca. 1 min. In the presence of both orthosilicic acid and aluminium the time for which pH remained constant decreased to ca. 1 min, 1.5 min and 1.6 min for precipitations including 75 μM Al and 0.082, 0.204 and 0.409 mM orthosilicic acid respectively.

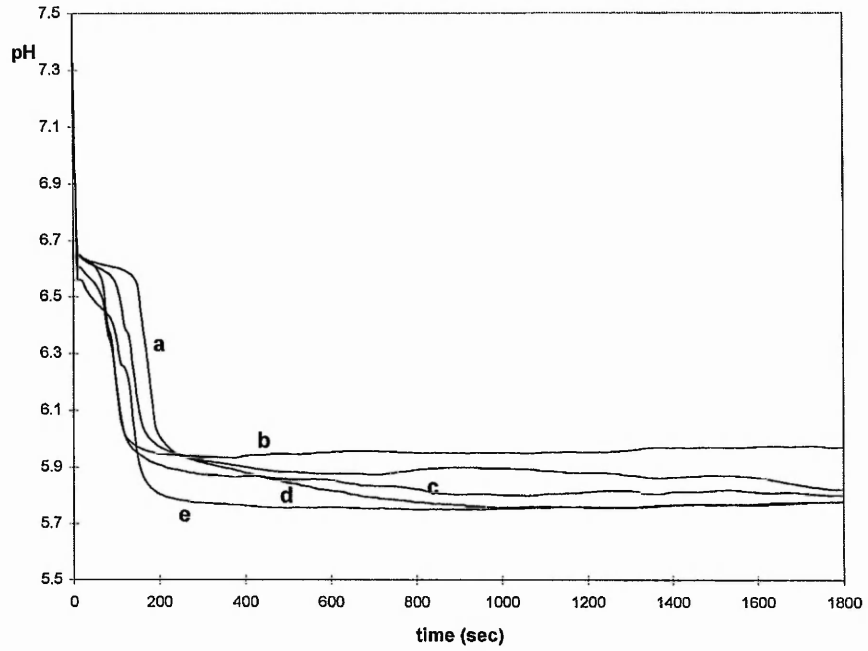

Figure 6.2 Changes in pH with time for reaction carried out at 37°C in the presence of a) 0, b) 75 μM Al(III), c) 75 μM Al(III) and 0.082 mM $Si(OH)_4$, d) 75 μM Al(III) and 0.204 mM $Si(OH)_4$, and e) 75 μM Al(III) and 0.409 mM $Si(OH)_4$.

The precipitates formed were analysed for aluminium content by atomic absorption spectroscopy. When orthosilicic acid was added to the reaction mixture there was a reduction in the incorporation of aluminium into the materials (table 6.1). No silicon was detected by atomic emission spectroscopy indicating no incorporation of silicon into the crystals at concentrations higher than 1 ppm (detection limit 1 ppm).

	Al ($mg.g^{-1}$) mean ± SD	
(mM)	**23 °C**	**37°C**
0	2.060 ± 0.013	3.055 ± 0.0003
0.075 Al(III)	28.931* ± 0.366	23.826* ± 0.343
0.075 Al(III) + 0.041 $Si(OH)_4$	24.285* ± 0.279	23.745 ± .0711
0.075 Al(III) + 0.102 $Si(OH)_4$	18.000* ± 0.531	15.270* ± 0.098
0.075 Al(III) + 0.409 $Si(OH)_4$	17.900* ± 0.412	20.842* ± 5.321

Table 6.1 Concentration of aluminium in precipitates dried at 250 °C for 1h after 30 min of reaction. (*$p<0.05$, n=2)

FT-IR spectra obtained from the control samples prepared at room temperature and heated at 250°C showed the bands expected for HAP and the presence of DCP (see chapter 3). The band at 3420 cm^{-1} (control) attributed to absorbed water was shifted to higher wavenumber indicating an increase in the hydrophilicity of the material formed in the presence of aluminium and both aluminium and orthosilicic acid (figure 6.3) (see chapter 4 for FT-IR of precipitate formed in the presence of orthosilicic acid at 23°).

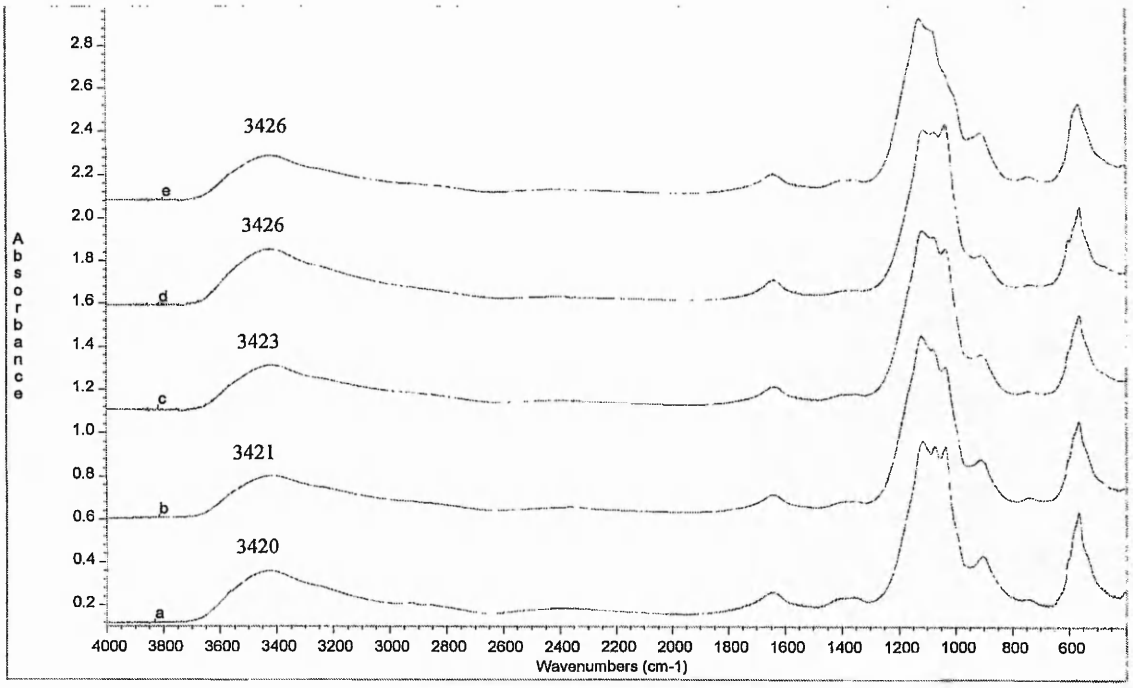

Figure 6.3 FT-IR spectra of precipitate formed at 23°C in the presence of a) 0, b) 75 μM Al(III), c) 75 μM Al(III) and 0.082 mM $Si(OH)_4$, d) 75 μM Al(III) and 0.204 mM $Si(OH)_4$, and e) 75 μM Al(III) and 0.409 mM $Si(OH)_4$ after drying at 250°C for 1h.

For samples prepared at 37°C the control spectrum corresponded to that expected for HAP (see chapter 3). The presence of aluminium increased the hydrophilicity of the precipitate. The band at 3420 cm^{-1} (control) was also shifted to higher wavelenght number. When orthosilicic acid was added to the reaction mixtures the hydrophilicity was reduced but still

higher than the control (figure 6.4) (see chapter 4 for FT-IR of precipitate formed in the presence of orthosilicic acid at 37°C).

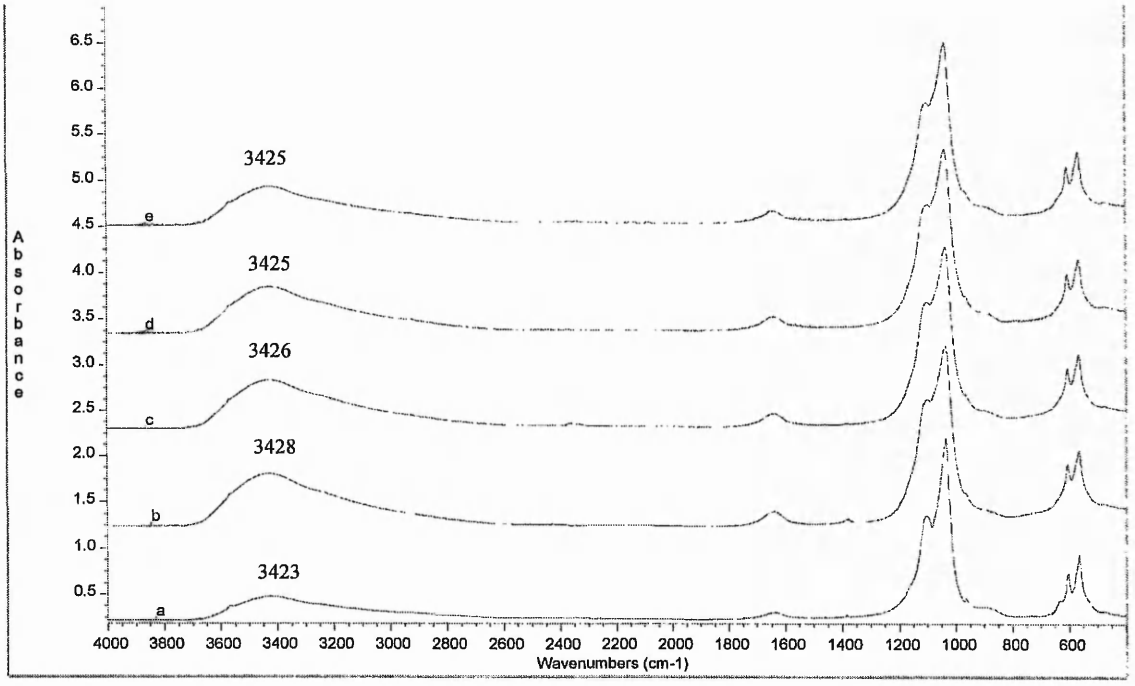

Figure 6.4 FT-IR spectra of the precipitate formed at 37°C in the presence of a) 0, b) 75 μM Al(III), c) 75 μM Al(III) and 0.082 mM $Si(OH)_4$, d) 75 μM Al(III) and 0.204 mM $Si(OH)_4$, and e) 75 μM Al(III) and 0.409 mM $Si(OH)_4$ after drying at 250°C for 1h.

XRD diffraction data showed that the addition of aluminium to the precipitation mixture at 23°C and 37°C resulted in a broadening of the reflections indicating that the crystals formed in the presence of aluminium were less crystalline (figure 6.5, 6.6). The XRD data for the precipitate formed at 23°C in the presence of both aluminium and orthosilicic acid showed not only a broadening of the DCP reflections but also the appearance of a new phase corresponding to HAP (figure 6.5c, 6.5d, 6.5e). The effect was larger at 0.082 mM orthosilicic acid.

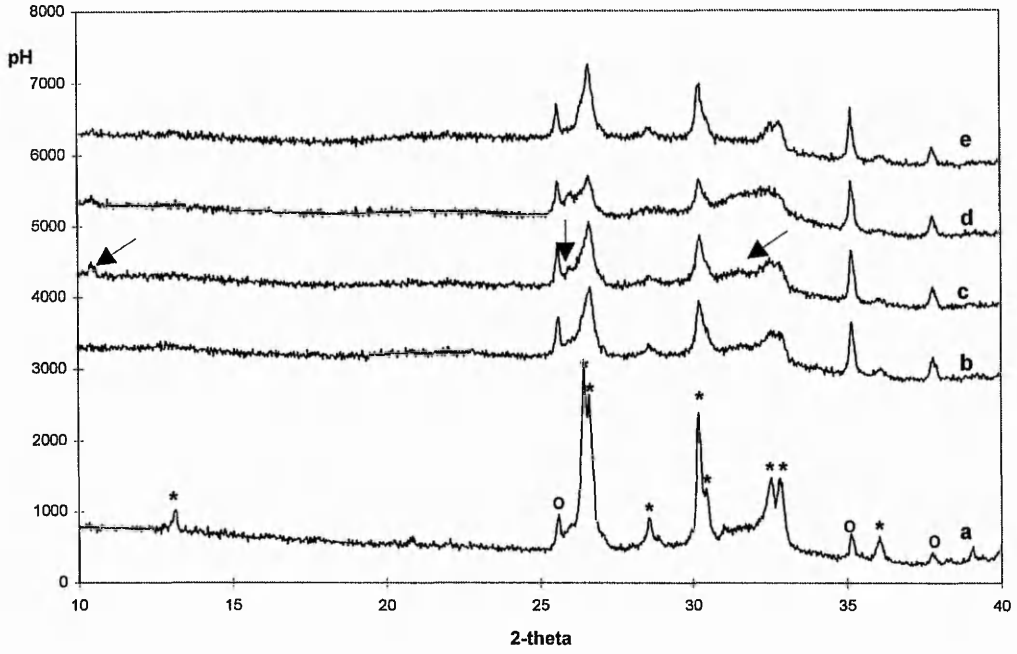

Figure 6.5 XRD spectra of the precipitate formed at 23°C in the presence of a) 0, b) 0.075 mM Al(III), c) 0.075 mM Al(III) and 0.082 mM $Si(OH)_4$, d) 0.075 mM Al(III) and 0.204 mM $Si(OH)_4$, and e) 0.075 mM Al(III) and 0.409 mM $Si(OH)_4$ after drying at 250°C for 1h. * DCP, ° SRM, arrows indicate the presence of reflections arising from apatite crystals.

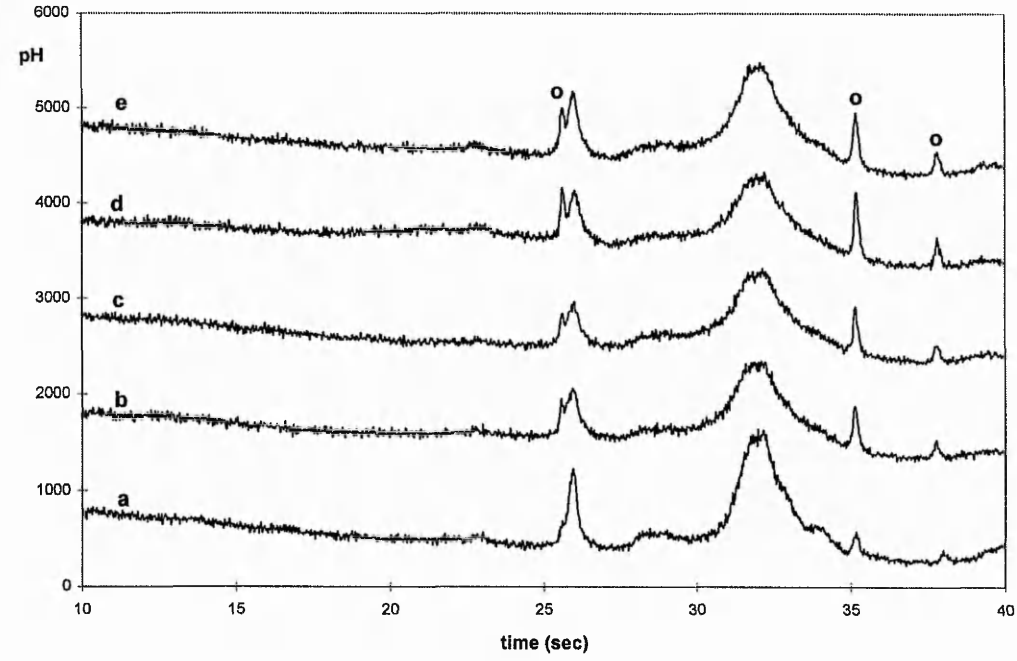

Figure 6.6 XRD spectra of the precipitate formed at 37°C in the presence of a) 0, b) 0.075 mM Al(III), c) 0.075 mM Al(III) and 0.082 mM $Si(OH)_4$, d) 0.075 mM Al(III) and 0.204 mM $Si(OH)_4$, and e) 0.075 mM Al(III) and 0.409 mM $Si(OH)_4$ after drying at 250°C for 1h. °SRM.

An X-ray broadening analysis and particle size determination based on the Debye-Scherrer equation was performed using the (2 2 0) and (1 1 2) reflections for the precipitate formed at 23°C corresponding to DCP (JCPDS 9-80) and the (0 0 2) and (2 1 1) reflections for the precipitate formed at 37°C corresponding to HAP (JCPDS 9-432) (table 6.2). The presence of aluminium reduced the crystalline size (see chapter 5). Orthosilicic acid seemed to ameliorate the aluminium effect on the crystalline size.

	Crystallite size (Å)			
	23°C		**37°C**	
(mM)	**(-2 2 0)**	**(1 1 2)**	**(0 0 2)**	**(2 1 1)**
0	341	451	285	109
0.075 Al(III)	$168^{*,*}$	$159^{*,*}$	$156^{*,*}$	$24^{*,*}$
0.075 Al(III) + 0.082 $Si(OH)_4$	225^{*}	350^{*}	185^{*}	62^{*}
0.075 Al(III) + 0.204 $Si(OH)_4$	-	-	225^{*}	83^{*}
0.075 Al(III) + 0.409 $Si(OH)_4$	235^{*}	480^{*}	209^{*}	70^{*}

Table 6.2 Crystallite size (Å) for the main phases precipitate at 23°C and 37°C after drying at 250°C for 1h. (* $p<0.05$ compared to 0.075 mM Al(III), *,* $p<0.05$ compared to control).

Transmission electron microscopy was used to investigate the structure, morphology and composition of precipitates. Samples were taken between 1 min and 30 min after the start of the reaction (see chapter 2). For samples prepared in the presence of aluminium see chapter 5. For samples prepared in the presence of both aluminium and orthosilicic acid at 23°C, amorphous aggregates were observed from 5 min of the start of reaction (fig 6.7b,e,f, fig. 6.8b,d and fig. 6.9b,d,e). Flakes were observed at all time points (fig 6.7c-d,h, fig. 6.8c,f,g and fig. 6.9a,c). They had a poorly polycrystalline diffraction pattern. Occasionally, flakes were observed growing within the aggregate structure (fig. 6.8e). DCPD crystals were also observed after 1 min of the start of the reaction (fig. 6.7g, fig. 6.8h, and fig. 6.9h).

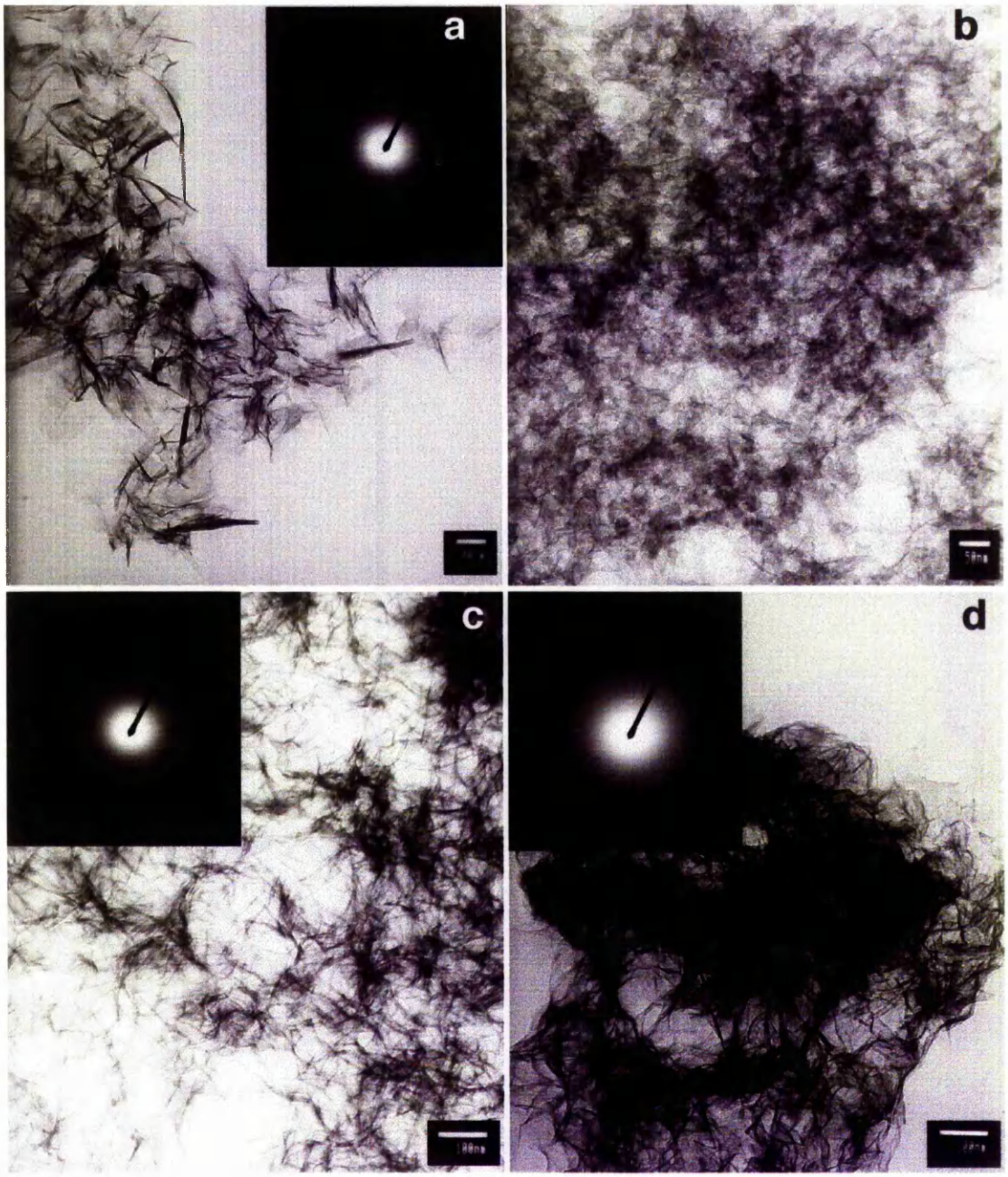

Figure 6.7 Calcium phosphate was precipitated from a solution containing 10 mM $Ca(NO_3)_2$ and 6 mM$(NH_4)_2HPO_4$ at 23°C in the presence of 75 μM Al(III) and 0.082 mM $Si(OH)_4$. During precipitation reaction samples were taken for TEM analysis at a)1 min, b) and c) 5 min, d) 15 min (see appendix III for d-spacings values calculated from the electron diffraction data).

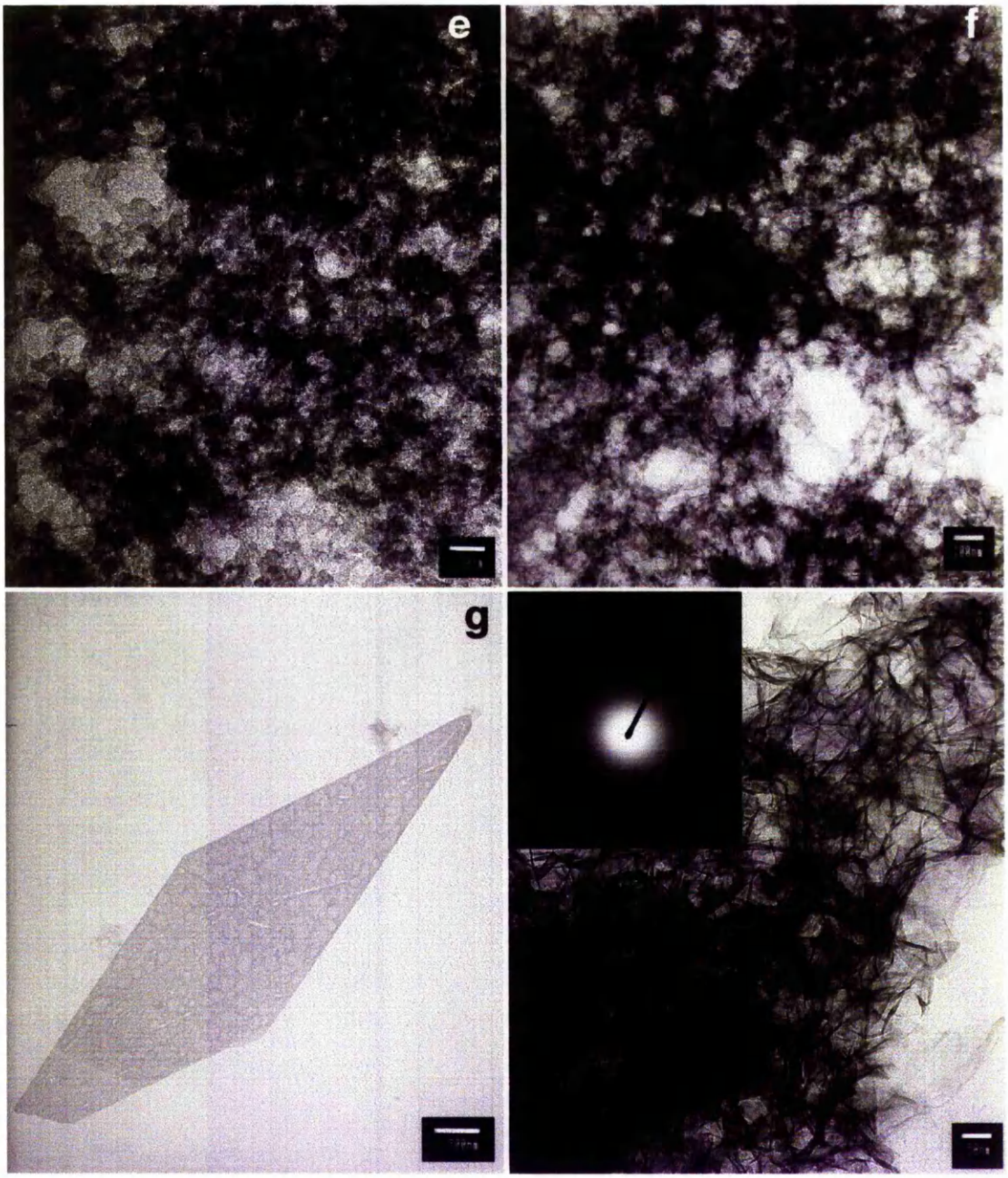

Continuation Figure 6.7 e) 15 min and f), g) and h) 30 min of reaction (see appendix III for d-spacings values calculated from the electron diffraction data).

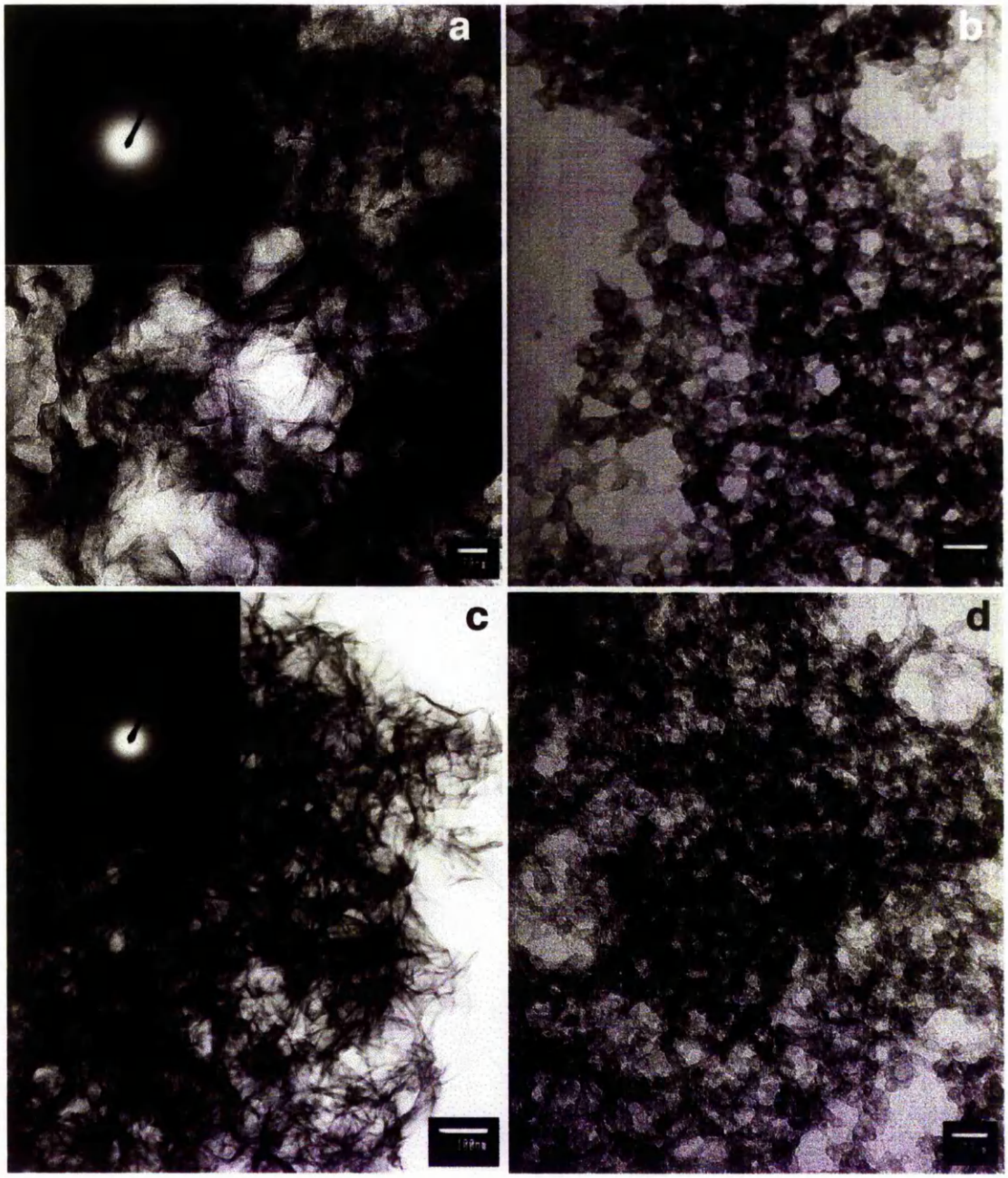

Figure 6.8 Calcium phosphate was precipitated from a solution containing 10 mM $Ca(NO_3)_2$ and 6 mM $(NH_4)_2HPO_4$ at 23°C in the presence of 75 μM Al(III) and 0.204 mM $Si(OH)_4$. During precipitation reaction samples were taken for TEM analysis at a) and b) 1 min, c) and d) 5 min (see appendix III for d-spacings values calculated from the electron diffraction data).

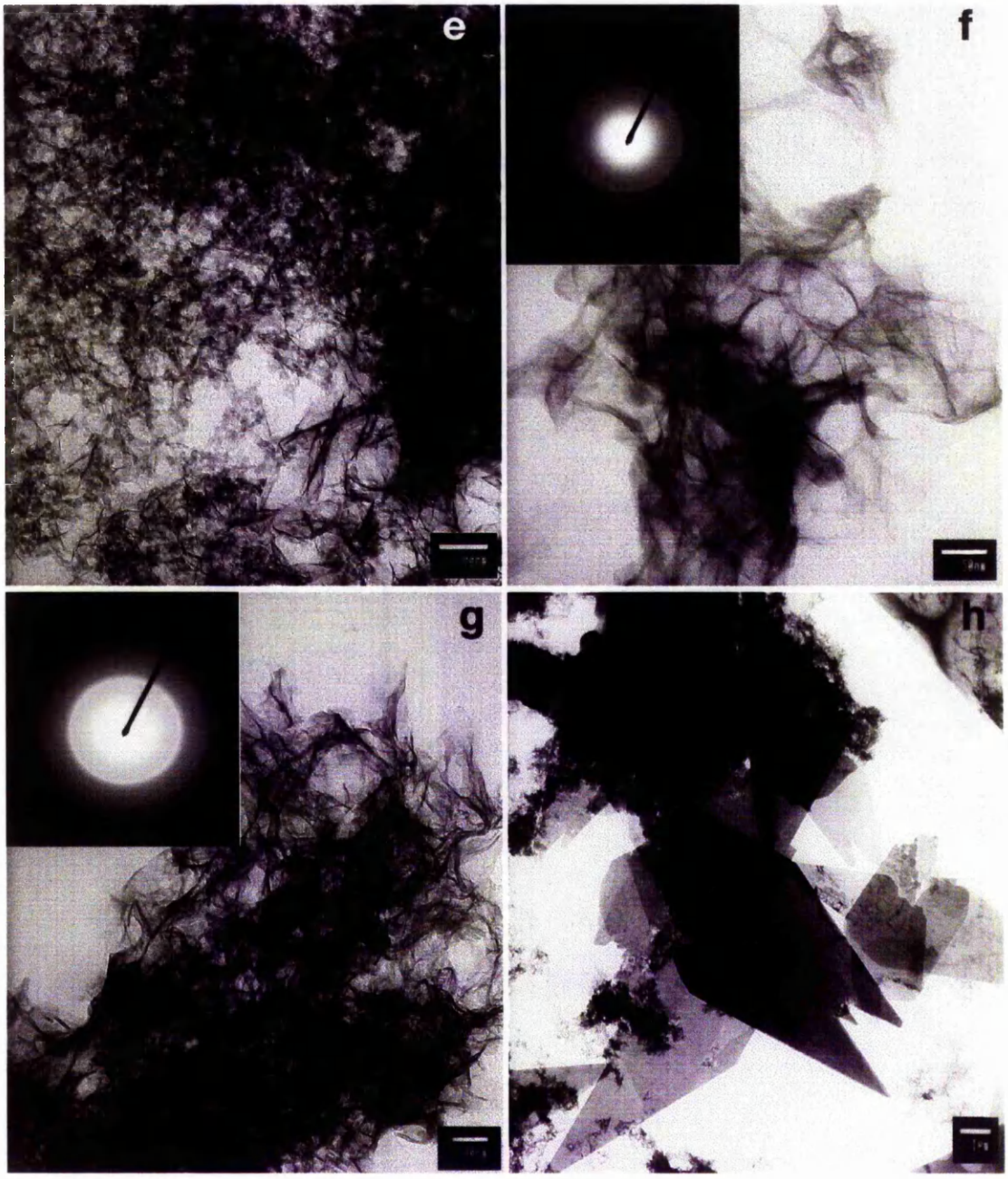

Continuation Figure 6.8 e) and f) 15 min and g) and h) 30 min of reaction (see appendix III for d-spacings values calculated from the electron diffraction data).

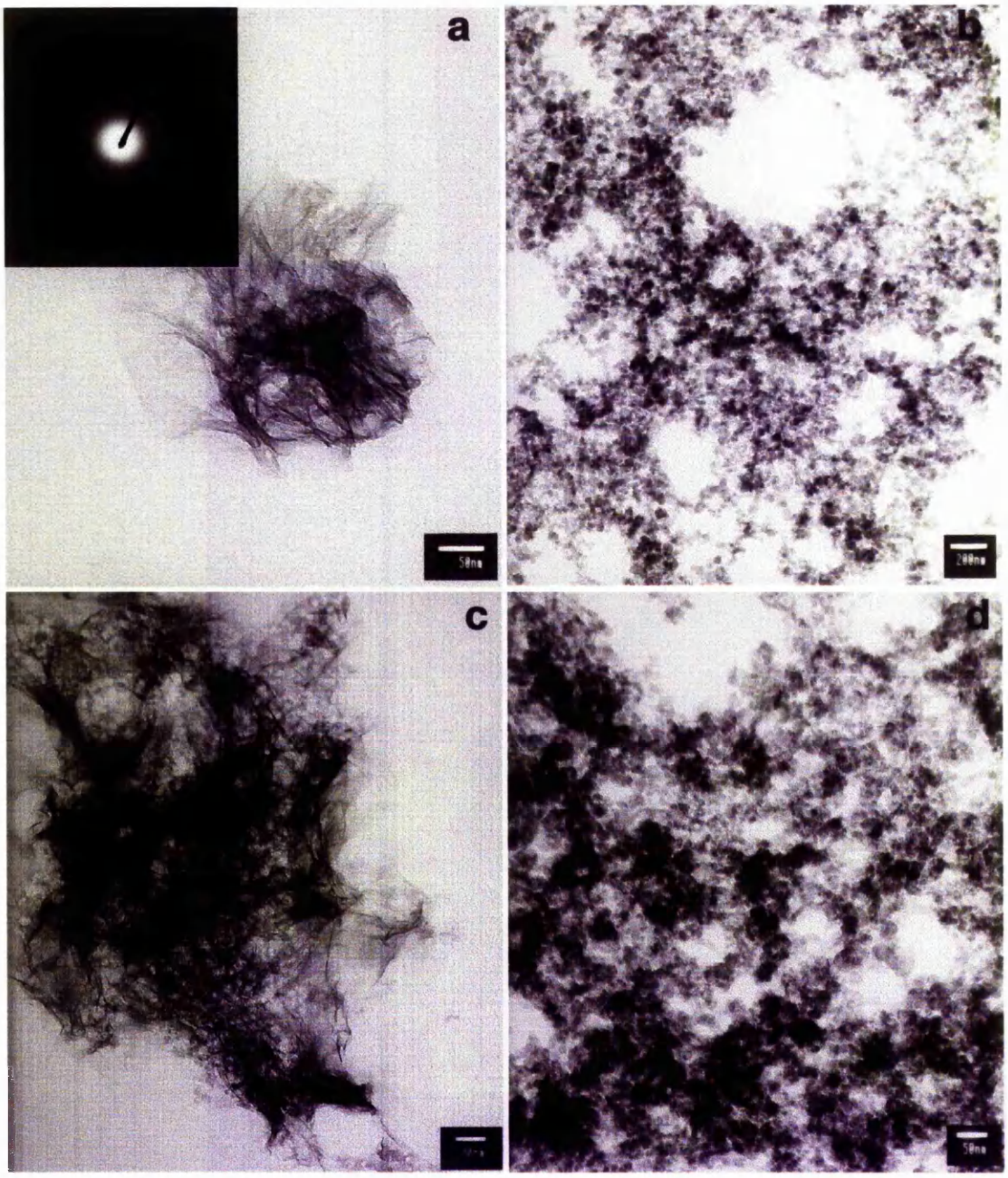

Figure 6.9 Calcium phosphate was precipitated from a solution containing 10 mM $Ca(NO_3)_2$ and 6 mM $(NH_4)_2HPO_4$ at 23°C in the presence of 75 μM Al(III) and 0.409 mM $Si(OH)_4$. During precipitation reaction samples were taken for TEM analysis at a)1 min, b) and c) 5 min, d) 15 min (see appendix III for d-spacings values calculated from the electron diffraction data).

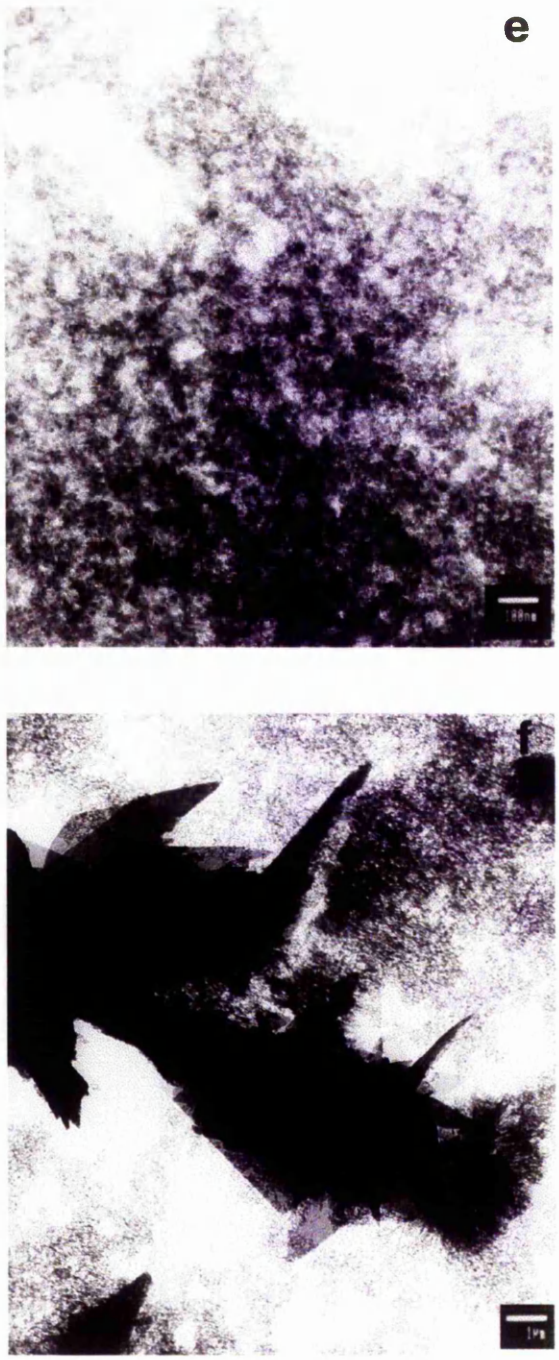

Continuation Figure 6.9 e) and f) 30 min of reaction (see appendix III for d-spacings values calculated from the electron diffraction data.

The Al/P ratio measured by EDXA decreased with time with increasing concentrations of orthosilicic acid for the flakes. However for the amorphous aggregates, the Al/P molar ratio increased with time with increasing concentrations of orthosilicic acid except for samples prepared with 0.204 mM orthosilicic when the Al/P molar ratio decreased with time (table 6.3). XRD analysis had shown this concentration of orthosilicic acid to have the greatest effect on the crystal phase formation for precipitations carried out at 23°C (see chapter 4). The Ca/P molar ratios were usually lower that the control and a high Ca/P molar ratio of the amorphous aggregates was accompanied with a low Ca/P molar ratio of the flake structures.

	spheres		amorphous aggregates		flakes		plate-like DCPD	
	Ca/P	Al/P	Ca/P	Al/P	Ca/P	Al/P	Ca/P	Al/P
1								
0	1.09 ±0.35	-	-	-	-	-	-	-
0.075 Al(III)	-	-	0.57 ±0.16	0.91 ±0.18	1.44 ±0.19	0.04 ±0.01	0.87 ±0.04	0.08
0.075 Al(III) + 0.082 $Si(OH)_4$	1.29 ±0.12	-	0.54 ±0.15	1.94 ±0.07	1.14 ±0.33	0.28 ±0.45	0.98 ±0.05	-
0.075 Al(III) + 0.204 $Si(OH)_4$	-	-	1.12 ±0.31	-	0.72	0.96	1.29	0.09
0.075 Al(III) + 0.409 $Si(OH)_4$	-	-	0.95 ±0.17	0.26 ±0.07	1.45 ±0.16	0.09 ±0.03	-	-
5								
0	-	-	-	-	1.39 ±0.23	-	-	-
0.075 Al(III)	-	-	0.82 ±0.27	0.18 ±0.002	1.45 ±0.38	0.06 ±0.01	1.05 ±0.16	-
0.075 Al(III) + 0.082 $Si(OH)_4$	-	-	0.88 ±0.01	0.56 ±0.06	1.24 ±0.30	0.12 ±0.06	1.49	-
0.075 Al(III) + 0.204 $Si(OH)_4$	-	-	0.75	0.59	1.32 ±0.10	0.05 ±0.03	-	-
0.075 Al(III) + 0.409 $Si(OH)_4$	-	-	1.01 ±0.07	0.24 ±0.05	-	-	1.02 ±0.08	0.14 ±0.09

Table 6.3 Ca/P, Al/P molar ratio for the different morphologies observed during precipitation at 23°C (mean ± SD, n=1-10).

	spheres		amorphous aggregates		flakes		plate-like DCPD	
time (min)	**Ca/P**	**Al/P**	**Ca/P**	**Al/P**	**Ca/P**	**Al/P**	**Ca/P**	**Al/P**
15								
0	-	-	-	-	1.49 ±0.20	-	1.03	
0.075 Al(III)	-	-	1.10 ±0.48	0.60 ±0.21	1.24 ±0.34	0.07 ±0.04	0.92 ±0.20	-
0.075 Al(III) + 0.082 $Si(OH)_4$	-	-	1.48 ±0.12	0.18 ±0.02	1.07 ±0.50	-	0.84 ±0.19	0.60 ±0.26
0.075 Al(III) + 0.204 $Si(OH)_4$	-	-	0.68 ±0.11	0.73 ±0.04	1.63 ±0.27	0.10 ±0.11	-	-
0.075 Al(III) + 0.409 $Si(OH)_4$	-	-	0.81 ±0.05	0.32 ±0.03	-	-	0.98 ±0.03	0.08
30								
0	-	-	-	-	1.31 ±0.34	-	0.90 ±0.11	-
0.075 Al(III)	-	-	0.66 ±0.02	0.63 ±0.04	1.13 ±0.11	0.16 ±0.06	0.94 ±0.04	-
0.075 Al(III) + 0.082 $Si(OH)_4$	-	-	0.53 ±0.11	0.14 ±0.09	0.91 ±0.15	0.14 ±0.08	0.99 ±0.06	-
0.075 Al(III) + 0.204 $Si(OH)_4$	-	-	0.71 ±0.57	0.94 ±0.01	1.25 ±0.16	0.17 ±0.04	0.83 ±0.28	-
0.075 Al(III) + 0.409 $Si(OH)_4$	-	-	0.89 ±0.11	0.44 ±0.02	-	-	0.95 ±0.15	0.04 ±0.02

continuation Table 6.3 Ca/P, Al/P molar ratio for the different morphologies observed during precipitation at 23°C (mean ± SD, n=1-10).

Silicon was also detected in the structures by EDXA analysis. The Si/P molar ratio (table 6.4) decreased with time with increasing concentrations of orthosilicic acid for the amorphous aggregate and flakes structure. There was no clear relationship between Al(III) and orthosilicic acid.

	spheres	amorphous aggregates	flakes	plate-like DCPD
time (min)	**Si/P**	**Si/P**	**Si/P**	**Si/P**
1				
0	-	-	-	-
0.075 Al(III)	-	-	-	-
0.075 Al(III) + 0.082 $Si(OH)_4$	-	0.11 ±0.03	0.06 ±0.03	-
0.075 Al(III) + 0.204 $Si(OH)_4$	-	0.47	0.35	0.11
0.075 Al(III) + 0.409 $Si(OH)_4$	-	0.15 ±0.04	0.13 ±0.09	-
5				
0	-	-	-	-
0.075 Al(III)	-	-	-	-
0.075 Al(III) + 0.082 $Si(OH)_4$	-	0.11 ±0.03	0.07 ±0.03	-
0.075 Al(III) + 0.204 $Si(OH)_4$	-	0.26	0.05 ±0.03	-
0.075 Al(III) + 0.409 $Si(OH)_4$	-	0.09 ±0.04	-	0.05
15				
0	-	-	-	
0.075 Al(III)	-	-	-	-
0.075 Al(III) + 0.082 $Si(OH)_4$	-	0.10	-	0.28
0.075 Al(III) + 0.204 $Si(OH)_4$	-	0.14 ±0.01	0.09 ±0.11	-
0.075 Al(III) + 0.409 $Si(OH)_4$	-	-	-	-
30				
0	-	-	-	-
0.075 Al(III)	-	-	-	-
0.075 Al(III) + 0.082 $Si(OH)_4$	-	0.05 ±0.01	0.10	0.06
0.075 Al(III) + 0.204 $Si(OH)_4$	-	-	0.05	-
0.075 Al(III) + 0.409 $Si(OH)_4$	-	0.12	-	-

Table 6.4 Si/P molar ratio for the different morphologies observed during precipitation at 23°C (mean ± SD, n=1-10).

For precipitation reactions carried out at 37°C, when orthosilicic acid was present in the reacting solution at 0.204 mM, round spheres were detected at 1 min of reaction (fig. 6.11a). The Ca/P molar ratio was higher compared to the control. At the rest of the orthosilicic acid concentrations used OCP plates, needles and flakes but not spheres were detected at 1 min (fig.6.10a, 6.12a). Amorphous aggregates were detected for all the samples precipitated in the presence of orthosilicic acid (fig. 6.10c, fig.6.11e, g). From 5 min onwards flakes, plates and amorphous aggregates were observed for samples prepared

in the presence of the 0.082 mM and 0.204 mM orthosilicic acid (fig. 6.10d, fig 6.11b,c,d,f, fig. 6.12b, c, d).The electron diffraction patterns obtained from the flakes formed in the presence of orthosilicic acid and aluminium showed that the structures were a more crystalline than the flakes formed in the presence of aluminium only (see chapter 5 for samples prepared in the presence of aluminium only).

The Ca/P, Al/P and Si/P molar ratios for the different structures are shown in table 6.6 and table 6.7. The Al/P ratio calculated by EDXA increased with time with increasing concentrations of orthosilicic acid for the amorphous aggregates whilst the Al/P molar ratio decreased. The Ca/P molar ratio for the OCP plates, needles and flakes varied with time and concentrations of orthosilicic acid but there was no significant difference between them. However the Al/P molar ratio for the flake-like structures remained more or less constant.

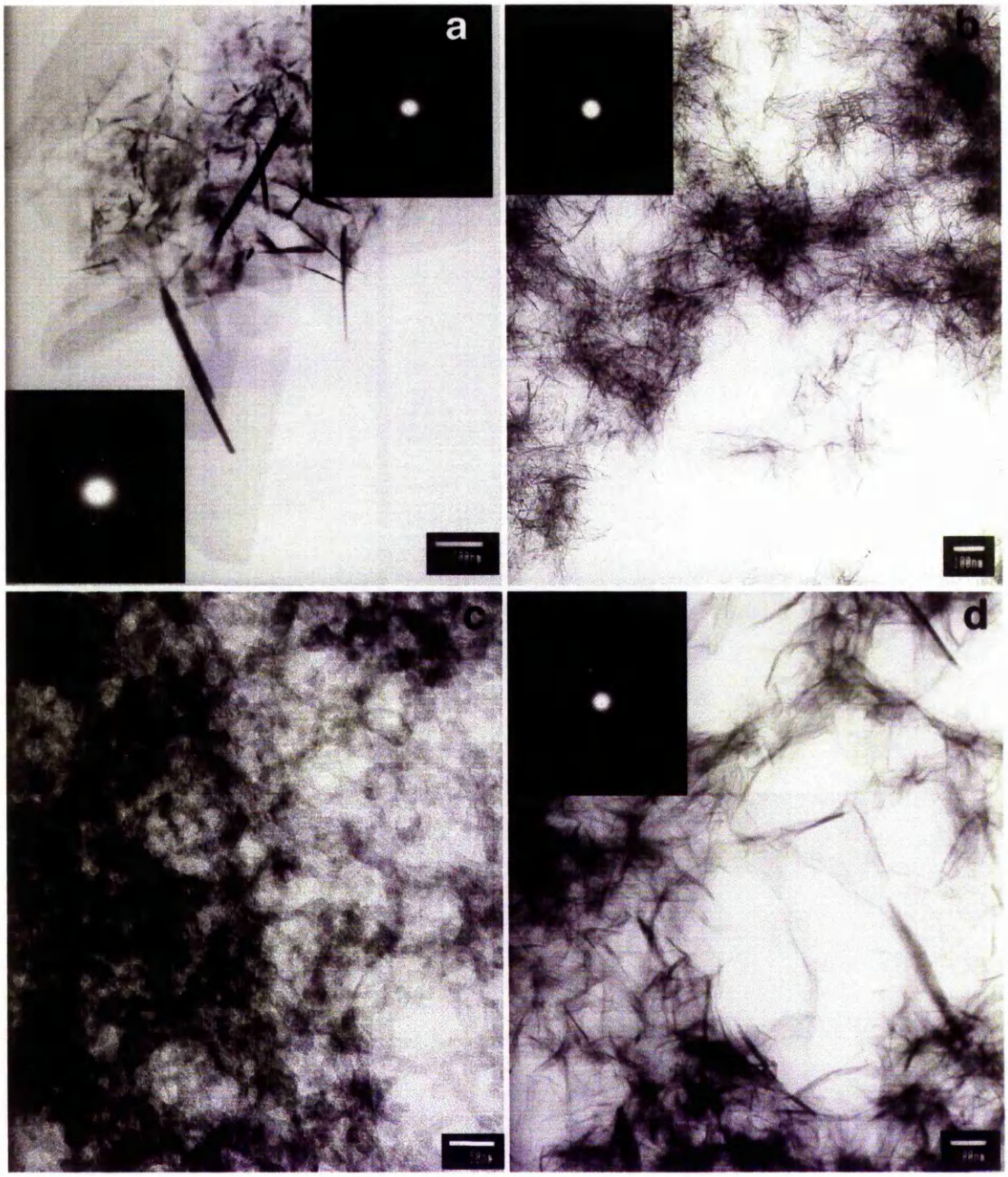

Figure 6.10 Calcium phosphate was precipitated from a solution containing 10 mM $Ca(NO_3)_2$ and 6 mM$(NH_4)_2HPO_4$ at 37°C in the presence of 75 μM Al(III) and 0.082 mM $Si(OH)_4$. During precipitation reaction samples were taken for TEM analysis at a) 1 min, b) 5 min, c) 15 min and d) 30 min (see appendix III for d-spacings values calculated from the electron diffraction data).

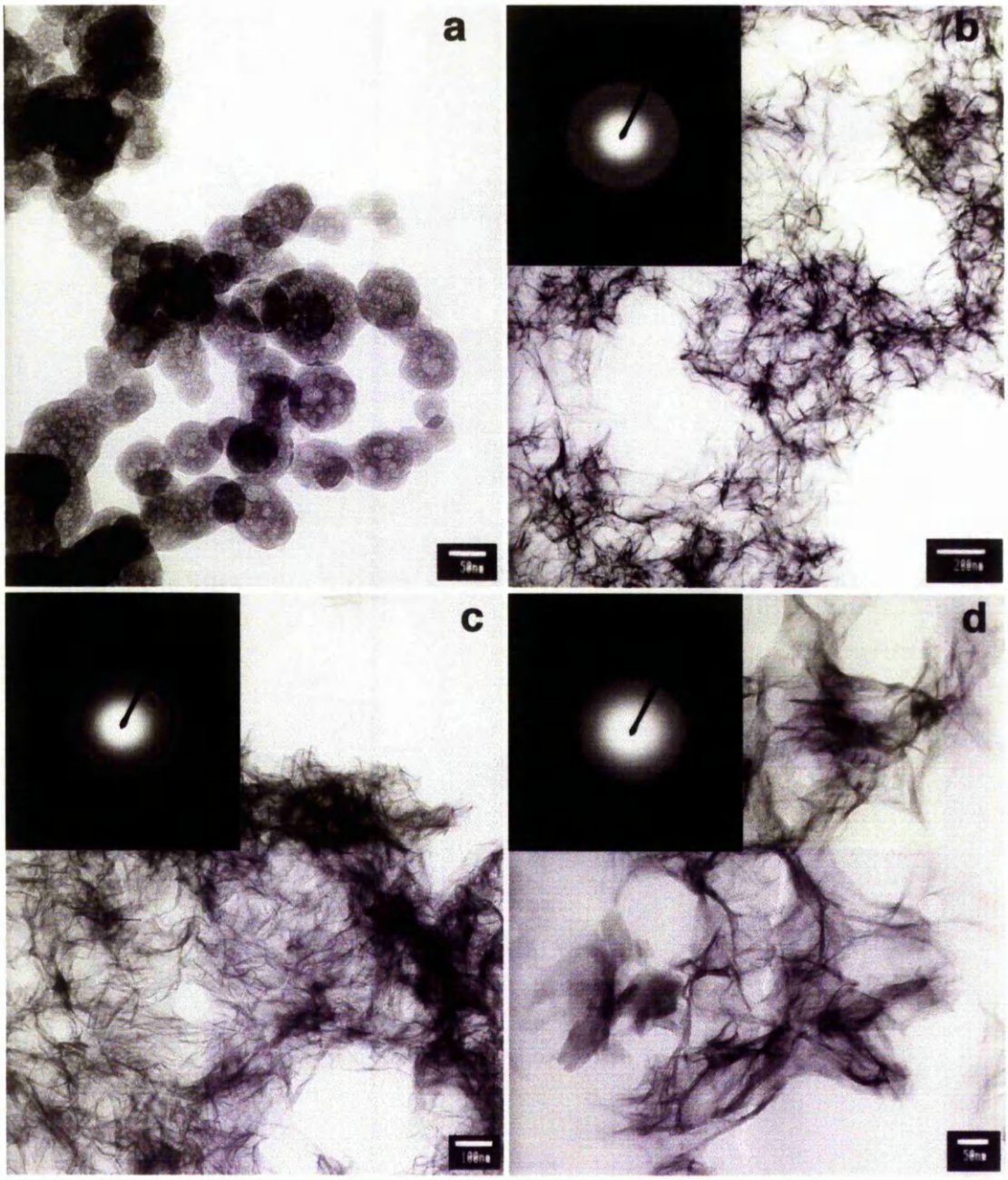

Figure 6.11 Calcium phosphate was precipitated from a solution containing 10 mM $Ca(NO_3)_2$ and 6 mM $(NH_4)_2HPO_4$ at 37°C in the presence of 75 μM Al(III) and 0.204 mM $Si(OH)_4$. During precipitation reaction samples were taken for TEM analysis at a) 1 min, b) 5 min, c) and d) 15 min (see appendix III for d-spacings values calculated from the electron diffraction data).

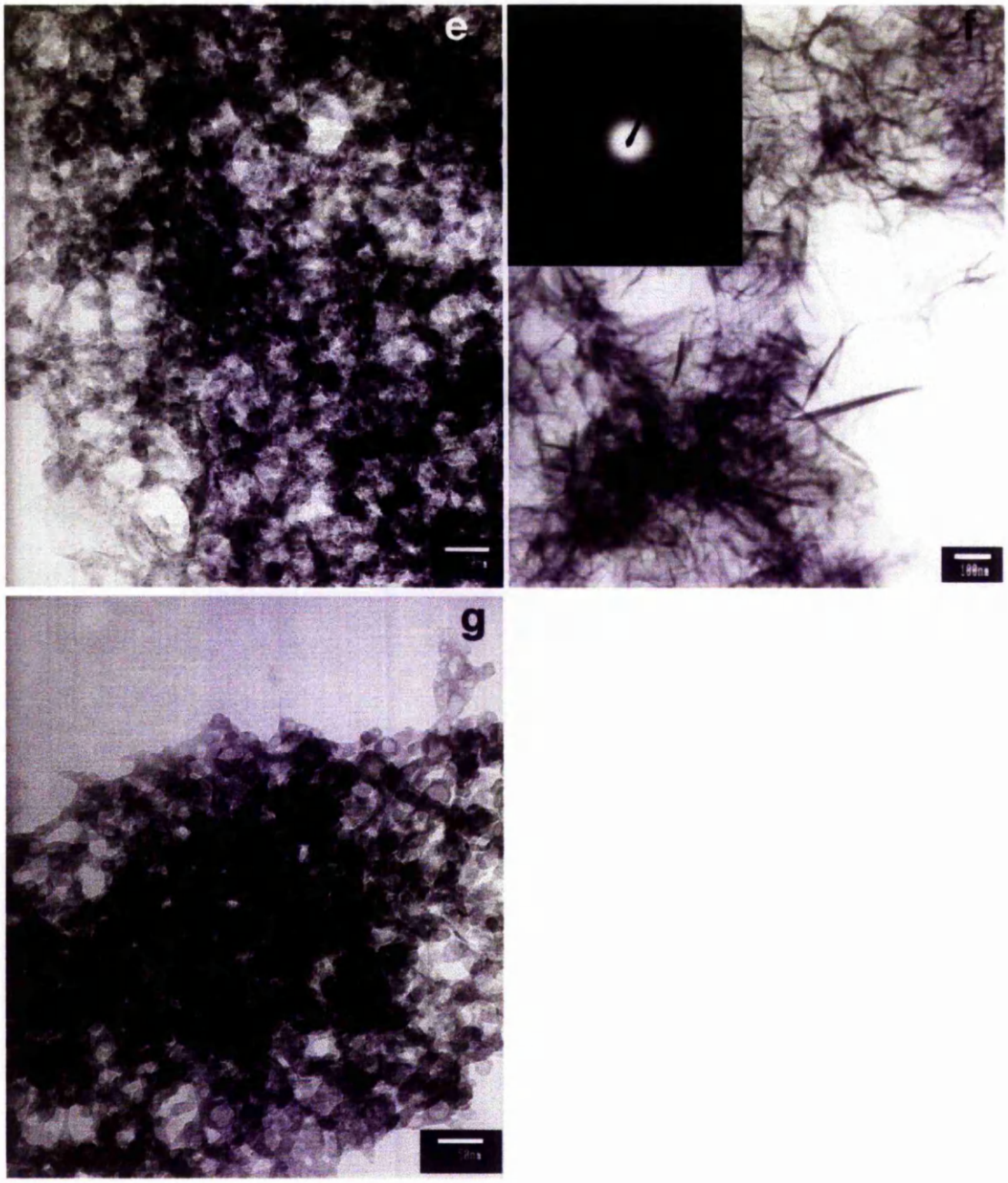

Continuation Figure 6.11 e) 15 min and f) and g) 30 min (see appendix III for d-spacings values calculated from the electron diffraction data).

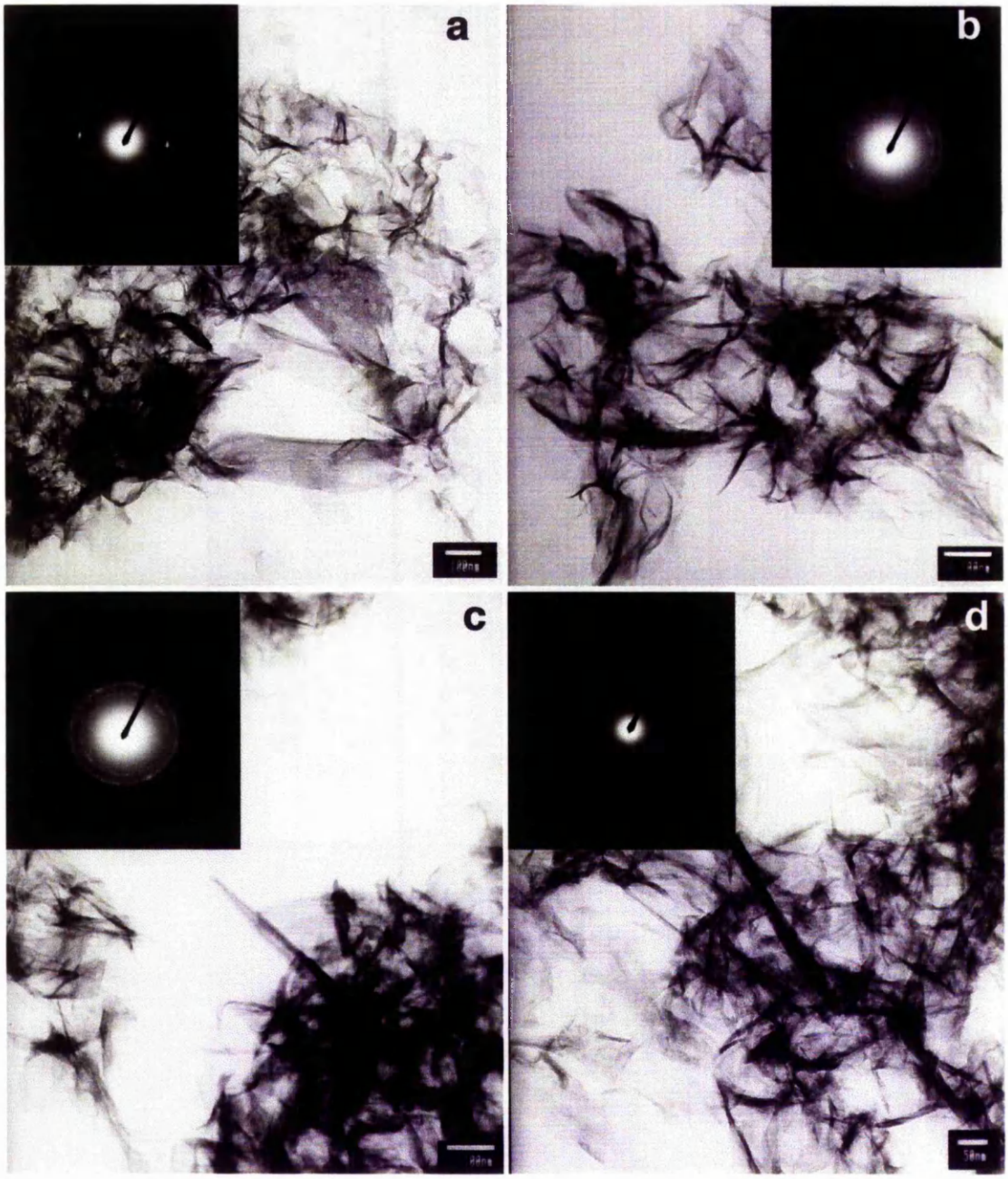

Figure 6.12 Calcium phosphate was precipitated from a solution containing 10 mM $Ca(NO_3)_2$ and 6 mM $(NH_4)_2HPO_4$ at 37°C in the presence of 75 μM Al(III) and 0.409 mM $Si(OH)_4$. During precipitation reaction samples were taken for TEM analysis at a) 1 min, b) 5 min, c) 15 min and d) 30 min (see appendix III for d-spacings values calculated from the electron diffraction data).

time	complex aggregates		flakes		plate(OCP)		needle	
	Ca/P	Al/P	Ca/P	Al/P	Ca/P	Al/P	Ca/P	Al/P
1								
0	-	-	-	-	1.62 ±0.34	-	1.58 ±0.11	-
0.075 Al(III)	-	-	1.34 ±0.07	0.02 $\pm 1x10^{-4}$	2.25 ±0.58	-	1.63 ±0.02	0.04
0.075 Al(III) + 0.082 $Si(OH)_4$	0.48 ±0.13	1.09 ±0.11	1.46 ±0.19	-	1.36 ±0.04	-	1.56	-
0.075 Al(III) + 0.204 $Si(OH)_4$	-	-	1.61 ±0.46	0.14 ±0.09	-	-	-	-
0.075 Al(III) + 0.409 $Si(OH)_4$	0.27 ±0.06	1.32 ±0.30	1.51 ±0.15	0.06 ±0.03	1.75 ±0.29	-	1.07	0.37
5								
0	-	-	1.78 ±0.28	-	1.69 ±0.29	-	1.75 ±0.32	-
0.075 Al(III)	0.63 ±0.004	0.67 ±0.07	1.64 ±0.33	0.04 ±0.02	-	-	1.51 ±0.22	0.05 ±0.02
0.075 Al(III) + 0.082 $Si(OH)_4$	0.74 ±0.34	0.50 ±0.38	1.32 ±0.02	0.08 $\pm 6x10^{-4}$	-	-	1.19 ±0.19	0.09 ±0.09
0.075 Al(III) + 0.204 $Si(OH)_4$	-	-	1.54 ±0.20	0.05 ±0.03	-	-	-	-
0.075 Al(III) + 0.409 $Si(OH)_4$	0.39 ±0.14	1.08 ±0.14	1.42 ±0.18	0.07 ±0.06	-	-	-	-
15								
0	-	-	1.50 ±0.12	-	1.57 ±0.29	-	1.49 ±0.34	-
0.075 Al(III)	0.52 ±0.11	0.86 ±0.24	1.36 ±0.30	0.09 ±0.02	-	-	1.70 ±0.52	0.29
0.075 Al(III) + 0.082 $Si(OH)_4$	0.83 ±0.39	0.71 ±0.58	1.37 ±0.03	0.06 ±0.02	1.36	-	1.27 ±0.12	0.08 ±0.03
0.075 Al(III) + 0.204 $Si(OH)_4$	0.44 ±0.06	0.94 ±0.19	1.41 ±0.10	0.09 ±0.03	-	-	-	-
0.075 Al(III) + 0.409 $Si(OH)_4$	0.31 ±0.01	0.91 ±0.03	1.84 ±0.23	0.04 ±0.05	-	-	-	-
30								
0	-	-	-	-	1.56 ±0.18	-	1.90 ±0.29	-
0.075 Al(III)	0.68 ±0.26	0.66 ±0.26	1.56 ±0.19	0.12 ±0.04	-	-	-	-
0.075 Al(III) + 0.082 $Si(OH)_4$	0.90	0.08	1.26 ±0.03	0.07 ±0.03	1.22	-	1.39	-
0.075 Al(III) + 0.204 $Si(OH)_4$	1.29 ±0.49	0.34 ±0.39	1.79 ±0.33	0.06 ±0.01	-	-	1.86 ±0.47	0.04 ±0.02
0.075 Al(III) + 0.409 $Si(OH)_4$	0.47 ±0.12	0.61 ±0.10	1.40 ±0.22	0.04 ±0.02	-	-	-	-

Table 6.5 Ca/P, Al/P ratio for the different morphologies observed during precipitation at 37°C (mean ± SD, n=1-10).

The Si/P molar ratio for the flake-like structures remained more or less constant (table 6.6). Occasionally Si was detected for the OCP plates and needles.

time (min)	complex aggregates	flakes	plate(OCP)	needle
	Si/P	Si/P	Si/P	Si/P
1				
0	-	-	-	-
0.075 Al(III)	-	-	-	-
0.075 Al(III) + 0.082 $Si(OH)_4$	0.30 ±0.04	0.13 ±0.12	0.23	-
0.075 Al(III) + 0.204 $Si(OH)_4$	-	0.04 ±0.02	-	-
0.075 Al(III) + 0.409 $Si(OH)_4$	0.24 ±0.003	0.06 ±0.05	0.08 ±0.06	-
5				
0	-	-	-	-
0.075 Al(III)	-	-	-	-
0.075 Al(III) + 0.082 $Si(OH)_4$	0.13 ±0.02	0.09 ±0.05	-	0.11 ±0.07
0.075 Al(III) + 0.204 $Si(OH)_4$	-	0.05 ±0.03	-	-
0.075 Al(III) + 0.409 $Si(OH)_4$	0.06 ±0.02	0.08 ±0.05	-	-
15				
0	-	-	-	-
0.075 Al(III)	-	-	-	-
0.075 Al(III) + 0.082 $Si(OH)_4$	0.27 ±0.14	0.09 ±0.02	0.15	0.11 ±0.09
0.075 Al(III) + 0.204 $Si(OH)_4$	0.21 ±0.05	0.06 ±0.01	-	0.05
0.075 Al(III) + 0.409 $Si(OH)_4$	0.09 ±0.08	0.04 ±0.01	-	-
30				
0	-	-	-	-
0.075 Al(III)	-	-	-	-
0.075 Al(III) + 0.082 $Si(OH)_4$	-	0.18 ±0.09	0.16	0.20
0.075 Al(III) + 0.204 $Si(OH)_4$	-	-	-	-
0.075 Al(III) + 0.409 $Si(OH)_4$	0.18 ±0.11	0.13	-	-

Table 6.6 Si/P ratio for the different morphologies observed during precipitation at 37°C (mean ± SD, n=1-10).

Appendix (III) shows the d-spacings obtained from the electron diffraction pattern of the structures detected during precipitation at 23°C and 37°C.

6.4 DISCUSSION

In this study, the ability of orthosilicic acid to ameliorate the aluminium inhibitory effects on calcium phosphate formation was assessed.

Calcium phosphate crystals were precipitated in the presence of aluminium(III) and silicic acid at 23°C and 37°C. For experiments at 23°C, orthosilicic acid appeared to ameliorate the inhibitory effects of aluminium on the formation of calcium phosphates. When 0.204 mM silicic acid was present in the precipitating solution which also contained aluminium, the formation of ACP was favoured over the formation of DCPD. When both silicic acid and aluminium were present in the reacting solution there was a synergic effect (as evidenced from XRD data). For precipitations carried out at 37°C, orthosilicic acid up to a concentration of 0.204M appeared to increase the crystallinity of the calcium phosphate crystals (as evidenced from TEM data) compared to the crystals formed in the presence of aluminium.

Carlisle (1986 CIBA symposium discussion session after Birchall's paper presentation)[9] was the first scientist to point out that silicon and aluminium worked synergistically in certain tissues and that both were essential elements in these tissues.

Since no strong organic binding of silicon has been found in biology, the effects of silicic acid have been tried to be explained through its inorganic chemistry. At the concentration and pH range found under physiological conditions, silicic acid has little chemistry in biological systems: Si-O-C bonds are hydrolytically unstable, although associations via hydrogen bonding are possible. However, silicic acid interacts with basic metal species, and in particular with aluminium[10]. Interactions of silicic acids (and its oligomers and colloidal particles) with aluminium can be detected from pH 4.5 upwards and the formation of species such as $[AlOSi(OH)_3]^{2+}$ has been conjectured[10]. There are interactions with all basic aluminium species, from $[Al(H_2O)_5(OH)]^{2+}$ to $Al(OH)_4^-$, to form hydroxyaluminosilicate species. Silicic acid and hydroxy-aluminium species start to combine at pH $\geq$ 4 and the stability of the hydroxy-aluminosilicate species formed

increases with increasing pH[4]. The strength of the binding of silicate to hydroxy-aluminium species exceeds that of sulphate above pH 7, of phosphate above pH 6 and of strong organic chelators such as citrate above pH 7[4]. The ability of aluminium to limit the bio-availability of essential phosphate is reduced when silicic acid is present and hydroxyaluminosilicates are formed[11]. However, at pH 6.6 previous experiments have shown a switch of Al^{3+} binding from silicate to phosphate when the latter was present under blood plasma conditions[12].

The mechanism by which silicic acid restricts the gastro-intestinal absorption of aluminium is postulated to be the formation of hydroxyaluminosilicate species, the rapid and stable formation of which requires a minimum of 100 μM Si[7]. When Al was administered in the presence of 100 μM dissolved Si, a concentration which permits the formation of stable hydroxyaluminosilicates in solution, plasma concentrations of Al after 60 min were only 15% of those observed after ingestion in the absence of Si. Hydroxyaluminosilicates form in aqueous solution, essentially when the Si concentration exceeds 100 μM and they probably form in the gastrointestinal tract and reduce the amount of Al absorbed. This level is rarely reached in plasma, so that hydroxyaluminosilicate formation in plasma is unlikely. However, the concentration of silicic acid in urine rarely falls below 100 μM, and rises to 200-300 μM following a silicon-rich drink. Thus aluminium excreted into the tubular fluid in the kidney could there interact to form hydroxyaluminosilicate species. This could restrict the re-absorption of aluminium and thus transiently enhance its excretion[13,14].

The formation of solids in aqueous solutions containing $Si(OH)_4$ and basic aluminium species at concentrations relevant to water chemistry and to physiology is slow, but sub-colloidal species form early[15-17], and their formation does influence the bio-availability of aluminium. Employing the techniques of membrane filtration and ion exchange Exley *et.al*

(1992) were successful in identifying hydroxyaluminosilicate formation in near-physiological solution[16]. HAS formation was recognisable only at pH 6.0 and 500 μM silicic acid concentration.

Although the silicic acid concentrations used in the experiment described in this chapter were below the polymerisation boundary in the present of ammonium species[19], some polymerisation of orthosilicic acid might have occurred at the nucleation site of calcium phosphate. Other authors have attributed the precipitating effect of calcium phosphate to polymeric silicon species[20, 21].

It has been reported that $Si(OH)_4$ is not well able to combine with Al(III) in acidic natural waters. It has also been reported that the size of polysilicic acids decreases with increasing concentrations of aluminium[22]. The growth of particles of polysilicic acid was found to be increasingly retarded with increasing concentration of aluminium up to 26 ppm [22]. Aluminium can be bonded to polysilicic acid. Iler presumed that at pH 8 an aluminium atom adsorbed on the surface of amorphous silica is co-ordinated with four oxygen atoms, forming a negative charged aluminosilicate site[11]. Although the growth of particles of polysilicic acid by the reaction between polymers proceeds rapidly at high temperature, aluminium retards the reaction between polymers. It may be reasonable to assume that the growth of particles of polysilicic acid is retarded by repulsion between the polymer particles due to the formation of negative aluminosilicate sites.

The ameliorating effect of orthosilicic acid on the effect of aluminium (III) species in the precipitation of calcium phosphate depended on the concentration of silicic acid present in solution. It has been shown that at the same concentrations of SiO_2, the affinity for aluminium depends dramatically on the method by which the silica solution is prepared[23]. Thus, at 0-2 mM total SiO_2 which is below the polymeralisation boundary, a solution of

oligomeric silica prepared by pH neutralisation (7.2) at 42 mM and then diluted, clearly bound aluminium more strongly than that diluted and then neutralised[23]. Dilution of oligomeric silica below 2 mM led to depolymerisation and loss of affinity for aluminium within 24 h. However when oligomeric silica was diluted well below the boundary region and then aluminium immediately introduced, depolymerisation was inhibited, and high affinity for aluminium was maintained at least 17 days[23]. Taylor *et al.* (1997) stated that it might not be safe to assume that monomeric silica in bulk solution remains monomeric at the site of its aluminium protection action[23].

In this study, aluminium was immediately added to the phosphate solution after the addition of orthosilicic acid to the phosphate solution. If polymerisation of orthosilicic acid had occurred due to the addition of aluminium, then HAS could have formed, and the negative aluminosilicate sites could have acted as nucleating sites of apatite thus favouring the formation of HAP over DCPD for the precipitations carried out at 23°C as evidenced by XRD analysis.

Although increasing the reaction temperature can speed up the polymerisation of orthosilicic acid[22], it has been reported that aluminium retards the polymerisation of silicic acid at high temperature. This may explain why although the crystallinity of the calcium phosphate phases formed at 37°C seemed to improve when precipitating in the presence of both aluminium and silicic acid, the synergic effect observed for the experiments performed at 23°C was not observed for the experiements carried out at 37°C.

Solid HAS were not detected by any of the techniques used in this study to characterise the calcium phosphates formed. Further experiments on the solution should be carried out to identify the soluble species involved in the mechanism of calcium phosphate formation in the presence of both aluminium and silicic acid.

In conclusion orthosilicic acid not only was shown to be able to ameliorate the aluminium inhibitory effect on the formation of calcium phosphates and the transformation of ACP to HAP, but both ions seemed to work in a synergistic way stimulating the formation of apatite over DCPD for precipitations performed at 23°C. For precipitations performed at 37°C, the presence of orthosilicic acid in solution seemed to decrease the loss of crystallinity, due to the effect of aluminium (III), on the calcium phosphate phases formed. The inhibitory effect of aluminium (III) on the transformation of ACP to HAP was also decreased by the presence of orthosilicic acid in the reaction solution.

6.5. REFERENCES

1. Birchall, J.D. (1990). The Role of Silicon in Biology. *Chem. Brit.*, **26**:141.
2. Birchall, J.D. (1991). The Toxicity of Aluminium and the Effect of Silicon on its Bioavailability. In Aluminium in Biology and Medicine, pp.53. Edited by Nicolini, M., Zatta, P.F. and Corrain, Raven Press. New York.
3. Exley, C. and Philips M.J. (1988). Recent Advances in Aquaculture, vol. 3, pp. 225. Edited by Muir, J.F. and Roberts, R.J. Croom Helm. London.
4. Birchall, J.D., Exley, C., Chappel, J.S. and Phillips, M.J. (1989). Acute Toxicity to Fish Eliminated in Silicon-Rich Acid Waters. *Nature*, **328**(6211):146.
5. Mjöberg, B., Hellquist, E., Mallmin, H. and Lindh, U. (1997). Aluminium, Alzheimer's Disease and Bone Fragility. *Acta Orthop. Scand.* **68**(6):511.
6. Sebert, J.L., Marie, A., Gueris, J., Herve, M.A., Leflon, P., Garabedian, M. Smadja, A. and Fournier, A. (1985). Assessment of the Aluminium Overload and of its Possible Toxicity in Asymptomatic Uremic Patients: Evidence for a Depressive Effect on Bone Formation. *Bone* **6**:373.
7. Edwarson, J.A., Moore, P., Ferrier, I.N., Lilley, J.S., Newton, G.W.A., Barker, J., and Day, J.P. (1993). Effect of Silicon on the Gastrointestinal Absorption of Aluminium. *Lancet*, **342**:211.

8. Bellia, J.P., Birchall, J.D., Roberts, N.B. (1996). The Role of Silicic Acid in the Renal Excretion of Aluminium. *Ann. Clin. Lab. Sci.* **26**:227.
9. Silicon Biochemistry. CIBA Foundation Symposium 121. Wiley, Chischester
10. Iler, R.K. (1970). The Chemistry of Silica. Edited by John Wiley&Sons. Wiley-Interscience. New York.
11. Exley, C. and Birchall, J.D. (1993). A Mechanism of Hydroxyaluminium Formation. *Polyhedron*, **12**(9):1007.
12. Martin, R.B. (1990). Aluminosilicate Stabilities under Blood Plasma Conditions. *Polyhedron*, **9**(2/3):193.
13. Birchall, J.D., Bellia, J.P, and Roberts, N.B. (1996). On the Mechanisms Underlying the Essentiality of Silicon—Interactions with Aluminium and Copper. *Coord. Chem. Rew.*, **149**:237.
14. Birchall, J.D. and Espie, A.W. (1986). Biological Implication of the Interaction (via silanol groups) of Silicon with Metal Ions in Silicon Biochemistry. (CIBA Foundation Symposium 121), pp. 140. Wiley, Chischester.
15. Exley, C., Tollervey, A., Gray, G., Roberts, S., and Birchall, J.D. (1993). Silicon, Aluminium and the Biological Availability of Phosphorus in Algae. *Proc. R. Soc. Lond. B*, **253**:93.
16. Exley, C. and Birchall, J.D. (1992). Hydroxyaluminosilicate Formation in Solutions of Low Total Aluminium Concentration. *Polyhedron*, **11**(5):1901.
17. Birchall, J.D. (1994). Silicon-Aluminium Interactions in Biology, in Bergna, H.C. (Ed.). The Colloid Chemistry of Silica. Amer. Chem. Soc., Washington, DC, pp 601.
18. Rowatt, E. and Williams, R.J.P. (1996). The Interaction of Aluminium with Silicic Acid in the Presence and Absence of a Phosphorylated Protein. *Coord. Chem. Rew.*, **149**:167.
19. Perry, C.C. and Keeling-Tucker, T. (1998). Aspects of the Bioinorganic Chemistry of Silicon in Conjunction with the Biometals Calcium, Iron and Aluminium. *J. Inorg. Biochem.* **69**:181.
20. Damen, J.J.M. and Ten Cate, J.M. (1989). The Effect of Silicic Acid on Calcium Phosphate Precipitation. *J. Dent. Res.*, **68**(9):1355.
21. Tanizawa, Y. and Suzuki, T. (1995). Effects of Silicate Ions on the Formation and Transformation of Calcium Phosphates in Neutral Aqueous Solutions. *J. Chem. Soc. Faraday Trans.*, **91**(19):3499.

22. Yamanka, C., Yokotama, T. and Tarutani, T. (1986). Retarding effect of aluminium on the polymerization of silicic acid particles. *J Chromatog.* **367**:419.

23. Taylor, P.D., Jugdaohsingh, R. and Powell, J.J. (1997). Soluble Silica with High Affinity for Aluminium under Physiological and Natural Conditions. *J. Am. Chem. Soc.* **119**:8852.

CHAPTER 7: EVALUATION OF THE BIOACTIVITY OF A SILICA SOL-GEL-BASED SURFACE *IN VITRO*

7.1. Introduction

In the early 1970s, Hench and co-workers discovered and developed bioactive glasses. These glasses were registered as Bioglass® with the constituents Na_2O-CaO-P_2O_5-SiO_2[1]. Other researchers such as Kokubo, (1992)[2], and Li, (1994)[3] have developed glass-ceramics by modifying Bioglass®, decreasing or substituting Na_2O and adding MgO. Nowadays, bioactive glasses and glass-ceramics are used clinically for the replacement and reconstruction of damaged bone [4,5] since they have the ability to bind to bone through an apatite layer that is formed on their surfaces in the body[6-8].

Ohtsuki *et al.* (1993) showed that pure silica hydrogel also induced the formation of apatite on its surface when the gel was soaked in simulated body fluid (SBF) with ion concentrations nearly equal to those in human blood plasma[9].

Bioactive sol-gel coatings of hydroxycarbonateapatite (HCA) have been made on various substrates such as porous sol-gel silica[10-13], sol-gel organically modified silicates[14], etc..

SBF has been used as an *in vitro* model to study apatite formation or precipitation on the surfaces of different types of biomaterials[15,16]. Furthermore, the SBF precipitation process has been suggested as a coating process to produce a thin layer of physiological HAP on an implant surface to replace the plasma-coated HAP[17]. Over the last 10 years, the chemical composition of the precipitates in relation to the ion composition[9], calcium and phosphorous concentration[18], and pH changes in the solution[19], heat treatment[20] and structure of the silica substrates[21,22] during precipitation have been investigated.

The aim of this work was to assess the bioactivity of a silica sol-gel based surface. The bioactivity of the coatings was assessed using the SBF process. The osteoblast response to the silica surface was also assessed.

7.2. Materials and Methods

Materials

TEOS 98% from Aldrich, dry EtOH (distilled from EtOH over Mg), HCl (31-33%) from Fisher, NaCl (99%) from Aldrich, $NaHCO_3$ (99.99%) from Aldrich, KCl (99.5%) from BDH, K_2HPO_4 (99.5%) from East Anglia Chemicals, $MgCl_2 \cdot 6H_2O$ (98%) from BDH, $CaCl_2$ (98%) from Aldrich and Na_2SO_4 (97%) from Aldrich.

Methods

Thermanox® discs (Nunc) were coating by a silica solution prepared by the sol-gel method (see chapter 2 for sol-gel and coating procedures).

The bioactivity of the silica gel based-coated disc was assessed using a simulated body fluid (SBF). SBF was prepared as described previously[11,12] using the reagents NaCl, $NaHCO_3$, KCl, K_2HPO_4, $MgCl_2 \cdot 6H_2O$, $CaCl_2$, Na_2SO_4 added in that order to give an ionic concentration almost equal to that of human plasma (table 7.1). The pH of the solution was brought to 7.4 using HCl and Tris buffer.

Ion	SBF (mM)	Human plasma (mM)
Na^+	142.0	142.0
K^+	5.0	5.0
Mg^{2+}	1.5	1.5
Ca^{2+}	2.5	2.5
Cl^-	147.8	103.0
HCO_3^-	4.2	27.0
HPO_4^{2-}	1.0	1.0
SO_4^{2-}	0.5	0.5

Table 7.1 Ion Concentrations of SBF and Human Blood Plasma at pH=7.4 .

Silica sol-gel-based coated discs were incubated in 1xSBF, and 1.5xSBF at 37°C for 28 days. They were vertically placed in a plastic box held below the surface of the solution as shown in Figure 7.1. The plastic container containing the silica gel coated coverslips was placed in a shaking thermostatically controlled water bath maintained at 37°C.

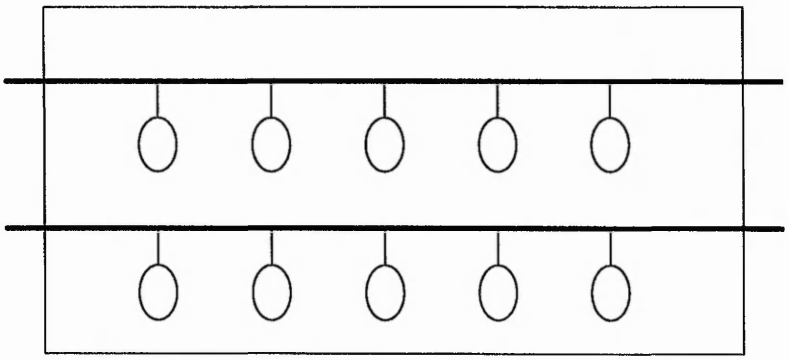

Fig. 7.1 : Formation of SBF on the silica gel coated thermanox-coverslips.

The SBF solution was renewed every three days. Non-coated Thermanox® discs were used as controls. The surfaces were analysed by SEM. The material deposited on the disc was carefully removed from the surface and deposited onto an holey copper carbon coated grid. TEM and EDX analysis were performed on the precipitate.

Cell Culture

As part of an ongoing collaboration between The Nottingham Trent University (NTU) and The Medical School at Nottingham University (NU), silica surfaces prepared by spin coating a silica sol-gel solution onto thermanox discs at NTU were investigated for osteoblast response by Ms S. Anderson at the NU. The effect of the surface itself and the release of orthosilicic acid into the medium have both been investigated.

Primary Human Osteoblasts (HOBs) were seeded onto the discs in sterile, 24 well cell culture plates at a density of $8x10^5$ cell/ml and cultured in complete, phenol red free, Dulbeccos modified eagles medium (prfDMEM) supplemented with 150 mg/l L-Ascorbic acid. The plates were incubated at 37°C, 5 % CO_2 for up to 31 days. For full protocol see reference 23.

Cells were processed at NU and send back to the NTU for examination by TEM and EDX analysis of any precipitates formed.

7.3. Results

SEM analysis of the silica sol-gel coating prior to incubation, showed that the surface was flat and featureless. Some cracks were observed. The coating were ca. 200-300 nm in thickness measured from the cracks (fig. 7.2).

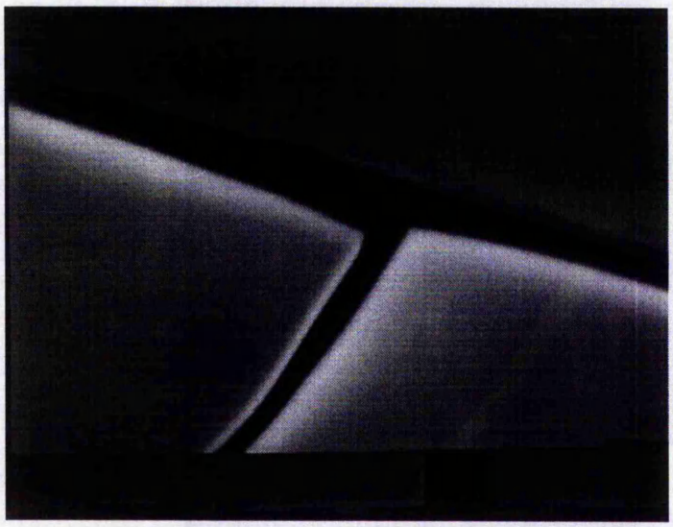

Figure 7.2 SEM image of a silica sol-gel based coating before soaking in SBF.

Figure 7.3 shows the FT-IR diffuse reflection spectra of the silica sol-gel based coating prior to soaking in SBF. The IR peaks at 470 and 810 cm^{-1} are assigned to the Si-O-Si

bending vibration, that at 1100 cm^{-1} to the Si-O stretching vibration and that at 960 cm^{-1} to the Si-OH stretching vibration[24].

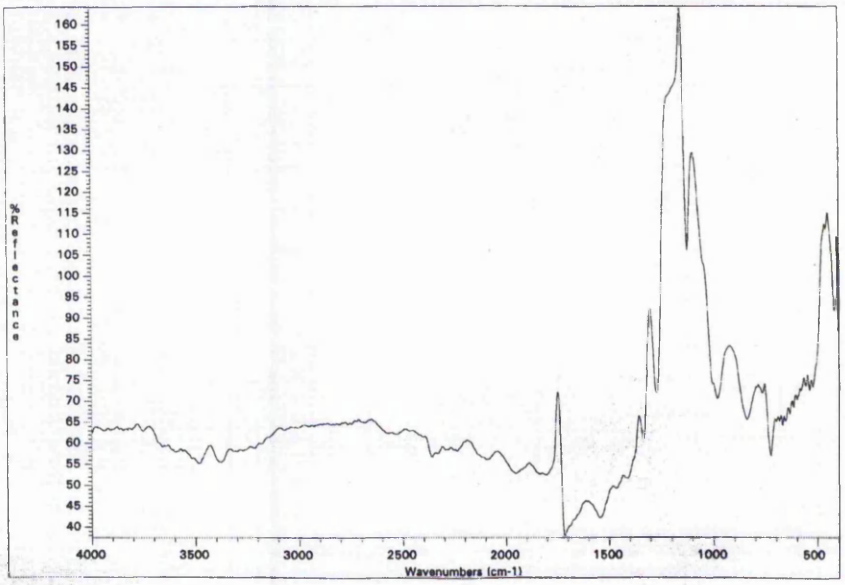

Figure 7.3 FT-IR diffuse reflectance spectrum of a silica sol-gel based coating prior soaking in SBF.

SEM analysis of the silica coatings after being soaked for 4 weeks in SBF and 1.5xSBF showed the formation of precipitate on the surface. Compared to the control, the surface of the silica-coated discs were regularly covered with precipitate (fig. 7.4).

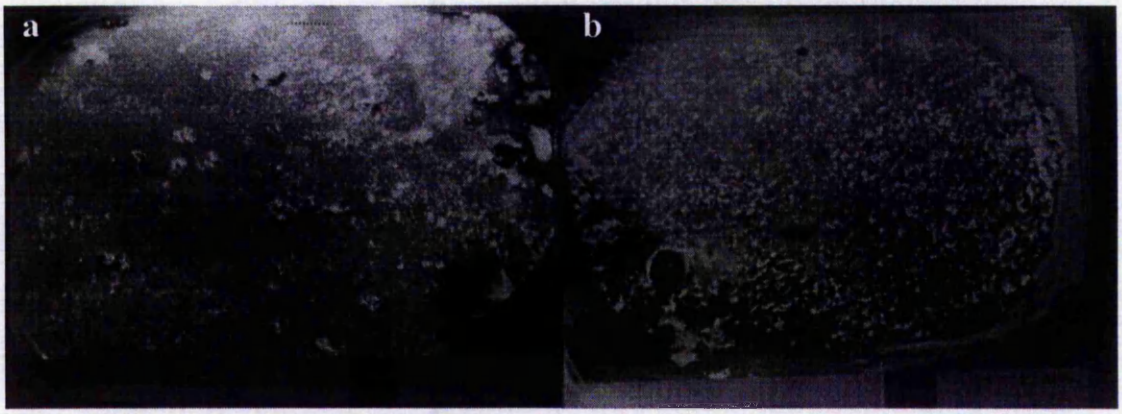

Figure 7.4 SEM images of discs a) control and b) coated with silica after 4 weeks incubation in 1xSBF at 37°C.

TEM analysis of the precipitate deposited on the surfaces incubated in 1xSBF and 1.5xSBF showed that the material was apatite. The crystals presented the flake-like structure characteristic of non-stoichiometric hydroxyapatite (fig. 7.5a,c and see chapter 3). Electron diffraction of the precipitate formed on the control and silica-coated discs gave the d-spacings values of 2.81 and 3.51 Å corresponding to the Miller indices of (2 1 1) and (2 0 1) of hydroxyapatite (JDCPS 9-432) (fig. 7.5).

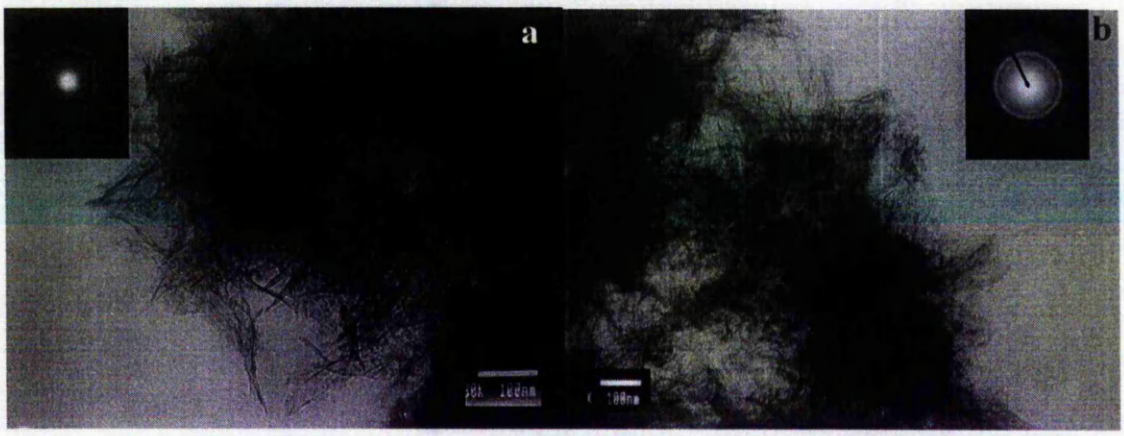

Figure 7.5 TEM image of precipitate formed on a) control and b) silica-coated discs after being incubated in 1.5xSBF for 4 weeks at 37°C.

The Ca/P molar ratios of the precipitate were those corresponding to non-stoichiometric hydroxyapatite. There was no significant difference between the Ca/P molar ratios obtained for the precipitate formed on the silica coatings and the controls (table 7.3).

	1xSBF	**1.5xSBF**
control	1.64 ± 0.21	1.68 ± 0.07
silica-coated discs	1.69 ± 0.10	1.59 ± 0.03

Table 7.2 shows the Ca/P molar ratios obtained for the precipitate after 4 weeks incubation in 1xSBF and 1.5xSBF at 37°C (n=3).

HOB cells cultured on silica sol-gel based coated surfaces and controls were confluent by 48h. Nodules were formed earlier on the silica-coated discs than on the controls. Sometimes the shape of the nodules formed on the silica-coated discs was elongated compared to the controls[23]. HOBs were also grown on inverted silica-coated discs. No significant difference between the controls and silica-coated discs was observed in cell activity, DNA content and AP activity[23]. Nodules on silica-coated surfaces started to mineralise earlier than the control[23].

Mineral was detected in these cultures by TEM analysis. The crystals which presented a needle-like morphology characteristic of apatite were analysed by EDX (fig. 7.6). The absence of phosphorous in the EDX analysis and the shape of the crystals might indicate that the crystals are a carbonateapatite mineral. They were highly hydrated and it was not possible to obtain an electron diffraction pattern.

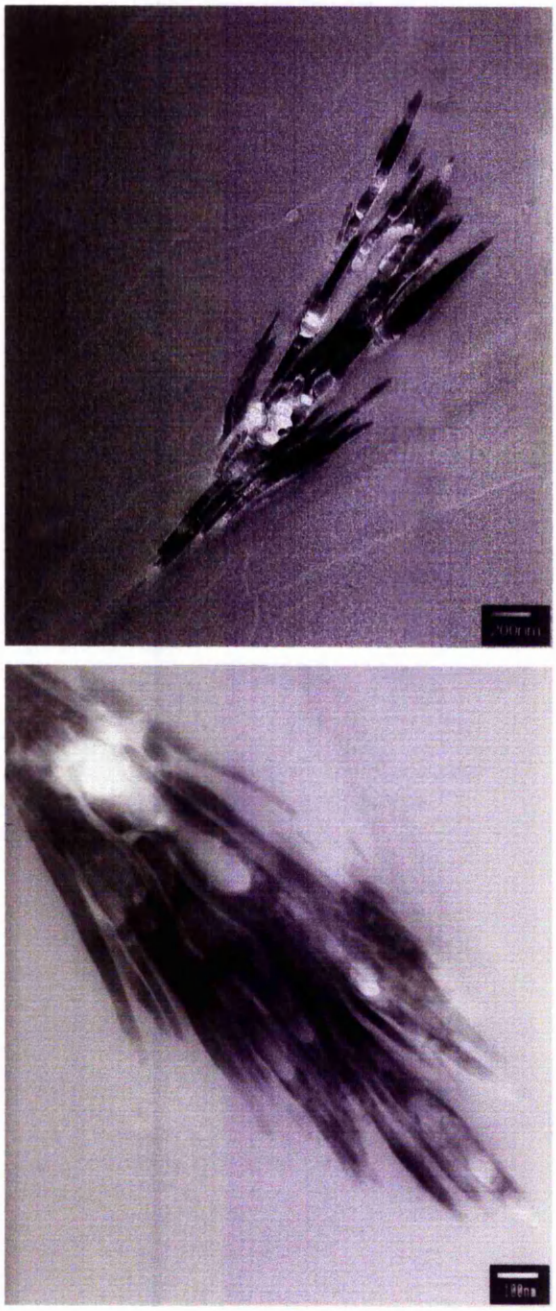

Figure 7.6 TEM images of crystals present in osteoblast cultures grown on silica-coated discs.

7.4. Discussion

In this study the biactivity of a silica sol-gel derived surface was assessed. The behavior of osteoblast cells grown on that surface was also investigated.

Although, SBF is supersaturated with respect to apatite, it is a metastable solution[26].

As shown in figure 7.4 , apatite precipitated in clusters and covered regularly the surface of the coated disc compared to the control. A higher magnification view (fig. 7.5) showed that the clusters were formed of flakes, a characteristic morphology of non-stoichiometric hydroxyapatite (see chapter 3) with Ca/P ratios between 1.5-1.7. Li *et al.* (1993) also reported the precipitation of apatite from SBF on silica gel[17]. They found that the apatite precipitated on silica gel had the form of very small spherulites with each one consisting of a large number of flakes[17].

The mechanisms of nucleation and growth of HAP on silica gel substrates are still in debate. Silanol group[25,26], surface structural defects[27], pore size and pore volume[17,25] and adsorption of silicate ions dissolved from the silica gels[28] may be involved in the rate of formation and the structure of the HAP precipitate from SBF. It could be possible that more than one of the aspects mentioned above would be involved in the process of HAP precipitation.

SEM analysis of the silica surfaces used in this study did not show the presence of pores (fig. 7. 2). FT-IR analysis showed the existence of silanol groups on the silica surface (fig. 7.3). It has already been suggested that the ability of silica to induce the formation of HAP depends on the presence of silanol groups on its surface which could act as nucleation sites[25,26]. An attempt has been made to show the involvement of silanol groups on the nucleation process. It was shown that apatite could form on silica gels immersed in SBF but not on dense silica glass or quartz[25]. However the differences between silica gel and

dense silica is not only in the number of silanol groups on the surface but also in the presence of pores in the silica gel and differences in the network of the silica gel and dense silica[24]. When these silica gels were heat treated, HAP formation was found to decrease with increasing temperature[17]. However the decrease of HAP precipitation on heat treated silica gels could have not only been due to the decrease of silanol groups but also the effect of the heat on the pore size and distribution[10].

Another hypothesis suggests that soluble silicate ions dissolved from silica gels induce apatite formation[28]. When Ca^{2+} ions were added in combination with $HSiO_3^-$ ions to a SBF solution containing an apatite-wollastonite glass-ceramic A-W(Al) an apatite layer formed on the surface[28]. The researchers suggested that the silicate ions could provide favorable sites for the nucleation of apatite.

Previous experiments using orthosilicic acid have shown that soluble silica species promote calcium phosphate precipitation (see chapter 4). The effect of the soluble silica species depended on the concentration of calcium and phosphorous present in solution (see chapter 4). It has also been proposed that the way these species act is through interactions of the hydroxyl groups with Ca^{2+} or HPO_4^{2-}. However the type of silanol groups present on the silica surface after being soaked in SBF and involved in the formation of HAP have yet to be determined.

HOBs were grown on a thin film of silica in order to establish the effect of a silica surface on osteoblast growth and differentiation. The earlier nodule formation on the silica-coated discs compared to the controls may have been due to the physical topography of the surface since in some cases osteoblasts aligned along defects in the silica coating and nodules formed in these areas[23]. However, when cells were grown on inverted discs, nodules also formed earlier than the controls. In this way cells had access to silica that had

been released from the discs[23] but the surface available to the cells was the same as that exposed to the controls. It demonstrated that topography alone was not responsible for the early mineralisation of HOBs on silica surfaces. It is still unclear if the response of the osteoblast cells was due to the silanol groups alone present on the surface of the silica coating which have been suggested to act as favourable sites for apatite nucleation[25,26]. Another possibility is that when the silica coated thermanox dics were immersed into the media, they would have become more hydrated and consequently some silicate ions dissolved, the surfaces developing additional silanol groups. These might also provide favorable sites for cell attachment. The silicate ions released into solution could be taken up by the cells and also promote apatite precipitation.

The results obtained from this study showed that silica coated surfaces stimulate apatite precipitation and may promote mineralisation of osteoblast cells *in vitro*.

7.5 References

1. Hench, L.L., Splinter, R.J.M., Allen, W.C., Greemlee, T.K. (1971). Bonding Mechanisms at the Interface of Ceramic Prosthetic Materials. *J. Biomed. Mater. Res. Biomed. Mater. Symp.* **2**:117.
2. Kokubo, T. (1992). 'Bioactivity of Glasses and Glass-Ceramics'. Bone-Bonding. Reed Healthcare Communications, pp 31-46. Ducheyne, Kokubo & Van Blitterswijk eds.
3. Li, P., and De-Groot, K. (1994). Better Bioactive Ceramics Through Sol-Gel Process *J. Sol-Gel Sci. Techn.*, **2**:797.
4. Yamamuro, T, Okumra, H., Kitsugi, T., Kakutani, Matsui, T. and Kokubo, T. (1990). Replacement of the Lumbar Vertebras of Sheep with Ceramic Prostheses. *J. Bone Joint Surg.* **72B**:889.
5. Kokubo, T. (1991). *J. Ceram. Soc. Jpn.* **99**:965.
6. Ohura, K., Yamamuro, T., Nakamura, T., Kokubo, T. Ebisawa, Y., Kotoura, Y. and Oka, M. (1991). *J. Biomed. Mater. Res.* **25**:357.

7. Hench, L.L. (1995). Bioactive Implants. *Chem. Ind.*.**14**:547.
8. Kokubo, T. (1993). Bioactive of Glasses and Glass Ceramics. In Bone Bonding Biomaterials, pp. 31. Edited by Ducheyne, P., Kokubo, T. and Blitteswijk, C., Reed Healthcare Communication, The Neatherlands.
9. Li, P., Ohtsuki, C., Kokubo, T., Nakanishi, K., Soga, N., Nakamura, T., and Yamamuro, T. (1993). Effects of Ions in Aqueous Media on Hydroxyapatite Induction by Silica Gel and Its Relevance to Bioactivity of Bioactive Glasses and Glass-Ceramics. *J. App. Biomater.* **4**:221.
10. Pereira, M. and Hench, L.L. (1996). Mechanisms of Hydroxyapatite Formation on Porous Gel-Silica Matrices. *J. Sol-Gel. Sci. Technol.* **7**:45.
11. Cho, S.B., Nakanishi, K., Kokubo, T., Soga, N., Ohtsuki, C. and Nakamura, T. (1996). Apatite Formation on Silica Gel in Simulated Body Fluid: Its Dependence on Structures of Silica Gels Prepared in Different Media. *J. Biomed. Mater. Res.* **33**:145.
12. Cho, S.B., Miyagi, F., Kokubo, T., Nakanishi, K., Soga, N., and Nakamura, T. (1996). Apatite-Forming Ability of Silicate Ion Dissolved from Silica Gels. *J. Biomed. Mater. Res.* **32**:375.
13. Li, P., Kokubo, T., Nakanishi, K. and de Groot, K. (1993). Induction and Morphology of Hydroxyapatite, Precipitated from Metastable Simulated Body Fluids, on Sol-Gel Prepared Silica. *Biomaterials* **14**:963.
14. Tsuru, K., Ohtsuki, C. and Osaka, A. (1997). Bioactivity of Sol-Gel Derived Organically Modified Silicates. *J. Mater.Sci. Mater. Med.* **8**(3):
15. Yoshihara, S., Kokubo, T., Nishimura, N., Yamamuro, T., Nakamura, T. (1994). Effects of Glass Composition on Compressive Strength of Bioactive Cement Based on CaO-SiO_2-P_2O_5 Glass Powders. *J. Mater. Sci. Mater. Med.* **5**:123.
16. Filho, O.P., LaTorre, G.P. and Hench, L.L. (1996). Effect of Crystallisation on Apatite-Layer Formation of Bioactive Glass 45S5. *J. Biomed. Mater. Res.* **30**:509.
17. Li, P., Ohtsuki, C., Kokubo, T., Nakanishi, K., Soga, N., Nakamura, T., and Yamamuro, T. (1993). Process of Formation of Bone-like Apatite Layer on Silica Gel. *J. Mater. Sci. Mater. Med.* **4:**127.
18. Cho, S., Miyaji, F., Kokubo, T., Nakanishi, K., Soga, N., and Nakamura, T. (1996). Apatite Formation on Various Silica Gels in a Simulated Body Fluid Containing Excessive Calcium Ion. *J. Ceram. Soc. Jpn.* **104**(5):399.

19. Li, J., Liao, H., and Sjöström, M. (1997). Characterisation of Calcium Phosphates Precipitated from Simulated Body Fluid of Different Buffering Capacities. *Biomaterials* **18**(10):743.
20. Cho, S., Nakanishi, K., Kokubo, T., and Soga, N. (1995). Dependence of Apatite Formation on Silica Gel on Its Structure: Effect of Heat Treatment. *J. Am. Ceram. Soc.* **78**(7):1769.
21. Pereira, M.M., Clark, A.E., and Hench, L.L. (1994). Calcium Phosphate Formation on Sol-Gel-Derived Bioactive Glasses *in vitro*. *J. Biomed. Mater. Res.* **28**:693.
22. Pereira, M.M., Clark, A.E., and Hench, L.L. (1995). Effect of Texture on the Rate of Hydroxyapatite Formation on Gel-Silica Surface. *J. Am. Ceram. Soc.* **78**(9):2463.
23. Anderson, S.I., Downes, S., Perry, C.C. and Caballero, A.M. (1998). Evaluation of the Osteoblast Response to a Silica Gel *in vitro*. *J. Mater. Sci. Mater. Med.* **9**:731.
24. Iler, R.K. (1970). The Chemistry of Silica. Edited by John Wiley&Sons. Wiley-Interscience. New York.
25. Li, P., Ohtsuki, C., Kokubo, T. Nakanigh, K., Soga, N., Nakamura, T. and Yamamuro, T. (1992). Apatite Formation Induced by Silica-Gel in a Simulated Body Fluid. *J. Am. Ceram. Soc.* **75**:2094.
26. Li, R., Clark, A.E. Clark, and Hench L.L. (1991). An Investigation of Bioactive Glass Powders by Sol-Gel Processing. *J. App. Biomater.* **2**:231.
27. Wallace, S., West, J.W., and Hench, L.L (1993). Interactions of Water with Trisiloxane Rings. I. Experimental Analysis. *J. Non. Cryst. Solids* **152**:101.
28. Kokubo, T., Ito, S., Huang, Z.T., Hayashi, T., Sakka, S., Kitsugi, T. and Yamamuro, T. (1990). Ca, P Rich Layer Formed in High-Strength Bioactive Glass-Ceramic A-W. *J. Biomed. Mater. Res.* **24**:331.

CHAPTER 8: CONCLUSIONS AND FUTURE WORK

This thesis was concerned with the formation of calcium phosphate crystals. A method to identify and characterise calcium phosphate materials has been developed. The formation and transformation of calcium phosphates in the presence of soluble silicon species and aluminium has been studied. The ameliorating effect of silicon on the aluminium toxic effects on the formation of calcium phosphate crystals has also been investigated. Finally, the bioactivity of a silica sol-gel based coating was assessed.

The nature of the calcium phosphate phase which formed during precipitation from aqueous solution was dependent upon the calcium and phosphate concentration, pH, T, ionic strength. At high supersaturation concentrations of calcium (0.242M) and phosphate (0.145M) ions, DCPD formed for precipitations carried out at both 23°C and 37°C. However when the pH was kept constant at 7.4 during precipitations carried at 23°C, apatite formed instead. At moderate supersaturation concentrations of calcium (10 mM) and phosphate (6 mM) ions, DCPD (main product), OCP and non-stoichiometric HAP formed from precipitation reactions carried out at 23°C. For precipitation reactions performed at 37°C, non-stoichiometric HAP and OCP formed.

When NaH_2PO_4 was used as precursor, Na^+ favoured the formation of DCPD over HAP when high concentrations of calcium (0.242M) and phosphate (0.145M) were used. The transformation of ACP to HAP occurred by the Ostwald ripening process. ACP transformed directly to HAP and also through the OCP intermediate.

Due to the difference in crystal sizes, the presence of the apatite phase was hidden by the low intensity of its reflections (x-ray diffraction) and the high intensity of the reflections from the DCP crystals which were much larger in size for precipitations carried out at 23°C

when 10 mM calcium and 6 mM phosphate were used. In contrast, the IR absorbance of the apatite phase was much higher than the absorbance for DCP. This inability to detect phases present at significant levels could lead to confusion when interpreting FT-IR data. The presence of OCP was also hidden in the x-ray diffraction patterns obtained from the precipitate formed at 37°C from a solution containing 10 mM calcium and 6 mM phosphate. Other techniques such as TEM must be used to confirm the presence of these crystal phases.

The effect of orthosilicic acid on calcium phosphate precipitation *in vitro* depended on the experimental conditions. At high concentrations of calcium (0.242M) and phosphate (0.145M), orthosilicic acid increased the crystallinity of the calcium phosphate crystal phases formed at both 23°C and 37°C. When lower concentrations of calcium (10 mM) and phosphate (6 mM) were used, the presence of orthosilicic acid seemed to favour the formation of apatite over DCP. The stimulatory effect of silicon on calcium phosphate formation seems to be associated with the silanol groups. It may be possible that the silanol groups are involved in the nucleation process. Orthosilicic acid also shortened the induction time thereby accelerating the precipitation process. Orthosilicic acid seemed to affect the crystal growth of apatite in an anisotropic way. TEM analysis showed that silica affected the length of the apatite crystals formed at 23°C. The apatite crystals precipitated in the presence of orthosilicic acid were longer compared to those precipitated in the absence of orthosilicic acid. However, only the apatite crystals precipitated in the presence of 0.082 mM orthosilicic acid at 37°C were longer compared to those precipitated in the absence of orthosilicic acid. The x-ray data showed a decrease in the c lattice and an increase in the a(=b) lattice parameters compared to the control for the apatite crystals

precipitated in the presence of orthosilicic acid at 37°C. The concentration of orthosilicic acid at which the greatest effect on crystallinity was observed was found to be 0.082 mM. Al(III) seemed to stop the transformation of ACP into HAP and the further development of the crystal by precipitating with Ca and P and forming a very insoluble amorphous material. Al and the amorphous material may adsorb as crystal growth poisons. Orthosilicic acid was able to ameliorate the aluminium inhibitory effect on the formation of calcium phosphates and the transformation of ACP to HAP. Both ions present simultaneously seemed to work in a synergistic way stimulating the formation of apatite over DCPD for precipitations performed at 23°C. For precipitations performed at 37°C, the presence of orthosilicic acid in solution seemed to decrease the loss of crystallinity, due to the presence of aluminium (III), on the calcium phosphate phases formed. The inhibitory effect of aluminium (III) on the transformation of ACP to HAP was also decreased by the additional presence of orthosilicic acid in the reaction solution.

The data presented in this study was obtained from analyses performed on the calcium phosphate precipitates. A single crystal study performed in fine detail is necessary to identify how orthosilicic acid affects the hydroxyapatite crystal structure at the molecular level. Further studies to determine the silicon, aluminium and HAS molecular species present in solution should also be carried out. Experiments to determine if silicic acid remains monomeric or polymerises at the sites of calcium phosphate nucleation should be done since it is not safe to assume that silicic acid may remain monomeric at the nucleation sites. Studies to determine if silicic acid polymerises or forms HAS when aluminium is added to the reacting solution and the nature of these molecular species would help to understand the synergic effect observed in the precipitation reactions carried out at 23°C in the presence of both aluminium and silicic acid.

Finally silica coated surfaces stimulated apatite precipitation and might promote mineralisation of osteoblast cells *in vitro*.

APPENDIX I

FT-IR and XRD spectra of the standards

1. Monocalcium phosphate (MCP)

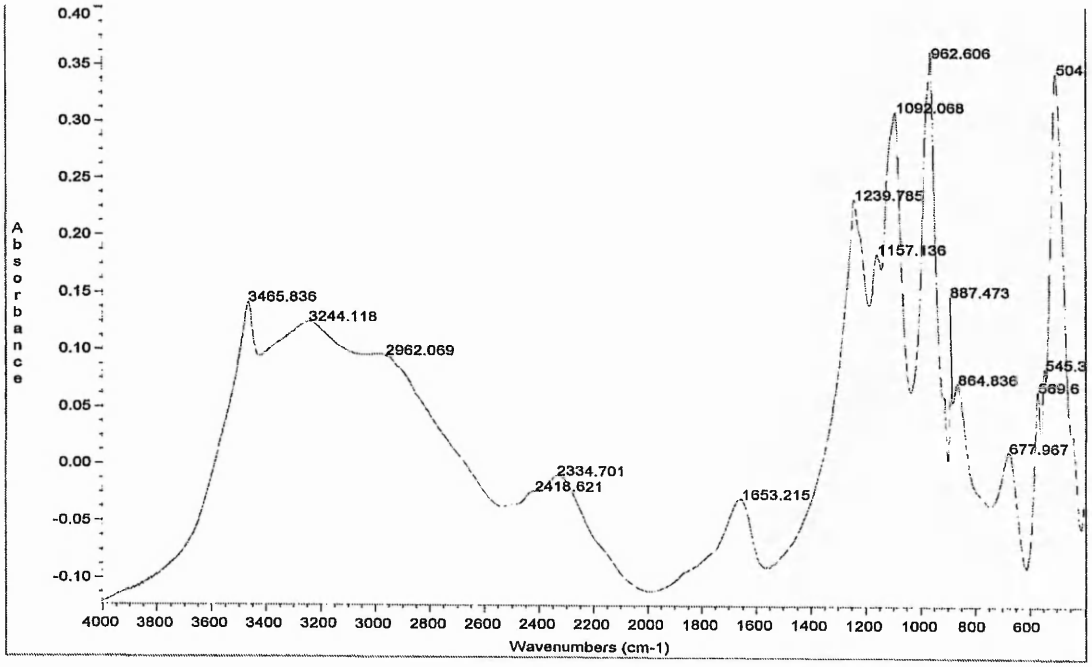

Fig 1 FT-IR spectrum of MCP

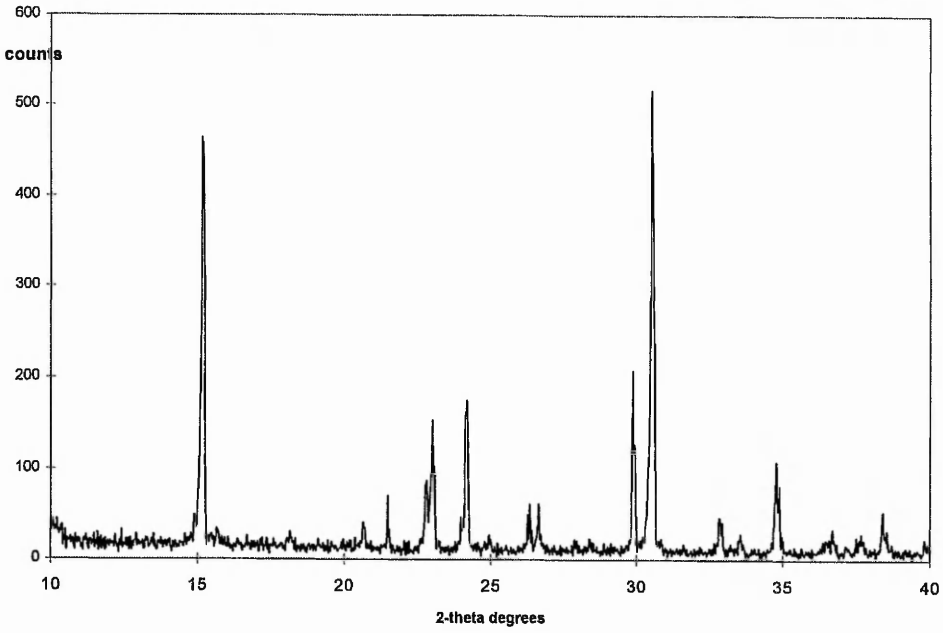

Fig 2 XRD pattern of MCP.

2.Dicalcium Phosphate (DCP)

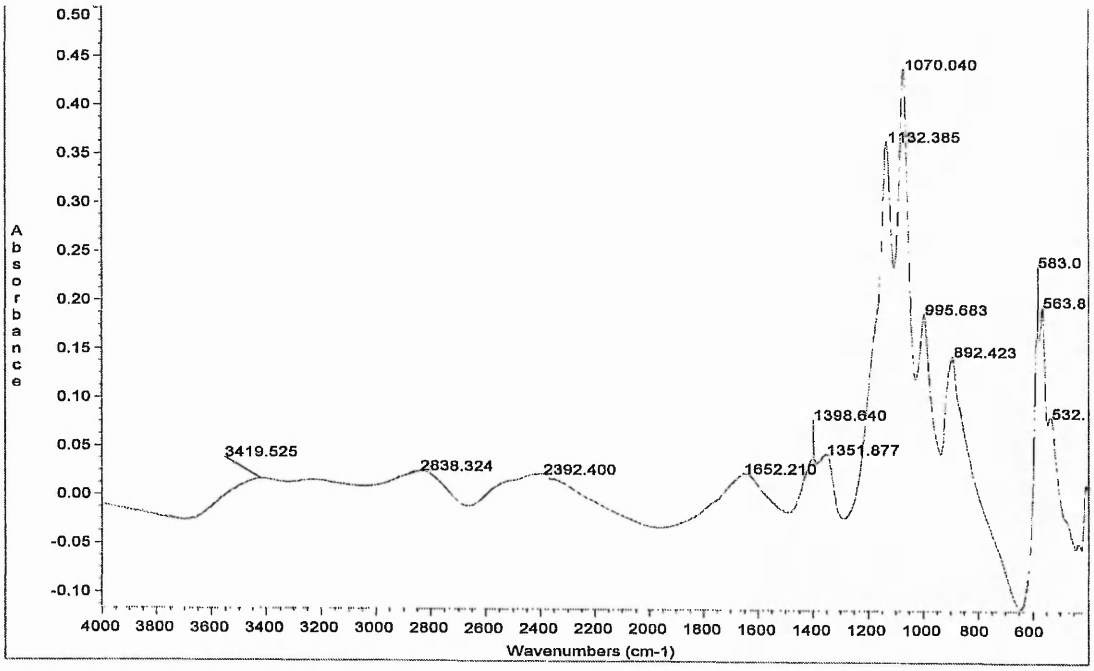

Fig 3 FT-IR spectrum of DCP.

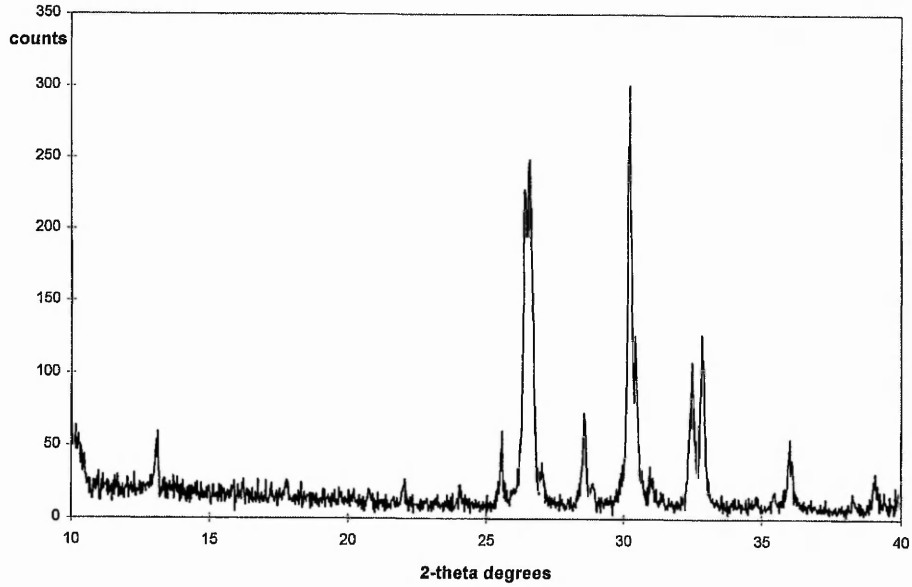

Fig 4 XRD pattern of DCP.

3. Hydroxyapatite (HAP)

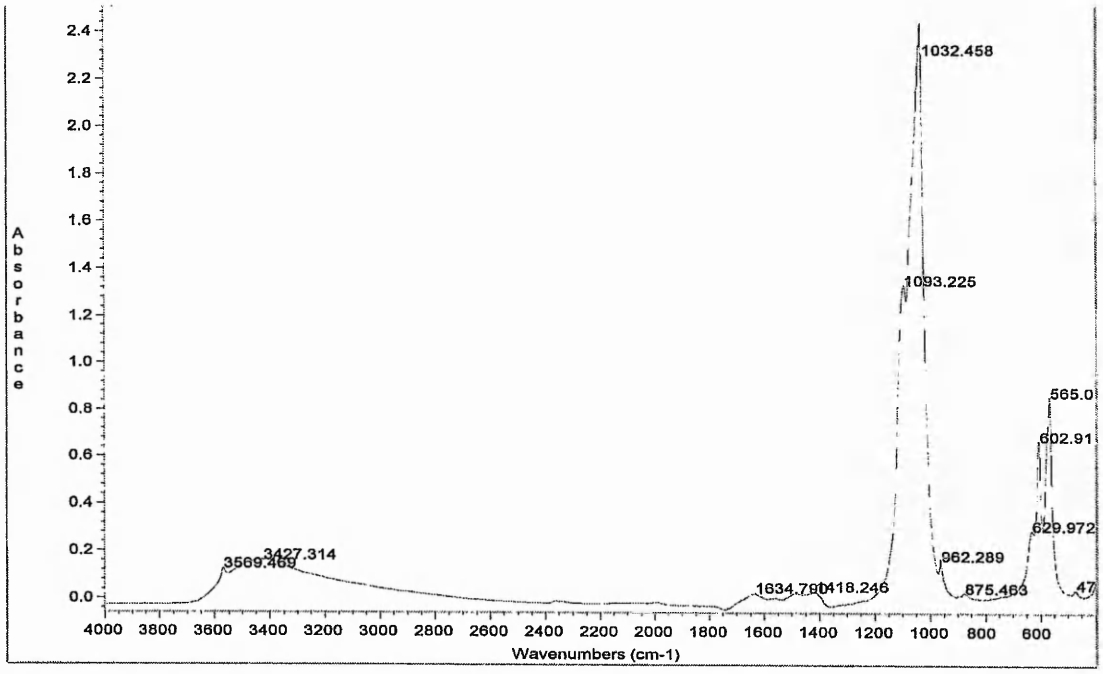

Fig 5 FT-IR spectrum of HAP.

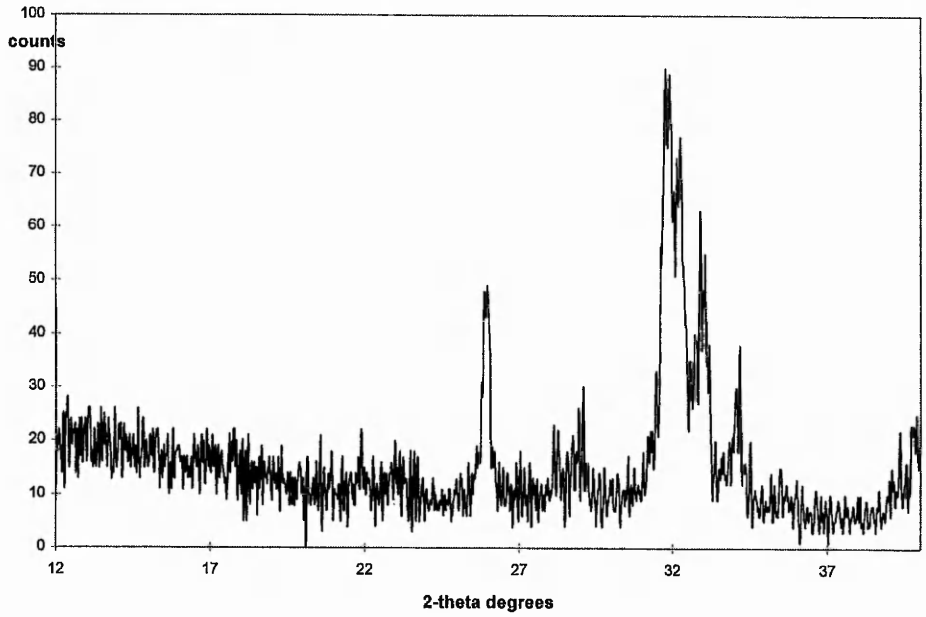

Fig 6 XRD pattern of HAP.

4. Calcium pyrophosphate (CPP)

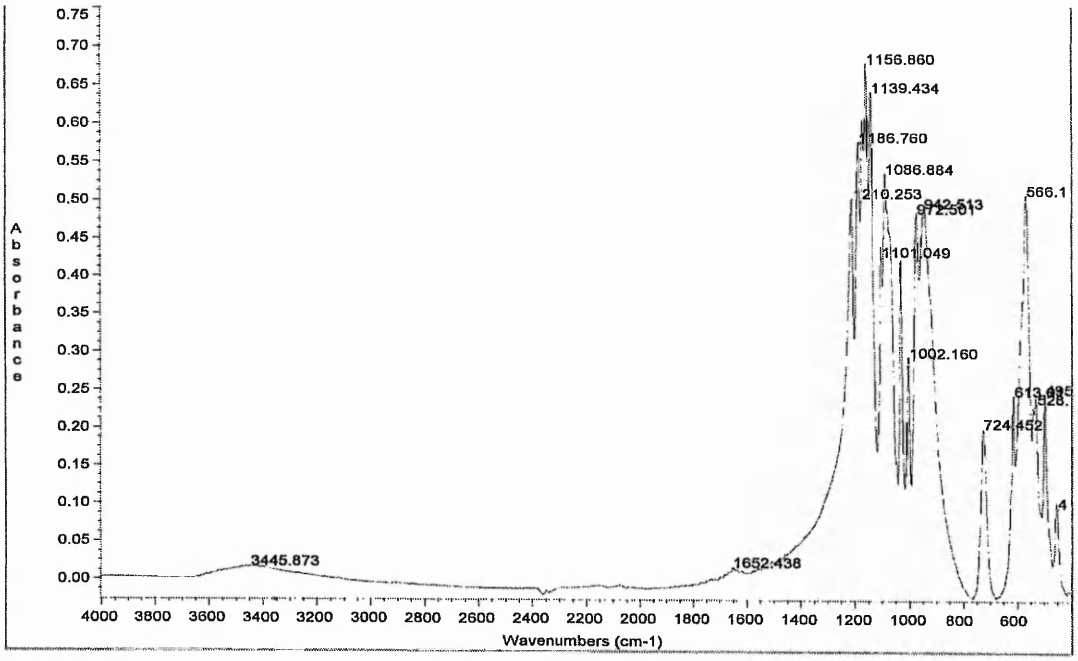

Fig 7 FT-IR spectrum of CPP.

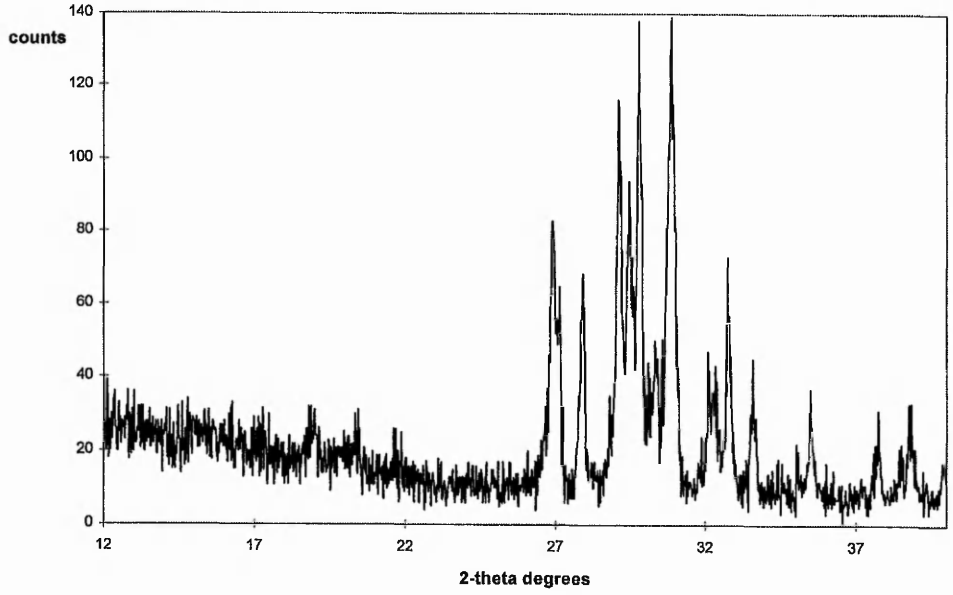

Fig 8 XRD pattern of CPP.

5. β-*Tricalcium Phosphate* (β-*TCP*)

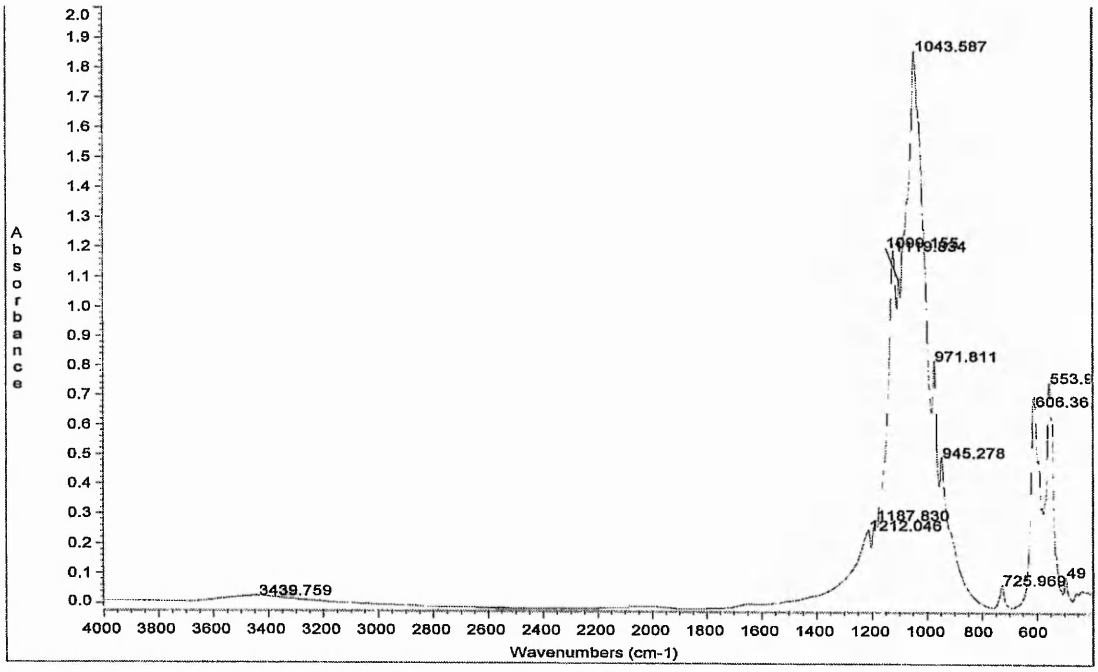

Fig 9 FT-IR spectrum of β-TCP.

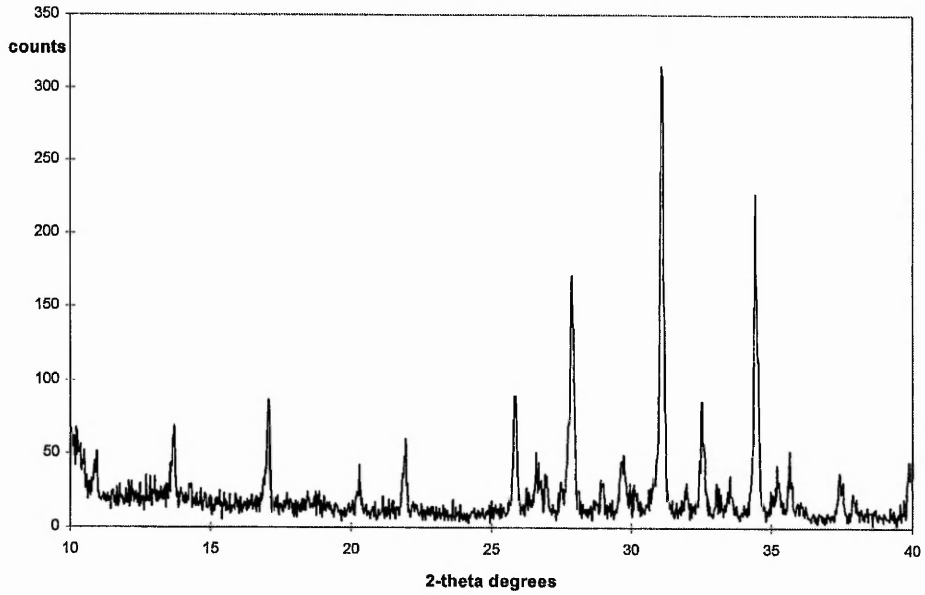

Fig 10 XRD pattern of β-TCP.

6. Aluminium Phosphate

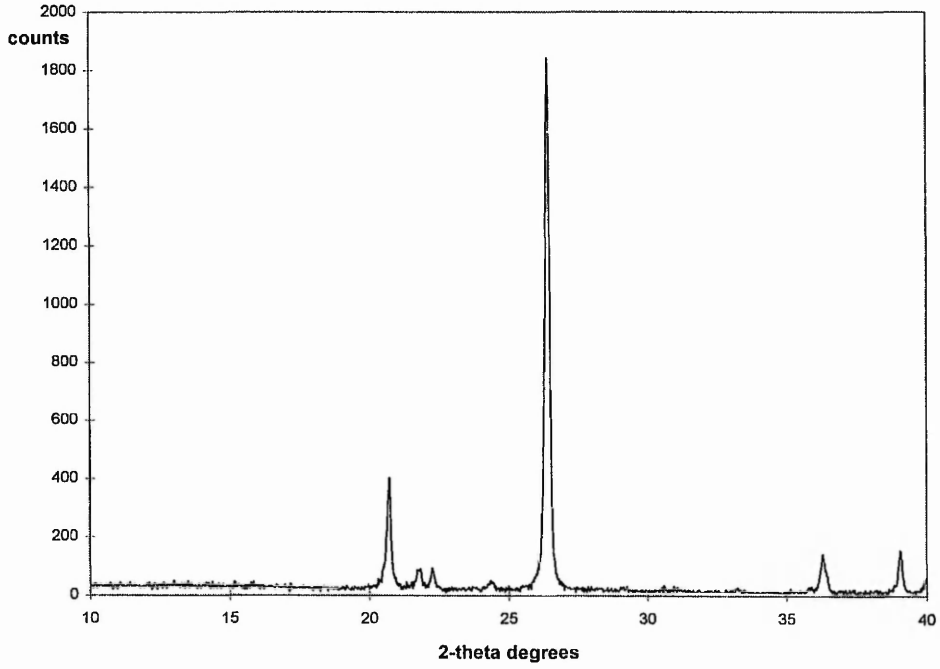

Fig 11 XRD pattern of aluminium phosphate.

APPENDIX II

Interpretation of Electron Diffraction Patterns

A diffraction pattern contains two basic types of information, (a) spatial arrangement, that is, distances R, between the central spot and the other diffraction spots and rings, and the angles Φ, between lines joining the central spot to each diffraction spot, and (b) intensities, in comparative values between the central spot and the other diffraction maxima.
From the R values it is possible to derive values of the d-spacings in the specimen.
Consider the electron microscope as a simple electron diffraction camera, with the electron beam striking a specimen and being diffracted to form a diffraction spot on the photographic plate, at distance R from the center of the diffraction (Fig. 1). The distance between the specimen and the plate, the *camera length*, is designated L, and by simple geometry

$$\tan 2\theta = R/L.$$

The Bragg Law states that

$$\lambda = 2d \sin \theta,$$

and since the angles θ, through which the electrons are diffracted are very small, only 1°-2°, the approximation

$$\tan 2\theta = 2\sin \theta,$$

can be made with very little error. Then,

$$R/L = \lambda/d,$$

or

$$Rd = \lambda L.$$

So if values of R, L and λ for a particular diffraction spot or ring can be measured, then the d-spacings of the set of lattice planes giving rise to that spot or ring can be determined. This procedure can be repeated for all the spots and rings in the diffraction pattern, and a list of d-spacings can be compiled for all the sets of planes in the specimen which are reflecting.

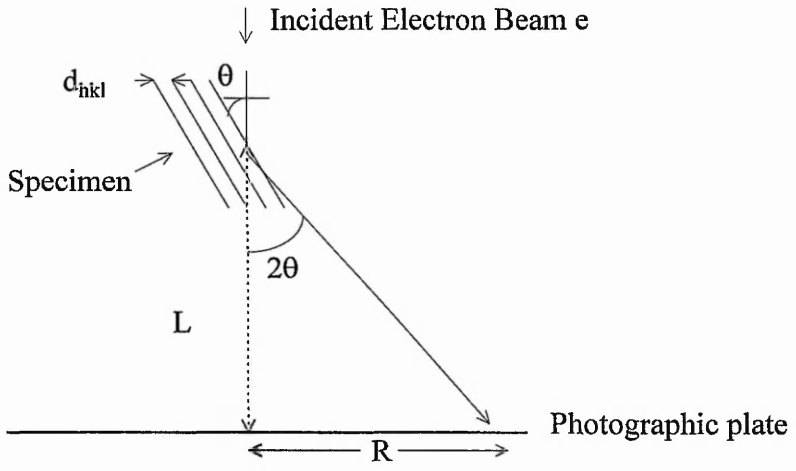

Fig. 1 The electron microscope considered as a simple electron diffraction camera.

R can be determined by measuring the distances between the central spot and each of the other spots in the diffraction pattern in turn. Since the pattern is symmetrical, this should be done by measuring between spots on either side of the central spot and dividing by two, or else by measuring the overall spacing of a large number of spots in a row passing through the central spot, and dividing by the number of spaces between the spots.

The diffraction patterns reportedf in this thesis were recorded with the microscope operating at an accelerating voltage of 200 kV, $\lambda = 0.00251$ nm and camera length, L = 200 cm.

So,

$$d\ (\text{nm}) = (\lambda\ (\text{nm}) \times L\ (\text{mm})) / R\ (\text{mm}).$$

When the *d*-spacings are obtained, by comparison to the *d*-spacings of the 9-432 JPCDS card for hydroxyapatite, it is possible to assign a set of Miller Indices to the spots or rings in the diffraction pattern. From the *d*-spacing formula for the hexagonal system

$$1/d^2 = 4(h^2+hk+k^2)/3a^2 + l^2/c^2,$$

the lattice parameters can be calculated .

APPENDIX III

Table 1. d-spacings calculated from the electron diffraction patterns obtained from the samples precipitated at 23°C from a solution containing 10 mM $Ca(NO_3)_2$ and 6 mM $(NH_4)_2HPO_4$ and 0.082 mM $Si(OH)_4$

time (min)	plates	needles	flakes	OCP (JCPDS 26-1056)	HAP (JCPDS 9-432)
1	-	-	-		
5	-	-	-		
15	4.747	-	-	4.706	4.72
	3.940			3.919	
	3.456			3.441 (m)	3.44 (s)
	2.834			2.833 (s)	
	2.814				2.814 (s)
	2.775			2.779 (m)	2.778 (s)
	1.950			1.957	
	1.941			1.948	1.943 (s)
	1.846			1.848	
	1.698				
	1.683				
30	3.940			3.919	
		3.456	3.456	3.441 (m)	3.44 (s)
	3.414			3.424 (m)	
	2.834			2.833 (s)	
	2.794				
		2.775	2.775	2.779 (m)	2.778 (s)
			2.755	2.745 (m)	
	2.264			2.265	2.262 (s)
	1.941			1.948	1.943 (s)
		1.894			
				1.891	1.890 (m)

Table 2 . d-spacings calculated from the electron diffraction patterns obtained from the samples precipitated at 23°C from a solution containing 10 mM $Ca(NO_3)_2$ and 6 mM $(NH_4)_2HPO_4$ and 0.204 mM $Si(OH)_4$

time (min)	plates	needles	flakes	OCP (JCPDS 26-1056)	HAP (JCPDS 9-432)
1	4.747		-	4.706	4.72
	3.940			3.919	
	3.863			3.862	
	3.456			3.441 (m)	3.44 (s)
		2.855		2.873 (m)	
	2.814			2.820 (s)	2.814 (s)
	2.238				2.228
	1.970			1.990	
		1.950		1.948	
	1.931			1.929	
		1.824		1.832	
		1.438			1.433
5	-		3.487	3.492	
		3.426		3.441 (m)	3.44 (s)
		2.814	2.814		2.814 (s)
		2.775	2.775	2.779 (m)	2.778 (s)
			2.755	2.745 (m)	
		1.876			1.871
15	9.163		-	9.05 (m)	
		3.487		3.492	
	3.456			3.441 (m)	3.44 (s)
	2.814			2.820 (s)	2.814 (s)
		2.775		2.779 (m)	2.778 (s)
	2.755			2.745 (m)	
	2.698				2.631 (s)
		1.931		1.929	
		1.858			1.871
30	3.518			3.492	3.51
			3.423	3.441 (m)	3.44 (s)
	3.396		3.396		
		3.203		3.209	
		2.824		2.820 (s)	2.814 (s)
			2.775	2.779 (m)	2.778 (s)
			2.755	2.745 (m)	
	2.736				2.720 (s)
	1.894			1.891	1.890 (m)
		1.824		1.832	
	1.698				1.684

Table 3. d-spacings calculated from the electron diffraction patterns obtained from the samples precipitated at 23°C from a solution containing 10 mM $Ca(NO_3)_2$ and 6 mM $(NH_4)_2HPO_4$ and 0.409mM $Si(OH)_4$

time (min)	plates	needles	flakes	OCP (JCPDS 26-1056)	HAP (JCPDS 9-432)
1	3.456	3.456	-	3.441 (m)	3.44 (s)
	3.127			3.132	
		2.845		2.833 (s)	
	2.814	2.814		2.82 (s)	2.814 (s)
	1.970			1.990	
5		5.710		5.52	
	4.614			4.67	
	3.863			3.862	
	3.396		3.396	3.378	
	2.814	2.814	2.814	2.82 (s)	2.814 (s)
		2.775		2.779 (m)	2.778 (s)
	2.755			2.745 (m)	
			2.736		2.720 (s)
		2.627		2.637 (m)	2.631 (s)
15	4.477		-	4.492	
		3.426		3.44 (m)	3.44 (s)
	3.396			3.378	
	2.814			2.82 (s)	2.814 (s)
		2.794			
	1.858			1.848	
		1.669			1.644 (m)
30		5.880		5.52	
	3.426		3.426	3.44 (m)	3.44 (s)
		2.985			
	2.855			2.873 (m)	
			2.814	2.82 (s)	2.814 (s)
		2.794			
	1.941			1.948	1.943 (s)
	1.720				1.722 (s)

Table 4. d-spacings calculated from the electron diffraction patterns obtained from the samples precipitated at 37°C from a solution containing 10 mM $Ca(NO_3)_2$ and 6 mM $(NH_4)_2HPO_4$ and 0.082 mM $Si(OH)_4$

time (min)	plates	needles	flakes	OCP (JCPDS 26-1056)	HAP (JCPDS 9-432)
1	3.964		-	3.919	
	3.887			3.879	3.88 (m)
		3.448		3.441 (m)	3.44 (s)
	3.249			3.278	
		3.223			
	3.146			3.132	3.17 (m)
		3.122		3.117	
	2.894			2.873 (m)	
	2.832	2.832		2.833 (s)	
		2.792		2.779 (m)	2.778 (s)
		2.305		2.304	
	1.982			1.990	
	1.953			1.957	
	1.943			1.948	1.943 (s)
	1.827			1.832	
		1.724			1.722 (s)
5		8.435	-		8.17 (m)
	3.964			3.919	
		3.540			3.51
		3.478		3.492	
	3.447			3.441 (m)	3.44 (s)
	3.249	3.249		3.278	
	3.146	3.146		3.132	3.17 (m)
	2.832	2.832		2.833 (s)	
	2.812			2.82 (s)	2.814 (s)
		2.792		2.779 (m)	2.778 (s)
	2.574			2.567	
		1.982		1.990	
	1.953			1.957	
		1.943		1.948	1.943 (s)
	1.870				1.871
		1.852		1.848	
	1.844				1.841 (s)
		1.754			1.754 (m)
	1.709				1.722 (s)
15		3.478		3.492	
			3.171	3.180	3.17 (m)
			2.981	2.946	
		2.873		2.873 (m)	
			2.832	2.833 (s)	
	2.792	2.792	2.792	2.779 (m)	2.778 (s)
	2.753			2.745 (m)	2.720 (s)
	1.852	1.852		1.848	

continuation table 4

time (min)	plates	needles	flakes	OCP (JCPDS 26-1056)	HAP (JCPDS 9-432)
30	9.219			9.36 (m)	
	3.964				4.07 (m)
	3.925	3.925		3.919	
	3.508			3.492	3.51
	3.447	3.447	3.447	3.441 (m)	3.44 (s)
	3.418	3.418		3.424 (s)	
	3.146			3.132	3.17 (m)
	3.097			3.055	3.08 (m)
		2.915		2.914	
	2.873	2.873	2.832	2.873 (m)	
	2.832	2.832		2.833 (s)	
	2.792	2.792			2.814 (s)
	2.772			2.779 (m)	2.778 (s)
		2.715		2.707	2.720 (s)
			2.278	2.271	
	1.982			1.990	
		1.972			
	1.962			1.957	
	1.870				1.871
		1.844		1.848	1.841 (s)
			1.835	1.837	
	1.746			1.745	
	1.724	1.724			1.722 (m)

Table 5. d-spacings calculated from the electron diffraction patterns obtained from the samples precipitated at 37°C from a solution containing 10 mM $Ca(NO_3)_2$ and 6 mM $(NH_4)_2HPO_4$ and 0.204 mM $Si(OH)_4$

time (min)	plates	needles	flakes	OCP (JCPDS 26-1056)	HAP (JCPDS 9-432)
1	3.887			3.879	3.88 (m)
	3.478	3.478	3.478	3.492	3.51
	3.447			3.441 (m)	3.44 (s)
	3.122			3.117	3.17 (m)
	2.873			2.873 (m)	
	2.832		2.832	2.833 (s)	
	2.812			2.82 (s)	2.814 (s)
	2.792	2.792			
	2.109			2.106	
		2.086		2.088	
	1.943			1.948	1.943 (s)
	1.861				1.871
5	9.439			9.36 (m)	
	9.010			9.05 (m)	
		8.435			8.17 (m)
	5.584			5.52	
	5.286			5.21	5.26
		4.129		4.111	
	4.004				4.07 (m)
	3.964			3.919	
	3.705			3.745	
	3.478			3.492	
	3.447	3.447	3.447	3.441 (m)	3.44 (s)
	3.197			3.180	3.17 (m)
	3.146			3.132	
	3.097			3.055	3.08 (m)
	2.873			2.873 (m)	
	2.852	2.852			
	2.832		2.832	2.833 (s)	
	2.792				2.814 (s)
		2.772		2.779 (m)	2.778 (s)
	2.643			2.637 (m)	
	2.625			2.617	2.631 (s)
		2.346		2.335	
		2.065		2.063	2.065
	1.982	1.982		1.990	
		1.879			1.890 (m)
	1.870				1.871
	1.835	1.835		1.837	
		1.762			1.754 (m)
	1.680				1.684

continuation table 5

time (min)	plates	needles	flakes	OCP (JCPDS 26-1056)	HAP (JCPDS 9-432)
15	-	3.540			3.51
		3.418		3.424 (s)	
		2.873		2.873 (m)	
			2.832	2.833 (s)	
		2.812			2.814 (s)
		2.772		2.779 (m)	2.778 (s)
		1.818		1.832	
		1.802		1.804	1.806 (s)
30	3.508			3.492	3.51
			3.418	3.424 (s)	
	3.197			3.180	3.17 (m)
		2.873		2.873 (m)	
			2.832	2.833 (s)	
	2.792				2.814 (s)
			2.753	2.745 (m)	
		2.661		2.671 (m)	
	2.086			2.088	
		2.002		2.002	2.000
		1.982		1.990	
	1.962			1.957	
		1.888		1.891	1.890 (m)
	1.879				1.871
	1.754				1.754 (m)

Table 6. d-spacings calculated from the electron diffraction patterns obtained from the samples precipitated at 37°C from a solution containing 10 mM $Ca(NO_3)_2$ and 6 mM $(NH_4)_2HPO_4$ and 0.409 mM $Si(OH)_4$

time (min)	plates	needles	flakes	OCP (JCPDS 26-1056)	HAP (JCPDS 9-432)
1	-	3.887		3.879	3.88 (m)
			3.508	3.492	3.51
		2.873		2.873 (m)	
		2.792	2.792		2.814 (s)
			2.753	2.745 (m)	
		1.924		1.929	
		1.879			1.890 (m)
			1.870		1.871
5	5.286			5.211	5.26
		3.501			3.51
	3.478		3.478	3.492	
	3.447		3.447	3.441 (m)	3.44 (s)
	3.146			3.132	3.17 (m)
	2.873			2.873 (m)	
	2.832		2.832	2.833 (s)	
			2.812		2.814 (s)
	2.792	2.792			
	2.753			2.745 (m)	
	2.643			2.637 (m)	
	2.618			2.617	
	2.332			2.335	
	2.065			2.063	2.065
	1.943			1.948	1.943 (s)
	1.852			1.848	
		1.754			1.754 (m)

continuation table 6

time (min)	plates	needles	flakes	OCP (JCPDS 26-1056)	HAP (JCPDS 9-432)
15	5.357			5.417	
	5.216			5.211	
	3.964			3.919	
	3.887			3.879	3.88 (m)
	3.540			3.492	3.51
			3.418	3.424 (s)	
	3.249			3.278	
	3.122			3.132	
		3.050		3.055	
	3.026			3.015	
	2.915			2.914	
	2.894				
	2.873			2.873 (m)	
			2.852		
	2.832	2.832		2.833 (s)	
	2.772			2.779 (m)	2.778 (s)
	2.677			2.671 (m)	
		1.982		1.990	
	1.962			1.957	
	1.943			1.948	1.943 (s)
	1.933			1.936	
	1.906				
	1.870				1.871
30	3.887			3.879	3.88 (m)
	3.478		3.478	3.492	
	3.447	3.447		3.441 (m)	3.44 (s)
	3.146			3.132	
	2.852			2.873 (m)	
		2.832		2.833 (s)	
	2.792		2.792		2.814 (s)
		2.772		2.779 (m)	2.778 (s)
	2.753			2.745 (m)	
	2.643			2.637 (m)	
		2.558		2.567	
	2.278			2.271	
	1.934	1.934		1.936	
	1.844			1.848	1.841 (s)
		1.716			1.722 (s)

Table 7. d-spacings calculated from the electron diffraction patterns obtained from the samples precipitated at 23°C from a solution containing 10 mM $Ca(NO_3)_2$ and 6 mM $(NH_4)_2HPO_4$ and 75 μM $AlCl_3$.

time (min)	plates	needles	flakes	OCP (JCPDS 26-1056)	HAP (JCPDS 9-432)
1	-	3.447	3.447	3.441 (m)	3.44 (s)
			3.417	3.424 (s)	
			3.121	3.132	
			2.832	2.833 (s)	
			2.812		2.814 (s)
		2.772		2.779 (m)	2.778 (s)
		1.739		1.743	1.722 (s)
5	3.925			3.919	
			3.540		
		3.508	3.508		3.51
	3.478	3.478		3.492	
			3.447	3.441 (m)	3.44 (s)
			3.418	3.424 (s)	
	3.223			3.278	
		3.197			3.17 (m)
	3.146			3.132	
		2.873		2.873 (m)	
	2.852				
			2.832	2.833 (s)	
	2.812		2.812	2.82 (s)	2.814 (s)
			2.792		
	2.734	2.734		2.745 (m)	
			2.086	2.088	
		2.012		2.002	
	1.870				1.871
	1.852			1.848	
		1.746		1.745	
	1.731				1.722 (s)
15	-	-	3.447	3.441 (m)	3.44 (s)
			2.832	2.833 (s)	
30	-	-	3.418	3.424 (s)	
			2.792		2.814 (s)
			2.772	2.779 (m)	2.778 (s)

Table 8. d-spacings calculated from the electron diffraction patterns obtained from the samples precipitated at 37°C from a solution containing 10 mM $Ca(NO_3)_2$ and 6 mM $(NH_4)_2HPO_4$ and 75 μM $AlCl_3$.

time (min)	plates	needles	flakes	OCP (JCPDS 26-1056)	HAP (JCPDS 9-432)
1	8.259	8.259	-		8.17 (m)
		4.129		4.111	
	3.964			3.919	
	3.478	3.478		3.492	
	3.197			3.180	
	3.122			3.117	
	3.097				3.08 (m)
		3.073		3.055	
	2.894				
	2.832			2.833 (s)	
		2.753		2.745 (m)	
	1.982			1.990	
	1.934				1.943 (s)
	1.879				1.871
		1.870			
	1.754				1.754 (m)
	1.739			1.743	
	1.490				1.503 (m)
5	-	3.478		3.492	
		3.447		3.441 (m)	
		2.873		2.873 (m)	
		2.832	2.832	2.833 (s)	
15	-	-	3.478	3.492	
			2.832	2.833 (s)	
			2.792		2.814 (s)
30	-	-	3.478	3.492	
			3.418	3.424 (s)	
			2.852	2.833 (s)	
			2.812		2.814 (s)
			2.792		

Table 9. d-spacings calculated from the electron diffraction patterns obtained from the samples precipitated at 23°C from a solution containing 10 mM $Ca(NO_3)_2$ and 6 mM $(NH_4)_2HPO_4$ and 75 μM $AlCl_3$ and 0.082 mM $Si(OH)_4$

time (min)	plates	needles	flakes	OCP (JCPDS 26-1056)	HAP (JCPDS 9-432)
1	-	-	3.493	3.492	
			2.832	2.833 (s)	
			2.799		2.814 (s)
5	-	-	3.540		3.51
			3.508		
			3.478	3.492	
			3.447		3.44 (s)
			3.418	3.424 (s)	
			2.832	2.833 (s)	
			2.812		2.814 (s)
			2.792		
15	-	-	2.812		2.814 (s)
30	-	-	3.540		3.51

Table 10 . d-spacings calculated from the electron diffraction patterns obtained from the samples precipitated at 23°C from a solution containing 10 mM $Ca(NO_3)_2$ and 6 mM $(NH_4)_2HPO_4$ and 75 μM $AlCl_3$ and 0.204 mM $Si(OH)_4$

time (min)	plates	needles	flakes	OCP (JCPDS 26-1056)	HAP (JCPDS 9-432)
1	-	-	-		
5	-	-	3.478	3.492	
			2.873	2.873 (m)	
			2.832	2.833 (s)	
			2.812		2.814 (s)
15	-	-	3.478	3.492	
			3.418	3.424 (s)	
			2.832	2.833 (s)	
			2.792		2.814 (s)
30	-	-	3.478	3.492	
			2.812		2.814 (s)

Table 11 . d-spacings calculated from the electron diffraction patterns obtained from the samples precipitated at 37°C from a solution containing 10 mM $Ca(NO_3)_2$ and 6 mM $(NH_4)_2HPO_4$ and 75 μM $AlCl_3$ and 0.082 mM $Si(OH)_4$

time (min)	plates	needles	flakes	OCP (JCPDS 26-1056)	HAP (JCPDS 9-432)
1	5.286		-	5.211	5.26
	3.964				4.07 (m)
	3.925			3.919	
	3.447	3.447		3.441 (m)	3.44 (s)
	3.418			3.424 (s)	
	3.197			3.180	
	3.122			3.117	
	2.894			2.914	
	2.873	2.873		2.873 (m)	
	2.852			2.833 (s)	
	2.772			2.779 (m)	2.778 (s)
	2.661			2.671 (m)	
	1.982			1.990	
	1.962				
	1.953			1.957	
	1.861				1.871
	1.844			1.848	1.841 (s)
		1.716			1.722 (s)
5	-		3.508		3.51
		3.478		3.492	
		3.447		3.441 (m)	3.44 (s)
			2.852	2.873 (m)	
		2.832		2.833 (s)	
15	3.197	-	-	3.180	
	2.812				2.814 (s)
	2.792				
	2.715				2.720 (s)
	2.661			2.671 (m)	
	2.252			2.258	2.262 (s)
	1.943			1.948	1.943 (s)
30	3.146			3.132	
		3.418		3.424 (s)	
	2.894			2.914	
		2.832	2.832	2.833 (s)	
	2.792				2.814 (s)
	2.625			2.617	2.631 (s)
		1.709			1.722 (s)

Table 12. d-spacings calculated from the electron diffraction patterns obtained from the samples precipitated at 37°C from a solution containing 10 mM $Ca(NO_3)_2$ and 6 mM $(NH_4)_2HPO_4$ and 75 μM $AlCl_3$ and 0.204 mM $Si(OH)_4$

time (min)	plates	needles	flakes	OCP (JCPDS 26-1056)	HAP (JCPDS 9-432)
1	-	-	3.478	3.492	
			3.418	3.424 (s)	
			2.832	2.833 (s)	
			2.792		2.814 (s)
5	-	-	3.478	3.492	
			3.418	3.424 (s)	
			2.873	2.873 (m)	
			2.792		2.814 (s)
			2.753	2.745 (m)	
			1.739	1.743	
15	-	-	3.478	3.492	
			2.832	2.833 (s)	
			2.792		2.814 (s)
30	-		5.663	5.52	
		3.478	3.478	3.492	
			3.448	3.441 (m)	3.44 (s)
		3.418		3.424 (s)	
		3.146		3.132	
			2.832	2.833 (s)	
		2.812			2.814 (s)
		2.792	2.792		
			2.772	2.779 (m)	2.778 (s)
		2.753		2.745 (m)	
		1.943	1.943	1.948	1.943 (s)
		1.835		1.837	1.841 (s)
		1.739		1.743	
			1.731		
		1.724			1.722 (s)

Table 13. d-spacings calculated from the electron diffraction patterns obtained from the samples precipitated at 37°C from a solution containing 10 mM $Ca(NO_3)_2$ and 6 mM $(NH_4)_2HPO_4$ and 75 μM $AlCl_3$ and 0.409 mM $Si(OH)_4$

time (min)	plates	needles	flakes	OCP (JCPDS 26-1056)	HAP (JCPDS 9-432)
1	3.925			3.919	
	3.540				3.51
	3.508				
	3.478			3.492	
		3.448	3.448	3.441 (m)	3.44 (s)
			3.418	3.424 (s)	
	3.304			3.311	
	3.122	3.122		3.117	
	3.073				3.08 (m)
		2.873	2.873	2.873 (m)	
	2.832			2.833 (s)	
			2.792		2.814 (s)
			2.734	2.745 (m)	2.720 (s)
	1.982			1.990	
	1.943			1.948	1.943 (s)
	1.934			1.936	
		1.888		1.891	1.890 (m)
	1.870				1.871
	1.746			1.745	
	1.740		1.723	1.743	
		1.716			1.722 (s)
5	-	-	3.540		3.51
			3.478	3.492	
			3.447	3.441 (m)	3.44 (s)
			3.418	3.424 (s)	
			2.792		2.814 (s)
			1.924	1.929	
			1.818		1.806 (s)
			1.731	1.743	
			1.716		1.722 (s)
15			3.508		3.51
			3.478	3.492	
		3.447	3.447	3.441 (m)	3.44 (s)
	3.418	3.418		3.424 (s)	
		3.122	3.122	3.117	
	2.873	2.873		2.873 (m)	
			2.832	2.832 (s)	
			2.812		2.814 (s)
	2.792	2.792	2.792		
	2.252			2.258	2.262 (s)
			1.962	1.957	
	1.835			1.837	
			1.731	1.743	
			1.724		1.722 (s)

continuation table 13

time (min)	plates	needles	flakes	OCP (JCPDS 26-1056)	HAP (JCPDS 9-432)
30		-	3.508		3.51
	3.478		3.478	3.492	
			3.447	3.441 (m)	
			3.418	3.424 (s)	
			2.832	2.833 (s)	
	2.812		2.812		2.814 (s)
			2.792		
			2.772	2.779 (m)	2.778 (s)
	2.734				2.720 (s)
	2.278			2.271	
			1.972	1.990	
	1.934			1.936	
			1.746	1.745	
			1.731	1.743	
			1.727		1.722 (s)

APPENDIX IV

Preparation of femoral head bone samples for transmission electron microscopy analysis.

Full-depth blocks of bone were taken from the superior and posterior regions of the femoral head. The tissues samples were subdivided to full-depth blocks of ca. 1 mm in the two remaining dimensions. The tissue blocks were fixed overnight in 1.5% glutaraldehyde in 0.1M sodium cacodylate buffer (pH=7.4). Samples were washed in three changes of 0.1M sodium cacodylate buffer containing 6% sucrose, prior staining with OsO_4 for 1h. Samples were washed in three changes of 0.1M sodium cacodylate buffer containing 6% sucrose and then dehydrated through a graded alcohol series (60%, 80% and 100% absolute ethanol). Samples were transfer to propylene oxide twice for 20 min, prior filtration with 1:1 propilene:araldite CY212 resin mixture overnight followed by infiltration in neat CY212 resin under vacuum three times for 2 hours and then embedding in fresh resin at 60°C for 48 hours. Ultrathin (90 nm) sections were cut with a Diatome diamond knives and floated onto 0.1M sodium cacodylate buffer prior to collection onto fomvar-coated copper grids. Unstained sections were analysed using a JEOL 2010 TEM with a LaB_6 electron gun filament operating at 200 Kv. The microscope had attached a PentafetST detector and the LikIsis software from Oxford Instruments for Energy Dispersive X-ray Analysis.